Development of a Human Cell Model of Amyloid β Seeding and Aggregation to Investigate Alzheimer's Disease Pathology

A thesis submitted in partial fulfilment of the requirements for the degree of Doctor of Philosophy from University College London

Ludmila Martinova Sheytanova

Department of Neurodegenerative Disease

Institute of Neurology

University College London

2018

Declaration

I, Ludmila Martinova Sheytanova, confirm that the work presented in this thesis is my own. Where information has been derived from other sources, I confirm that this has been indicated in the thesis.

Acknowledgements

First off, I would like to thank my parents, Maria and Martin, for their endless support, understanding, and guidance during the three years of my PhD, the biggest challenge I have faced so far.

My warmest thanks go to Frank Cooper, Jonathan Wadsworth, Elizabeth Fisher, and Bart De Strooper whose competent and empathetic leadership helped me overcome situations when continuing seemed impossible. Kevin Williams has also been an invaluable friend who has made me laugh with his vibrant humor more times than I care to remember.

I would like to thank my good friends Lawrence Vandervoort, Billy West, Justin Tosh, Victoria Nicholls, Conrad De Kerckhove, Bernardo Esteves, Alexandra Philiastides, Ruchi Kumari, Xun Yu Choong, and Luke Dabin with whom I have shared many happy moments and who were always by my side in times of need. It is not an exaggeration to say that without them I would not be here today. I would also like to thank everyone else with whom I have shared the PhD office for the camaraderie and the memories through which I grew so much: Lucianne Dobson, James Miller, Amy Nick, Charlotte Ridler, Prasanth Sivakumar, David Thomas, Julia Ravey, Madeleine Riley, Grace O'Regan, Carolin Koriath, Caroline Casey, Angelos Armen, Rachele Saccon, Daniel Wright, Francesca De Giorgio, Rhia Ghosh, and Alan Mejia-Maza.

I would also like to briefly talk about my friend and colleague Laura Pulford who was incredibly knowledgeable, bright, and caring and who was always ready to help anyone if they were struggling. No one can say with certainty what her innermost thoughts were, but she tragically took her own life during her thesis write up. I would like to take this opportunity to stress how much pressure an academic environment puts on aspiring scientists and how lacking in support we often find ourselves. Mental health is a serious issue and an adequate response can save lives. With this in mind, I would also like to extend my gratitude to my own therapist, Catherine McAteer, who has worked with me since Laura's passing. Laura will be sorely missed.

I'm grateful to Silvia Purro, Emma Clayton, Sarah Mizielinska, Nunu Arora, Emmanuelle Viré, Karen Cleverley, Claire Sarell, Iryna Benilova, Anny Devoy, Cassandra Terry, Adam Wenborn, Ronald Druyeh, Adrian Isaacs, and Andrew Nicoll for the invaluable scientific discussions and for their kind guidance. Thanks are due to Henrik Zetterberg, Erik Portelius, Rita Persson, and Jamie Toombs for performing the mass spectrometry experiments, which are a central part of my thesis and also to Parmjit Jat, Mark Farrow, Michael Farmer, Emmanuel Risse, Juan Ribez, and Anna Harvey for help with data analysis, experiment planning, and protocols. I would also

like to thank the people in the IT and administration office who made my work possible, namely Ryan Peter, Samantha MacLeod, Oke Avwenagha, Rosie Baverstock-West, Sandra Porteus, Amir Mayahi, David Ruegg, Naho Ollason, and Alison Church.

This work would also not have been possible without the funding provided by John Collinge through the Medical Research Council and also by Alzheimer's Research UK.

Finally, I would like to thank my supervisor, Peter-Christian Kloehn, for his support, guidance, and for creating an environment in which I learned how to think independently, ask questions, and trust my own judgment on the road to becoming an independent scientist.

Abstract

Alzheimer's disease (AD) is characterized by extracellular plaques of amyloid β (Aβ) and intracellular tangles of microtubular tau proteins. Aβ is produced through sequential cleavage of amyloid precursor protein (APP) by β-secretase (BACE1) and γ-secretase. Seeded aggregation of oligomeric Aβ (AβO) contributes to disease progression as demonstrated by intracerebral inoculation of transgenic mice with human-derived AD brain homogenates. To date, however, there is no high-throughput cell model for Aβ seeding and the present project investigated an approach to address this gap. Eleven human neuroblastoma lines were evaluated for their endogenous APP, BACE1, γ-secretase, and Aβ levels. Wild-type or mutant (Swedish, Iberian, or NL-F) APP695 was cloned with BACE1 into a retroviral vector and was stably overexpressed in two cell lines with opposite levels of APP and BACE1 expression, SK-N-BE(2) and GI-ME-N. The Aβ peptides secreted by each mutant were evaluated via mass spectrometry and relative amounts of Aβ1-38, 1-40, and 1-42, were quantified with a highly sensitive enzyme-linked immunosorbent assay (ELISA). Aβ levels were compared to those produced by 7PA2 cells, a well-characterized model of APP processing. APP-overexpressing SK-N-BE(2) cells secreted equivalent or higher Aβ amounts; the NL-F line had the highest levels of Aβ1-42, which is particularly prone to oligomerization. This line was inoculated with diluted homogenate from human AD brain with proven seeding ability, in parallel to 7PA2 and native GI-ME-N cells, in which Aβ was not detected. The lines were grown for several splits post-seeding. Cell supernatant from each split was evaluated for sustained AβO secretion post-seeding with an AβO-specific ELISA. Seed uptake and propagation was quantified at each split by immunocytochemistry. No AβOs were detected in cell supernatants due to assay sensitivity limitations and intracellular uptake was too variable. Hence, pilot experiments to explore seeded aggregation were not conclusive and further exploration of this system is needed.

Table of Contents

List of Figures

List of Tables

List of Abbreviations

%CV	Percent coefficient of variation
α7nAChR	α7 nicotinic acetylcholine receptor
AD	Alzheimer's disease
ADAM10	A-disintegrin-and-metalloproteinase domain-containing protein 10
ADDL	Amyloid β-derived diffusible ligands
AEBSF	4-(2-aminoethyl)benzenesulfonyl fluoride hydrochloride
AF 488	Alexa Fluor 488
AICD	Amyloid precursor protein intracellular domain
ANOVA	Analysis of variance
APH1	Anterior pharynx defective 1
APLP	Amyloid precursor-like protein
ApoE	Apolipoprotein E
APP	Amyloid precursor protein
Aβ	Amyloid β
Aβ3(pE)-42	Pyroglutamate amyloid β
AβO	Oligomeric amyloid β
BACE	β-Site cleaving enzyme
BCA	Bicinchoninic acid
bp	Base pair
BSA	Bovine serum albumin
BSE	Bovine spongiform encephalopathy
CAA	Cerebral amyloid angiopathy
CDS	Coding sequence
CHO	Chinese hamster ovary
CJD	Creutzfeldt-Jakob disease
CLU	Clusterin
CM	Cultured medium
CMV	Cytomegalovirus
CNS	Central nervous system
CSF	Cerebrospinal fluid

CTF	C-terminal fragment
DAPI	4',6-diamidino-2-phenylindole, dihydrochloride
DMEM	Dulbecco’s Modified Eagle Medium
DMSO	Dimethyl sulfoxide
DNA	Deoxyribonucleic acid
DNase	Deoxyribonuclease
dNTP	Deoxyribose nucleoside triphosphate
DPBS	Dulbecco's Phosphate-Buffered Saline
dsDNA	Double-stranded deoxyribonucleic acid
EDTA	Ethylenediaminetetraacetic acid
ELISA	Enzyme-linked immunosorbent assay
ELISPOT	Enzyme-linked immunospot assay
EOAD	Early-onset Alzheimer's disease
ERAV	Equine rhinitis A virus
FBS	Fetal bovine serum
FRET	Fluorescence resonance energy transfer
GALV	Gibbon ape leukemia virus
GAPDH	Glyceraldehyde 3-phosphate dehydrogenase
GSK3β	Glycogen synthase kinase 3β
HD	Huntington's disease
HFIP	Hexafluoro-2-propanol
HRP	Horseradish peroxidase
IDE	Insulin-degrading enzyme
IDT	Integrated DNA Technologies
IF	Immunofluorescence
IP	Immunoprecipitation
iPSC	Induced pluripotent stem cells
kbps	Kilobasepairs
LB	Luria broth
LDLR	Low-density lipoprotein receptor
LLOD	Lower limit of detection

LLOQ	Lower limit of quantification
LOAD	Late-onset Alzheimer's disease
low-n	Low number; low molecular weight
LS-MS/MS	Liquid chromatography - mass spectrometry
LTP	Long-term potentiation
LTR	Long terminal repeat
MALDI TOF/TOF	Matrix-assisted-laser-desorption/ionization time-of-flight/time-of-flight
MALS	Multi-angle static light scattering
MAMs	Mitochondrial-associated ER membranes
MES	2-(N-morpholino)ethanesulfonic acid
MAPK	Mitogen-activated protein kinase
MMLV	Murine leukemia virus
mRNA	Messenger ribonucleic acid
MTA	Material transfer agreement
NCSTN	Nicastrin
NMDA	N-methyl-D-aspartate
NEB	New England Biolabs
NFTs	Neurofibrillary tangles
PBS	Phosphate-buffered saline
PBS-T	Phosphate-buffered saline with Tween 20
PCR	Polymerase chain reaction
PD	Parkinson's disease
PEN2	Presenilin enhancer 2
Pen-Strep	Penicillin-streptomycin
PI	Protease inhibitor
PICALM	Phosphatidylinositol clathrin assembly lymphoid-myeloid leukemia
PrP	Prion protein
PrP^{C}	Cellular prion protein
PrP^{Sc}	Scrapie prion protein
PS	Presenilin
PVDF	Polyvinylidene fluoride

Ram-1	Amphotropic retrovirus receptor 1
RIPA	Radio immunoprecipitation assay
RML	Rocky Mountain Laboratory
RNA	Ribonucleic acid
RNase	Ribonuclease
RNA-seq	Ribonucleic acid sequencing
RPMI	Roswell Park Memorial Institute
RT	Room temperature
SAD	Sporadic Alzheimer's disease
sAPP	Soluble amyloid precursor protein fragment
SDM	Site-directed mutagenesis
SDS	Sodium dodecyl sulfate
SEM	Standard error of the mean
SOC	Catabolite repression
SORL1	Sortilin related receptor 1
TDP-43	TAR DNA-binding protein 43
Tg	Transgenic
TM	Transmembrane
TMB	3,3',5,5'-tetramethylbenzidine
TREM2	Triggering receptor expressed on myeloid cells 2
TSE	Transmissible spongiform encephalopathy
ULOD	Upper limit of detection
ULOQ	Upper limit of quantification
v/v	Volume-to-volume
VSV-G	Vesicular stomatitis virus glycoprotein
w/v	Weight-to-volume
WB	Western blot
WT	Wild type

1. Introduction

1.1. Alzheimer's Disease

1.1.1. Overview

Alzheimer's disease (AD) is the most prevalent form of dementia, primarily affecting individuals aged above 60-65 in its late-onset form (LOAD) or individuals entering middle age in its early-onset (EOAD) form (Alzheimer's Association 2016). It was first identified in 1906 by the German psychiatrist Alois Alzheimer as a case study of presenile dementia in one of his patients, Auguste Deter. Histopathological staining of Ms. Deter's brain revealed two distinct types of protein aggregate lesions, which have since been identified to be extracellular fibrillar plaques of amyloid β (Aβ) and intracellular neurofibrillary tangles (NFTs) of hyperphosphorylated microtubular tau. It is now known that apart from these two canonical pathological manifestations, AD pathology can be mixed with features characteristic of other types of dementia (McKhann et al. 2011, Schneider et al. 2007). These are invariably accompanied by chronic cerebral inflammation manifesting as hyperactivated microglia, synaptic degeneration, and overall neuronal dystrophy (reviewed in Serrano-Pozo et al., 2011). Ultimately, these events lead to pervasive neurodegeneration, which gives rise to all-encompassing cognitive deficits and progress to complete loss of agency and death. Tau lesions analyzed in post-mortem tissue have been shown, unlike Aβ plaques, to spread through specific brain regions in a predictable manner and to correlate with cognitive decline; this has led to the development of the Braak staging system of tau pathology (Braak & Braak 1991, 1995; Braak et al. 2011). Although Aβ spread does not progress as consistently as tau, a similar staging system has also been developed and is shown in Figure 2 (Thal et al. 2002). Braak and Thal stages, together with assessment of the grade of cognitive decline and pathophysiological changes in live patients (e.g. Bateman *et al.*, 2012; Wilson *et al.*, 2012; Villemagne *et al.*, 2013), have contributed to the development of guideline sets of diagnostic criteria for clinicians (Boluda et al. 2014, Fillenbaum et al. 2008, McKhann et al. 1984, 2011).

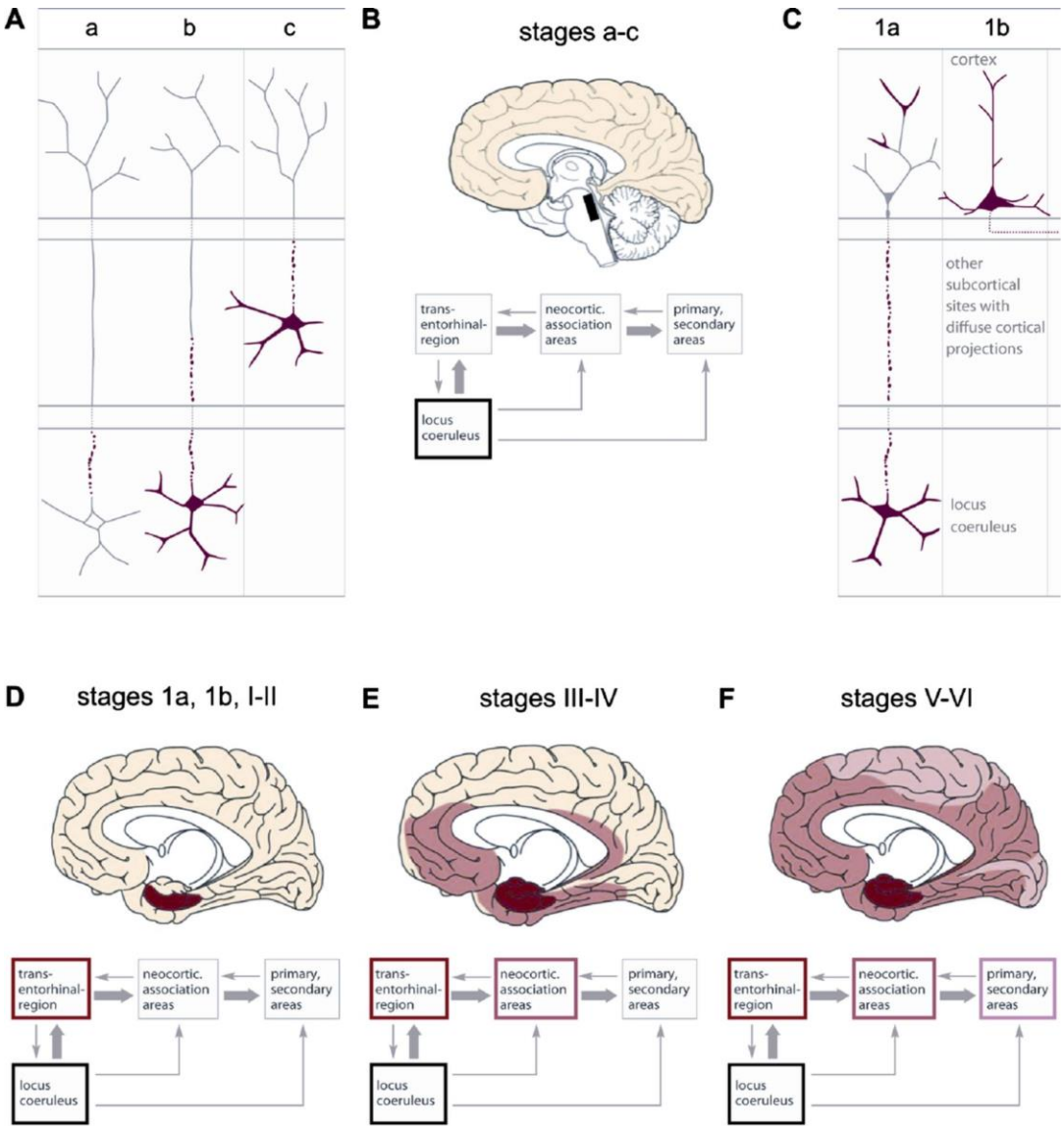

Figure 1. Braak stages of the progression of AD pathology (from Braak et al., 2011).

a) Stages a-c begin primarily in the locus coeruleus (**b), black boxes**) when pre-tangle material starts accumulating in axons, after which it enters the soma and dendrites of neurons. By stage c, the material has entered neurons which project into the cortex. The relationship between regions involved in stages a-c is shown in **b)**. **c)** Pre-tangle material spreads to the transentorhinal region in stage 1a and fills pyramidal neurons in stage 1b. **d) – f)** The spread of pre-tangle stages 1a and 1b and early NFT stages I and II are shown in dark red. Light red refers to NFT stages III and IV and pink to the latest NFT stages V and VI.

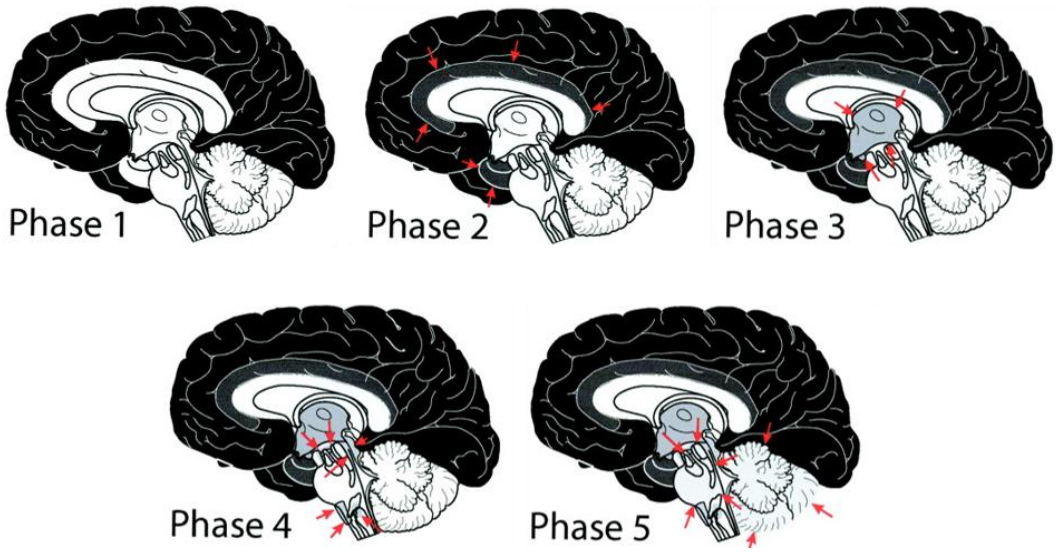

Figure 2. Thal staging of Aß pathology in AD (from Thal et al. 2002).

Cerebral amyloidosis has been proposed to progress in 5 stages. Stage 1 begins with deposits in the neocortex (black). Stage 2 sees movement (arrows) of deposits into the allocortex, which includes the hippocampus and the amygdala. In Stage 3 other subcortical structures including the striatum, thalamus, and hypothalamus become involved and by Stage 4 amyloid deposition progresses into the brainstem. The final Stage 5 is characterized by deposits in the pons and the cerebellum.

1.1.2. Causes and Risk Factors

1.1.2.1. Sporadic Alzheimer's Disease (SAD)

Currently, there is no consensus on a unifying cause of AD. Between 95-99% of AD cases are sporadic, have no known cause, and increase exponentially with age after 65, which makes age the number one risk factor for acquiring the disease (Mayeux & Stern 2012). A number of additional genetic, environmental, and behavioral risk factors that increase the likelihood of SAD have been identified (Figure 3, reviewed in Karch and Goate, 2015 and Scheltens *et al.*, 2016); however, these have not been linked to a single causal cellular event and it is likely that in order for SAD to begin, multiple conditions need to be fulfilled. The primary genetic risk factor for AD is homozygosity for the ε4 allele of Apolipoprotein E (ApoE) (Corder et al. 1993, Saunders et al. 1993) and this is associated with faster and more abundant cerebral Aβ plaque deposition and with a corresponding reduction of peripheral Aβ in the cerebrospinal fluid (CSF) (Morris et al. 2010). ApoE is a key lipid transporter in the central nervous system (CNS) and is responsible for maintaining cholesterol levels, as well as binding Aβ and participating in its clearance (Castellano et al. 2011, Lee et al. 2011). Heterozygous individuals have reduced risk, which is still higher than non-

carriers; conversely, carriers of the ε2 allele are protected (Corder et al. 1993). Clusterin (CLU, Figure 3, bottom right) is another AD risk factor that exists as several splice variants with a wide range of suggested biological functions covering inflammation, lipid transport, and regulating apoptosis, which makes interpreting its effects difficult (Jones & Jomary 2002, Karch & Goate 2015). For example, through a synergistic interaction with ApoE, CLU has been proposed to facilitate Aβ clearance and impede deposition (DeMattos et al. 2004), but CLU-deficient mice show reduced fibrillization of Aβ aggregates and limited neuritic damage (DeMattos et al. 2002). Another example is the lipid transporter triggering receptor expressed on myeloid cells 2 (TREM2), which is found on CNS microglia and has functions towards Aβ phagocytosis during the microglial inflammatory response to plaques (Guerreiro et al. 2013, Jonsson et al. 2013). TREM2 interacts with apolipoproteins like ApoE and CLU during microglial uptake of Aβ for degradation; thus, risk variants of TREM2 impede this process (Yeh et al. 2016).

Additional SAD/LOAD risks arise from genetic variation or abnormal hyperphosphorylation of other proteins with functions not only in lipid transport, but in the inflammatory response, endocytosis, and other processes, which are often interdependent, as seen in the example of ApoE, CLU, and TREM2. TAR DNA-binding protein 43 (TDP-43), an RNA-binding nuclear protein that can become hyperphosphorylated and bears high risk for amyotrophic lateral sclerosis (ALS) when mislocalized to the cytoplasm, has been shown to form inclusions in a vast proportion of SAD patient brains together with plaques and NFTs (Geser et al. 2009, Josephs et al. 2014). TDP-43 has been shown to increase tau aggregation, but to reduce the formation of fibrillar Aβ aggregates and modulate the intracellular trafficking of amyloid precursor protein (APP) from which Aβ is synthesized (Davis et al. 2017). Sortilin related receptor 1 (SORL1) also has roles in lipid trafficking and its insufficient neuronal expression leads to errors in vesicle recycling of APP (Rogaeva et al. 2007). Similarly, phosphatidylinositol clathrin assembly lymphoid-myeloid leukemia (PICALM) protein is central to membrane recycling and internalization of APP into endosomes, favoring Aβ production (Xiao et al. 2012). Albeit rarer, these variants may present the same level of risk as ApoE ε4 (Guerreiro et al. 2013, Jonsson et al. 2013). Type II diabetes and cardiovascular disease and, by extension, an unhealthy diet and sedentary lifestyle, also increase the risk of developing LOAD; so does head injury (Huang et al. 2014, Liu et al. 2014, Peila et al. 2002, Zetterberg & Mattsson 2014).

1.1.2.2. Familial Alzheimer's Disease (FAD)

FAD, on the other hand, accounts for between 1-5% of all cases and arises through approximately 300 (Bai et al. 2015) autosomal dominant mutations within the *APP, PSEN1,* or *PSEN2* genes. *PSEN1 and 2* encode the two homologous proteins presenilin 1 and 2 (PS1 and PS2), which house the active site of γ-secretase, an aspartyl intramembrane enzymatic complex with multiple cellular substrates including APP and thus indispensable for Aβ production. Most of these mutations occur in the presenilins, with those in PS1 far outnumbering those in PS2 (Bai et al. 2015). Typically, FAD and EOAD are synonymous, but it is also possible for some FAD cases to manifest in later life; equally SAD, which is typically late-onset, can also manifest at a younger age (Strobel). In addition, there are multiple mutations along the sequence of the *MAPT* gene, which encodes tau, but while these mutations facilitate tau hyperphosphorylation and exacerbate pathology, they are not causative (Bekris et al. 2010). Amyloidogenic and non-amyloidogenic processing, γ-secretase complex heterogeneity, and particular mutations are discussed later in the Introduction, but briefly APP, PS1, and PS2 mutations have two main effects on the outcome of Aβ production: they either increase total Aβ load or they modulate the cleavage of APP to preferentially produce longer, more hydrophobic, and therefore more aggregate-prone Aβ species (Chávez-Gutiérrez et al. 2012, Szaruga et al. 2015, Veugelen et al. 2016). The latter mutation type progressively destabilizes the interaction of the complex with intermediate APP substrates as they get shorter; it also increases the flexibility of γ-secretase, so that it assumes an "open" conformation more frequently and thus is more likely to release Aβ prematurely (Elad et al. 2015, Szaruga et al. 2017). Factors such as multiple simultaneously occurring mutations, membrane composition, and temperature further modulate the interaction between the complex and its APP-derived substrates, resulting in altered secretion of Aβ peptide species both *in vitro* and *in vivo* (Szaruga et al. 2017). Furthermore, a handful of causative PS1 mutations represent a partial loss-of-function of γ-secretase because they impair the maturation of the active site, in addition to destabilizing the integrity of the enzyme-substrate assembly through the above mechanisms (Saito et al. 2011, Szaruga et al. 2017, Veugelen et al. 2016).

1.1.3. Economic and Societal Implications

It is estimated that by 2030 65.7 million people worldwide will live with dementia and that 63% of them will reside in poorer countries (Prince et al. 2013), where birth rates are consistently higher and therefore more people will enter older age in the next decade, compared to Europe and the US (Scheltens et al. 2016). The number of cases is expected

to double by 2050 (Prince et al. 2013). A mathematical cost analysis estimates that a single AD patient in the UK costs approximately £210,000, depending on the time of diagnosis and the level of treatment (Getsios et al. 2012), which also includes the indirect costs of deteriorating lifestyle and caregiving. In the US, the 2016 Alzheimer's Association Facts and Figures report estimates that the total hours of unpaid care amounted to $221.3 billion in 2015, whereas in 2016 the total healthcare expenditure on all dementias, of which AD will constitute approximately 60-80%, has amounted to $236 billion. Considering these figures together with the emotional repercussions of the disease, which impact not only the patient, but families and caregivers, it becomes clear that AD and other dementias are an enormous societal burden and that treatment, which is currently unavailable, is urgently needed.

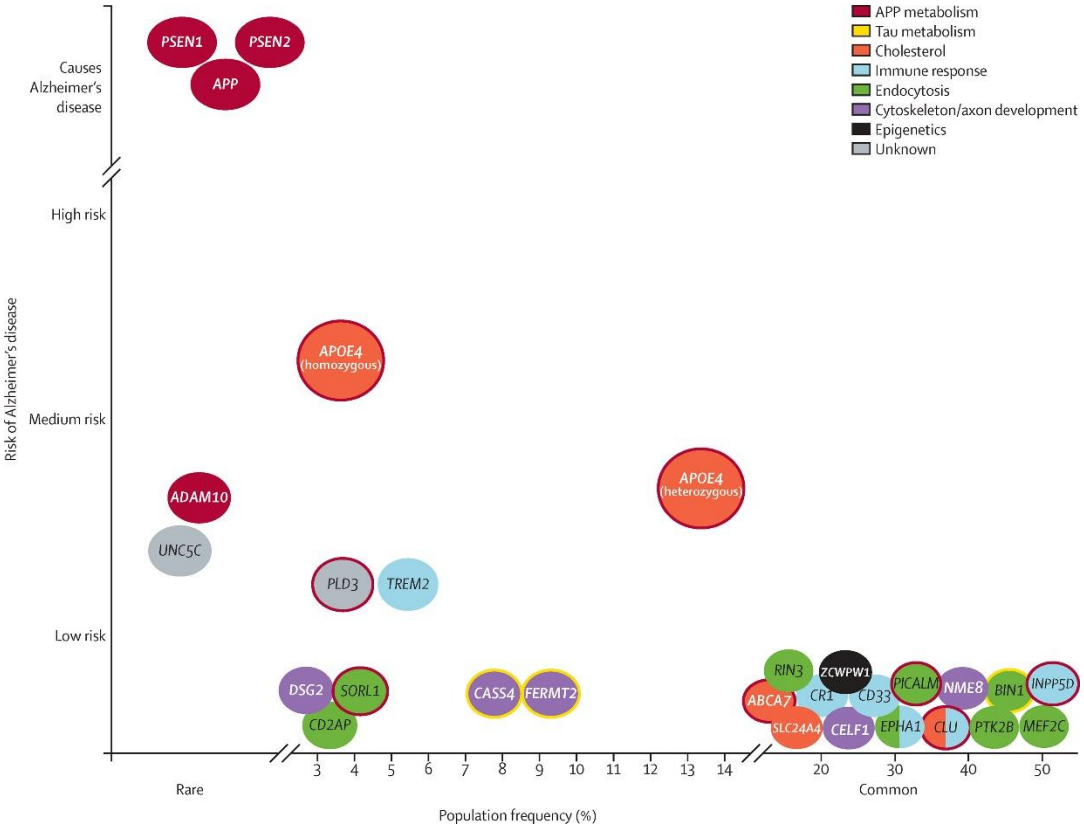

Figure 3. Genetic risk factors linked to AD (from Scheltens et al., 2016).

Disease-associated risk genes are color-coded based on their suggested function (legend top right). Genes circled in red relate to Aβ production and metabolism, while genes circled in yellow relate to tau. The risk which these genes pose to AD onset is plotted on the y axis and their frequency in AD cases is plotted on the x axis.

1.2. Proteolytic Processing of Amyloid Precursor Protein and Aβ Production

1.2.1. Non-amyloidogenic Processing

APP is a single-span transmembrane (TM) protein with a long extracellular N-terminal domain and a short intracellular C-terminus (Dyrks et al. 1988, Kang et al. 1987). Its protein family includes two other members, amyloid precursor-like proteins 1 and 2 (APLP1 and APLP2), which carry some functional redundancy (Shariati & De Strooper 2013). Among the splice variants of APP, APP695 is the predominant neuronal isoform, whereas APP751 and APP770 exist in other CNS cell types and their sequences differ by the presence of one or two extracellular domains (Kang *et al.*, 1987; Dyrks *et al.*, 1988; Ponte *et al.*, 1988; Beyreuther *et al.*, 1993; reviewed in Müller, Deller and Korte, 2017). APP is processed along two main pathways (Figure 4a) in the context of AD – the amyloidogenic, which leads to Aβ production, and the non-amyloidogenic, in which the Aβ sequence is interrupted and a shorter peptide, p3, is produced (comprehensively reviewed in De Strooper, Vassar and Golde, 2010). Both pathways occur physiologically. The non-amyloidogenic pathway is more prevalent and a-disintegrin-and-metalloproteinase domain-containing protein 10 (ADAM10 or α-secretase) cleavage at position 16/17 within the Aβ sequence (or 687/688 according to APP770 nomenclature) is the rate-limiting step (Kuhn et al. 2010). At this point, the N-terminal APP segment termed soluble APP α (sAPPα) is shed and the resultant C-terminal fragment C83 (or CTF-α) remains embedded in the membrane.

1.2.2. Amyloidogenic Processing

An alternative cleavage of APP at position 671/672 by β-site cleaving enzyme 1 (BACE1 or β-secretase) (Vassar et al. 1999) initiates the amyloidogenic pathway and liberates sAPPβ from C99 (or CTF-β). BACE1 is a secretase which localizes to the Golgi network and late endosomes, which provide the acidic environment necessary for its function (Vassar et al. 2014). It is therefore highly expressed in the CNS, while BACE2 is the predominant peripheral β-secretase (Bennett et al. 2000, Marcinkiewicz & Seidah 2002). An APP mutation that elevates the total production of Aβ would favor the interaction of APP and BACE1. In both the amyloidogenic and non-amyloidogenic pathways, C83 and C99 are additionally cut by the γ-secretase complex in an endopeptidase step termed ε-cleavage at a locus C-terminal to the Aβ sequence (Aβ48/49 or Aβ49/50) (De Strooper et al. 2010). The APP intracellular domain (AICD), which has multiple roles including nuclear signaling and gene regulation (Cao & Südhof 2001), modulating neuronal growth and maturation (Zhou et al.

2012), and regulating apoptosis (Ha et al. 2011, Kögel et al. 2012), is released into the cytoplasm at this point. Finally, amyloidogenic processing is completed when γ-secretase sequentially removes 3 residues at a time from the Aβ precursors in a series of carboxypeptidase events, which determine the length of the shed Aβ peptide, usually between 38-43 residues long.

Of the canonical Aβ species, Aβ1-40 appears to be the most common and in some cases has been suggested to be protective against AD (Kim et al. 2007, Zou et al. 2003), but the two/three additional residues on Aβ1-42/Aβ1-43 increase hydrophobicity and therefore the propensity to aggregate into oligomers (AβO). Depending on whether the product of ε-cleavage has 48 or 49 residues, two Aβ production lines are initiated, so that Aβ1-38 is produced from Aβ1-42 and Aβ1-40 from Aβ1-43 (see Figure 4c). One of the first indications of pre-clinical AD is largely acknowledged to be the reduction of Aβ1-42 in CSF as the peptide begins to accumulate in the brain and the Aβ40/42-43 ratio drops (e.g. Motter *et al.*, 1995; Galasko *et al.*, 1998; Blennow and Vanmechelen, 2003; Bateman *et al.*, 2012). In addition, subtle changes in this ratio alter the aggregation rate of Aβ mixtures and the oligomers thus produced have variable potency in inducing toxicity in neurons (Kuperstein et al. 2010). It was previously thought that the insoluble β-sheet-rich Aβ plaques cause neurodegeneration, but more recent evidence suggests that plaques are relatively inert and it is the small prefibrillar soluble AβO which are neurotoxic and capable of inducing tau hyperphosphorylation (Ferreira et al. 2015, Jin et al. 2011, Yang et al. 2017).

1.2.3. APP Mutations

Numerous APP mutations flanking or within the Aβ sequence increase overall Aβ production, decrease the Aβ40/42-43 ratio towards species with elevated or altered aggregation properties (Gessel et al. 2012, Portelius et al. 2010), impair cellular mechanisms like cholesterol transport (Nomura et al. 2013), and exacerbate inflammatory and tau pathology and memory impairment (Saito et al. 2011, 2014; Umeda et al. 2017). These mutations are typically named after the origin of the carrier families, e.g. the KM670/671NL Swedish mutation, which is the only described pathogenic mutation adjacent to the BACE1 cleavage site and preferentially increases total amyloidogenic processing (Johnston et al. 1994, Mullan et al. 1992); the I716F Iberian (Guardia-Laguarta et al. 2010, Guerreiro et al. 2010) and V717F Indiana mutations (Murrell et al. 1991, Tamaoka et al. 1994), which reduce the stability of the APP-γ-secretase interaction and lead to the production of longer Aβ species; or the E632Δ Osaka deletion (Tomiyama et al. 2008), which does not alter the amounts, but the propensity of the Aβ peptide itself to oligomerize without fibrillization,

resulting in species that are more resistant to clearance mechanisms (Nomura et al. 2013). Conversely, a protective A673T mutation just after the BACE1 cleavage site in the APP sequence has been identified, which results in a lower baseline production of Aβ and preserved cognitive ability at older age (Das et al. 2015, Jonsson et al. 2012). Moreover, as APP is found on chromosome 21, it is observed that individuals with classic trisomy 21 (Down syndrome) develop plaques and AD symptoms if they survive to middle age (McCarron et al. 2014), while in cases where only a part of the chromosome is copied or translocated, only those with an extra copy of APP develop AD (Rovelet-Lecrux et al. 2006). These are compelling observations that demonstrate a clear relationship between APP copy number and amino acid sequence and disease, albeit being more relevant to familial cases.

Figure 4. Canonical and non-canonical APP processing (from Müller et al. 2017).

a) Schematic representation of non-amyloidogenic and amyloidogenic processing of full-length APP by α- and β-secretases and of the differences in length between the fragments produced. **b)** Two examples of non-canonical processing by δ- and η-secretases (left) and the subsequent possibility of further processing by the three canonical secretases. **c)** A close-up illustration of the amino acid sequence and positions in APP695 where secretase cleavage sites are found and corresponding length of Aβ peptides secreted. The Aβ sequence is colored in orange. ➢

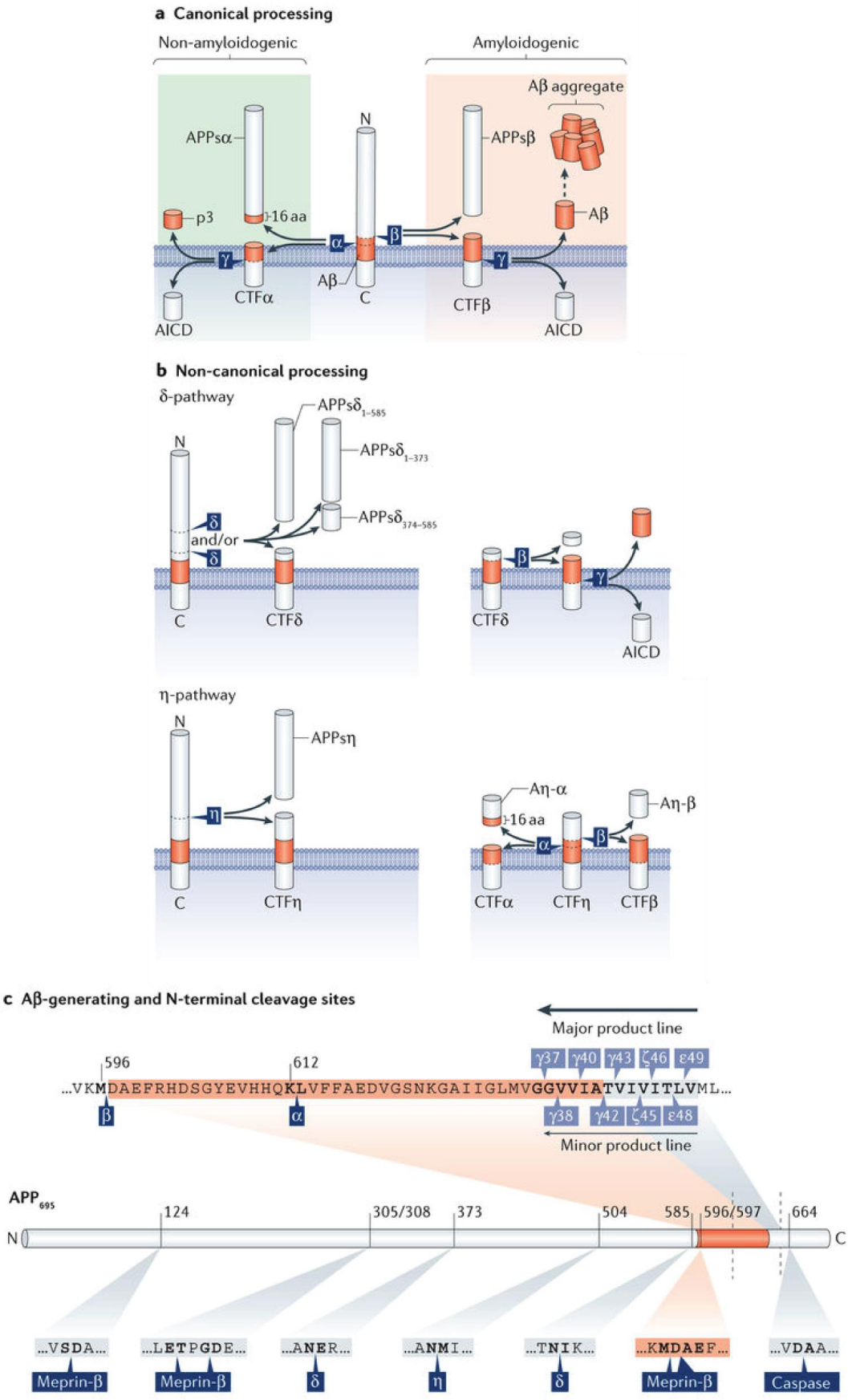
a Canonical processing
Non-amyloidogenic
Amyloidogenic
Aβ aggregate
APPsα
APPsβ
N
p3
16 aa
Aβ
α
β
γ
Aβ
C
CTFα
CTFβ
AICD
AICD
b Non-canonical processing
δ-pathway
APPsδ1–585
APPsδ1–373
APPsδ374–585
N
δ
and/or
δ
C
CTFδ
β
γ
CTFδ
AICD
η-pathway
N
APPsη
η
C
CTFη
Aη-α
16 aa
Aη-β
α
β
CTFα
CTFη
CTFβ
c Aβ-generating and N-terminal cleavage sites
Major product line
596
612
γ37 γ40 γ43 ζ46 ε49
...VKMDAEFRHDSGYEVHHQKLVFFAEDVGSNKGAIIGLMVGGVVIATVIVITLVML...
β
α
γ38 γ42 ζ45 ε48
Minor product line
APP695
124
305/308
373
504
585
596/597
664
N
C
...VSDA...
...LETPGDE...
...ANER...
...ANMI...
...TNIK...
...KMDAEF...
...VDAA...
Meprin-β
Meprin-β
δ
η
δ
Meprin-β
Caspase

1.2.4. The γ-Secretase Complex

1.2.4.1. Components

The transmembrane γ-secretase complex is made up of four proteins: nicastrin (NCSTN), which is the gateway to the hydrophilic pocket of the active site and is thought to have a role in substrate recognition (Bai et al. 2015, Shah et al. 2005); the α or β homologues of anterior pharynx defective 1 (APH1), which acts as an essential scaffold for complex integrity (Bai et al. 2015); presenilin enhancer 2 (PEN2), which helps stabilize the complex during transport, assembly, and maturation (Holmes et al. 2014b); and one of the two presenilin homologues (De Strooper 2003, Kimberly et al. 2003). γ-Secretase matures when PS undergoes self-cleavage between TM helices 6 and 7 to reveal residues Asp257 and Asp385, which are highly conserved and formulate the active site (Thinakaran et al. 1996, Wolfe et al. 1999). The substrate recognition motif is located in helix 9 and since the amino acid environment in that region is relatively disordered, it is thought that substrate binding induces the alignment of the catalytic residues (Bai et al. 2015). The structure of γ-secretase is illustrated in Figure 5. The first two components to assemble are APH1 and an immature form of NCSTN and they do so in the endoplasmic reticulum; subsequently, PS holoprotein binds to this intermediate, which promotes NCSTN maturation through glycosylation, and only after is PEN2 added to complete and trigger activation of the complex (LaVoie et al. 2003). Immature and mature NCSTN differ in the extent and type of their glycosylation and correspondingly in their molecular weight (LaVoie et al. 2003). Even though both PS1 and 2 are abundantly expressed, it appears that PS1 is responsible for most of the Aβ produced in the CNS (Acx et al. 2014, De Strooper et al. 1998) and its complete knockdown in mice yields an embryonic lethal phenotype due to side effects unrelated to APP processing (e.g. Shen et al. 1997). This and the fact that most FAD presenilin mutations occur in PS1 explains why this isoform receives more attention compared to PS2 in the context of AD. Similarly, in mice, complete APH1α deficiency is also embryonic lethal and its complete knockout results in a marked decrease of PS1, NCSTN, and PEN2 level, together with a ~70% loss in overall complex activity, while the same is not true for complete APH1β knockouts (Serneels et al. 2005). The above observations point to the idea that the "essential" γ-secretase complex is made up of PS1, APH1α, PEN2, and NCSTN and this component combination is most frequently quoted in research publications.

Nevertheless, the component heterogeneity of the complex means that at least four different types of γ-secretases can exist and when factoring in the fact that APH1α and both

presenilins also have several splice variants, the number rises further (De Strooper et al. 2012). Depending on this heterogeneity and whether APP or PS harbor an AD-relevant mutation, the endo- and carboxypeptidase activities of γ-secretase and thus the length and propensity of Aβ species to aggregate can be modulated (Sharples *et al.*, 2008; Acx *et al.*, 2014; Elad *et al.*, 2015; Szaruga *et al.*, 2015). An important study performed an elegant functionality comparison of the four possible γ-secretase combinations and revealed that PS2-containing complexes exhibit lower ε-cleavage as measured by total AICD production and showed suboptimal conversion of Aβ1-42 into Aβ1-38 along the minor Aβ production line (Acx et al. 2014). Neither PS1 nor PS2, however, exhibited a preference for the initiation of either line. In addition, APH1β complexes were less efficient at the last carboxypeptidase step because they secreted more Aβ1-42 and Aβ1-43, while the canonical PS1-APH1α complex was the most efficient (Acx et al. 2014). The authors concluded that at least in terms of Aβ production, APH1 is a likely regulatory factor of the final γ-cleavage step, while PS affects all activities of the complex. γ-Secretase inhibitors and modulators represent one treatment approach investigated so far and it has been shown that it is possible to selectively target PS1, so that side effects are mitigated by PS2 (Borgegård et al. 2012). In addition, as the lethal effects of APH1α knockout reported above are not necessarily related to γ-secretase processivity of APP, it is possible that in the context of AD, APH1β could be more relevant (Serneels et al. 2005). The combined information from such studies on the biological effects of complex heterogeneity could be valuable in further exploring the concept of selective γ-secretase targeting for the development of therapeutics.

Figure 5. Simulated atomic structure of human γ-secretase (from Bai et al. 2015).

a) The dimensions and organization of γ-secretase components are shown in cartoon (left) and surface (right) representation as seen parallel to the membrane. The heavily glycosylated "lid" of nicastrin (NCT) extends outside the membrane and covers the hydrophilic pocket of the active site. **b)** The complex is viewed from the bottom perpendicular to the membrane to clearly visualize the position of all PS1 TM helices and the two Asp residues of the active site (red). ➢

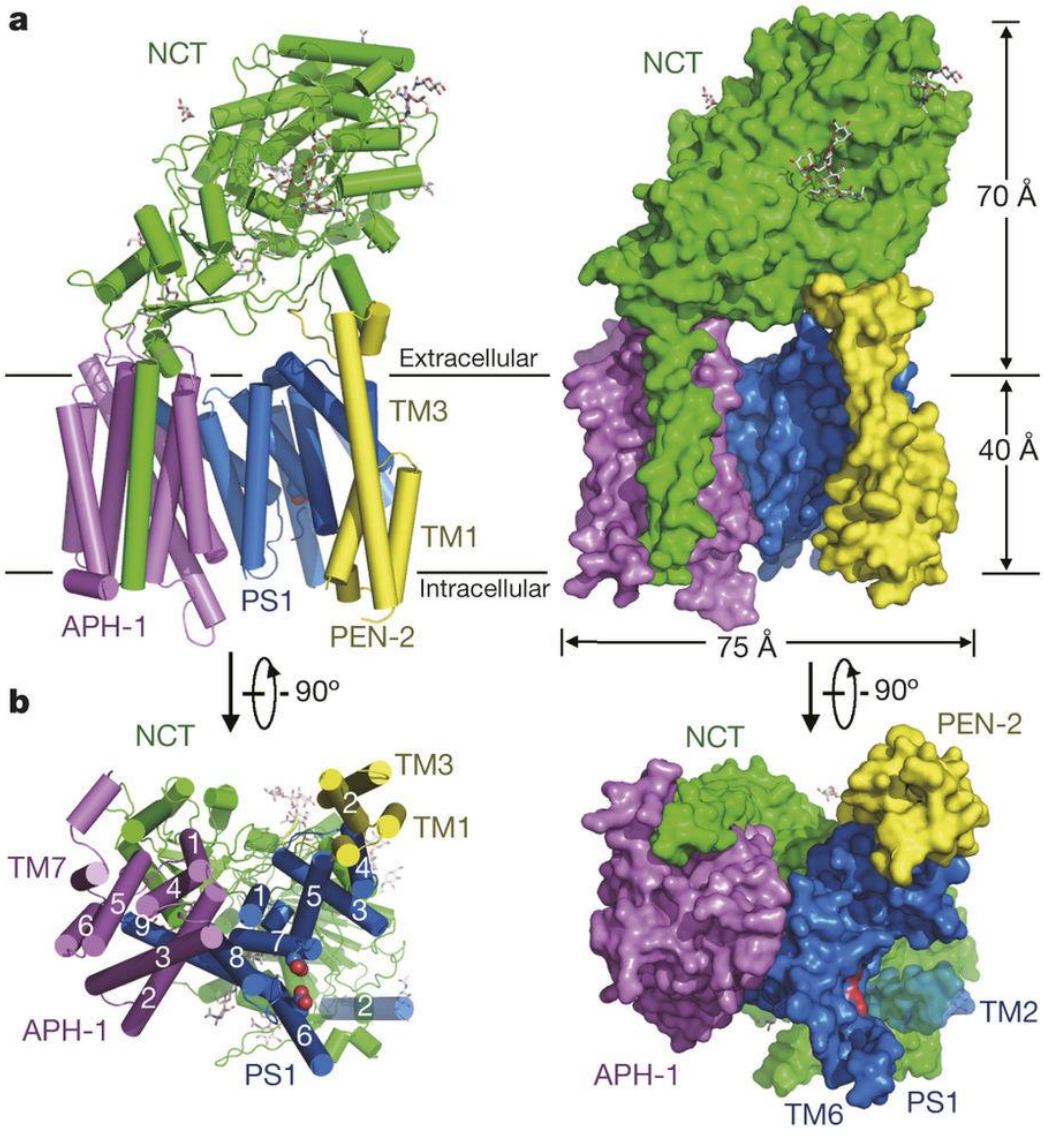

1.2.4.2. Presenilin Mutations

According to a detailed structural analysis of γ-secretase, approximately half of all PS1 mutations map to just 35 amino acid residues found within the adjacent cores of TM helices 2-5 and 6-9, where the two catalytic residues are located (Bai et al. 2015). As introduced above, mutations can have a markedly different effect on the mechanism of γ-secretase activity but have the same net outcome of producing longer Aβ. For example, the structural study looked at the specific effects *in vitro* of ten reported mutations and discovered that while all led to decreased Aβ1-40/Aβ1-42 ratios and correspondingly to lower carboxypeptidase activity, four (I202F, V248R, F237I, and V261F) severely impaired endopeptidase activity, three (I143V, F177L, and M233L) had no impact, and three (I213L, L226F, and L424V) actually increased it (Bai et al. 2015). Other groups have demonstrated

similar effects in cells for some of these, like I143V, F177L, and L226F, the latter two of which are particularly aggressive and cause very early disease (Bialopiotrowicz et al. 2012, Li et al. 2016). In support of the proposed mechanism that mutations destabilize APP-γ-secretase interaction, Li et al. (2016) found that I143V increases Aβ1-42 levels by reducing its truncation to Aβ1-38, while other mutations also reduced Aβ1-40 generation from Aβ1-43. An important aspect of the study by Bialopiotrowicz and colleagues (2012) is that it provides a potential clue towards the averse cellular effects that mutations might have. The authors discovered that another aggressive PS1 mutant, P117R, not only leads to a similar Aβ production profile as L226F, but it additionally disrupts the cell cycle in patient-derived lymphocytes, an effect independent of overall γ-secretase activity. A more extreme example of γ-secretase impairment already mentioned is through mutations R278I, C410Y, and L435F, which inhibit PS1 autoproteolysis and produce mostly inactive complexes, but the minimal γ-secretase function they allow also elevates Aβ1-42 and Aβ1-43 (Veugelen et al. 2016).

Although mutations also occur in PS2, they are much rarer and few are causative; in addition, their clinical manifestation and age of onset can be variable and not entirely consistent with the effects of APP and PS1 mutations (Bekris et al. 2010, Canevelli et al. 2014). For this reason, they are less studied. A relatively recent literature review investigation found that most cases of FAD caused by PS2 mutations are attributable to the N141I Volga-German and M239V mutants and all have European ancestry (Canevelli et al. 2014); this study reports that 13 of all PS2 mutations have confirmed AD pathogenicity, while Alzforum's Mutations database reports 16. It appears that the two mutations do not impart a loss-of-function mechanism, as they do not affect the maturation of presenilin, but lower the Aβ1-40/Aβ1-42 ratio through increased Aβ1-42 levels (Walker et al. 2005). It is unclear, however, which mechanism of dysfunction in the interaction of APP and γ-secretase is responsible. Taken together, the findings about FAD-causing mutations indicate that even if these do not occur in APP directly, they have several common mechanisms of exacerbating amyloidogenic processing, which then leads to Aβ aggregation, cell toxicity, and neurodegeneration through yet unidentified mechanisms and interactions (discussed later) (Veugelen et al. 2016).

1.2.4.3. Non-APP Substrates and Their Importance for AD Treatment

In addition to C83 and C99, γ-secretase cleaves a vast array of proteins with the same structural features (a Type I single-span α-helix TM domain and an ectodomain of less than 50 amino acids) (Lichtenthaler et al. 1999, Struhl & Adachi 2000, Wakabayashi & De

Strooper 2008). So far, there are more than 90 described substrates with functions in development, cell proliferation and differentiation, signaling, and apoptosis, which makes γ-secretase an indispensable all-round peptidase (summarized in Haapasalo & Kovacs 2011, Wakabayashi & De Strooper 2008). Of these, arguably the Notch cell receptor receives the most attention, apart from APP; embryogenesis, neural, vascular, and hematopoietic differentiation are only a handful of its functions and consequently errors in its processing and signaling are responsible for several types of cancers and hereditary development disorders (reviewed in Andersson & Lendahl 2014). The concept of γ-secretase inhibitors and modulators for treatment of AD was introduced earlier and considering the crucial roles of Notch and other substrates, it is easy to understand why such compounds need to be explored with caution (De Strooper 2014). An example is the inhibitor semagacestat, which failed at Phase 3 clinical trials because of severe Notch-related gastrointestinal side effects, on top of greater cognitive deterioration compared to placebo controls, increase in skin cancer and infection incidence, as well as cardiac and hepatic abnormalities (Doody et al. 2013, Henley et al. 2014). What is more, it appears that semagacestat, similarly to other available inhibitors, is actually much more effective in inhibiting Notch, not APP (Chávez-Gutiérrez et al. 2012). Factors that affect the binding affinities of the complex towards its substrates are just now being uncovered and these will provide the much needed mechanistic insights for the better design of treatment compounds and clinical trials (De Strooper 2014, Voytyuk et al. 2018). For instance, the improved understanding of the effect of APP and PS mutations has diversified the simplistic complete inhibition concept into targeting distinct γ-secretase subtypes, stabilizing particular interactions with the Aβ precursors to avoid premature dissociation, or blocking APP binding before it fully enters the complex (Voytyuk et al. 2018).

1.2.5. Non-canonical Secretases

Recent evidence has exposed additional secretases which contribute to the heterogeneity of the peptides produced from APP (Figure 4b) and which may contain a part or the entire Aβ sequence (Baranger et al. 2015, Willem et al. 2015, Youssef et al. 2008, Zhang et al. 2015). For example, membrane-bound matrix metalloproteinase MT5-MMP or η-secretase cleaves APP upstream of the BACE1 site, releasing sAPPη and CTF-η, and Aη-α and Aη-β after α- or β-secretase cleavage (Willem et al. 2015). The peptides generated through this activity depress neuronal function in mouse models, while knockdown of this secretase reduces amyloidosis and cerebral inflammation (Baranger et al. 2015, Willem et al. 2015). Evidence also suggests that upon BACE1 inhibition, the levels of η peptides and

their corresponding adverse effects increase (Willem et al. 2015), which adds another dimension to the question of reducing Aβ production through therapeutic inhibition of its rate-limiting proteases (thouroughly discussed in Voytyuk et al. 2018). Similarly, asparagine endopeptidase AEP or δ-secretase cleaves APP upstream of the α and β sites and appears to synergistically work with BACE1 towards Aβ production, possibly within late endosomes as both secretases require an acidic environment to function (Vassar et al. 1999, Zhang et al. 2015). Such newly-discovered Aβ peptides are the object of current research and their involvement in disease will become clearer in due course.

1.3. The Amyloid Hypothesis and Evidence for AβO Toxicity

The above observations, which establish a strong causative link between mutations affecting APP processing and Aβ species type, together with more isolated cases of altered APP copy number, are at the core of the amyloid hypothesis of AD. The amyloid hypothesis was formulated approximately 25 years ago (Beyreuther & Masters 1991, Hardy & Allsop 1991, Hardy & Higgins 1992) and while its original version has been revised to be more flexible and inclusive, its basic principle has remained the same; it states that Aβ accrual is causative or at least contributive to disease onset and pathogenesis, as opposed to being a downstream effect of other disease-relevant molecular mechanisms (reviewed in Selkoe and Hardy, 2016). This hypothesis has received valid criticism over the years for several reasons: the correlation between cognitive impairment and neurodegeneration is much weaker for plaques than for tangles; plaques have been observed in individuals without dementia symptoms; transgenic (Tg) APP mouse models accumulate amyloid deposits with age, but these do not cause neurodegeneration although they are associated with poorer performance in behavioral tests; and clinical trials have been largely unsuccessful (Herrup 2015, Morris et al. 2014). Nevertheless, while this theory is imperfect, it is arguably the best current model that fits the collective data available to date (Veugelen et al. 2016) and what follows is a brief discussion of the contribution of Aβ and tau to AD toxicity in favor of the amyloid hypothesis.

1.3.1. Roles of Intracellular and Extracellular AβO in SAD

In SAD where the disease is not associated with APP and PS mutations, Aβ and its oligomers still play central roles in mediating adverse cellular events and these can be modulated by the risk factors discussed earlier. Given that both BACE1 and γ-secretase are aspartyl proteases, they function optimally at an acidic pH, where BACE1 requires a lower pH of approximately 4.5 (Cole & Vassar 2007), while γ-secretase prefers a mildly acidic

environment of pH 6.3 (Xia et al. 2000). These requirements determine the cellular sites of Aβ production – the rate-limiting step of BACE1 cleavage, for which the substrate has to be membrane-bound (Cole & Vassar 2007), must therefore occur in acidic vesicles in later stages of the secretory pathway (Koo & Squazzo 1994); on the other hand, γ-secretase also cleaves substrates embedded in the cell membrane, in addition to late endosomes. Consequently, Aβ is produced both intracellularly and extracellularly and the majority of Aβ appears to be expelled from the cell, either by being shed off the membrane or secreted through vesicles (LaFerla et al. 2007). Subsequent reuptake of shed Aβ also occurs, but whether this process is dependent on the endocytic pathway or not seems to be influenced by the length of the Aβ species (Omtri et al. 2012). The location of Aβ production and the dynamic exchange between the two Aβ pools could therefore determine where Aβ would exert its toxic effects and where it will begin to oligomerize.

The cellular origin of Aβ oligomerization, plaque formation, and the interplay between the various toxic effects of Aβ are not well understood. Recent immunocytochemistry experiments in the 3xTg AD mouse model (Oddo et al. 2003) yielded support to the theory that oligomerization begins intracellularly, invades the nucleus, and leads to cell lysis over time and to the release of fibrillar Aβ into the extracellular space (Pensalfini et al. 2014). In SAD patients, the presence of ApoE ε4 alleles strongly correlated with the amount of intraneuronal Aβ as detected by immunohistochemical staining of post-mortem hippocampal tissue with oligomer and Aβ-specific antibodies (Christensen et al. 2010). Sucrose gradient fractionation experiments have demonstrated that low-n Aβ oligomers associated in particular with mitochondria and mitochondrial-associated ER membranes (MAMs) are able to induce the oligomerization of monomeric Aβ *in vitro* and also accelerate the accrual of amyloid deposits in the brains of Tg mice (discussed in detail below) (Marzesco et al. 2016). Primary neurons from APP-overexpressing mice which accumulate intracellular Aβ1-42 demonstrated altered vesicular trafficking, which was due to impaired deubiquitination and proteasome activity (Almeida et al. 2006). The injection of intracellular AβO into primary neurons reduces the magnitude and frequency of postsynaptic action potentials by impairing glutamate release and also reduces long-term potentiation (LTP), which is frequently used as a measurement of cognitive performance, in mouse hippocampal slices (Ripoli et al. 2014). That being said, the injection of oligomers directly into the cytoplasm does not necessarily represent the effects of endogenously-derived or re-internalized secreted oligomers, nor does it distinguish between the two, which makes it difficult to attribute particular events to intracellular or extracellular AβO, since the two pools are constantly cycling. Moreover, the detection of intracellular Aβ has often been

questionable because of the cross-reactivity of commonly used antibodies with cellular APP and APP processing fragments (Wirths & Bayer 2012). One therefore needs to be careful when attributing effects to one of the two Aβ pools.

Prefibrillar AβO applied extracellularly are toxic to neurites through a multitude of interactions. AβO-dependent LTP reduction and synaptic plasticity impairment have been demonstrated *in vivo* (Walsh et al. 2002) and in mouse hippocampal slices, where the effects were due to the disruption of glutamatergic/GABAergic homeostasis (Lei et al. 2016, Shankar et al. 2008). Aβ3(pE)-42, or "pyroglutamate Aβ", is a particularly toxic species found in the brains of AD patients and intracerebral injections of this peptide in mice reduced spatial memory and learning, concomitant with an increase in hippocampal oxidative stress, caspase-mediated apoptosis, and inflammation (Youssef et al. 2008). Pyroglutamate Aβ was also able to bind more strongly to membranes than Aβ1-42 and abnormally elevated Ca^{2+} in mouse cortical neurons with the involvement of the N-methyl-D-aspartate (NMDA) receptor (Gunn et al. 2016). A similar disruption of Ca^{2+} homeostasis, which resulted in dendritic spine loss, was also observed when Tg mouse brains were treated with conditioned medium containing Aβ1-40 and Aβ1-42 from selfsame cortical neuron preparations (Arbel-Ornath et al. 2017). AβO elevated the circulation of pro-inflammatory factors in mouse CSF and disrupted the tight junctions of the brain-CSF barrier through elevating the expression of matrix metalloproteinases (Brkic et al. 2015). Likewise, uptake of extracellularly applied non-fibrillar AβO by microglia induced their activation and the release of interleukin-1β, which was facilitated by cathepsin B and the presence of reactive oxygen species (Taneo et al. 2015). Reports also exist of AβO's ability to insert themselves in lipid bilayers and disturb cellular homeostasis (Evangelisti et al. 2016, Tofoleanu & Buchete 2012, Wood et al. 2003), including via binding through the prion protein (PrP; Laurén et al. 2009) and thus altering cholesterol metabolism (West et al. 2017). Moreover, insufficient Aβ clearance (Domert et al. 2014, Lee et al. 2011), exacerbated by the presence of ApoE ε4 and enhanced by the protective ApoE ε2 alleles, likely also contributes to the pathogenic effects of Aβ. It is beyond the scope of this introduction to fully discuss the cellular effects of AβO and its binding promiscuity, but see Smith and Strittmatter, 2017 for a detailed review.

1.3.2. Aβ-mediated Tau Toxicity

Tau spans sixteen exons and alternative splicing of Exons 2, 3, and 10 gives rise to six adult brain isoforms that differ in the presence of repeat copies of an amino terminal insert (0N, 1N, or 2N) and three or four highly-conserved microtubule-binding repeats (3R or 4R)

(Wang & Mandelkow 2015). It is predominantly found in axons, where it binds to microtubules to stabilize them and this is a process regulated by phosphorylation of its many serine, threonine, and tyrosine residues (Polanco et al. 2018, Wang & Mandelkow 2015). If tau becomes excessively phosphorylated, it dissociates from microtubules and can aggregate and localize to the soma and dendrites where it is normally found in low concentrations, which leads to cell toxicity through impaired transport of organelles and other proteins (Ittner et al. 2008, Li et al. 2007, Polanco et al. 2018, Yoshiyama et al. 2007). With respect to AD, tau is excessively phosphorylated (Köpke et al. 1993) and mutations which facilitate this are abundant, but other tauopathies like Pick's disease, frontotemporal and lobar dementia, and corticobasal degeneration are caused by a shift in the balance between the numbers of 3R and 4R isoforms (Dickson et al. 2011, Wang & Mandelkow 2015). The aggregation of tau is mediated by two hexapeptide motifs in the second and third microtubule binding repeats respectively; these motifs are occluded in the protein's native relaxed structure, but become exposed when tau misfolds and thus promote aggregation (Mirbaha et al. 2018).

Similarly to AβO, tau oligomers impair hippocampal LTP and learning ability in mice (Lasagna-Reeves et al. 2012). This could be explained in part by structural changes of the axon which increase the action potential threshold and limit neuronal excitability, caused by tau hyperphosphorylation at distinct residues (Hatch et al. 2017). Tau aggregates also promote dendritic spine atrophy and this effect seems to be dependent on the degree of aggregation of the tau sample, rather than hyperphosphorylation (Merino-Serrais et al. 2013). The importance of cell structural integrity mediated by tau is further highlighted by the discovery that mutant tau causes neurodegeneration through heterochromatin relaxation, which is accompanied by oxidative stress and aberrant changes in gene expression (Frost et al. 2014). In a tau Tg mouse model, soluble pre-tangle tau had no effect on spatial memory which depends on the hippocampus, but led to presynaptic alterations that promoted neurotransmitter release and a reduction of postsynaptic LTP, which could be due to impaired Ca^{2+} homeostasis, altered dynamics of the presynaptic vesicle reserve pool, or errors in the modulation of GABA or mGlu receptors (Polydoro et al. 2014). Like prefibrillar soluble AβO, pre-tangle hyperphosphorylated tau also promotes microglial activation, neuroinflammation, and synaptic dysfunction in Tg mice, which accompanies hippocampal and neocortical neuronal loss and precedes astrogliosis (Yoshiyama et al. 2007). Specific detrimental effects on microglia as a result of phospho-tau include dystrophic processes and a reduction of the area covered by this cell type, in addition to a restriction of the surveillance area of individual microglia (Sanchez-Mejias et al. 2016). Tak-

ing this evidence together with that presented in Section 1.3.1., the similarities between the toxic effects of abnormally phosphorylated and misfolded tau and those of Aβ and its oligomers are easily identifiable. At the same time, what is likely to be most relevant for AD research and treatment development is investigating the adverse cellular events arising from the crossover of the two pathogenic proteins. In this relationship, Aβ seems to be the instigator and tau the perpetrator of pathology.

Aβ induces tau hyperphosphorylation and NFT formation through a variety of proposed mechanisms. Firstly, tau is a phosphorylation target of mitogen-activated protein kinases (MAPK), which are activated through the binding of Aβ1-42 to α7 nicotinic acetylcholine receptors (α7nAChR) (Wang et al. 2003); these receptors are expressed in pre- and postsynaptic terminals of pyramidal neurons, which are vulnerable in AD (see Figure 1). This phosphorylation is likely a physiological process, as it is completely reversible in cells, but becomes exacerbated particularly under stress conditions (Wang et al. 2003). In Tg mice overexpressing the Swedish mutation, α7nAChRs are upregulated as a result of Aβ exposure and this leads to chronic hyperactivation of the MAPK pathway, which critically affects learning and memory mediated by the hippocampus (Dineley et al. 2001). Moreover, upregulation of α7nAChRs and their co-immunoprecipitation with Aβ is also seen in post-mortem AD patient samples (Wang et al. 2000). Secondly, tau is a target of glycogen synthase kinase 3β (GSK3β) and its pharmacological inhibition reduces tau phosphorylation and rescues Aβ-mediated impairment of LTP in hippocampal organotypic slices from WT mice (Shipton et al. 2011). This can also be achieved by fully knocking out tau (Shipton et al. 2011). In addition, AβO-mediated hyperphosphorylation of tau conveys a degree of insulin resistance in mouse neuroblastoma cells and primary neurons through a reduction in protein kinase B phosphorylation and a corresponding decrease in inactivation of GSK3β (Tokutake et al. 2012). None of these pathways are mutually exclusive, nor are they the only ones affected by Aβ and tau; nevertheless, while more conclusive evidence is necessary to directly prove the steps in these interactions, they provide broad mechanistic links between Aβ overproduction, tau hyperphosphorylation, and neural dysfunction associated with AD.

Hyperactivation of the MAPK pathway as a result of Aβ could mediate the neurodegenerative effects of tau through the critical upstream action of the tyrosine protein kinase Fyn (Li & Götz 2017). Treating primary neurons with AβO enhances not only tau phosphorylation, but also *de novo* tau translation in the somatodendritic neuronal compartment, rather than in the axons where tau is normally localized (Li & Götz 2017). Positive feedback

exists between Fyn and tau, as each promotes the other's overexpression (Li & Götz 2017) and tau is required for the dendritic localization of Fyn (Ittner et al. 2010). Disruption of this physiological process through tau knockout results in reduced signaling via postsynaptic NMDA receptors that are normally stabilized by Fyn, which is consistent with elevated excitotoxic damage as a result of increased Aβ exposure and a corresponding increase in phospho-tau in AD (Ittner et al. 2010). The removal of tau in the context of toxic priming with Aβ and a Fyn cascade also attenuates memory deficits and prolongs lifespan in APP Swedish Tg mice, showing a link between cellular neurodegenerative events and behavior (Ittner et al. 2010). Fyn is a kinase central to many physiological signaling pathways, from inflammation and immunity, cell growth and differentiation, to regulating neuronal activity (Ohnishi et al. 2011). Given its high expression in the hippocampus, a brain region particularly vulnerable to AD and indispensable for learning and memory (see Figure 2), and its role in regulating synaptic plasticity and protein trafficking (Ohnishi et al. 2011), it is unsurprising to find this kinase directly implicated in AD disease mechanisms, which makes it a potential therapeutic target (Li & Götz 2017, Polanco et al. 2018).

More generalized molecular evidence in support of the driving role of Aβ at the level of the synapse demonstrates that synaptic Aβ accumulation occurs in AD, but not in age-related non-neurodegenerative amyloidosis (Bilousova et al. 2016). In this study of AD brain-derived synaptosomes, significant synaptic elevation of phospho-tau did not occur until later disease (Braak stages V and above), but its levels were still higher in Aβ-containing synapses early on (Braak stages IV and below) compared to controls (Bilousova et al. 2016). In live patients, CSF levels of phospho-tau also rise with disease progression (Hampel et al. 2009), but this occurs much later than the initial drop in Aβ1-42, which could be consistent with a scenario where Aβ accumulates, triggers tau pathology, and then becomes sequestered in inert plaques (Bateman et al. 2012). Confusingly, experts have also suggested that the accumulation of pre-tangle material in neurons precedes cerebral amyloid deposition by decades (see Figure 1; Braak *et al.*, 2013). Clearly, a complex "chicken and egg" interplay between the two culprit proteins is occurring that involves diverse disease mechanisms, and it is likely that many of them occur simultaneously. Going back to the criticism of failed clinical trials, they have so far taken a single-faceted approach targeting only one pathological aspect of the disease; another important argument is that patients were recruited too late when clinical symptoms were already prominent and damage was irreversible (De Strooper 2014, Selkoe 2011, Selkoe & Hardy 2016). It may be that tau, not Aβ itself, is the limiting factor for the vast neurodegeneration seen in patients , but evidence overwhelmingly points towards errors in Aβ

metabolism being an earlier trigger for AD through yet putative interactions. It is therefore necessary to investigate how Aβ and tau work together to cause AD, rather than argue which is more important, and to design further clinical trials with a broader outlook.

1.4. Prion-like Properties of AβO and Models of Seed Propagation

1.4.1. Overview of Prion Diseases

Over the years it has emerged that AD and other clinically and pathologically distinct dementias such as Parkinson's (PD) and Huntington's disease (HD) are in fact mechanistically similar, as all are characterized by the accumulation of aggregates of misfolded protein, which are able to self-propagate and multiply (α-synuclein for PD and huntingtin for HD) (Costanzo & Zurzolo 2013, Walker & Jucker 2015, Walker et al. 2016). As such, they have been dubbed prion-like to reflect their resemblance to "true" prion dementias, which are directly caused by pathogenic aggregates of misfolded cellular prion protein (PrP^{C}), some of which acquire protease resistance and are classically designated PrP-scrapie (PrP^{Sc}). The concept of the proteinaceous infectious particle, from where the term prion was coined, was first proposed in the 1980s by Stanley Prusiner and colleagues (Prusiner 1982), who were researching rodent-adapted strains of natural scrapie, a transmissible spongiform encephalopathy (TSE) in sheep. Scrapie was unusual because it had a long incubation period and could not be linked to a bacterium or virus despite being highly infectious, until the pathogen was proven to be the host's own protein (Prusiner 1982, 1998). TSEs occur in humans and several other non-human species, notably cattle which suffer from bovine spongiform encephalopathy (BSE, colloquially known as "mad cow" disease), and deer and elk, which suffer from chronic wasting disease. Humans are affected by TSEs which include Creutzfeldt-Jakob disease (CJD), kuru, and fatal familial insomnia. Most cases of CJD arise sporadically through a spontaneous misfolding event of PrP^{C}, which is ubiquitously expressed in the CNS and peripheral tissue (Collinge 2016, Oesch et al. 1985). The mechanisms that lead to PrP^{C} misfolding are unknown. A smaller fraction of CJD is inherited via autosomal dominant mutations in the *PRNP* gene, which encodes human PrP. Pathologically, TSEs are defined by accumulation of disease-associated PrP that leads to the vacuolation of neurons, which gives the brain a sponge-like appearance upon histopathological examination, and to inflammatory astrogliosis (Budka et al. 1995). These aberrant microscopic abnormalities lead to neurodegeneration and thereby to memory loss, motor dysfunction, and a range of psychotic behaviors. TSEs are always fatal and there is currently no treatment.

1.4.2. Infectivity of TSEs

While CJD predominantly arises through the rare spontaneous misfolding of PrP or as a consequence of mutations in its sequence, prions are also infectious pathogens. Recognized human prion transmission routes include peripheral and central inoculation as a result of medicinal accidents, oral transmission through consumption of prion-contaminated tissue, and blood transfusion (Collinge 2016). Prion diseases can transmit between species to some extent, as demonstrated by the 1980-1990 BSE epidemic in the UK (Will et al. 1996), which caused individuals who had consumed the meat of diseased animals to develop vCJD years later. In addition, experimental evidence has shown that human prions can successfully infect non-human primates (Gajdusek 1977). An interesting occurrence of human-to-human transmission of prions is kuru, which occurred among indigenous tribes in Papua-New Guinea that historically partook in ritual endocannibalism, leading to recycling of human prions in the population (Wadsworth et al. 2008a). More recently, iatrogenic cases of CJD have been reported as a result of surgical procedures with contaminated equipment or by transfer of body fluids (Brown et al. 2012, Llewelyn et al. 2004), as prions are extraordinarily resistant to conventional hospital sterilization methods (Brown et al. 1990). People who were treated for short stature with cadaveric growth hormone injections between 1950 and 1985 have also succumbed to prion disease because some hormone samples were obtained from infected individuals (Ritchie et al. 2017, Rudge et al. 2015, Swerdlow et al. 2003). Notably, some of these recently deceased vCJD patients also demonstrated abundant Aβ pathology, which was morphologically identical to that seen in AD, unlike what is typically seen in CJD patients (Jaunmuktane et al. 2015). Even though there were only eight cases examined in this study, the authors postulated that based on this preliminary data, it may be possible that Aβ pathology and perhaps AD could be transmitted iatrogenically. Although CJD is relatively rare, it presents a unique disease pattern where the pathogen is a conformational variant of a host protein and therefore evades the immune system over its long incubation period (Walker & Jucker 2015).

1.4.3. Strains, Amyloids, and Seeding

Misfolded PrP^{Sc} is enriched in cross β-sheets (Pan et al. 1993) and assembles into long fibrils and other polymers. Fibrillar assemblies of PrP forming plaques in diseased brain show the distinct biophysical properties of an amyloid structure (Eisenberg & Jucker 2012). Many other proteins, such as Aβ, tau, α-synuclein, and huntingtin are also able to form amyloid conformations, which are usually associated with disease. Functionally, as seen for PrP, the most distinct feature of amyloids is their ability to self-propagate their patho-

genic fibrillar conformations by inducing the misfolding of native functional proteins in a process called seeded aggregation. This means that a small amyloid assembly can grow by acting as a seed through which monomers are misfolded and added onto the fibril (Eisenberg & Jucker 2012). The precise mechanism of how this template-based conversion begins in PrP is not known, neither is the precise structure of the PrP amyloid, but recent studies have shed more light onto the subject (Terry et al. 2016, Trevitt et al. 2014). This seeding process is what defines the acute transmissibility of prion diseases. As already introduced, the ability of proteinaceous aggregates to seed themselves is a broad disease mechanism shared by a number of common dementias, which places great importance on uncovering the factors that govern this template-mediated replication and the ways through which it contributes to cytotoxicity and neurodegeneration. It is conceivable that due to this similarity, the impact of key discoveries in individual diseases will be relevant to the field of dementia study as a whole and could greatly accelerate the development and applicability of new treatments.

While a rigid β-sheet spine is the telltale characteristic shared by all amyloid fibrils, conformational variations within the monomer affect the way in which the fibril is assembled and thus alter its properties (Eisenberg & Jucker 2012). Structurally distinct assemblies, or strains, of PrP^{Sc} exist and they are thought to be responsible for the selective transmissibility of prion disease between and within species, as some strains may better proliferate in different host environments (Collinge 2016, Li et al. 2010, Telling et al. 1996). Several strains can exist simultaneously in a single CJD patient, where one strain may be dominant and others may exist in minute quantities (Oelschlegel & Weissmann 2013). Interestingly, a similar scenario of active oligomeric intermediate and inert fibrillar amyloid conformations has also been emerging for Aβ and tau in AD (discussed below). Therapeutic targeting of a particular prion strain would pose a challenge in a situation where multiple strains exist in the same host, as this would simply shift the balance between them and not halt misfolding altogether (Collinge 2016). It would also be very difficult to target already misfolded PrP, due to the conformational differences between strains, to which a drug would bind with variable affinity and accessibility. Therefore, the target substrate would have to be normal PrP^{C} and passive immunization studies targeting normal PrP^{C} are being carried out in mouse models (Collinge 2016).

1.4.4. Evidence for In Vivo Aβ and Tau Seeding

A collection of landmark experiments with Tg mouse models has unequivocally demonstrated that inoculation with patient-derived Aβ seeds is able to induce potent amyloido-

sis in the mouse brain. Most of these experiments were conducted using three models, which either overexpress Swedish mutant human APP only (APP23 and R1.40 mice; Lamb *et al.*, 1997; Sturchler-Pierrat *et al.*, 1997) or together with L166P mutant human PS1 (APPPS1 mice; Radde *et al.*, 2006). APP23 and APPPS1 mice naturally deposit Aβ and develop robust plaques as they age, but R1.40 mice do not develop Aβ deposits until approximately 13-15 months of age. It has been systematically shown that injecting young pre-depositing mice with human AD brain-derived homogenates or extracts accelerates amyloid deposition, which mimics human AD pathology, as it spreads through interconnected regions in the brain and is particularly strong in the hippocampus (Eisele et al. 2009, 2010; Fritschi et al. 2014a, George et al. 2014, Heilbronner et al. 2013, Kane et al. 2000, Langer et al. 2011, Meyer-Luehmann et al. 2006, Morales et al. 2011, Rönnbäck et al. 2012, Rosen et al. 2012, Ye et al. 2017). In particular, Ye and colleagues (2015b) showed that hippocampal injections of R1.40 and APP23 mice with aged Tg brain extracts induced amyloidosis which spread further into the limbic system and into regions directly connected to it, the longer the incubation time. The seeding effect has been observed with brain extracts from aged Tg mice, but not with those from wild-type (WT) or with Aβ-depleted brain extracts (Duran-Aniotz et al. 2014, Eisele et al. 2009, Ye et al. 2015a,b). In addition, in R1.40 mice, the deposition of Aβ depends on the incubation time, rather than the age of the mouse at the time of injection (Hamaguchi et al. 2012). The severity of amyloidosis corresponds to the Aβ aggregate, but not total Aβ, content of the injected material, which can seed aggregation even at subattomolar concentrations, and on the abundance of Aβ and APP in the brain (Eisele et al. 2014, Fritschi et al. 2014b). Interestingly, human AD CSF has so far failed to induce seeding *in vivo* but not *in vitro*, despite containing high Aβ peptide amounts (Fritschi et al. 2014b), which may indicate that brain-derived cofactors are necessary for Aβ seed propagation or that it does not contain the appropriate AβO conformations (Fritschi et al. 2014b, Walker & Jucker 2015). This idea is corroborated by the mixed success of experiments involving synthetic AβO preparations, also known as Aβ-derived diffusible ligands (ADDLs), to induce robust responses on their own even at high, non-physiologically relevant concentrations, similarly to experiments involving synthetic prion strains (Collinge 2016, Novotny et al. 2016, Stöhr et al. 2012, 2014). Moreover, seeding of APP23 and APPPS1 mice with extracts from young and old mice showed that the ability of the extracts to induce amyloidosis tapers off with age, despite an ever-increasing cerebral Aβ load, but rapidly peaks when using young extracts, which contain less Aβ overall in the form of low-n prefibrillar AβO (Ye et al. 2017). The au-

thors used their data to argue in support of targeting patients for treatment as early as possible before widespread pathology is manifest (Ye et al. 2017).

Other modes of Aβ seed introduction have been successfully employed in these Tg mice that show similarities between PrP and Aβ amyloids. Of particular interest is an experiment carried out by Eisele et al., (2009), which demonstrated that implanting steel wires dipped in aged APP23 brain extract into the brains of pre-depositing mice also induces spreading amyloidosis. This was not observed when the wires were dipped in WT extract or buffer, which shows that the seeding effect is proprietary to the aged brain and is not due to the introduction of a foreign body. This process mimics the iatrogenic transmission route of disease-associated PrP. In addition, while peripheral administration experiments were unsuccessful at first (Eisele et al. 2009), subsequent tests with prolonged incubation times showed that Aβ deposits can be induced in the brain and its vasculature in this way as well (Eisele et al. 2010). Another similarity with disease-associated PrP is that naturally-derived AβO with seeding potency have a degree of proteinase K resistance, unlike synthetic AβO, and treatment with this proteinase is routinely used in prion infectivity assays to remove non-infectious material (Langer et al. 2011). Proteinase K digestion distinguishes between infectious and benign PrP because PrP^{Sc} is fully resistant to this enzyme. The study in question further supported the importance of Aβ strain over concentration by showing that ultracentrifuged Tg mouse brain preparations, which contain a low concentration of low-n, soluble AβO free from organelles, are strongly bioactive but also sensitive to proteinase K (Langer et al. 2011). Evidence also points towards the existence of AβO strains with variable structure and bioactivity in patient brain, which may be linked to pathological differences in patients with various types of amyloidosis (Petkova et al. 2005, Yang et al. 2017). It has been suggested that this may be a determining factor towards differences in disease manifestation (Cohen et al. 2016, Lu et al. 2013, Yang et al. 2017). For example, depending on the rate of AD progression, different Aβ1-40 and Aβ1-42 structures with different abundances were identified, but a few of these were common for all cases (Qiang et al. 2017). Cross-seeding experiments between APP23 and APPPS1 mice showed that the induced Aβ deposits are the same in morphology and composition as those found in the brain-derived inoculum (Heilbronner et al. 2013). Similarly, mice seeded with SAD and FAD extracts demonstrated a difference in the induced amyloidosis pattern, which also varied in terms of the ratios of Aβ species involved and in mutation-specific effects seen in patients, such as cerebral amyloid angiopathic (CAA) deposition of Aβ1-38 (Watts et al. 2014). These results were maintained after a second round of trans-

mission in mice, which is consistent with the idea that AβO are conformationally stable and propagate pathology in a prion-like manner (Watts et al. 2014).

Mouse studies involving tau have analogically demonstrated that intracerebral injections with AD patient-derived phospho-tau induces robust hippocampal deposits after a prolonged incubation period and that the extent of the spread depends on hyperphosphorylation (Hu et al. 2016). Similarly to the different potency of synthetic and naturally-derived AβO, recombinant tau oligomers disrupted LTP in hippocampal organotypic slices to a significantly lower degree than oligomers derived from patient brain; the latter also impaired memory in WT in a novel/familiar object recognition task several days post injection, but these effects were not sustained long-term (Lasagna-Reeves et al. 2012). Despite the cognitive recovery, mice had accumulated profuse hyperphosphorylated filamentous tangles, unrestricted to the area of injection, which promotes the idea that low-n soluble tau oligomers are toxic, not fibrils (Lasagna-Reeves et al. 2012). Unsurprisingly, intracerebral inoculation of human tau Tg mice with synthetic tau fibrils (Stancu et al. 2015) and brain extracts from mutant tau mice also induced seeding of tau aggregates through interconnected brain regions (Clavaguera et al. 2009). This was recapitulated when the same mice were seeded with extracts from the brains of not only AD, but also argyrophilic brain disease, progressive supranuclear palsy, and corticobasal degeneration patients (Clavaguera et al. 2013). What is more, the induced murine lesions had the same morphologies as those found in patients (Clavaguera et al. 2013), similarly to the results for Aβ strain transmission described above (Heilbronner et al. 2013, Watts et al. 2014).

Particularly interesting is a study by Vasconcelos and colleagues (2016), which demonstrated that inoculating mice with tau oligomers whose aggregation has been seeded by Aβ, a process the authors term heterotypic seeding, induced tau pathology more potently than homotypic tau seeds, adding another layer to the pathogenic interaction of the two proteins. In addition, PS19 is a well-characterized Tg model expressing human tau with the P301S mutation; it recapitulates many aspects of tau pathology like hyperphosphorylation, pervasive NFT accrual, hyperactivated glia, and synapse and neuronal loss associated with hippocampal-mediated motor deficits (Yoshiyama et al. 2007). In this model, misfolded tau aggregates increase with age and preceded the onset of hyperphosphorylation by three months; this translated into an age-dependent increased seeding activity of brain homogenates in a fluorescence resonance energy transfer (FRET) cell-based aggregation assay, indicating that an increase in seeding activity is a reliable marker for the progression of tau pathology (Holmes et al. 2014a). The same model has been employed in a

study looking at the propagation rates and selective neuronal vulnerability to distinct cell-derived tau strains and revealed that while some strains were able to propagate regardless of the brain region injected, others were restricted (Kaufman et al. 2016). Detailed knowledge of the behavior of different strains would be invaluable in predicting the pattern, extent, and rate of pathological spread, which could help tailor appropriate treatment (Kaufman et al. 2016, Sanders et al. 2014). The collection of studies presented in this section are only a small fraction of the vast amount of work performed on AD-related seeding, but they show that there are key mechanistic similarities between the propagation of prion-like amyloid structures and have begun to fill an important conceptual gap by providing an explanation of how brain pathology progresses and what the biggest culprits are.

1.5. The Case for an Aβ Cell Seeding Model

1.5.1. Shortcomings of Mouse Models

This large body of work clearly demonstrates the ability of oligomer-containing seeding material to induce AD-like pathology in mice, thereby providing a deeper understanding into disease mechanisms, particularly into the way pathology spreads through brain regions and the cognitive and behavioral effects it has, all of which could be differently affected by strains. However, an important caveat is that while these studies recapitulate pathological aspects such as inflammation, gliosis, and synapse dystrophy and loss, they do not induce widespread neurodegeneration, which is characteristic of human dementia, nor do they show the co-existence of Aβ and tau pathology and are therefore not representative of true AD (Walker, Schelle and Jucker, 2016). They also lack resolution capacity to demonstrate what factors govern the spread of pathology on a cellular and molecular level and so only partially explore the seeding concept. A plausible explanation for the lack of tau pathology in APP or PS Tg mice is the lack of human tau (e.g. Sanchez-Mejias et al. 2016), which, as already stated, correlates better with cognitive decline in patients and is more directly linked to neuronal death. Aβ is able to induce tau misfolding and hyperphosphorylation (Jin et al., 2011; Bilousova et al., 2016; Vasconcelos et al., 2016), but the reverse is not true; therefore, Aβ may require tau as a downstream agent to exert deleterious effects (Bloom 2014). Additionally, it is possible that a longer incubation time is needed for Aβ-induced toxicity to arise, which is limited by the murine lifespan. It can be argued that mouse models based on APP overexpression create unrepresentative test conditions because human and mouse APP are both present and copy number is elevated many times above normal, which has prompted a preference for the use of knock-in

mouse models (Nilsson et al. 2014). Another limitation of mouse experiments is that they are hugely expensive, particularly when the mice need to be aged as long as possible, which puts a cap on the experimental turnover and output. Following from this, mouse models are particularly unsuitable to screen for drugs that ameliorate key aspects of AD pathology like seeded Aβ and tau propagation. While mouse models are favored in AD research due to their complex biological organization, simpler, more widely-accessible *in vitro* tools like cell models would allow for more versatile experimentation, particularly for the study of molecular mechanisms and disease pathways, though the limitations of such reductionist approaches should always be considered. The applications of cell models to study seeding are therefore discussed below.

1.5.2. Cell Studies of Prion-like Amyloid Propagation

1.5.2.1. Aβ Seeding

A requirement for seeding to occur is for prion-like structures to get transferred between cells at their points of contact either freely or through designated transport mechanisms and thus corrupt naïve cells (**Error! Reference source not found.**) (Guo & Lee 2014). This concept would explain why and how AD pathology spreads through synaptically connected brain regions (Clavaguera et al. 2009, 2013; Guo & Lee 2014; Stöhr et al. 2012, 2014; Ye et al. 2015b). It is important to note that oligomers termed bioactive because of their seeding propensity are not necessarily the same oligomers that are toxic and it is difficult to recapitulate this accurately in a cell assay because of the high risk of direct cytotoxicity of any foreign material introduced in culture and the absence of clearance mechanisms, which would be present in a mouse brain (Guo & Lee 2014). This concept is particularly relevant when investigating AβO strain diversity in AD patients to attempt to distinguish between active and inert conformations. In addition, technical limitations, mainly due to Aβ's notorious "stickiness" and spontaneous self-aggregation, make it difficult to isolate and distinguish between these assemblies in culture, which is another reason why mouse models are preferred for seeding experiments. Studies in cells are fewer, more are performed for tau than for Aβ, and these mainly look at Aβ toxicity, which leaves a gap in the understanding of the exact cellular mechanisms that govern Aβ template-based propagation.

In cell cultures, AβO are indeed transmitted from cell to cell in human neuroblastoma lines and in primary neuronal preparations. The transmission is associated with cytoskeletal and endosomal disruption, mitochondrial toxicity, and is fully dependent on cell con-

tact (Nath et al., 2012; Domert et al., 2014). Neuroblastoma cells and murine cortical neurons readily take up AβO seeds and accumulate them into lysosomes and early endosomes, where further aggregation is promoted by the acidic environment, which in turn may mean that Aβ can be secreted through vesicle-mediated exocytosis during clearance, as well as being shed off the cell membrane during APP cleavage (Domert et al. 2014, Hu et al. 2009, Nath et al. 2012, Song et al. 2014). The species of Aβ appears to play a role in the degree of aggregation and the extent of lysosomal toxicity because a slightly different peptide structure gives rise to oligomer strains with variable biophysical properties and resistance to degradation; for this reason, Aβ3(pE)-42 oligomer seeds induced more toxicity than Aβ1-42 seeds in a cell model (De Kimpe et al. 2013). In addition, it has been shown that once taken up by SH-SY5Y neuroblastoma cells, AβO increase in size the longer the cells are in culture (Hu et al. 2009). The demonstration that seeding-competent AβO are associated with mitochondria, which in turn are intimately associated with microtubules during transport, reveals a potential intercellular location for the crossover of Aβ and tau seeding (Marzesco et al. 2016). Cell studies such as these complement the large body of mouse work by showing that seeding is not a passive but a cell-mediated process and by linking template-based amyloid accumulation and propagation to cytotoxicity.

An interesting recent experiment attempted to bridge the gap between cell and mouse seeding by using hippocampal organotypic slices cultured for a period of approximately three months (Novotny et al. 2016). Upon seeding with APP Tg mouse extract, deposits were induced in the slices, provided that the medium was continuously supplemented with Aβ monomer, which would mimic the continuous Aβ production *in vivo* (Novotny et al. 2016). Of note, seeds formed in the slices were of the same potency as those derived directly from brain, even though the former were assembled from the supplemented synthetic monomers; this supports the notion that the brain-derived seeds were able to seed biologically-relevant conformations that are not normally recapitulated by synthetic oligomers (Novotny et al. 2016). An advantage of this platform is that it contains both neurons and glia and allows for the simultaneous study of the simplified response of multiple cell types to seeding. In particular, the study demonstrated that microglia were partly responsible for the extent of fibrillization of the observed Aβ deposits (Novotny et al. 2016). Because Aβ is continuously shed off the cell membrane and would accumulate in the cultured medium, 3D cultures grown in porous gels which would trap secreted Aβ have been explored (Nath et al. 2012). Such models allow the use of neuroblastoma cells which are immortalized due to their cancerous background, but also have the potential to differentiate into a more neuron-like phenotype and provide a potential alternative to neuronal

preparations. A successful model of Aβ seeding would have to employ cells which are able to survive for a prolonged period in culture, in order to allow adequate time for seed formation and propagation and would also need to be fairly robust to survive the stresses associated with AβO treatment. This makes commercially available cell lines like the commonly used SH-SY5Y good candidates.

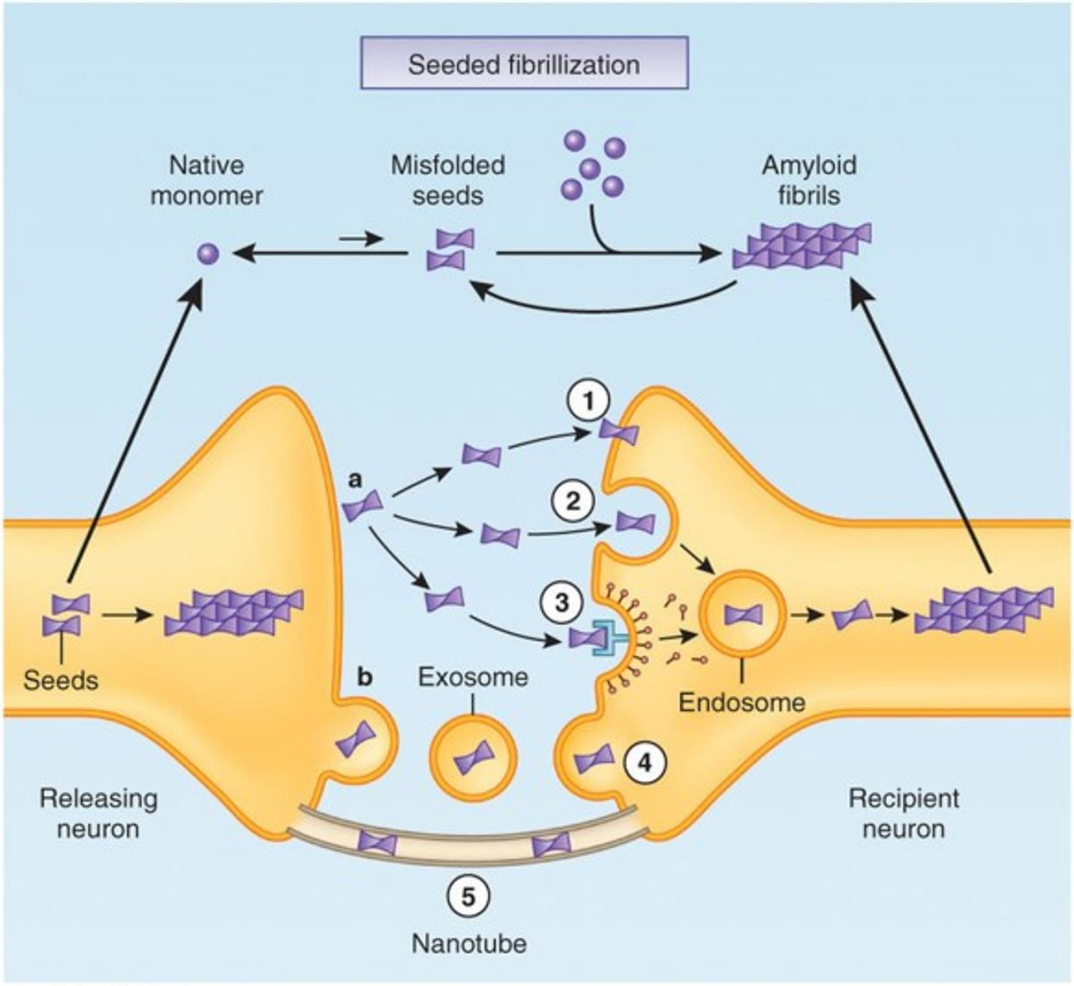

Figure 6. Intercellular seeding of misfolded protein aggregates (from Guo & Lee 2014).

Several modes of amyloid cell-to-cell transmission have been proposed. Monomers misfold and aggregate intracellularly and are subsequently released either freely (**a**) or in exosomes (**b**), which fuse with the recipient cell (**4**) where they can act as seeds and induce misfolding of naïve monomers. Freely released oligomers can directly insert themselves in membranes (**1**) or be endocytosed by the recipient cell (**2**). Alternatively, receptor-mediated endocytosis is also possible (**3**). In both cases, mechanisms must be then in place for the seeds to exit the vesicles. Finally, some oligomers are also able to travel directly between the cytoplasms of neighboring cells through tunneling nanotubes (**5**).

1.5.2.2. Tau Seeding

Seeding assays involving tau have been more successful so far and a lot can be learned from the principles they were built upon. In the heterotypic Aβ-tau seeding study described above (Vasconcelos et al. 2016), cross-seeding was also verified in a non-neuronal cell system which relies on lipid-mediated transduction of pre-aggregated tau or Aβ directly into the cell. The level of aggregation can then be quantified and it revealed that homotypic tau seeding is stronger than Aβ-tau cross-seeding, but both also occurred in these cells (Vasconcelos et al. 2016). Moreover, Aβ seeding following a round of tau seeding yielded an even stronger response, showing synergy between the two proteins that aggravates aggregative pathology (Vasconcelos et al. 2016). While this system is useful in reporting the amount of aggregation that occurs as a result of purified seed treatment, it does not represent Aβ seeding accurately, as it relies on the transfection of seeds directly into the cell, which bypasses any uptake mechanisms the cells would naturally have. As such, it is likely not suitable for studying naturally-derived Aβ seeds, which cannot be purified to the same extent and would likely be toxic to the cell system if introduced in this manner.

Another assay already mentioned uses human embryonic kidney HEK293 cells that express P301S mutant tau tagged with green or yellow fluorescent protein, which generate a quantifiable FRET signal during aggregation in response to transduction of pre-aggregated seeds (Holmes et al. 2014a). This assay propagated recombinant tau seeds, as well as those contained in human AD and tau Tg mouse brain and also worked when applied to primary neurons, demonstrating that the mechanism can be harnessed into multiple cell types (Holmes et al. 2014a). In addition, it was specific enough to discriminate between amyloids from different proteins, circumventing the important potential problem of aberrant aggregation in seeding assays (Holmes et al. 2014a). Attaching a fluorescent protein of about 27 kDa to tau whose monomeric molecular weight ranges from 36 to 46 kDa is an elegant and easy approach to directly observe its aggregation. However, this method is arguably not suitable for Aβ studies because tagging this tiny monomer of approximately 4 kDa with a disproportionally large fluorescent tag will likely considerably affect its aggregation properties. A similar interference was observed with PrP^{Sc} propagation in a cell assay when tags were attached to different parts of the protein (discussed below, Goold et al. 2011). The current tau assay also used lipid-mediated transduction of seeds and seemed to apply this method to seeding with crudely centrifuged patient brain

as well, but did not report toxicity resultant from the protocol, which is surprising, but is perhaps dependent on cell type.

Finally, the hypothesis that tau is a prion was further supported when structurally and functionally distinct toxic strains able to propagate their conformations in naïve cells were generated after seeding HEK293 cells with recombinant fibrils and isolating competent stable clones (Sanders et al. 2014). These strains were bioactive not only in cells, but in multiple generations of tau Tg mice, and produced distinct pathologies, notably through the presence or absence of disease-associated rod-shaped microglia, which shows yet another link between seeding and cytotoxicity (Sanders et al. 2014). The authors postulate that tau strains, similarly to PrP, could evolve in culture and their cellular turnover could impart selection pressures on their conformation and if this were true, it could open a new dimension of understanding the relationship between the pathology and manifestation of tauopathies (Sanders et al. 2014). Another potential problem for a sell ceding assay would be a limit to the number and types of strains it could propagate, and Sanders and colleagues found this was true for their model – it was permissive for several strains only and thus a proportion of their patient samples did not seed. Equally, strains from other samples were acutely toxic and killed the cells before clones could be established. Notably, however, this does not necessarily mean that these samples are incapable of seeding, but that perhaps a different platform is required. With a protein as heterogenous as tau, it cold be difficult to match the "raw material" requirements of an exogenous seed for its successful propagation; equally, certain seed conformations could be less stable, which would affect their ability to propagate faithfully (Sanders et al. 2014). Such considerations need to be kept in mind when working on an Aβ seeding model where a huge panel of Aβ peptides with various lengths and post-translational modifications exist.

1.5.2.3. The Scrapie Cell Assay for PrP

The Scrapie Cell Assay (SCA) for PrP^{Sc} (Klöhn et al. 2003) is currently the best example of a versatile, reproducible, and quantifiable amyloid seeding model, created in response to the need to quickly quantify the infectivity of prion-containing samples without the use of mice, and today is routinely used for this purpose. The assay uses mouse neuroblastoma N2a cells, which were exposed to the Rocky Mountain Laboratory (RML) PrP^{Sc} strain and were subcloned to yield susceptible PK1 cells and refractory cells for this strain in particular. The susceptibility to infective prions relied entirely on clonal differences arising through the continuous passage of cells and not on genetic modifications like PrP overexpression because this does not guarantee the ability of cells to propagate infectious prions.

Cells in the SCA are inoculated with PrP^{Sc} without the use of transfection agents because PrP aggregates on the cell surface and upon antibody treatment individual infected cells can be counted. Thus, the number of PrP^{Sc}-positive cells is a direct function of the infectivity titer of an RML sample. Importantly, the assay assures that the original seeds are diluted out by passaging the cells several times, so that only *de novo* formed prions are visualized. The downside of the SCA, however, is that generally it is only susceptible to the RML strain and work in our department is currently underway to adapt it to other mouse and human strains and to uncover potential cell differences that account for this variable susceptibility.

In our group, the SCA has notably been used to expand the knowledge behind cell susceptibility to prion infection by identifying genes which modulate PrP^{Sc} propagation through a comparison between PK1 cells and revertant clones, which had spontaneously lost their ability to propagate PrP^{Sc} (Marbiah et al. 2014). These genes were primarily related to differentiation and development, showing that revertant cells were less differentiated than PK1 cells and that their permissibility was greatly elevated by inducing differentiation with retinoic acid (Marbiah et al. 2014). Moreover, when comparing prion titers in different spleen cell types, it was clearly shown that in early stages of prion infection natural killer and plasmacytoid dendritic cells, which are immune cells and had not been previously associated with prion disease pathogenesis, have highest titers (Castro-Seoane et al. 2012). This evidence supports the important concept that susceptibility towards prion seeding is dependent on cell background and could be a plausible explanation for why certain cell types are particularly vulnerable to seeding (Marbiah et al. 2014). Within our department, the SCA has been used to show that the overall rate of prion titer increase does not correlate with disease clinical onset *in vivo*; instead, aggregation occurs rapidly and exponentially post-inoculation and then reaches a prolonged plateau phase, the length of which is affected by PrP overexpression (Sandberg et al. 2011). This study further highlights the importance of strain contribution to prion spread and toxicity and indeed it was later shown that together with classical PrP^{Sc}, another distinct prion structure that correlates to total PrP^{C} levels was emerging during the course of infection (Sandberg et al. 2014). This species was sensitive to proteinase K and unlike total PrP or PrP^{Sc} rose with the development of clinical symptoms, showing that neither of these factors is rate limiting towards propagation and toxicity (Sandberg et al. 2014). Such findings may also be of relevance to Aβ studies, since total Aβ does not correlate with disease.

The SCA has become a readily available and adaptable tool to the field and other groups have used it to uncover more information about the way prions behave in culture. Li et al. (2010) challenged PK1 cells with different mouse prion assemblies and were able to generate clones permissive to strains other than RML, showing that through consistent exposure to infectious material cells will evolve to propagate the prions contained therein. It was not clear, however, whether this evolution reflected a changed cellular response to a heterogenous pool of prion strains contained in the mouse brain from the start of the inoculation, or whether the original PrP^{Sc} seed underwent a subtle conformational change that facilitated its propagation (Li et al. 2010). The assay has also been adapted in a manner similar to the tau assays described above, where an epitope tag was inserted into the PrP sequence in a way that would not interfere with its cellular localization, processing, and aggregation properties, so that newly formed seeds could be readily distinguished from the inoculum (Goold et al. 2011). This method increased the experimental resolution of the initial events in prion formation and demonstrated that template-mediated replication of prions in culture begins within minutes of exposure to exogenous seeds, is already robust several hours after inoculation, and cell susceptibility does not increase with increased seed concentration (Goold et al. 2011). If Aβ propagated so rapidly as well, perhaps the evidence from mice that amyloidosis is dependent on the Aβ concentration of the inoculum could mean that cell susceptibility per se is not so important when compared to overwhelmed clearance mechanisms, the over-abundance of seeds, or strain heterogeneity. Through seeding as a quantitative output, the assay showed that PrP^{Sc} aggregation begins in the plasma membrane, aggregates are subsequently endocytosed in a dynamin/clathrin-independent manner, and seeding is likely limited by cell factors because of the absence of correlation between seed concertation and cell response (Goold et al. 2011). Investigating such mechanisms, how they facilitate seeding propensity, and vice versa could yield more information about these proteins' physiological roles and potentially how they go wrong in disease.

1.5.3. The 7PA2 Model of APP Processing

Looking at all the research avenues opened by the ability to quantify the process of cell-to-cell seeding in a reproducible, high-throughput system such as an immortalized cell line, it is obvious that the SCA, although conceptually simple, is an exceptionally useful research tool. If such a tool existed for Aβ that could allow groups to modify cell components to investigate the factors which control Aβ seeding, assess the infectivity of a patient sample, distinguish between the bioactivity of different AβO strains, and screen

drugs which block or modulate seeding, it would represent a huge development in the AD field and would significantly cut experimental costs. Adapting the SCA could be a viable approach for the quantification of AβO seeded aggregation due to the mechanistic similarities in the spread of misfolding between Aβ and PrP. Currently, a widely-studied model of AβO production and APP processing is the 7PA2 cell line (Podlisny et al. 1995). 7PA2 cells overexpress the 751 isoform of human APP, bearing the V717F Indiana mutation on a Chinese hamster ovary (CHO) cell background. Interestingly, soluble non-fibrillar oligomers secreted by these cells induced long-term synaptic depression in rats (Freir et al. 2011, Walsh et al. 2002, Welzel et al. 2014), triggered synapse damage in cultured neurons via PrP binding (Bate & Williams 2011), and induced excessive formation of cofilin-actin rods, which modulate microtubular integrity (Davis et al. 2011). The cells also display a reduction of oxidative phosphorylation and an increased production of reactive oxygen species (Krako et al. 2013). It is important to note, however, that despite the diverse toxic cellular effects of AβO from 7PA2 medium, *in vivo* seeding of amyloid has not been reported. A mass spectrometry evaluation revealed that these cells secrete more than ninety APP fragments which contain parts of or the entire Aβ sequence (Portelius et al., 2013). Nevertheless, the exact composition of the secreted oligomers has not been tested and it is only known that they are of low molecular weight. Clearly defined protocols for culturing AβO from this cell line are available (Shankar et al. 2011) and even though the genetic background of this model is not human, the 7PA2 line is an excellent point of comparison for an AβO seeding assay because it produces bioactive AβO and is well-characterized.

1.5.4. Thesis Aims

In this PhD study, I genetically engineered and characterized a series of human neuroblastoma cell lines as an approach to generate a cell model capable of faithfully propagating AβO. Eleven cell lines were obtained and screened for expression of APP, BACE1, and the γ-secretase proteins, to arrange them along a spectrum of high and low expression. While efforts have been made to identify factors which may predict the susceptibility of cells to prion infection (Marbiah et al. 2014), it is not known what the conditions are which determine permissiveness of oligomer propagation. Therefore, after the initial characterization step, I selected two cell lines at opposite ends of the spectrum – SK-N-BE(2), which had high levels of full-length APP and BACE1, and GI-ME-N, which had negligible amounts of both – and compared these to the 7PA2 line. One wild-type or one of three mutant (Swedish, Iberian, and NL-F) APP695 variants were assembled together with BACE1 in four gene constructs, to be introduced into the two neuroblastoma lines to elevate Aβ produc-

tion. The presence of Aβ was confirmed by western blot and immunoassays and an initial mass spectrometry screen of secreted Aβ peptides was performed to reveal the signature profile of each line. Finally, diluted AD and control brain homogenate with proven seeding ability was applied to the cells and extracellular and intracellular propagation of oligomers were assessed. Propagation could not be detected in any of the conditions and it appeared that seeds which were taken up were cleared by the cells as they were expanded post-seeding. Due to time and resource constraints, these experiments could not progress beyond the pilot phase and yield more conclusive results. Therefore, at this point it cannot be ascertained whether the studies lines can serve as a template for AβO seeding and more tests are needed to explore this concept and determine the usefulness of these lines as an APP processing model.

2. Materials and Methods

2.1. Cell Culture

2.1.1. Conditions and Cell Lines

Eleven human neuroblastoma cell lines were purchased for their reported morphology and growth properties. Table 1 below summarizes their culture conditions and sources. 7PA2 and CHO cells were a kind gift from Dr. Dominic Walsh (Center for Neurologic Diseases, Brigham & Women's Hospital, Boston, MA). In addition, RetroPack PT67 cells were used for viral packaging and stocks of those were already present in-house. All media, supplements, and equipment were bought from ThermoFisher Scientific and their catalog numbers are: Dulbecco's Modified Eagle Medium (DMEM)/F12 GlutaMAX – 31331093, DMEM GlutaMAX – 31966047, Roswell Park Memorial Institute (RPMI) 1640 medium – 21875091, 0.05% Trypsin/EDTA (ethylenediaminetetraacetic acid) Phenol Red – 25200072, fetal bovine serum (FBS) of South American origin – 10270-106, penicillin-streptomycin (Pen-Strep) 10000 units/ml – 15140-122, and geneticin (G418 sulfate) powder – 11811-023. All cells were grown in a HERACell 150i incubator at 37°C, 5% CO_2.

Table 1. Culturing conditions of cell lines.

Cell Line	Supplier	Culture Medium	Split Method	Split Ratio	G418 Selection
7PA2	Dominic Walsh Lab	DMEM/F12, 10% FBS, 1% Pen-Strep	Trypsin/EDTA	1:50	200 µg/ml
BE(2)-M17	Sigma-Aldrich 95011816-1VL	DMEM/F12, 10% FBS, 1% Pen-Strep	Pipetting	1:10/1:20	800 µg/ml
CHO	Dominic Walsh Lab	DMEM/F12, 10% FBS, 1% Pen-Strep	Trypsin/EDTA	1:50	N/A
CHP-134	DSMZ ACC 653	RPMI 1640, 10% FBS, 1% Pen-Strep	Pipetting	1:5/1:10	200 µg/ml
GI-ME-N	DSMZ ACC 654	RPMI 1640, 10% FBS, 1% Pen-Strep	Trypsin/EDTA	1:20/1:40	300 µg/ml
IMR-32	DSMZ ACC 165	RPMI 1640, 10% FBS, 1% Pen-Strep	Pipetting	1:5/1:10	400 µg/ml
KELLY	DSMZ ACC 355	RPMI 1640, 10% FBS, 1% Pen-Strep	Pipetting	1:10	600 µg/ml
LS	DSMZ ACC 675	RPMI 1640, 10% FBS, 1% Pen-Strep	Trypsin/EDTA	1:10/1:20	400 µg/ml
NBL-S	DSMZ ACC 656	DMEM/F12, 10% FBS, 1% Pen-Strep	Pipetting	1:5/1:10	400 µg/ml

NGP	DSMZ ACC 676	DMEM/F12, 10% FBS, 1% Pen-Strep	Pipetting	1:10	500 µg/ml
NMB	DSMZ ACC 657	DMEM/F12, 10% FBS, 1% Pen-Strep	Pipetting	1:10	600 µg/ml
RetroPack PT67	N/A	DMEM, 10% FBS, 1% Pen-Strep	Trypsin/EDTA	1:20/1:40	400 µg/ml
SH-SY5Y	DSMZ ACC 209	DMEM/F12, 10% FBS, 1% Pen-Strep	Trypsin/EDTA	1:5/1:10	600 µg/ml
SK-N-BE(2)	DSMZ ACC 632	DMEM/F12, 10% FBS, 1% Pen-Strep	Trypsin/EDTA	1:10/1:20	800 µg/ml

2.1.2. Antibiotic Kill Curves

One of the project's aims was to overexpress APP and BACE1 in the cell lines. This was to be done using a retroviral vector with a neomycin/kanamycin resistance gene. Therefore, kill curves for G418 (geneticin, a structural analog to neomycin) were carried out either in 10-cm or 6-well cell culture dishes. Cells were plated at a density of 1 million per dish or 200 thousand per well respectively and after 24 h were resuspended in fresh medium, supplemented with a range of antibiotic concentrations depending on the susceptibility of each line. Due to the slow action of G418, the cells were selected for approximately one week. The antibiotic concentration immediately preceding the concentration which left no viable cells was established as the selection and maintenance concentration for that line. The maintenance concentration for 7PA2 cells has already been established and that was 200 µg/ml (Table 1).

2.1.3. Serum Titration

APP and BACE1 overexpression would lead to the increased secretion of Aβ in the cell medium, which would then be analyzed by immunoassays (see Section 13 below). The presence of serum is known to interfere with protein detection, so the cells were tested for their ability to tolerate growth under serum-depleted conditions. They were plated in a 6-well format at a density of 400 thousand, 500 thousand, or 1 million. Upon reaching ~80% confluence, the cells were washed with sterile Dulbecco's phosphate buffered saline without Ca^{2+} and Mg^{2+} (DPBS, ThermoFisher Scientific, Cat.# 14190094) and were incubated in 5 ml fresh medium, supplemented with 1% Pen-Strep and either 10%, 8%, 6%, 4%, 2%, or 0% FBS. After four to six days of incubation, cells were imaged and their health and viability were visually assessed.

2.2. Gibson Assembly

Gibson Assembly was the cloning method of choice for assembling the APP/BACE1 constructs into the retroviral vector. The method joins double-stranded DNA (dsDNA) sequences termed gBlocks by means of short (20-50 base pairs, (bps)) terminal overlapping regions. The gBlocks are mixed together in a proprietary Gibson Assembly Master Mix (New England Biolabs, Cat.# E2611L), which contains a thermosensitive exonuclease, a polymerase, and a ligase. The exonuclease acts in a 3' -> 5' direction, partially removing one strand of the dsDNA to expose complementary overhangs at the end of each gBlock, which can then anneal. The polymerase fills in any gaps in the DNA created during the annealing process and the ligase joins any nicks in the sequence. About five gBlocks can be successfully assembled into a single segment, one of which can be a vector cut with a restriction enzyme.

2.2.1. gBlock and Construct Design

Firstly, the BACE1 sequence was retrieved by its National Center for Biotechnology Information reference number (NM_012104.4) and its coding sequence (CDS) was identified. The CDS was split into three fragments with overlapping termini and the properties of each were evaluated with the Integrated DNA Technologies (IDT) tool for gBlock design (http://eu.idtdna.com/site/order/gblockentry). Where necessary, a number of silent mutations were introduced before ordering to reduce GC content and nucleotide repeats, according to IDT's instructions. The three gBlocks were assembled and the BACE1 product was amplified via polymerase chain reaction (PCR, see Section 3.2).

BACE1 was cloned in the same transcript together with APP by means of a self-cleaving 2A peptide overhang. 2A peptides are short viral sequences whose secondary structure inhibits the ribosome from adding amino acids to the peptide chain, causing the already synthesized peptide to be released. The ribosome is then able to continue translating the same transcript further downstream. This process is known as ribosomal skipping and theoretically allows for the relatively equal expression of multiple proteins from the same amplicon, without the need for multiple start and stop codons. In this work, I used the equine rhinitis A virus (ERAV) 2A peptide sequence. Vector pLNCX2, blunt-cut by restriction digest with enzyme StuI for 1 h at 37°C (New England Biolabs, Cat.# R0187L), was taken for the backbone of the construct. The insert was assembled in the order APP-ERAV-BACE1, using the appropriate 5' and 3' overhangs. APP and BACE1 also contained a

5’ and a 3’ overhang sequence respectively, complementary to the cut vector. All gBlocks are sequence-verified by IDT before shipping.

2.2.2. Reaction Setup

The amounts of gBlocks needed per reaction were calculated according to the following formula, provided in the manufacturer's protocol.

$$pmols = \frac{(weight\ in\ ng) \times 1000}{bps \times 650\ Da}$$

Equimolar amounts (0.2 pmol) from each gBlock were then added to 10 µl 2x Gibson Assembly Master Mix. The reaction was topped up with pre-chilled nuclease-free water (QIAGEN, Cat.# 129114) to a final volume of 20 µl. It is crucial that all components are kept on ice throughout, as the exonuclease acts extremely rapidly at room temperature (RT) and will digest the DNA. The reaction was mixed well by pipetting and transferred immediately to a thermocycler (Biorad Tetrad II) pre-heated to 50°C for 1 h to inactivate the thermolabile enzyme and to anneal and ligate the fragments.

2.3. Polymerase Chain Reaction (PCR)

Gibson Assembly works with minute amounts of DNA, so the reaction product needed to be amplified via PCR before transforming into bacteria. The 695 isoform of APP bearing the Swedish mutation (KM670/671NL) was also amplified from a construct previously made in our lab to be cloned in the pLNCX2 vector together with BACE1. Finally, colony PCR was used to test for the presence of inserts into transformed bacteria after Gibson Assembly of the APP-ERAV-BACE1 construct and after site-directed mutagenesis (SDM, described in Section 4).

2.3.1. Primers

2.3.1.1. Design

Primers were designed manually from the sequences of APP and BACE1 (reverse primers were reverse complemented to their sense sequences) and their properties were assessed with the OligoAnalyzer tool available from IDT (https://eu.idtdna.com/calc/analyzer). Where possible the GC content was kept below 60% and melting temperatures around 65°C.

2.3.1.2. Sequences

APP was amplified with a forward primer containing a pLNCX2 overhang that ends at the StuI restriction site and a reverse primer which contains the complete sequence of ERAV. The opposite combination of primers was used for BACE1. In addition, diagnostic PCRs were run to amplify various fragments of the APP-ERAV-BACE1 sequence to evaluate the success of the Gibson Assembly reactions. Standard commercially available forward and reverse primers for the multiple cloning site of pLNCX2 (Clontech, Cat.# K1060-F) were used for colony PCR. The sequences of all primers are given in the Table 2 below.

Table 2. PCR primers.

Primer Name	Primer Features	Primer Sequence
pLNCX2_APPswef	Forward to APP, contains the pLNCX2 overhang	5'-GACTCAGATCTCGAGCTCAAGCTTGTT TGGCCGAGGCGGCCGCTTGTCGACAGGA TGCTGCCCGGTTTGGCACTGC-3'
APPswer_ERAV	Reverse to APP, contains the full sequence of ERAV 2A peptide	5'-GGGTCCGGGGTTGCTCTCCACGTCGCC GGCCAGCTTCAGAAGGGCGTAGTTGGTG CACTGGTTCTGCATCTGCTCAAAGAACTT GTAGGTTGGATTTTCGTAGCC-3'
APPfw	Forward to APP	5'-ATGCTGCCCGGTTTGGCACTGC-3'
ERAV_BACE1f2	Forward to BACE1, contains the full sequence of ERAV 2A peptide	5'-CAGTGCACCAACTACGCCCTTCTGAA GCTGGCCGGCGACGTGGAGAGCAACCC CGGACCCATGGCCCAAGCCCTGCCCT-3'
BACE1r1_pLNCX2	Reverse to BACE1, contains the pLNCX2 overhang	5'-AAAATCTTTTATTTTATCGATGTTAGG CCATTAAGGTCACTTCAGCAGGGAGATG TCATCAGCAAAGTCATCA-3'
BACE1 f1	Forward to BACE1	5'-ATGGCCCAAGCCCTGCCCTG-3'
BACE1 r2	Reverse to BACE1	5'-TCACTTCAGCAGGGAGATGTCATCAG CAAAGTCA-3'
BACE1 rmid2	Reverse to middle of BACE1	5'-AATACCACTCCCGCCGGATGGGTGTA TACC-3'
pLNCX2 seq f	Forward to pLNCX2 multiple cloning site	5'-AGCTCGTTTAGTGAACCGTCAGATC-3'
pLNCX2 seq r	Reverse to pLNCX2 multiple cloning site	5'-ACCTACAGGTGGGGTCTTTCATTCCC-3'

2.3.2. PCR Amplification

2.3.2.1. Reaction Setup

PCR amplification was carried out in 96-well polypropylene plates (Starlab, Cat.# E1403-5200), using AccuPrime Taq High Fidelity DNA polymerase (Invitrogen, Cat.# 12346-086). Each reaction was prepared with 1x Buffer I (provided at 10x stock), 1.5 µl anhydrous dimethyl sulfoxide (DMSO, Sigma-Aldrich, Cat.# 276855-250ML), 10 µM forward and reverse primer, 40 ng DNA, and 0.2 µl (1 unit) AccuPrime Taq polymerase and was topped up with nuclease-free water to a final volume of 50 µl. The plate was then sealed with a clear plastic lid (Starlab, Cat.# E2796-0793) and was briefly spun down to collect all reagents at the bottom of each well.

2.3.2.2. Program

The fragments of interest were amplified on a Biorad Tetrad II thermocycler. DNA strands were initially denatured at 94°C for 30 s. Each of the subsequent 35 amplification cycles consisted of DNA denaturation at 94°C for 15 s, annealing of primers at 67°C for 15 s, and elongation at 68°C for 3 min 20 s (~1 min/kilobase). Finally, the reaction was either immediately separated on a 1% agarose (Bioline, Cat.# BIO-41025) Tris-Acetate DNA gel, containing 1 µg/ml ethidium bromide, or frozen at -20°C.

2.3.3. Colony PCR

2.3.3.1. Reaction Setup

Screens of whole bacterial plates for the presence of the APP-ERAV-BACE1 insert in pLNCX2 were carried out on all plates after each transformation. Individual bacterial colonies were stirred into the wells of a 96-well polypropylene plate, each of which contained 5 µl nuclease-free water. A master mix was prepared using the GoTaq DNA polymerase kit (Promega, Cat.# M3171) or its replacement GoTaq G2 DNA polymerase kit (Promega, Cat.# M7841). Briefly, 20 µl master mix were added to each inoculated well to a total reaction volume of 25 µl. Each PCR reaction contained 10 µM pLNCX2 forward and reverse primer (flanking the insert), 1x green GoTaq reaction buffer (stock at 5x), 100 µM $MgCl_2$, 250 µM dNTPs, and 0.05 units/µl GoTaq G2 (stock at 5 units/µl). The plate was then sealed and centrifuged before cycling.

2.3.3.2. Program

Initial denaturation was at 95°C for 1 min, melting temperature was set to 95°C for 1 min, primers annealed at 58°C for 1 min, and extension time was 4 min at 72°C. The last three steps were repeated 30 times, after which a final elongation step of 5 min at 72°C was carried out before the samples were chilled to 4°C and separated on an agarose DNA gel as in Section 3.2.2.

2.4. Site-Directed Mutagenesis (SDM)

Four different APP mutant clones were generated using SDM to investigate the effects of different mutations on APP processing. The template was a single clone of APP695 previously produced in our lab, harboring the Swedish KM670/671NL mutation. The sequence of the original clone was verified (see Section 6), points in need of repair were identified, and primers with the correct sequences and the desired APP mutations were designed. SDM relies on the design of complementary primers, which contain the desired mutation as a mismatch to the original template. A PCR reaction is then set up and here the entire vector containing the construct (a total of 10 kilobase pairs (kbps)) was amplified.

2.4.1. Primer Design

Primers were designed using the IDT OligoAnalyzer tool, according to the guidelines provided with the QuikChange Site-Directed Mutagenesis kit (Stratagene, Cat.# 200519). Primers were fully complementary and contained one mutation per pair in the middle of their sequence. They were between 30 and 43 bps long, with GC content over 50% and ending in at least one or more G or C bases. A full list of all primers used is given in Table 3 below, where the mutation(s) introduced are highlighted in red.

Table 3. SDM primers.

Primer Name	Primer Features	Primer Sequence
APP_Leu491Phe_Fw	Corrects a random point mutation in the APP sequence at position 491	5'-CGGCCTCGTCACGTG**T**TCAATATGCTAAAG-3'
APP_Leu491Phe_Rev		5'-CTTTAGCATATTGA**A**CACGTGACGAGGCCG-3'
APP_Swe2WT_Fw	Corrects the Swedish mutation into the wild-type form	5'-CGGAGGAGATCTCTGAAGTGAA**GA**TGGATGCAGAATTCCGAC-3'
APP_Swe2WT_Rev		5'-GTCGGAATTCTGCATCCA**TC**TTCACTTCAGAGATCTCCTCCG-3'

APP_WT2Ibe_Fw	Corrects the wild-type form into the Iberian mutation	5'-GGTGTTGTCATAGCGACAGTGTTCGTC ATCACCTTGGTGATGC-3'
APP_WT2Ibe_Rev		5'-GCATCACCAAGGTGATGACGAACACT GTCGCTATGACAACACC-3'

2.4.2. Reaction Setup and Cycling

Each 50-µl reaction contained 5 µl of 10x reaction buffer, 1 µl miniprepped dsDNA (5-50 ng), 1 µl (approximately 125 ng) forward and reverse primers each (10 µM stock), 1 µl dNTP (100 µM stock), and 1 µl Pfu Turbo DNA polymerase (2.5 units/µl). The final reaction volume was adjusted to 50 µl with nuclease-free water. The SDM reactions were cycled on a Biorad Tetrad II thermocycler according to these settings: 95°C for 30 s, followed by 16 cycles of 95°C for 30 s, 55°C for 1 min, and 68°C for 10 min (1 min/kbps of plasmid length), and finally 68°C for an additional 5 min. The reactions were then placed on ice for 2 min to cool. One µl (10 units/µl) of *Dpn* I restriction enzyme was added to each reaction, after which they were incubated at 37°C for 1 h. *Dpn* I cuts methylated DNA which is produced in *E. coli* strains, while DNA produced in the PCR reaction is unmethylated. Therefore, any non-mutated DNA left over is digested to yield only the desired mutated DNA. The success of SDM was verified via sequencing as in Section 6 below and 1 µl of each digested reaction was then transformed in XL1-Blue Supercompetent cells.

2.5. DNA Gel Purification

All cut plasmids, PCR, and SDM products were extracted and purified after separation in DNA gels with the Wizard SV Gel and PCR Clean-up System (Promega, Cat.# A9281). The protocol supplied by the manufacturer requires the bands of interest to be cut out under low UV light, weighed, and dissolved in 10 µl Membrane Binding Solution per 10 mg gel slice at 50 – 65°C. The dissolved gel slices were incubated on a Minicolumn at RT for 1 min, after which they were centrifuged for 1 min at 16000 *g* in a table-top centrifuge. The flow-through was discarded and the column was washed with 700 µl Membrane Wash Solution, which contains ethanol. The column was centrifuged for 1 min and was again washed and centrifuged with 500 µl Membrane Wash Solution for 5 min. All flow-through was discarded and the column was centrifuged once again for 1 min for the ethanol to completely evaporate. The column was transferred to a clean 1.5-ml Eppendorf tube and was incubated with 50 µl nuclease-free water for 1 min, after which the DNA was eluted via a 1-min centrifugation step. DNA concentration was measured with NanoDrop.

2.6. Sequencing

All constructs were sequenced to make sure correct and functional proteins were expressed. This was outsourced to Eurofins Scientific. Sequencing results were analyzed using Sequence Scanner Software 2 (Applied Biosystems) and sequences were aligned using SnapGene Viewer 2.7.3 (GSL Biotech).

2.6.1. Primer Design

Primers were designed using the Eurofins sequencing Design-a-Primer tool. The APP-ERAV-BACE1 construct was divided into regions of 500 bps and one primer pair was designed per segment. In addition, a forward and a reverse pLNCX2 primer were used to reliably cover the beginning and the end of the construct. Sequencing was carried out with all forward and the reverse pLNCX2 primers and was of sufficiently good quality that proofreading it with the remaining reverse primers was not necessary. Below is the list of primers used in the reactions (Table 4).

Table 4. Sequencing primers.

Primer Name	Primer Sequence
APP_seq_F1	5'-TTGTAAGTGATGCCCTTCTCGTTC-3'
APP_seq_F3	5'-CCAGAGTGGAAGCCATGCTCAATG-3'
APP_seq_F4	5'-AAACGAAGTTGAGCCTGTTGATGC-3'
BACE1_seq_F1	5'-TCGAGAGACAGACGAAGAG-3'
BACE1_seq_F2	5'-ATCAGACAAGTTCTTCATCAACGG-3'
BACE1_seq_F3	5'-TTTCCCAGTCATCTCACTCTACC-3'
pLNCX2_seq_F	5'-TGTACGGTGGGAGGTCTATATAAG-3'
pLNCX2_seq_R	5'-GCTTGCCAAACCTACAGGTG-3'

2.6.2. DNA Preparation

DNA was extracted from transformed cells (Sections 7 and 8) and its concentration was assessed with NanoDrop using 1 µl of each sample. As per Eurofins' requirements, DNA was diluted down to 100 ng/µl and 15 µl was pipetted per Eppendorf Safe-Lock tube, to which a pre-paid barcode label was attached.

2.7. Transformation of Competent Cells

Transformations of Gibson Assembly reactions and plasmid DNA were carried out primarily in NEB 5-alpha Competent E. coli (High Efficiency) (New England Biolabs, Cat.# C2987H). Aliquots of competent cells were thawed on ice for 5 min, 2-3 µl (1 pg – 100 ng recommended amount) plasmid or Gibson Assembly DNA were added per aliquot and mixed by flicking, and the tubes were incubated on ice for 30 min. The bacteria were then heat-shocked for precisely 30 s at 42°C in a heat block and incubated on ice for a further 5 min. Each tube was supplemented with 950 µl 1x Super Optimal broth with Catabolite repression (SOC) medium (provided with the transformation kit) and was placed in an incubator-shaker for 1 h at 37°C, 5% CO_2. Between 100-250 µl of transformed bacteria were plated on LB (Luria broth)-agar plates containing 100 µg/ml ampicillin, which were then incubated overnight at 37°C. SDM DNA samples were transformed in XL1-Blue Supercompetent cells, which are supplied with the QuickChange Site-Directed Mutagenesis kit (Agilent Technologies, Cat.# 200519). The protocol is almost identical to the one described above, with the following differences. Bacteria were grown in pre-chilled 14-ml BD Falcon polypropylene round-bottom tubes (Corning, Cat.# 352059), as recommended by the supplier. They were heat-shocked for precisely 45 s in a water bath and incubated in 500 µl SOC medium pre-heated to 42°C. Finally, 250 µl of bacteria were spread on agar plates for incubation.

2.8. Bacterial DNA Extraction

2.8.1. Miniprep

Plasmid DNA was prepared from transformed NEB 5-alpha or XL1-Blue cells using the QIAprep Spin Miniprep kit (QIAgen, Cat.# 27106). Individual bacterial colonies were grown up overnight in 10 ml LB (Sigma-Aldrich, Cat.# L3522-1KG) supplemented with 100 µg/ml ampicillin to select for vector pLNCX2, after which they were spun down at 3000 *g* for 5 min. The broth was drained and the bacterial pellet was resuspended in 250 µl Buffer P1, containing RNase A (ribonuclease A) and LyseBlue reagents, and transferred to clean Eppendorf tubes. The bacteria were lysed with 250 µl Buffer P2 and neutralized with 350 µl Buffer N3. Lysates were spun down in a table-top centrifuge at full speed (used for all subsequent centrifugation steps) for 10 min until debris formed compact pellets. Supernatants were transferred to QIAprep Spin Columns and centrifuged for 1 min. The flow-through was removed and columns were washed with 500 µl Buffer PB, followed by DNA precipitation with 750 µl ethanol-containing Buffer PE. The columns were spun down for

an additional minute to remove residual ethanol. Finally, DNA was eluted in 50 µl Elution Buffer. The DNA concentration was measured using NanoDrop.

2.8.2. Maxiprep

Whenever larger and purer quantities of DNA were required, they wre prepared using the EndoFree Plasmid Maxi kit (QIAgen, Cat.# 12362). Individual colonies from NEB 5-alpha or XL1-Blue bacteria were seeded overnight in 2 ml LB supplemented with 100 µg/ml ampicillin. The resulting culture was then transferred to glass conical flasks containing 250 ml LB with 100 µg/ml ampicillin and was again expanded overnight. Cells were harvested by centrifugation at 6000 *g* for 15 min at 4°C. The pellets were resuspended in 10 ml Buffer P1, lysed with 10 ml Buffer P2, and neutralized with 10 ml cold Buffer P3. The lysate was poured into a QIAfilter Cartridge for a 10-min incubation at RT, after which it was filtered into a clean 50 ml Falcon tube. Endotoxins were removed during a 30-min incubation on ice with 2.5 ml Buffer ER added to the filtered lysate. In the meantime, a QUIAGEN-tip 500 column was equilibrated with 10 ml Buffer QBT. The lysate was poured in and the column was allowed to drain by gravity flow. It was washed twice with 30 ml Buffer QC, transferred to a clean tube, and the DNA was eluted with 15 ml Buffer QN, after which it was precipitated with 10.5 ml RT isopropanol. DNA pellets were collected by centrifugation at 8000 *g* for 15 min at 4°C. The location of the pellets was marked onto the tube and the supernatant was carefully removed. The DNA was washed with 1 ml RT 70% ethanol, transferred to a clean Eppendorf tube, and spun in a table-top centrifuge for 10 min at maximum speed. The supernatant was carefully removed and the pellets were left to air-dry. Finally, the DNA was re-dissolved in 100 µl Buffer TE before assessing its concentration via NanoDrop.

2.9. DNA Overexpression via Retroviral Infection

The four constructs were packaged into retroviruses to infect the human neuroblastoma lines using the RetroPack PT67 packaging line, which constitutively expresses a portion of the genes that encode a functional viral particle. Transfection with a retroviral vector which contains the remaining viral genes in addition to the DNA to be packaged (in this case pLNCX2) initiates viral production.

2.9.1. Transfecting Packaging Cells

RetroPack PT67 cells were plated at a density of 1 million in 10-cm culture dishes and were grown to ~70% confluence overnight. The medium was changed with a fresh 10 ml and transfection mixtures with Lipofectamine LTX/Plus Reagent (Life Technologies, Cat.#

15338100) were pipetted dropwise onto each dish. The transfection solutions were prepared in 500 µl unsupplemented OptiMEM (Life Technologies, Cat.# 31985070) per dish by combining 8 µg plasmid DNA of interest and 8 µg pmD2.G plasmid, which encodes the coat glycoprotein of vesicular stomatitis virus (VSV-G). Nineteen µl Plus Reagent were pipetted into each tube; these were then left at RT for 5 min. Lipofectamine LTX was thoroughly vortexed and 29 µl were added to complete the mixtures before incubating them for 30 min at RT. After transfection, the cells were incubated overnight, and then the medium was changed with a fresh 10 ml to collect the virus.

2.9.2. Harvesting and Concentrating Retroviral Supernatant

Seventy-two hours post-transfection the viral supernatants were passed through 0.45 µm filters to remove cell debris and were transferred to Falcon tubes. To infect GI-ME-N cells, the virus was cultured for 120 h and was concentrated with the polyethylene glycol solution Precipivir (Fundación Miguel Servet, Navarrabiomed). Precipivir was warmed up at RT for up to an hour and was thoroughly mixed before use. Viral supernatant was pipetted together with Precipivir into 15-ml Falcon tubes covered with aluminum foil at a 4:1 v/v ratio. The tubes were left to mix on a blood wheel overnight at 4ºC and were then centrifuged at the same temperature and 4000 rpm (3488 *g* in a Multifuge XR3 centrifuge, ThermoFisher Scientific) for 1 h. The supernatant was carefully removed and the viral pellet was resuspended with complete medium for immediate use in infection.

2.9.3. Infecting Human Neuroblastoma Cells

The eleven cells were screened for their expression of several proteins related to amyloidogenic processing (Results, Chapter 1) and SK-N-BE(2) and GI-ME-N cells were selected. They were plated in 6-well culture plates at a density of 300 thousand and 500 thousand respectively. The next day, each well was infected in two rounds about 8 h apart with 2 ml supernatant per round. SK-N-BE(2) cells were infected with unconcentrated supernatant cultured for 72 h. For GI-ME-N cells, 10 ml supernatant was concentrated down to 2 ml, so that each well of the 6-well plate was infected with a total of 20 ml unconcentrated supernatant. All supernatants were supplemented with 8 µg/ml polybrene. Twenty-four hours after the first infection round, the virus was taken off and the cells were left to recover for two days before being split into selection medium, supplemented with 800 and 300 µg/ml G418 respectively for SK-N-BE(2) and GI-ME-N. Within two weeks successfully infected cells had formed colonies and were expanded.

2.10. Western Blotting (WB) of Cell Lysates

Baseline protein expression and overexpression of APP/BACE1 constructs was confirmed via WB from cell lysates. Please refer to Sections 13.2 and 11.1.2 respectively for WB protocols for cell-secreted and brain-derived Aβ. All materials are from ThermoFisher Scientific unless otherwise stated.

2.10.1. Lysate and Sample Preparation

Cells were grown in 10-cm culture dishes to confluence. The medium was removed and the cells were washed twice with cold sterile DPBS. All liquid was aspirated and 1.5 ml cold radio immunoprecipitation assay (RIPA) lysis buffer, freshly supplemented with 4 µl/ml benzonase (25-29 U/µl, Merck Millipore, Cat.# 70664-3) and 10 µl/ml 100x Protease Inhibitor (PI) Cocktail Mix (Calbiochem, Cat.# 535142), was added per dish. The buffer was prepared with Triton X-100 (Sigma Aldrich, Cat.# T8787-250ML) and the components of 1x Cocktail Mix are: 500 µM 4-(2-aminoethyl)benzenesulfonyl fluoride hydrochloride (AEBSF), 150 nM animal-free aprotinin, 1 µM E-64 protease inhibitor, 0.5 mM disodium EDTA, and 1 µM leupeptin hemisulfate. The dishes were floated onto an ice-water bath and rocked every 3-4 min. After 20 min the lysates were transferred to Eppendorf tubes and were centrifuged for 20 min at full speed and 4°C in a table-top centrifuge. The supernatant was transferred to clean Eppendorf tubes and stored at -70°C for quantification via the BCA (bicinchoninic acid) Assay kit (Cat.# 23225) and for further use. After quantification of their protein content, the lysates were mixed with equal volumes of 2x Novex SDS (sodium dodecyl sulfate) sample buffer (Cat.# LC2676), containing 4% β-mercaptoethanol (Sigma-Aldrich, Cat.# M-3148), and were completely denatured for blotting by boiling at 100°C for 5 min.

2.10.2. Antibodies

The following two tables provide a full list of antibodies used in WB of cell lysate and immunoprecipitation of Aβ (IP, see Sections 13.1 and 13.2) and their working concentrations. Antibodies used for brain-derived Aβ blotting and other techniques will be specified where appropriate.

Table 5. Antibodies for WB and IP.

Clone	Target	Species	Clonality	Supplier	Cat.#
22C11	APP N-terminus 66-81	Mouse	Mono	Merck Millipore	MAB348

4G8 (Purified)	Aβ 17-24	Mouse	Mono	Biolegend	800701
6E10 (Purified)	Aβ 1-16	Mouse	Mono	Biolegend	803002
Biotin-6E10 (Purified)	Aβ 1-16	Mouse	Mono	Biolegend	803007
Anti-APH1α	APH1α 50-150	Rabbit	Poly	Abcam	ab12104
EPR3956	BACE1	Rabbit	Mono	Abcam	ab108394
2Q1055	B-actin 50-70	Mouse	Mono	Abcam	ab14128
Anti-GAPDH	Mouse GAPDH 314-333	Rabbit	Poly	Sigma-Aldrich	G9545
9C3	NCSTN, C-terminal 18 res.	Mouse	Mono	Merck Millipore	MAB5556
Anti-PEN2	PEN2	Rabbit	Poly	Cell Signalling	5451
PS1-loop	PS1 263-378	Mouse	Mono	Merck Millipore	MAB5232

Table 6. Working concentrations of WB antibodies.

Antibody	WB Concentration
22C11	0.2 µg/ml
Biotin-6E10 (Purified)	1 µg/ml
Anti-APH1α	0.5 µg/ml
EPR3956	0.17 µg/ml
2Q1055	0.1 µg/ml
Anti-GAPDH	0.1 µg/ml
9C3	0.2 µg/ml
Anti-PEN2	0.16 µg/ml
PS1-loop	1.5 µg/ml

2.10.3. Gel Loading, Running, and Blotting

Fifteen µg of cell lysate in a volume of 40 µl were loaded per well in a 10-well Bolt 4-12% Bis-Tris Plus Gel (Cat.# NW04120BOX). Five µl SeeBlue Plus2 Pre-stained protein standard

(Cat.# LC5925) were used per blot and empty wells were loaded with 10 µl 2x Novex SDS sample buffer or 3 µl ladder. Gels were ran for 35 min at 200 V in 1x Bolt MES (2-(N-morpholino)ethanesulfonic acid) SDS running buffer (Cat.# B0002). They were transferred onto polyvinylidene fluoride (PVDF) membranes (Merck Millipore, Cat.# IPVH00010) for 2 h at 35 V in methanol-containing 1x Tris-Glycine blotting buffer (National Diagnostics, Cat.# EC880).

2.10.4. Probing

All solutions were prepared in 0.05% PBS-T (phosphate buffered saline with Tween 20), which was also used for all washing steps. The blots were blocked for 1 h in 5% milk powder with no added calcium (Sigma-Aldrich, Cat.# 70166-500G). The milk was washed off with three 10-min washes and the membranes were incubated overnight at 4°C on a rocker in primary antibody, diluted in 1% BSA/PBS-T (bovine serum albumin, Sigma-Aldrich, Cat.# A9418-10G; Tween 20 (Sigma-Aldrich, Cat.# P7949-500ML)). The blots were washed three times for 10 minutes before the addition of secondary antibody solutions of 1:10000 (or 1:5000 (stock at 1 µg/ml) for NeutrAvidin-horseradish peroxidase (HRP), ThermoFisher Scientific, Cat.# 31001) in 1% BSA and were left to rock for 1 h at RT. They were again washed as above, carefully drained, and incubated for 2 min with 2-3 ml SuperSignal West Pico chemiluminescent substrate (Cat.# 34080) for hand-developing.

2.10.5. Developing

Membranes were placed in a developer cassette between two sheets of clear plastic. In a dark room a sheet of Kodak Carestream BioMax MR film (Sigma-Aldrich, Cat.# Z350397-50EA) or Amersham Hyperfilm ECL (GE Healthcare, Cat.# 28906836) was put on top of each blot and was exposed for the desired length of time. The film was immersed in Developer solution (Sigma-Aldrich, Cat.# P7042-5GA) for 1 min, rinsed with water, immersed in Fixer solution (Sigma-Aldrich, Cat.# P7167-5GA) for 1 min, rinsed again, and left to dry for analysis.

2.10.6. Stripping and Re-probing for β-actin

After developing, blots from cell lysates were washed once with PBS and then stripped for 15 min at RT in 10 ml Restore PLUS WB stripping buffer (ThermoFisher Scientific, Cat.# 46430). They were again washed once with PBS-T, blocked with 5% milk solution for 15 min, and re-probed for β-actin.

2.10.7. Data Analysis

Blots were quantified using the ImageJ software (Wayne Rasband, version 1.47) according to the following method. The areas surrounding the bands of interest were manually selected to yield sufficient distinction between band and background. Pixel blackness was measured and quantified by the software and reported as greyscale percent intensity, where white is 0% and black is 100%. In every blot, the loading control band with lowest percent intensity was selected as the reference and all loading control values were normalized to it to account for differences in protein content. Subsequently, the band percent intensities of the proteins of interest were divided by the corresponding loading control value to obtain percent expression of the protein of interest compared to the expression of the control protein. When comparing expression of proteins with respect to a control cell line, a final normalization step was performed where the thus obtained percent expression of the protein of interest was divided by the corresponding value for the control cell line and the resulting ratio was reported as fold difference, not percent expression.

The statistical analysis and graphs were generated in Microsoft Excel. Differences between samples were analyzed in the SPSS software (IBM, version 22) using the one-way analysis of variance (ANOVA) test. Errors due to multiple comparisons were corrected with the post-hoc Bonferroni method. Where outlier values were excluded from analysis, those were different by at least ten-fold from the remaining replicates in the group. In addition, statistical analyses for significance only include cell lines where expression was evident, in order to more accurately assess the differences between positive lines. Results are reported as averages with the corresponding standard error of the mean (SEM).

2.11. Mouse Intracerebral Seeding with AD Brain

Human AD and control brain samples were obtained and their capability to induce amyloidosis in transgenic mice was tested. Young NL-F animals were intracerebrally inoculated with human brain homogenates and after a period of aging were evaluated for the accretion of Aβ-positive material.

2.11.1. Human Brain Samples

2.11.1.1. Source and Preparation

An internal material transfer agreement was completed for the legitimate use of human AD brain with proven seeding activity and a non-diseased control. The study was ethically

approved by the North East – Newcastle & North Tyneside 2 Research Ethics Committee, REC Ref: 11/NE/0348. All samples were originally obtained under approved material transfer agreements (MTAs) and were handled according to authorized risk assessment and standard operating procedures. Post-mortem AD brain sample PDG 38623 was derived from the frontal cortex of a 76-year-old female with disease clinical duration of 11 years. At death AD had progressed to Braak stage VI. Secondary pathology was manifest as CAA and TDP-43 proteinopathy. The sample was originally supplied by the Queen Square Brain Bank for Neurological Disorders, UCL Institute of Neurology. Disease was confirmed by anonymized clinical and histology reports. Control brain sample PDG 55084 was derived from the same brain region of a 41-year-old male. It was originally supplied by the Oxford Brain Bank, University of Oxford and Oxford University Hospitals NHS Trust and the same clinical reports were provided to confirm disease and genetic risk factor absence. The ApoE genotype was established as 2/3. Grey matter from the samples was homogenized to 10% w/v in DPBS without Ca^{2+} or Mg^{2+} with a glass Duall tissue grinder (Anachem) for mouse and cell seeding experiments. The samples were prepared in this way and provided by Dr. Jonathan Wadsworth.

2.11.1.2. WB for Aβ in AD and Control Brain

The following protocol was adapted from Wadsworth et al. 2008. AD and control brain 10% homogenates were prepared for WB by mixing 20 µl of each sample together with 1 µl benzonase and incubating them for 10 min at RT to reduce viscosity. Subsequently, 21 µl 2x SDS sample buffer/4% β-mercaptoethanol were added to the homogenates and were boiled at 100°C for 10 min. Ten µl of each brain sample were ran alongside 10 µl SeeBlue Pre-stained protein standard (ThermoFisher Scientific, Cat.# LC5625) on a 10-well Novex 16% Tris-Glycine gel (ThermoFisher Scientific, Cat.# XP00160BOX) for 70 min at 200 V. Proteins were transferred onto a PVDF membrane as in Section 10.3 and the membrane was blocked as in Section 10.4 The primary antibody used for probing was 82E1 anti-human Aβ mouse IgG1 antibody (Immuno-Biological Laboratories, Cat.# 10323) at a concentration of 0.2 µg/ml and the secondary antibody was goat anti-mouse IgG (Fab specific) alkaline phosphatase (Sigma-Aldrich, Cat.# A2179) at a dilution of 1:10000. Both antibodies were diluted in PBS-T only. CDP-Star chemiluminescent substrate (Sigma-Aldrich, Cat.# C0712-100ML) and Kodak Carestream BioMax MR film were used for revelation.

2.11.2. Mice

2.11.2.1. Source

APP NL-F knock-in mice, which express the Swedish and Iberian APP mutations on an unmodified background, were obtained from Dr. Takaomi C. Saido and Dr. Takashi Saito (Laboratory for Proteolytic Neuroscience, RIKEN Brain Science Institute, Japan) under an approved joint MTA with Dr. Dominic Walsh. The mice were bred, maintained, and genotyped by Mr. Michael Farmer. All experiments were performed in accordance with the Animals Scientific Procedures Act 1986 with an established Home Office project license by Dr. Silvia Purro, who also kindly provided the following protocols.

2.11.2.2. Intracerebral Inoculation

Human brain homogenates were diluted to 1% w/v in DPBS without Ca^{2+} or Mg^{2+} for intracerebral inoculation. Female NL-F animals were injected in the right hemisphere with 30 µl 1% homogenate and were culled according to Schedule 1 four months later. The brain was harvested and the inoculated hemisphere was preserved for biochemical experiments, while the left hemisphere was prepared for immunohistochemistry.

2.11.2.3. Immunohistochemistry of Seeded Mouse Brain

All work was carried out by Ms. Tamsin Wilkins. Brain tissue was fixed with 10% buffered formal saline and was embedded in paraffin on a Leica Microsystems embedding machine. Serial slices with thickness of 5 µm were taken for staining with hematoxylin and eosin and 0.2 µg/ml biotinylated 82E1 anti-human Aβ mouse IgG1 antibody (Immuno-Biological Laboratories, Cat.# 10326). Slides were automatically revealed via diaminobenzidine treatment, imaged on a Ventana Discovery automated immunohistochemical staining machine (Roche), and scanned at 40x magnification and 65% export image compression on a SCN400F scanner (Leica). All files were stored and managed using the SlidePath application (Leica).

2.12. Seeding of SK-N.NL-F, 7PA2, and GI-ME-N Cells with Human AD and Control Brain

To assess whether the APP/BACE1 overexpressing cells were capable of propagating Aβ seeds, they were inoculated with the AD and control brain homogenate described in Section 11. Cells were plated in a 96-well format at a concentration of 20 thousand per well and were left to attach and recover overnight. AD and control brain homogenates were diluted to 1% in DPBS without Ca^{2+} or Mg^{2+} from their stock concentration of 10%. Subse-

quently, four AD brain (1:300, 1:500, 1:1000, and 1:5000) and two control brain (1:300 and 1:500) dilutions were prepared from the 1% stock using complete cell-appropriate medium. A positive control dilution of 100 nM ADDLs (described in Section 13.5.1) was also prepared. All medium was aspirated and 270 µl of seed solution were pipetted in quadruplicate onto each cell line. The seeded medium was incubated for 24 h and was then collected and frozen as below (Section 13.1). This medium was designated P0. The cells were then washed once with DPBS and 270 µl serum-free medium were incubated in each well overnight. The medium was collected, designated P1, and the cells were split with 20 µl StemPro Accutase cell dissociation solution (ThermoFisher Scientific, Cat.# A1110501) and 250 µl complete medium into a fresh 96-well plate (1:6 split) and into 8-well chamber slides (1:3.75 split, see section 14.5.1 below). The cells were left to reach confluence and were split twice more in this way; 270 µl serum-free medium per well were also collected before each split (P2 and P3) and once before the cells were discarded (P4). The oligomeric Aβ content of the medium was then analyzed by ELISA (Section 13.5) and the cells in chamber slides were fixed and analyzed by immunocytochemistry (Section 13.6).

2.13. Aβ Quantification

2.13.1. Culturing of Cell Medium

Secreted Aβ accumulates in the cell medium over time, so this was cultured to quantify the levels of the peptide. Cells were plated in 10-cm dishes at high densities to reach 95-100% confluence overnight. All medium was removed; cells were washed with sterile DPBS and were incubated in 5 ml serum-free medium for 17-24 h. Cultured medium (CM) was transferred to 15-ml polypropylene Falcon tubes and was supplemented with 1x PI Cocktail Mix (see Section 10.1). On several occasions where the cells needed to be cultured in a 96-well format for seeding with AD and control brain and ADDLs (see Section 12 above), 270 µl serum-free medium per well was conditioned and was collected in Protein LoBind Eppendorf tubes (Scientific Laboratory Supplies, Cat.# E0030108116) before the addition of 1x PI Cocktail Mix. The tubes were centrifuged for 10 min at 300 *g*, 4^{o}C to pellet dead cells. CM was aliquoted in Protein LoBind Eppendorf tubes and was frozen at -70^{o}C or used fresh for IP or quantification via ELISA.

2.13.2. IP and WB for CM-derived Aβ

Aβ was immunoprecipitated from CM for WB using magnetic µMACS Protein G MicroBeads (Miltenyi Biotec, Cat.# 130-071-101). CM was mixed with 1 µg each of 6E10 and 4G8 anti-Aβ antibody (Table 5). Fifty µl MicroBeads were added to the medium, mixed by

inversion, and incubated on ice for 30 min. Filtration µ Columns (Miltenyi Biotec, Cat.# 130-042-701) were placed on a magnetic stand and were equilibrated with 200 µl cold RIPA buffer. The medium/MicroBeads mixture was pipetted onto the columns and was eluted by gravity flow. The columns were washed four times with 400 µl 0.01% PBS-T. The residual PBS-T was eluted with 20 µl 1x Novex SDS sample buffer (4% β-mercaptoethanol) pre-heated to 95^{o}C. The captured Aβ was eluted in 100 µl of the same buffer for WB.

For WB, all steps were carried out as in Sections 10.3 and 10.4 with the following modifications. Forty µl of IP product were loaded per gel well and ran and blotted as above. In preparation for Aβ probing, membranes were individually submerged in clean plastic containers filled with ~250 ml DPBS and were boiled in a microwave for 1.5 min at maximum power. They were left to stand for 3.5 min, were turned over, and were boiled again under the same conditions. Membranes were incubated in the boiling DPBS for another 3.5 min and were washed with double-distilled water for blocking. Finally, 1 µg/ml biotinylated 6E10 antibody was used for probing and was detected with NeutrAvidin-HRP as in Section 2.10.4.

2.13.3. Total Aβ Quantification in CM and Brain

Estimated total Aβ amounts from CM and brain fractions were quantified using the V-Plex Aβ Peptide Panel 6E10 Kit (Meso Scale Discovery, Cat.# K15200E). This 96-well ELISA detects monomeric Aβ1-38, 1-40, and 1-42. Each well contains four spots, one BSA-blocked and three singly-coated with proprietary antibodies specific for each of the Aβ species above. The detection antibody is pan-Aβ 6E10, conjugated with an electrochemiluminescent MSD SULFO-TAG. Monomeric 40x preparations of synthetic Aβ1-38, 1-40, and 1-42 with lot-specific concentrations are supplied with each kit to calibrate the plates. The concentrations of the standards in the kit used for these experiments are 10775, 14975, and 1333 pg/ml for Aβ1-38, 1-40, and 1-42 respectively. The three peptides are mixed together to 1x their concentration in a volume of Diluent 35 (supplied with the kit) and are serially diluted 4-fold to prepare standards 1-7. Standard 8 is Diluent 35 only. Similarly, samples and controls need to be diluted at least 1:1 in Diluent 35 before they are applied to the plate. Detection antibody 6E10 is provided at 50x concentration and the 1x working solution is prepared with Diluent 100 (supplied with the kit).

To begin the experiment, the ELISA plate was blocked with 150 µl Diluent 35 per well on a rocker for at least an hour at RT, although overnight blocking is also possible. In the meantime, calibrators, samples, controls, and antibody were diluted as appropriate. All Aβ

standards were thoroughly vortexed before pipetting. The plate was washed three times with 0.05% PBS-T and 25 µl of 6E10 solution was added, followed by 25 µl of diluted calibrator, sample, or control in triplicate. It was then sealed and left to shake for 2 h at RT. A solution of 2x Read Buffer T (in the kit) was prepared during the incubation; the plate was washed three times as above, and 150 µl of read buffer were added per well. Fluorescence was read in a MESO SECTOR S 600 plate reader (Meso Scale Discovery). Data were analyzed in the manufacturer's software, MSD Discovery Workbench v. 4.0.12. The quantified fluorescence intensity was plotted against the known calibrator concentration to produce separate standards curves for Aβ1-38, 1-40, and 1-42. The concentration of each Aβ species was read off the corresponding standard curve and was reported as pg/ml.

2.13.4. Mass Spectrometry

Mass spectrometry was used to comprehensively characterize the Aβ signature of each overexpressing line. CM was shipped by Mr. Jamie Toombs and received by Prof. Henrik Zetterberg. The experiments and data normalization were carried out by Dr. Erik Portelius and Ms. Rita Persson. The full Aβ content from 1 ml CM was immunoprecipitated with 6E10 and 4G8 antibodies as described previously (Portelius et al. 2007). Briefly, 50 µl magnetic Dynabeads M-280 Sheep Anti-Mouse IgG (ThermoFisher Scientific, Cat.# 11201D) per sample were coupled with 4 µg of each antibody. Approximately 10 µl of 0.025% PBS-T were added to each CM sample before mixing with the antibody-coupled beads. The samples were then washed in three sequential washes with 0.025% PBS-T, PBS only, and 50 mM ammonium hydrogen carbonate (pH 8.0) in a KingFisher magnetic particle processor (ThermoFisher Scientific) and were eluted with 100 µl 0.5% formic acid. Matrix-assisted-laser-desorption/ionization time-of-flight/time-of-flight (MALDI TOF/TOF) mass-spectrometry was performed twice per sample on an ultrafleXtreme machine (Bruker Daltonics) to produce a peak area intensity reading for each peptide. The peak areas were then normalized to the sum area of Aβ peptides found in each sample to estimate the proportional contribution each species has to the total Aβ signature. The data were reported as percent normalized peak area. It is important to note that as ionization efficiency and hydrophobicity properties vary among isoforms, the measurements thus obtained are not accurate representations of the true amounts and breakdown of the Aβ species, but are relative quantifications.

2.13.5. Sandwich ELISA for Aβ Oligomers

An ELISA specific for AβO was established to detect their presence in cell CM. The ELISA relies on the same anti-Aβ antibody used for both capture and detection, as monomers will only have one binding site available.

2.13.5.1. Preparation and Quality Control of ADDLs

The following protocol was devised by the MRC Prion Unit's Amyloid Beta Project group, previously headed by Dr. Andrew Nicoll and the preparation of the ADDLs batch used for this project was handled by Dr. Clare Sarell and Mr. Emmanuel Risse. Approximately 15 g of purified lyophilized dry weight synthetic Aβ1-42 monomeric peptide (The ERI Amyloid Laboratory, LLC) was dissolved in 2% anhydrous DMSO by gently rolling the tube for 5 min. The monomer was then diluted to a final concentration of 0.5 mg/ml with warmed phenol red and L-glutamine-free Ham's F12 medium. The solution was then left to aggregate overnight on the bench at RT without shaking. After approximately 16 h, the oligomer content of the aggregated sample was characterized. To do this, a 150 µl aliquot was centrifuged at full speed in a table-top centrifuge and the top 100 µl were collected and run through a 1260 Infinity Liquid Chromatography system (Agilent), coupled with an Eclipse 3+ AF4 asymmetric-flow field-flow fractionation instrument (Wyatt Technology). The sample was injected into the AF4 channel fitted with a 10 kDa membrane and ran for 45 min at a speed of 1 ml/min and 1.5 ml/min cross flow, with 10 mM sodium acetate, pH 5.5 as the vehicle buffer. Oligomer size was estimated via light scattering and UV refraction at 275 nm with an Optilab T-rEX refractometer (Wyatt Technology) and molecular weight was further quantified with a DAWN HELEOS II multi-angle static light scattering (MALS) detector (Wyatt Technology). If the monomer concentration in solution was above 20%, the sample was tested at subsequent time points until this cutoff was reached. The sample was then divided into 2 ml aliquots, centrifuged again for 20 min at RT, the top 1.9 ml were pooled, re-aliquoted, and frozen at -70^{o}C.

2.13.5.2. Preparation of Aβ1-40 Monomer

The following protocol is an alternative method developed by the Amyloid Beta Project group to generate small batches of ADDLs and in the present work it was shortened to prepare a solution of Aβ1-40 monomer (The ERI Amyloid Laboratory, LLC). Purified lyophilized synthetic peptide was dissolved in ice-cold hexafluoro-2-propanol (HFIP, Sigma-Aldrich, Cat.# H8508)) in a fume hood to a concentration of 1 mM to reduce aggregates which may have formed to monomers. The vial was sealed, sonicated in a water bath for 5

min, and was then left at RT for 1 h so the peptide could fully dissolve. The solution was then transferred to a glass vial and the HFIP was left to evaporate in a fume hood, leaving a clear film of peptide at the bottom. Any residual HFIP was removed by blasting the vial with dry air. The peptide film was then dissolved by vortexing at full speed for 10 min in anhydrous DMSO to a concentration of 5 mM. Every 2-3 min the vial was swirled to make sure the DMSO droplet covers the entire surface of the film. Finally, the monomer solution was further diluted to a stock concentration of 100 µM in Ham's F12 phenol-red and L-glutamate-free medium (Promocell, Cat.# C-72117) and was frozen at -70°C in aliquots.

2.13.5.3. Preparation of Aβ1-11 Dimer Standard

A synthetic dimer with the Aβ1-11 sequence (DAEFRHDSGYE), C-terminally linked via a cysteine residue as described in Hölttä et al. 2013 was custom-ordered from rPeptide and supplied by Stratech. The peptide was purified by high-performance liquid chromatography and was lyophilized. According to the manufacturer's recommendations, the powder was reconstituted in 50:50 v/v H_2O and acetonitrile to a stock concentration of 1 mg/ml. The sample was briefly sonicated before being aliquoted and stored at -70°C.

2.13.5.4. ELISA Setup

The following protocol was published in Hölttä et al. 2013 and was adapted for the present work as necessary. A 96-well clear, flat-bottomed, chimney-well high-binding polystyrene microplate (Greiner Bio, Cat.# 655081) was coated overnight at 4°C with 1 µg/ml, 50 µl/well 82E1 antibody, diluted in 50 mM $NaHCO_3$ buffer, pH 9.6. The plate was washed five times with 300 µl/well 0.05% PBS-T and was blocked for 1 h at RT with 150 µl/well 2% BSA/PBS-T. In the meantime, the Aβ1-11 dimer standards were diluted in 0.1% BSA/PBS-T. The standard curve was made up of 2-fold dilutions, ranging from 3678 to 3.6 pg/ml. After blocking, the plate was washed as above and 50 µl/well of standard or sample were pipetted in triplicate. These were also incubated for 1 h at RT and were washed off as above. Biotinylated 82E1 was diluted to 0.75 µg/ml in 0.1% BSA/PBS-T, 50 µl/well and was incubated for 1 h at RT. It was washed as above and 0.2 µg/ml, 50 µl/well NeutrAvidin-HRP were added to the plate, which was then incubated for 1 h at RT. TMB (3,3',5,5'-tetramethylbenzidine) colorimetric substrate (1-Step Ultra TMB-ELISA Substrate Solution, ThermoFisher Scientific, Cat.# 34028) was equilibrated at RT for at least 30 minutes before reading. The plate was washed five times after the final antibody incubation, 100 µl TMB were added to each well, and were incubated for 15 min. The color reaction was

stopped with 100 µl/well 2 M H_2SO_4 and the plate was read at 450 nm in an Infinite M1000 Pro plate reader (TECAN).

2.13.5.5. ELISA Analysis

The data were analyzed and the graphs were generated in Microsoft Excel. The average reading from the three technical replicates and the standard deviation for each standard were calculated to determine each one's percent coefficient of variation (%CV). The lower limit of detection (LLOD) was calculated as 2.5 times the standard deviation of the blank standard. The acceptable limits for each sample's %CV value were then taken to fall between the LLOD percentage and 10%. The standard curve was plotted and the region of linearity with the best R-square value was determined empirically. The estimated concentration for each standard was calculated from the plot equation and was divided by the assigned concentration to assess their similarity (% backfit). The lower limit and upper limits of quantification (LLOQ and ULOQ) were set to fall between 80 and 120% of the % backfit values. The concentration of each sample was then determined according to the above limits.

2.13.6. Immunocytochemistry

In order to visualize and quantify intracellular uptake and clearance or propagation of AD brain-derived Aβ seeds, seeded cells were fixed, stained, and imaged using confocal microscopy.

2.13.6.1. Sample Preparation and Staining

Cells seeded with AD and control brain and ADDLs were plated in Nunc Lab-Tek 8-well chamber slides (ThermoFisher Scientific, Cat.# 155411) after a 1:3.75 split from a well of a 96-well plate (80 µl from 270 µl, see Section 12). They were grown until confluence, the medium was washed off with sterile DPBS, and 200 µl 1:1000 solution of Deep Red CellMask plasma membrane stain (ThermoFisher Scientific, Cat. # C10046) in serum-free medium was incubated in each well for 10 min. The solution was completely aspirated and the cells were fixed with 3.8% formaldehyde (Sigma-Aldrich, Cat.# F8775-500ML) for 12 min. The formaldehyde was completely aspirated and 200 µl 0.1% Triton X-100 in DPBS were added per well to permeabilize the cells. After 15 min, this solution was removed and the cells were stained with 200 µl/well 0.4 µg/ml (1:250) 82E1 antibody at 4°C for 24 h. The primary antibody was aspirated and a solution of 1 µg/ml (1:1000) Alexa Fluor 488 (AF 488) AffiniPure goat anti-mouse secondary antibody (Jackson ImmunoResearch, Cat.# 115-545-166) and 0.1 µg/ml (1:10000) 4',6-diamidino-2-phenylindole, dihydrochloride

(DAPI) nuclear stain was added at 200 µl/well and incubated overnight at 4^{O}C. Finally, the secondary antibody solution was aspirated, wells were filled with 1% Pen-Strep/DPBS, and the slides were stored in a fridge until imaging.

2.13.6.2. Imaging

Fixed seeded cells were imaged on an LSM710 confocal microscope (Zeiss) on a plan-apochromat 40x/1.4 Oil DIC M27 oil objective with Immersol 518 F immersion oil (Zeiss, Cat.# 12737327) and the ZEN 2.3 (black) software, v. 13.0.0518 (Zeiss). The imaging conditions were optimized to exclude noise for the cell line with the brightest Aβ signal and were then used for all lines. Z-stack images were taken at a distance of 1 – 0.64 µm through the cell layer. Where cell layers were particularly thick and this distance was not optimal, a fixed number of image slices (16 – 18) was used. A summary of the laser conditions is provided in Table 6 below, although occasionally the gain or laser power of the DAPI and CellMask channels needed to be adjusted to compensate for particularly strong staining. Each slice was an average of 4 measurements and z-stacks were saved at a depth of 16-bit. Six z-stacks were taken per seeding condition.

Table 7. Summary of laser specifications.

Laser	Target	Wavelength	Master Gain	Digital Offset	Power
Diode 405-30	DAPI	405 nm	583	-42537.77	2%
Argon	AF 488	488 nm	630	-5040.00	2%
HeNe633	CellMask	633 nm	861	-27594.00	1.2%

2.13.6.3. Image Analysis

Z-stacks were analyzed with the Volocity software, v. 5.5 (PerkinElmer). The volume of AF 488 green signal, which represents Aβ seed load, was summed for each z-stack and was normalized by cell number. Table 7 below provides detailed descriptions of the Volocity protocols for quantifying Aβ spots and number of cells. The normalized signal from the six z-stacks per seeding condition was then averaged and reported as µm^3/cell with SEM. Statistical analysis of the singular and combined effects of split number and seeding conditions on Aβ load was done in the SPSS software using two-way ANOVA tests and the Bonferroni correction for multiple and pairwise comparisons. Graphs were generated with Microsoft Excel.

Table 8. Volocity protocol for quantification of Aβ spots across Z-stacks for 7PA2 cells.

Cell Line and Task	Step	Details
SK-N.NL-F Seeded Aβ Spots	Find Objects, Channel ChS1-T2	Threshold using Intensity: Lower 2363/Upper 65535
		Minimum object size: 0.205 μm^3
7PA2 Seeded Aβ Spots	Find Objects, Channel ChS1-T2	Threshold using Intensity: Lower 5099/Upper 65535
		Minimum object size: 0 μm^3
GI-ME-N Seeded Aβ Spots	Find Objects, Channel ChS1-T2	Threshold using Intensity: Lower 1741/Upper 65535
		Minimum object size: 0.111 μm^3
SK-N.NL-F Nuclear Count	Find Objects, Channel Ch1-T1	Threshold using Intensity: Lower 10695/Upper 65535
		Minimum object size: 80 μm^3
	Remove Noise from Objects	Coarse filter
	Separate Touching Objects	Object size guide: 250 μm^3
	Exclude Objects by Size	< 80 μm^3
7PA2 Nuclear Count	Find Objects, Channel Ch1-T1	Threshold using Intensity: Lower 15793/Upper 65535
		Minimum object size: 50 μm^3
	Remove Noise from Objects	Medium filter
	Separate Touching Objects	Object size guide: 100 μm^3
	Exclude Objects by Size	< 9 μm^3
GI-ME-N Nuclear Count	Find Objects, Channel Ch1-T1	Threshold using Intensity: Lower 6715/Upper 65535
		Minimum object size: 300 μm^3
	Fill Holes in Objects	N/A
	Remove Noise from Objects	Fine filter
	Separate Touching Objects	Object size guide: 400 μm^3
	Exclude Objects by Size	< 230 μm^3

3. Characterization and Selection of Human Neuroblastoma Cell Lines as a Platform for the Model

3.1. Establishment of Culture Conditions

3.1.1. Media Selection

Eleven human neuroblastoma cell lines were purchased from the Leibniz institute DSMZ (German Collection of Microorganisms and Cell Cultures GmbH) and from Sigma-Aldrich to test their suitability as an AβO propagation model. The culture conditions described by the supplier were different for most lines and adhering to them strictly would have impeded work flow. I reviewed the literature for published culturing protocols and compared them to those provided by the supplier. DMEM, DMEM/F12, and RPMI 1640 were the three most frequently used media, 10% FBS was the most commonly used serum supplement concentration, and 5% Pen-Strep the most prevalent antibiotic. I therefore set up culturing experiments to compare the lines' compatibility to these nutrient mixtures. Each line was cultured with each medium in a 6-well format to observe the cells' growth and morphologies. It is necessary to point out that for this assessment of overall cell behavior no quantifications of doubling times, cell counts, etc. were performed and all observations were done empirically. Six lines (BE(2)-M17, NBL-S, NGP, NMB, SH-SY5Y, and SK-N-BE(2)) performed best in DMEM/F12, while the remaining five (CHP-134, GI-ME-N, IMR-32, KELLY, and LS) grew better in RPMI 1640. DMEM was always inferior to DMEM/F12 or RPMI 1640. In addition, four cell lines (GI-ME-N, LS, SH-SY5Y, and SK-N-BE(2)) were too adherent for resuspension by pipetting and required 0.05% Trypsin/EDTA for splitting. See Table 1 in Materials and Methods for a summary of all conditions established by this experiment.

3.1.2. Morphology and Behavior

The lines were markedly different in their morphologies, proliferation speed, and sensitivity to passaging (Table 8). BE(2)-M17, GI-ME-N, LS, SH-SY5Y, and SK-N-BE(2) grew in monolayers and were noticeably more tolerant to splitting than the other six lines. Among these, GI-ME-N and SK-N-BE(2) were particularly adherent and together with BE(2)-M17 had the fastest doubling times of approximately three days after a 1:10 split from a 10-cm Petri dish. LS and SH-SY5Y cells typically required five days to reach confluence after the same split ratio. Interestingly, growth in all of the above lines tended to slow after several splits, particularly in GI-ME-N and SH-SY5Y cells. In addition, BE(2)-M17 cells, which do not

adhere to each other when confluent, were interconnected by neuronal-like processes, similarly to CHP-134 and NBL-S cells.

CHP-134 cells had the highest counts from a confluent 10-cm dish, as they were the smallest among all eleven lines. However, despite their large numbers and distinct morphology, they were deemed unsuitable for future work because of their high mortality after each passage. NBL-S cells were interesting in that they had the slowest doubling times and grew in dense colonies, which slowly merged together through extending processes as they expanded. Nevertheless, as the aim is to create a high-throughput model which would ideally rely on rapidly dividing cells, I did not continue with the NBL-S line. Three of the cell lines, NMB, NGP, and IMR-32, were also deemed unsuitable as they grew in clumps and detached from the substratum despite a healthy appearance. Finally, KELLY cells were average in all parameters and did not demonstrate any distinct characteristics.

Table 9. Summary of culture properties of eleven human neuroblastoma lines.

Cell Line	Growth	Adherence	Sensitivity to Splitting	Monolayer	Reduced Serum Tolerance	Suitability
BE(2)-M17	Fast	Low	Sensitive	Yes	Excellent	Yes
CHP-134	Average	Low	Tolerant	Yes	Poor	No
GI-ME-N	Average	Very high	Sensitive	Yes	Good	Yes
IMR-32	Slow	Low	Tolerant	No	N/A	No
KELLY	Average	Average	Sensitive	Yes	N/A	No
LS	Average	Average	Sensitive	Yes	Good	Yes
NBL-S	Slow	Low	Average	Yes	Poor	No
NGP	Slow	Low	Tolerant	No	N/A	No
NMB	Slow	Low	Tolerant	No	N/A	No
SH-SY5Y	Average	Average	Average	Yes	Average	Yes
SK-N-BE(2)	Fast	High	Sensitive	Yes	Excellent	Yes

3.1.3. Serum Titration

Following from the culturing experiments described above, the tolerance of the cell lines towards reduced serum and serum-free conditions was tested. Since the quantification of the Aβ and AβO content in tissue culture medium by ELISA is one of the intended methods of analysis, the high protein content of serum is likely to interfere with the immunoassay. A set number of cells (400 thousand, 500 thousand, or 1 million) was plated in a 6-well format with serum concentrations ranging from 10% to 0% and incubated for 4-6 days (Figure 7). SK-N-BE(2) cells were least affected by serum reduction, as no change in morphology and growth rates were observed after 5 days (Figure 7m and 7n). Their sub-

clonal line BE(2)-M17 showed no change in morphology or growth rate after 4 days in all conditions, except 0% serum, where growth was slightly reduced (Figure 7a and 7b). LS cells were more sparse at 2% and 0% FBS with no visible changes in cell morphology (Figure 7g and 7h).

Doubling in SH-SY5Y cells was similarly reduced (Figure 7k vs. 7l); in addition, there was increased mortality at 0% FBS, cells had become more globular, and had begun to extend processes. At 2% and 0% serum, GI-ME-N cells were large, and their nuclei were darker and bulging (Figure 7e). In contrast to other lines, CHP-134 cells were becoming increasingly neuronal-like and at 0% serum had condensed in large compact colonies interconnected by very long axon-like structures (Figure 7c and 7d). Growth in NBL-S cells was slowing down progressively with the reduction of serum and at 0% clumps of cells were floating off, leaving large bare circular patches in the monolayer (Figure 7i and 7j). It is important to note that while there were considerable differences between the appearance and doubling times of the lines over the 4-6-day incubation period, none of them seemed visibly affected by the lack of FBS within a shorter timeframe of 24 h. Therefore, no cells were excluded based on their tolerance to reduced serum conditions.

3.2. Evaluating the Expression of Proteins Related to Amyloidogenic APP Processing in the Selected Cell Lines

After the initial shortlisting of the neuroblastoma lines based on culture conditions, it was necessary to determine their endogenous expression levels of APP and the enzymes responsible for Aβ production, BACE1 and the four components of γ-secretase, to select those that were most likely to favor amyloidogenic processing. In addition, while I deemed CHP-134 and NBL-S cells unsuitable for the model, I decided to include them in the protein analysis, as their behavior and morphology were intriguing.

3.2.1. APP

Denatured lysates from seven cell lines were probed with the N-terminal APP antibody 22C11, which recognizes all isoforms of the full-length protein, sAPPα, sAPPβ, as well as other processing fragments which contain the epitope, but not Aβ. The processing profiles of APP and the overall amounts of full-length protein were visibly different among the seven lines tested. With the exception of GI-ME-N cells, the remaining lines showed the same band patterns two by two: BE(2)-M17 and CHP-134; LS and SK-N-BE(2); and NBL-S and SH-SY5Y (Figure 8a). Two to three distinct bands, corresponding to the molecular weight of the different isoforms of full-length APP and to the sAPP fragments, are detect-

able around the 98 kDa marker in all lines. Notably, BE(2)-M17 and SK-N-BE(2) cells showed the highest expression levels, while expression was particularly low in GI-ME-N cells. In addition, a number of smaller bands between 62 kDa and 55 kDa are visible in GI-ME-N, LS, NBL-S, SH-SY5Y, and SK-N-BE(2) cells. Two bands in the middle between the 49 and 38 kDa markers occur in all lines.

Upon quantification and normalization, the amounts of APP were reported as percent expression relative to endogenous levels of β-actin (Figure 8b). After analysis with a one-way ANOVA and post-hoc corrections, it became apparent that BE(2)-M17 and SK-N-BE(2) lines expressed equal amounts of APP (20% ± 5% and 22% ± 2%), more than twice the levels found in SH-SY5Y cells (9% ± 0.5%, $p < 0.05$ and 0.01 respectively). NBL-S cells expressed 15% ± 1.5% APP, and while the amount in LS cells was half that of NBL-S (8% ± 0.7%), these differences were not significant. CHP-134 cells had the second lowest level of APP among the seven lines (4% ± 1.6%), while GI-ME-N cells revealed negligible amounts of detectable protein (0.4% ± 0.2%). Overall, there was a considerable difference in expression of total APP among the neuroblastoma lines tested ($p < 0.0001$), along with distinct processing profiles shown by the WB.

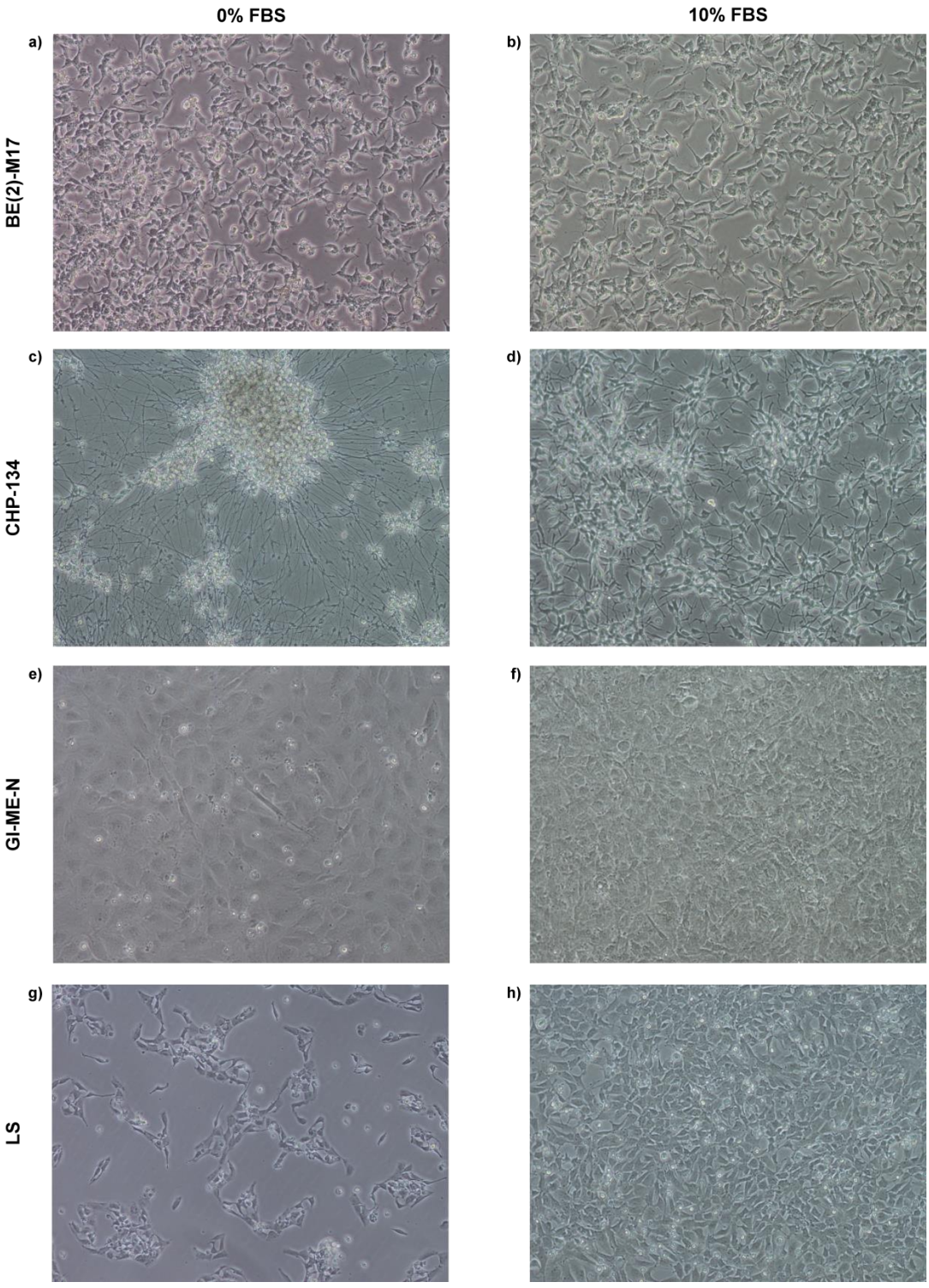

Figure 7. Morphologies of seven human neuroblastoma cell lines under serum-depleted and normal conditions after several days in culture.

a) and **b)** BE(2)-M17, 4 days; **c)** and **d)** CHP-134, 6 days; **e)** and **f)** GI-ME-N, 5 days; **g)** and **h)** LS, 6 days; **i)** and **j)** NBL-S, 5 days; **k)** and **l)** SH-SY5Y, 4 days; **m)** and **n)** SK-N-BE(2), 5 days. *(cont'd overleaf)*

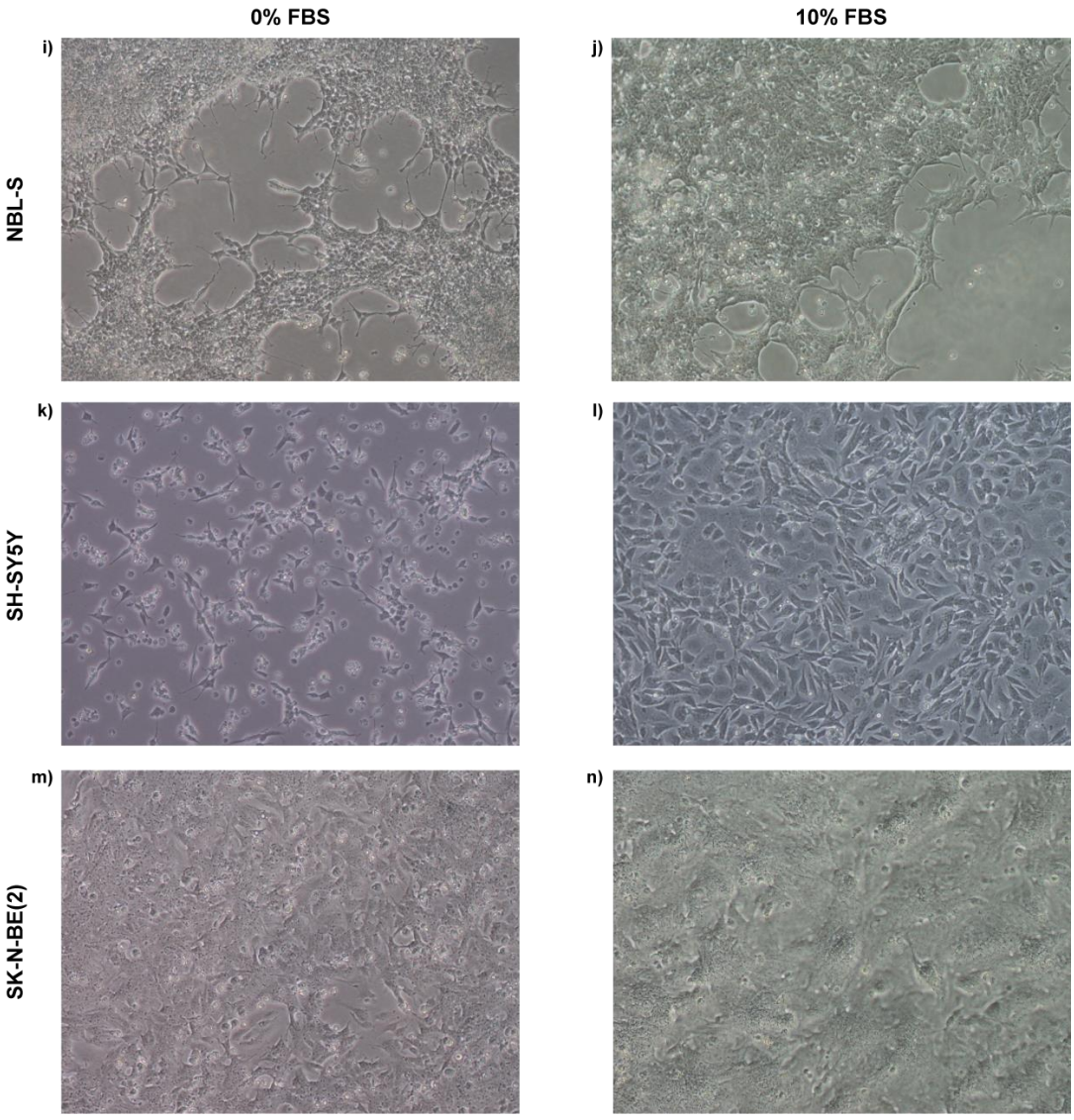
0% FBS
10% FBS
i)
j)
NBL-S
k)
l)
SH-SY5Y
m)
n)
SK-N-BE(2)

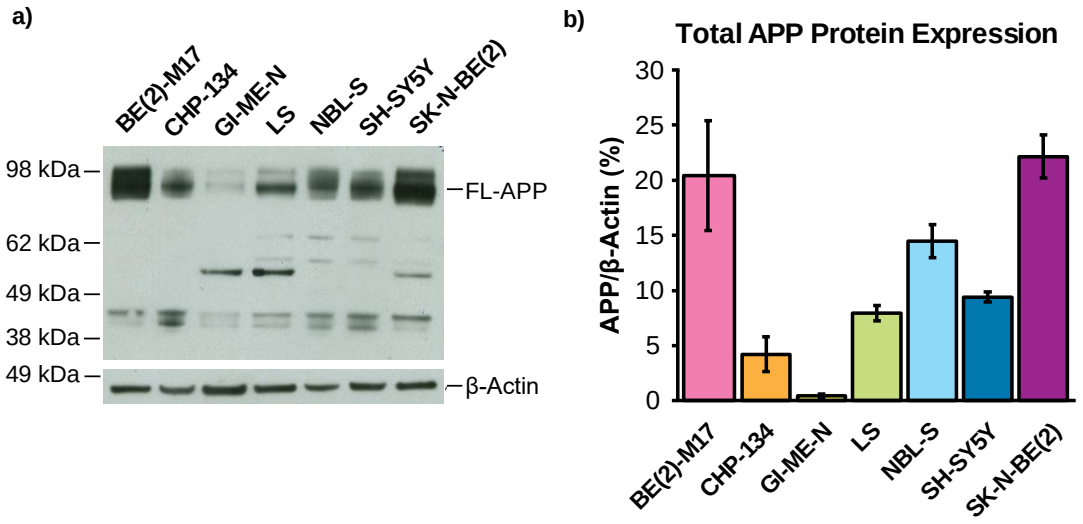

Figure 8. APP expression and processing in seven human neuroblastoma cell lines.

a) APP fragments were detected on WB with antibody 22C11. The housekeeping control β-actin was also probed. The APP blot was exposed for several minutes to obtain sufficient band clarity and β-actin was exposed for 2 s. FL = full-length. **b)** There was a significant difference in APP expression compared to β-actin ($p < 0.0001$, one-way ANOVA, Bonferroni correction for multiple comparisons). An outlier value was excluded from the analysis of BE(2)-M17 cells. N = 4. Error bars represent SEM.

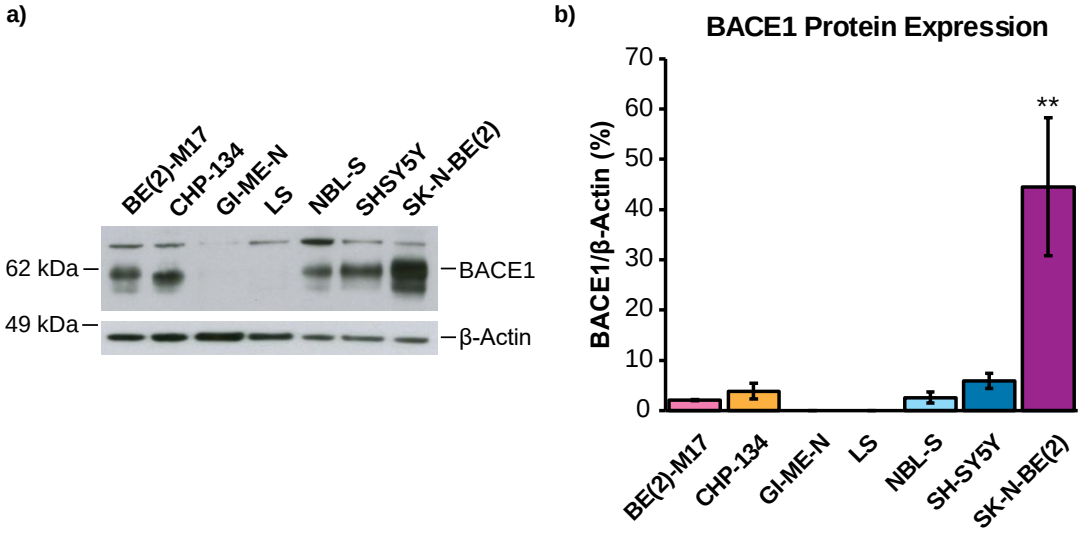

Figure 9. BACE1 expression in seven human neuroblastoma cell lines.

a) Endogenous expression of BACE1 and β-actin control were detected. The BACE1 blot was exposed for 10 min and β-actin for 2 s. **b)** SK-N-BE(2) significantly overexpressed BACE1 compared to other positive cells (** or $p \leq 0.008$, one-way ANOVA, Bonferroni correction), but there were no differences among the remaining lines ($p = 0.22$).GI-ME-N and LS cells were excluded from the analysis because they showed no signal. One excessively high value was excluded from the analysis of BE(2)-M17 cells. N = 4. Error bars represent SEM.

3.2.2. BACE1

Visible levels of BACE1 were detected in five lines, with the notable exception of GI-ME-N and LS cells, where BACE1 was undetectable under the experimental conditions (Figure 9a). Conversely, BACE1 expression in SK-N-BE(2) cells (45% ± 14%, $p < 0.01$) was between nine- and twenty-fold higher than in the remaining four lines with detectable expression levels (Figure 9b). Percent BACE1 compared to β-actin in these lines ranged from 6% ± 1.5% for SH-SY5Y to 2% ± 0.2% for BE(2)-M17 cells. Removing SK-N-BE(2) cells from the one-way ANOVA analysis revealed that BACE1 levels in the remaining four positive lines did not differ significantly ($p = 0.22$).

3.2.3. γ-Secretase

The components of γ-secretase (APH1α, NCSTN, PEN2, and PS1) were readily detectable in all cell lines, with the exception of APH1α (Figure 10a), which was highly expressed relative to β-actin only in CHP-134 (23% ± 5%) and NBL-S (37% ± 7%) and was marginally detectable in SH-SY5Y cells (0.4% ± 0.3%) (Figure 10b). Only one of four biological replicates of GI-ME-N cells showed APH1α traces (0.04%), while no expression was detected in the remaining three lines. Two bands were visible for NCSTN (Figure 10a), reflecting both glycosylation states of the protein, and both isoforms were taken into account when calculating the expression differences between cell lines. NBL-S cells showed highest NCSTN expression after normalization to GAPDH (glyceraldehyde 3-phosphate dehydrogenase; 16% ± 3%), but due to the high degree of signal variability among the replicates, the difference in expression was only significant when compared to BE(2)-M17 (2% ± 1.4%, $p < 0.002$) and GI-ME-N cells (3% ± 1.3%, $p < 0.003$) (Figure 10c). Visually, a strong signal was also observed in SH-SY5Y (12% ± 2%), SK-N-BE(2) (11% ± 3%), and LS cells (7% ± 0.5%), although the last were nearly identical to CHP-134 (7% ± 2%) when quantified. The signal for PEN2 was also highly variable among blots and therefore the analysis showed no statistical differences (Figure 10a and 10d). Nevertheless, LS cells (0.6% ± 0.2%) had consistently low amounts of PEN2, whereas GI-ME-N (7% ± 3%) and SH-SY5Y cells (10% ± 4%) were the strongest expressers (Figure 10d).

As PS1 gets incorporated into the γ-secretase complex, it undergoes self-cleavage between C-terminal TM helices 6 and 7, which exposes the two aspartyl residues that form the catalytic core of the complex (Thinakaran et al. 1996, Wolfe et al. 1999). Therefore, I chose an antibody targeting the loop between these two helices, in order to simultaneously detect both the full-length protein and its cleaved activated variant (e.g. Park et al.

2012, Thinakaran et al. 1996). Activated PS1 was abundant in all cell lines, as indicated by the strong bands migrating at 18 kDa (Figure 10a). Full-length PS1 was also readily visible in all samples as a double band close to the 38 kDa marker. I then used the sum of full-length and cleaved protein to calculate the total amounts of PS1 present in the neuroblastoma cells. However, despite a visible trend for LS and GI-ME-N cells to have less PS1 (both yielded 0.3% ± 0.1% for full-length and 3% ± 0.7% and 4% ± 1% for total respectively), high variability among the replicates did not allow me to establish statistically significant differences in expression between the individual cell lines (Figure 10e). The values for full-length protein in the remaining lines ranged from 2% ± 0.4% in SH-SY5Y to 1% ± 0.3% in SK-N-BE(2) cells and those for total PS1 were between 11% ± 4% in SH-SY5Y to 6% ± 1.7% in BE(2)-M17 cells.

To infer the activation state of γ-secretase, I replotted the data as the ratio of activated to full-length PS1. Interestingly, despite the visibly disparate amounts of PS1 protein, the activation ratios in five of the lines ranged from 4 ± 0.5 for BE(2)-M17 to 6 ± 0.3 for NBL-S, with little overall variability (Figure 10f). What is more, the two lines with lowest values for total PS1 yielded the highest activation ratios, where GI-ME-N cells reached significance at $p < 0.02$ when compared to the remaining five lines and LS did not. These observations may have implications towards the amount and quality of proteolytic processing carried out by γ-secretase and the turnover of its components with respect to their overall expression levels.

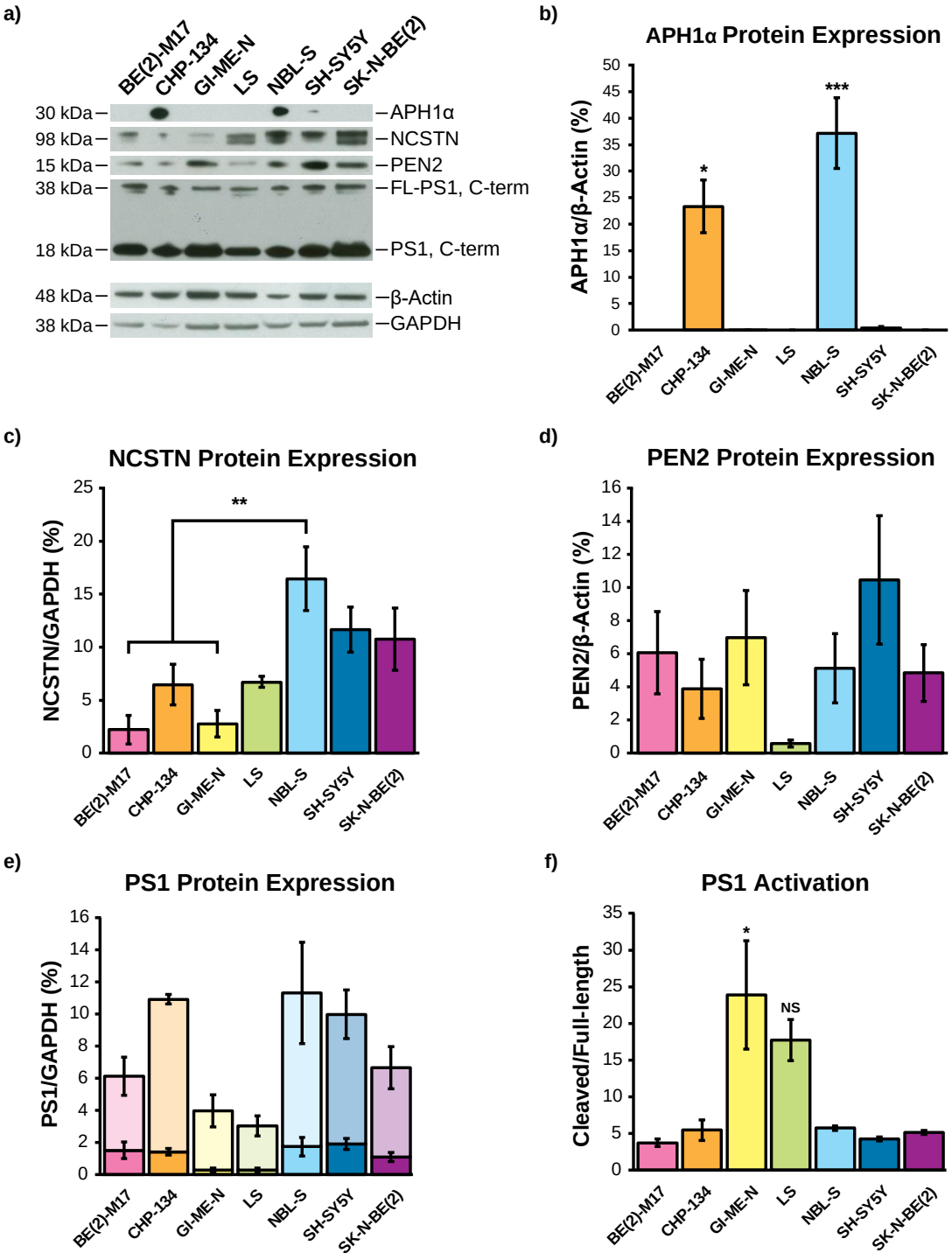

Figure 10. Expression of the γ-secretase components in seven human neuroblastoma cell lines.

a) Representative WBs of the four γ-secretase components and two endogenous controls are shown. **b)** Quantification of APH1α expression showed differences between lines where signal was detected ($p < 0.0001$). **c)** NCSTN was differentially expressed in the seven lines ($p < 0.0001$). **d)** Quantification of PEN2 expression was not significant ($p = 0.20$). **e)** Full-length and activated PS1 were quantified and plotted as fractions of total PS1. Dark shades – full-length. Light shades – activated. One-way ANOVA tests produced marginally significant p values (0.018 for full-length and 0.033 for activated), but post-hoc tests were not significant. **f)** The ratios between activated and

full-length PS1 were taken and plotted as a representation of the activation state of PS1 within the γ-secretase complex. One abnormally high and one low value were excluded from the analysis of BE(2)-M17 and LS cells respectively. Levels of significance: * = $p \leq 0.05$; ** = $p \leq 0.01$; *** = $p \leq 0.001$; NS = not significant. For all blots n = 4. The data were analyzed with one-way ANOVA and corrected for multiple comparisons using the Bonferroni correction. Error bars represent SEM.

3.3. Quantification of Secreted Aβ Species

Following the characterization of the amyloidogenic processing machinery in the cell lines of interest, it was necessary to assess its functionality by quantifying the amount of secreted Aβ. Serum-free medium from each cell line was cultured and immunoprecipitated with two anti-Aβ antibodies, 6E10 and 4G8, and probed with biotinylated 6E10 on WB. As shown in Figure 11, a band of 4 kDa, corresponding to monomeric Aβ, was detected in two out of the seven lines. Notably, BE(2)-M17 cells are a line subclonal to SK-N-BE(2). Following this initial assessment, the amounts of Aβ1-38, Aβ1-40, and Aβ1-42 secreted into the cultured medium were quantified with a highly sensitive commercial ELISA (see Materials and Methods and Figure 12). There was considerable variability in profiles among the lines as shown by one-way ANOVA tests, with BE(2)-M17 showing very high levels of Aβ1-40 (439.96 ± 16.26 pg/ml) and Aβ1-38 (151.93 ± 1.55 pg/ml). These concentrations were reduced by half in SK-N-BE(2) cells (212.83 ± 7.04 pg/ml for Aβ1-40 and 58.36 ± 3.75 pg/ml for Aβ1-38, $p < 0.0001$), but the amount of Aβ1-42 detected in SK-N-BE(2) and BE(2)-M17 cells was similar (18.66 ± 1.48 pg/ml and 21.85 ± 0.55 pg/ml respectively). With an Aβ1-40/1-42 ratio of 11.40, SK-N-BE(2) cells were found to secrete approximately twice as much Aβ1-42 as BE(2)-M17 cells, which had a ratio of 20.14. Aβ1-40 and Aβ1-42 levels were further reduced in SH-SY5Y cells compared to SK-N-BE(2) (126.02 ± 2.62 pg/ml, $p < 0.0001$ and 10.51 ± 0.39 pg/ml), but the drop in Aβ1-42 was not significant and therefore did not alter the Aβ1-40/1-42 ratio, which was 11.99 for SH-SY5Y cells.

No Aβ was detected in GI-ME-N cultured medium and only low amounts were present in the remaining cell lines. Aβ1-40 was the only species reliably detected in NBL-S cells (21.56 ± 0.58 pg/ml), as the remaining species were below the detection limit of the assay. Similar amounts of Aβ1-40 were detected in CHP-134 (25.79 ± 2.41 pg/ml) and LS cells (21.11 ± 0.80 pg/ml), but most of the Aβ1-38 and Aβ1-42 values were also outside the detection or quantification limits for both lines. The concentration of Aβ1-38 and Aβ1-42 in CHP-134 cells did not show significant differences due to high sample variations. Out of the four Aβ1-42 values from LS medium which fell within the detection and quantification

limits of the ELISA, two were excluded from analysis, as they were 10- and 100-fold larger than the remaining two. It is not known what factors make a cell permissive towards seed propagation. Therefore, based on the observations on culture conditions and the protein expression data, I chose to take forward SK-N-BE(2) and GI-ME-N cells, the two lines farthest apart in their expression of APP, BACE1, and Aβ. Both lines divide rapidly and appear robust, but their different expression profiles could give an indication on whether propagation depends on Aβ production alone, or whether other more complex factors are at play.

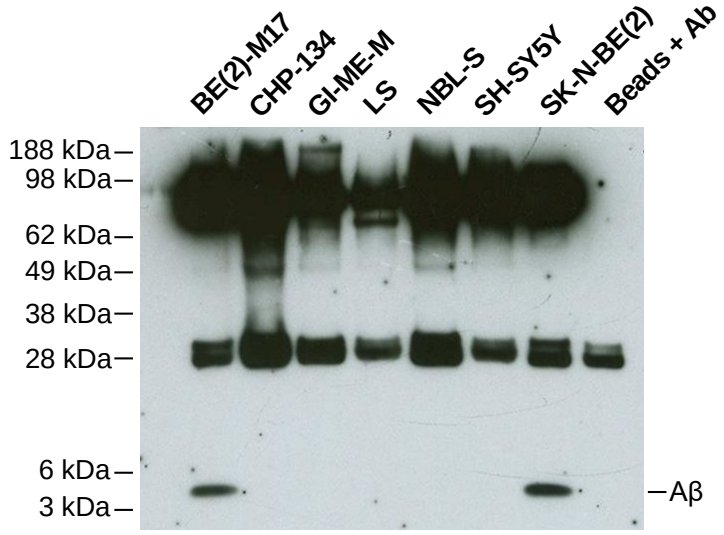

Figure 11. Western blot of immunoprecipitated Aβ in cultured medium from seven human neuroblastoma cell lines.

Serum-free medium was cultured for 3-4 days and 4 ml was IP'd with 6E10 and 4G8 anti-Aβ antibodies. Monomeric Aβ bands are visible at approximately 4 kDa in BE(2)-M17 and SK-N-BE(2) cells.

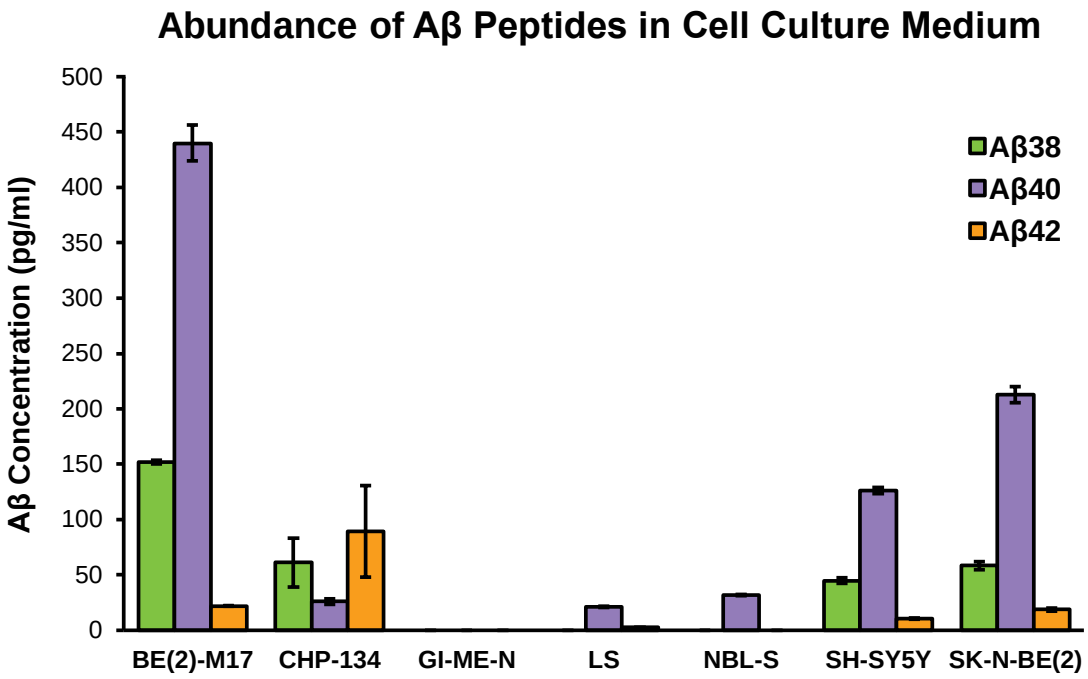

Figure 12. Quantification of secreted Aβ1-38, 1-40, and 1-42 in cultured medium from seven human neuroblastoma cell lines.

Serum-free medium was cultured for 3-4 days and average values from three biological with three technical replicates each are plotted. Where necessary, values below the detection and quantification limits of the assay were excluded, as well as outliers differing by ten-fold or more from the remaining values. Lines with zero signal were omitted from the analysis of the corresponding peptide. All three species were significantly different among lines ($p < 0.0001$, one-way ANOVA, Bonferroni correction). Error bars represent SEM.

4. Upregulation of the Amyloidogenic Pathway in Two Human Neuroblastoma Cell Lines

4.1. Design and Assembly of Retroviral Constructs Harboring APP695 Variants and BACE1

After SK-N-BE(2) and GI-ME-N lines were selected based on their high and low expression of APP, BACE1, and Aβ respectively, gene constructs were designed to upregulate the amyloidogenic pathway in these cells at the expense of α-secretase cleavage. BACE1 and α-secretase directly compete for APP processing; therefore, both APP and BACE1 were present in the constructs, as I expected that increasing the total Aβ produced by the cells and outcompeting non-amyloidogenic processing would improve their likelihood of propagating Aβ seeds. The coding sequence for the primary 695 neuronal isoform of APP bearing the Swedish KM670/671NL mutation was amplified via PCR from a construct previously assembled in our lab. Upon sequence verification, a point mutation from leucine to phenylalanine was discovered at position 491 and was corrected via SDM. SDM was then further used to generate four versions of the APP695 sequence by restoring it to its WT isoform and then introducing the Iberian I716F mutation into both the WT and the Swedish variants. In this way, four constructs (WT, Swedish-only, Iberian-only, and Swedish-Iberian or NL-F) with distinct properties were generated (Figure 13). The Swedish mutation favors β-secretase cleavage and produces more Aβ compared to a WT variant, while the Iberian mutation modulates cleavage at the γ-secretase site and leads to the production of longer aggregate-prone Aβ species. Designing BACE1 from its consensus coding sequence is described in detail in Section 2.1 in Materials and Methods. It was then cloned into the pLNCX2 retroviral vector together with each of the four APP variants via Gibson assembly, according to the vector (gene) map in Figure 14. APP is upstream of BACE1, interspaced by the ERAV 2A peptide. Whole bacterial plates were screened for the presence of an insert by means of colony PCR. Transformation efficiency was low and only a few colonies per construct were positive. All positive colonies were expanded and sequenced to verify the success of the SDM and that no mistakes had arisen within the sequences due to PCR-amplification. Example threads of the quality of the sequencing are given for both APP and BACE1 in Figure 15. Only colonies with correct sequences were used for future work.

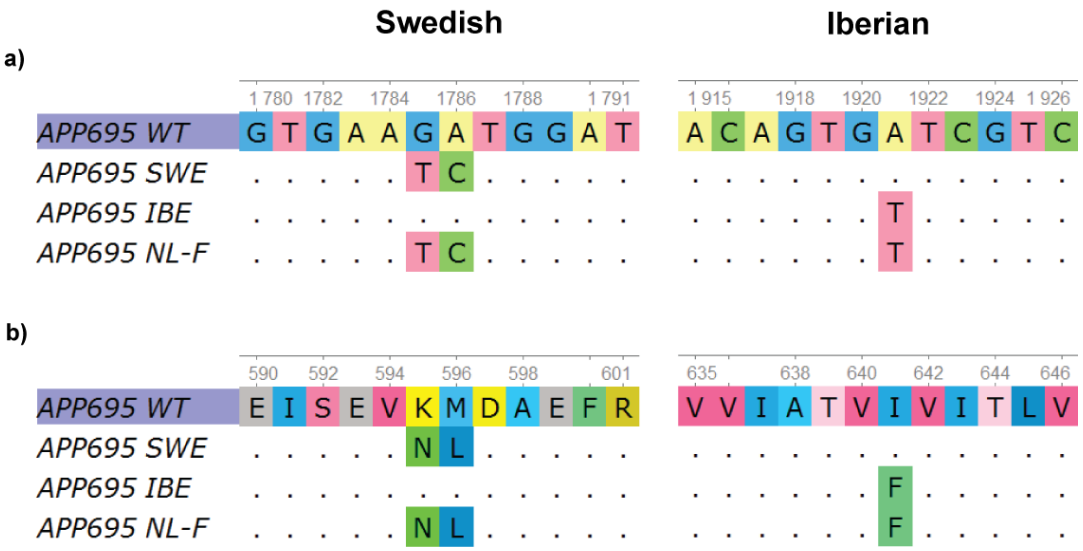

Figure 13. Schematic representation of the differences between four APP gene constructs.

APP695 constructs bearing the following mutations were generated for overexpression in cells: WT, Swedish (KM to NL), Iberian (I to F), and double Swedish-Iberian (NL-F). APP695 WT was taken as the reference sequence and is highlighted in purple. The nucleotide changes are shown in **a)** and the corresponding amino acid alterations are showed in **b)**. Dots represent matching bases or amino acids.

4.2. Generation of Stable APP/BACE1-overexpressing Cell Lines

4.2.1. G418 Kill Curves of Human Neuroblastoma Cell Lines

To generate cell lines which stably overproduce Aβ, the resistance of SK-N-BE(2) and GI-ME-N cells to geneticin (G418) was established. Resistance to G418 is conferred by the neomycin resistance gene which is present in the pLNCX2 vector (Figure 14, light green). Five antibiotic concentrations were tested for both cell lines in a 6-well format, along with an untreated control. G418 acts by inhibiting de-novo protein synthesis and for this reason selection is slow-acting and takes approximately two weeks. In this instance, the test cultures were maintained over one week under stringent selection. The antibiotic concentrations used for GI-ME-N cells ranged between 100 and 900 µg/ml. After three days, viable cells remained only in the 100, 300, and 500 µg/ml wells, and by seven days in culture only the first two wells contained surviving cells. SK-N-BE(2) cells had to be subjected to more stringent selection and initially a range between 200 and 1200 µg/ml G418 was chosen. After seven days, there were individual surviving cells in the 800 µg/ml well. The appropriate G418 selection concentrations were therefore taken to be 300 µg/ml for GI-ME-N and 800 µg/ml for SK-N-BE(2) cells.

4.2.2. Infection of Cell Lines with Retroviral Supernatant

Retroviral infection was the method of choice for introducing DNA into the neuroblastoma lines because the insert is incorporated directly into the genome and the stability of overexpression is improved, compared to standard transfection. The viral coat was pseudotyped with VSV-G, which is a pan-mammalian surface receptor, in addition to the 10A1 receptor, which is constitutively expressed in the RetroPack PT67 line. Two rounds of infection approximately 8 h apart were carried out to maximize the virus load. In the case of GI-ME-N cells, the virus needed to be concentrated prior to inoculation, as infection efficiency was low despite the preemptive pseudotyping. The cells were then left to recover for 48 h before selection was introduced; colonies began to form after about two weeks. The recovery of SK-N-BE(2) cells was much faster than that of GI-ME-N, although it was interesting to observe that some APP mutants grew faster than others. Particularly slow was the Iberian mutant from both cell lines. The recovered cells were pooled and expanded and their nomenclature henceforth will be an amalgamation of the first part of the mother cell line name and the introduced APP mutation, i.e. SK-N.WT, GI.SWE, etc.

4.3. Validation of Successful Construct Overexpression

4.3.1. Verification of APP, BACE1, and Aβ Overproduction

To verify that the retroviral infection had successfully induced overexpression of APP and BACE1 proteins in the neuroblastoma lines, cell lysates were blotted in the same way as in sections 2.1 and 2.2 from Chapter 1. Expression of the empty vector in GI-ME-N and SK-N-BE(2) cells was used to control for possible changes associated with the antibiotic selection. As full-length APP was already highly expressed in SK-N-BE(2) cells (see Chapter 1, Figure 8), the WB was saturated and differences in expression could not be reliably estimated (Figure 16a, c). On the other hand, BACE1 overexpression was extremely successful (Figure 16b) and when normalized to β-actin levels, it ranged from 18% ± 0.6% for SK-N.IBE to 22% ± 2% for SK-N.WT cells. When normalized to the vector-only control SK-N.V, BACE1 was overexpressed between 49% ± 10%, $p < 0.02$ for SK-N.IBE and 59% ± 10%, $p < 0.002$ for SK-N.WT cells (Figure 16d). The BACE1 content of SK-N.V and untreated SK-N-BE(2) cells was equal at 0.4% ± 0.1% for the former and 0.5% ± 0.1% (or 1.2% ± 0.1% after normalization to the control) for the latter.

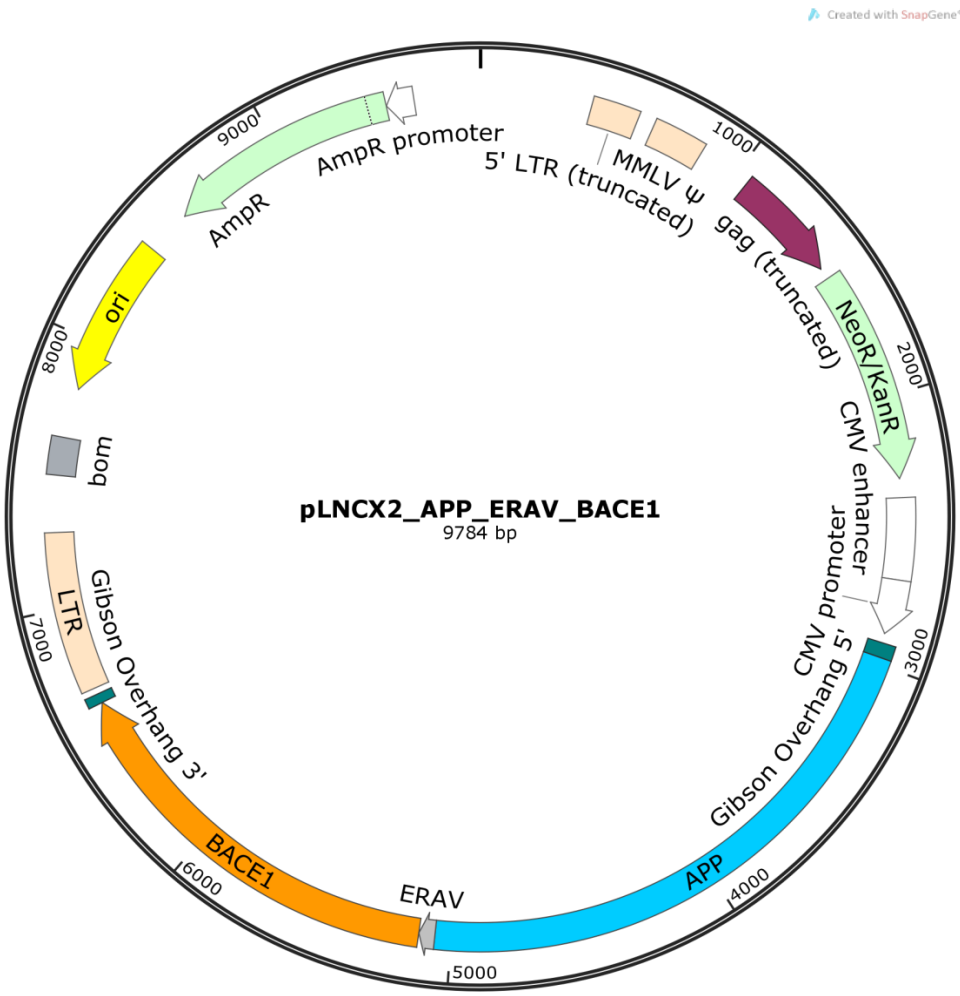

Figure 14. Map of pLNCX2 vector with the APP695 and BACE1 insert.

Expression of APP and BACE1, interspaced by the 2A ERAV peptide, is driven by the cytomegalovirus (CMV) promoter (white). The vector bears two selection markers, ampicillin and neomycin/kanamycin (light green). The length of the whole construct is 9784 bp, but only the region from the murine leukemia virus (MMLV) ψ packaging element to the 3' long terminal repeat (LTR) is packaged into the retrovirus (peach). The overhangs necessary for Gibson assembly, which was used to clone in the insert, are shown in dark green.

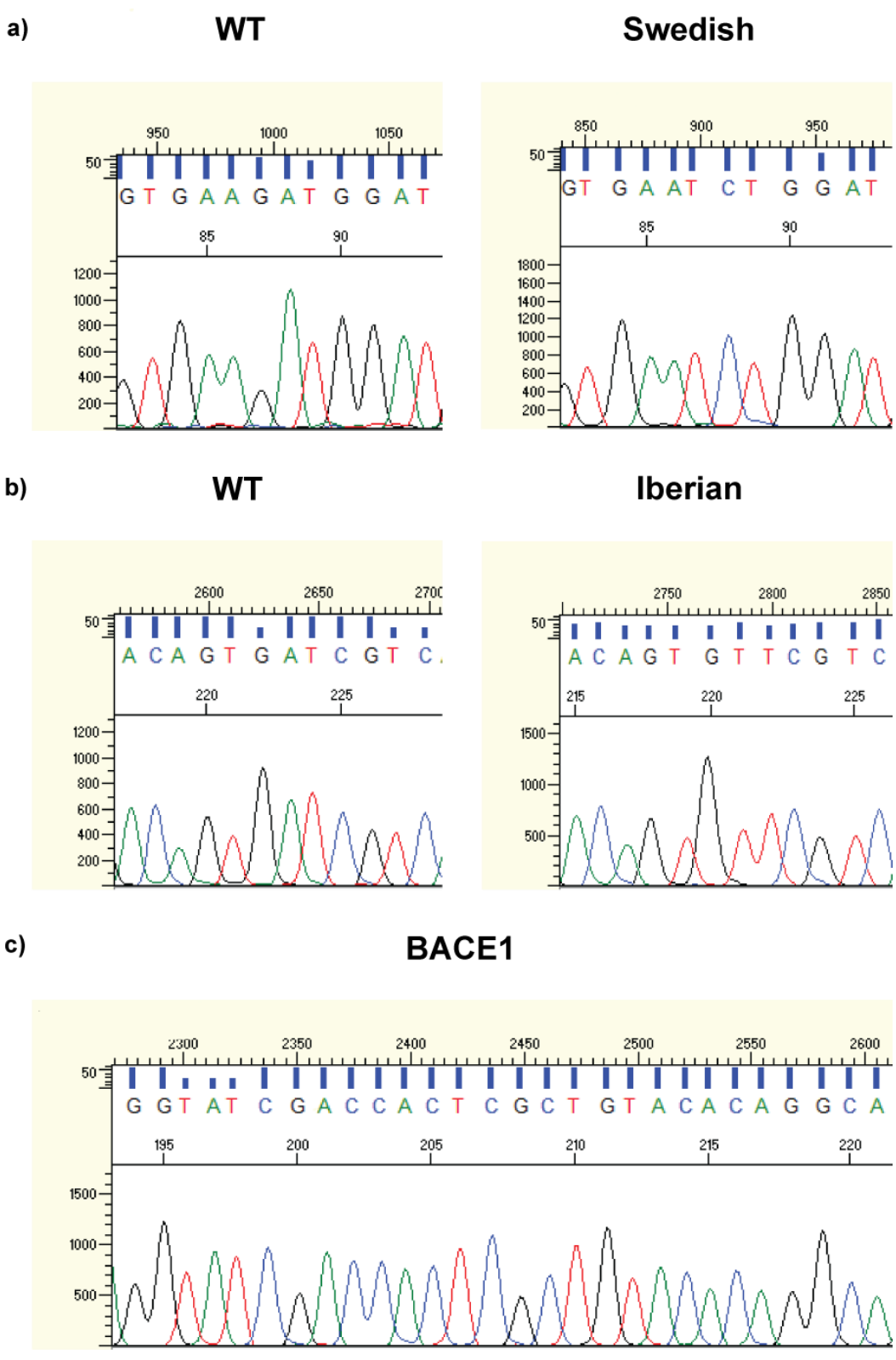

Figure 15. Example of sequence quality of APP and BACE1 constructs.

Panel **a)** shows traces for the regions containing the Swedish mutant and its WT counterpart and panel **b)** shows the same for the Iberian mutant. Panel **c)** shows an arbitrary region of the BACE1 coding sequence from the Swedish mutant construct. The y-axis corresponds to peak intensity and the x-axis to base number. Peaks are uniform, indicating sequencing of good quality.

In overexpressing GI-ME-N cells, APP expression was visibly higher than in untreated and vector-only controls, respectively (Figure 17a). In addition to the overall increase of FL-APP for all mutant lines, the Swedish and NL-F variants showed a stronger band at 62 kDa, compared to the Iberian and WT. All mutants also showed a thickening of a band just under the 36 kDa marker, as did GI.V cells. Overall, although the vector-only control does not contain the insert, its band signature was more similar to the four mutants than to the untreated control. Moreover, when the blots were quantified, an increase in total APP signal of 8% was calculated for this line in comparison to GI-ME-N cells. Upon normalization to GI.V, however, it became apparent that the increase in signal for the mutants was more subtle and therefore did not reach significance (Figure 17c). It ranged from 1.4% ± 0.3% for GI.WT to 1.8% ± 0.7% for GI.SWE (Figure 17c). In the case of BACE1, the difference in overexpression was a lot more variable than the one observed in SK-N-BE(2) cells, but was still much higher than control levels, which were below the blot's detection limit (Figure 17b and d). Quantification and normalization as above showed a highly significant difference of $p < 0.0001$ between the two controls and GI.SWE (38% ± 1.4%), GI.IBE (18% ± 1.7%), and GI.NL-F cells (22% ± 1.6%). The difference between controls and GI.WT (7% ± 1.6%, $p < 0.05$) was less pronounced. Evidently, the presence of the pLNCX2 vector in GI-ME-N cells, possibly combined with the associated selection stress, is enough to alter the overall amounts of APP as seen on a WB, but has no effect on the BACE1 signature.

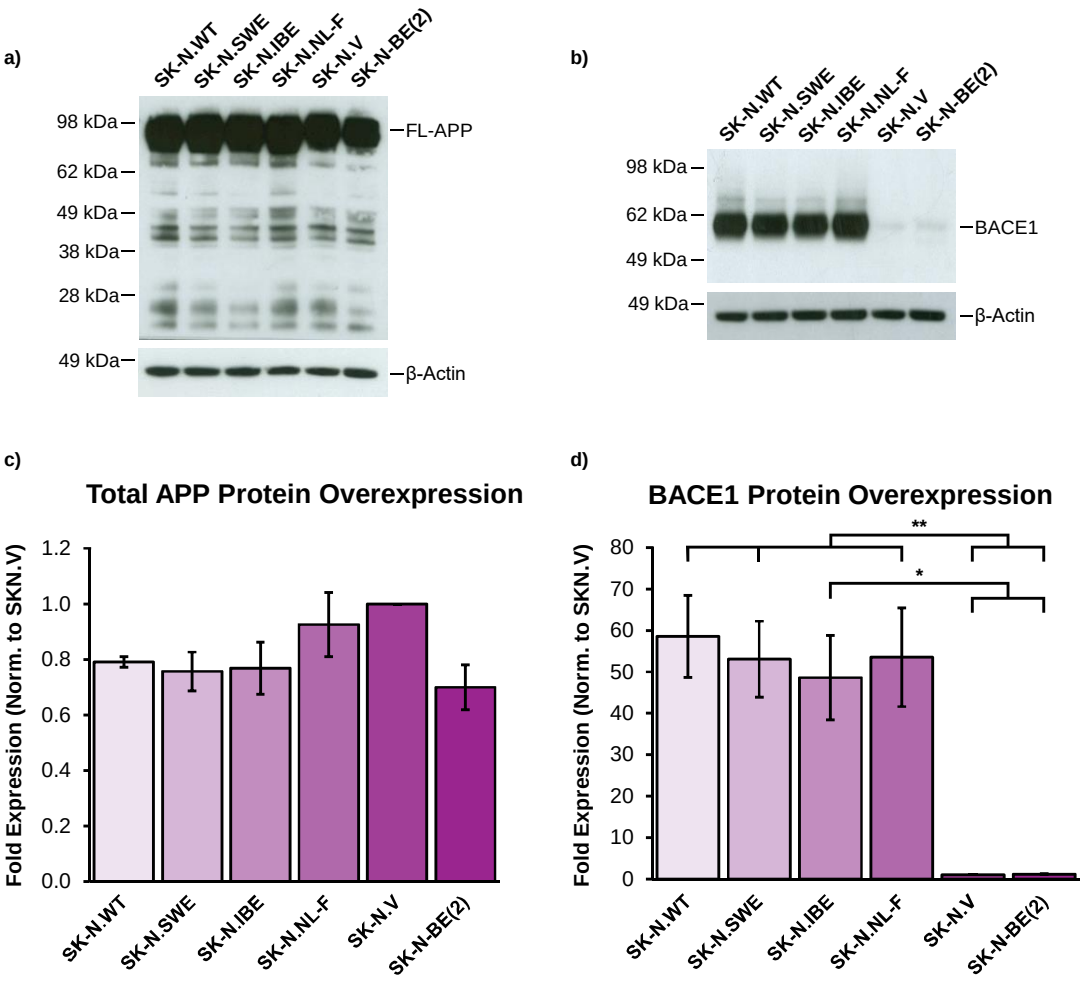

Figure 16. APP and BACE1 protein overexpression after retroviral infection of SK-N-BE(2) cells.

Representative WBs for APP **a)** and BACE1 **b)** show expression in the four mutants and in the vector-only and untreated controls. APP was detected with 22C11 antibody. Quantification after normalization to β-actin levels and SK-N.V cells reveals no detectable change in total APP levels ($p = 0.087$, one-way ANOVA) in **c)**, but shows significant elevation in β-secretase expression ($p < 0.0001$, one-way ANOVA). FL = full length. The Bonferroni correction for multiple comparisons was used for both quantifications. Levels of significance: * = $p \leq 0.05$; ** = $p \leq 0.01$. N = 4. Error bars represent SEM.

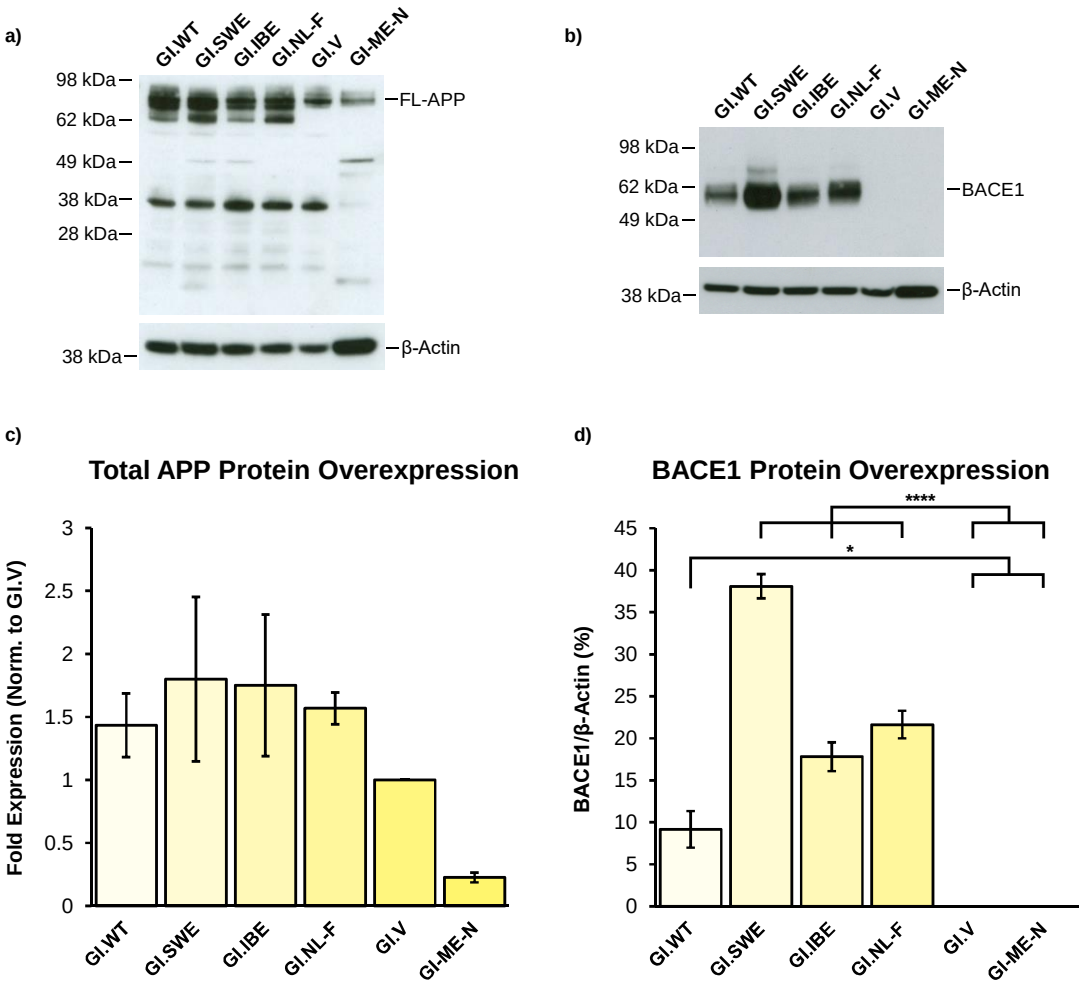

Figure 17. APP and BACE1 protein overexpression after retroviral infection of GI-ME-N cells.

As above, representative blots for APP **a)** and BACE1 **b)** are shown. The APP blot was normalized to GI.V vector-only control and signal showed no statistically significant elevation ($p = 0.139$, one-way ANOVA). **c)**BACE1 was highly overexpressed ($p < 0.0001$, one-way ANOVA), but normalization to GI.V was not possible because a BACE1 reading for the control line could not be obtained. Both tests were corrected for multiple comparisons with the Bonferroni method. FL = full-length. Levels of significance: * = $p \leq 0.05$; **** = $p \leq 0.0001$. N = 4. Error bars represent SEM.

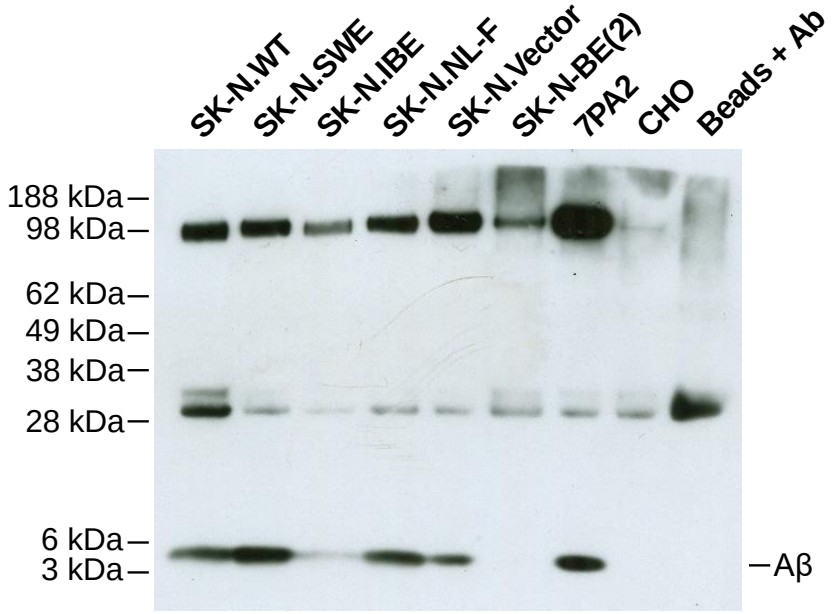

Figure 18. IP of Aβ secreted in CM from APP and BACE1-overexpressing SK-N-BE(2) cells.

Medium was cultured, IP'd, and blotted as in Figure 11, Chapter 1. Monomeric Aβ appears as a single band of approximately 4 kDa.

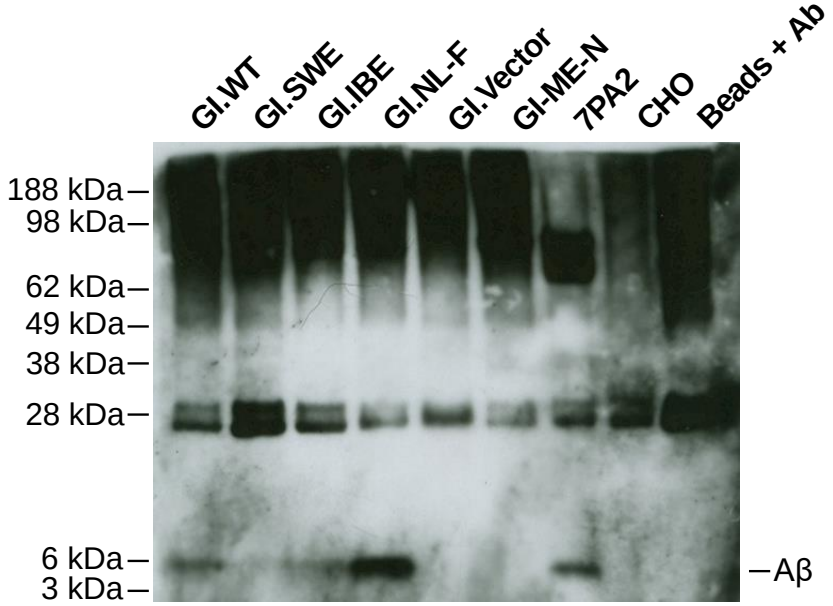

Figure 19. IP of Aβ secreted in CM from APP and BACE1-overexpressing GI-ME-N cells.

Medium was cultured, IP'd, and blotted as in Figure 11, Chapter 1 and Figure 18 above.

4.3.2. Quantification of Total Secreted Aβ

After verifying that APP and BACE1 are overexpressed in the infected cell lines, I sought to show that this translates into elevated secretion of Aβ into the CM, as we had originally

expected that higher Aβ production in the cells could facilitate seeding. Using the same method for immunoprecipitation and WB as described previously, Aβ from medium was detected for all overexpressing lines and was compared to 7PA2 and CHO cells as positive and negative controls, respectively. Aβ was present in all SK-N-BE(2) mutants, as well as the vector-only control (Figure 18). As expected, 7PA2 cells showed a clear signal, while Aβ was absent in the CHO control cells. Signal was variable, where SK-N.SWE cells showed the strongest Aβ band, while that was particularly faint in SK-N.IBE cells. It is interesting to note that while APP overexpression could not be verified in the SK-N.V line and BACE1 levels were comparable to the untreated control, Aβ amounts were prominent, as shown by the WB, but no peptide was detected in the SK-N-BE(2) line. Previously Aβ was detected in SK-N-BE(2) CM (Chapter 1, Figure 11); however, this was cultured for 3-4 days in contrast to the medium used in this experiment, which was cultured over ~17-24 h only. In contrast, GI.V cells did not express Aβ (Figure 19), even though the presence of the vector alone appeared to increase the amounts of APP found in the cell (Figure 17a). It is likely that treatment with this vector has variable effects depending on the cell line in which it is introduced. A particularly thick band was observed for GI.NL-F cells, while the remaining mutants showed a weak signal and no Aβ was found in GI-ME-N cells.

The secreted Aβ content was further quantified by ELISA as in Chapter 1 to gain a more accurate understanding of the precise amounts of common Aβ species produced by the cells. The SK-N mutants had elevated levels of Aβ, equivalent or higher than those secreted by the 7PA2 line (Figure 20). The proportional distribution of the three surveyed peptides was also consistent with the expected effect of the mutations on amyloidogenic APP processing. SK-N.SWE cells secreted the most peptides overall, mainly in the form of Aβ1-40 (1819.46 ± 94.82 pg/ml), and the pattern of peptide distribution was mirroring that shown by SK-N.WT, SK-N.V, and untreated SK-N-BE(2) cells. On the other hand, in SK-N.NL-F cells, the Aβ1-40 peak (1059.11 ± 69.42 pg/ml) was reduced at the expense of Aβ1-38 (1006.58 ± 48.00 pg/ml) and Aβ1-42 (560.16 ± 32.05 pg/ml). The Aβ1-40/1-42 ratio had correspondingly dropped to 1.89 compared to SK-N.WT, for example, which had a ratio of 10.25. Importantly, Aβ1-42 amounts in SK-N.NL-F cells were more than twice higher than in 7PA2 (231.61 ± 15.73 pg/ml, Aβ1-40/1-42 ratio of 3.95). The Iberian mutation alone did not noticeably increase Aβ1-42 production in SK-N.IBE cells (207.46 ± 42.56 pg/ml, Aβ1-40/1-42 ratio of 4.11), but levels were still higher than both SK-N.V (64.38 ± 2.40 pg/ml) and SK-N-BE(2) (18.66 ± 1.48 pg/ml). Again, here it is better shown that the pLNCX2 vector alone increases Aβ production in SK-N-BE(2) cells, but does not seem to alter the way in which it is processed, which is evident from the unaltered Aβ1-40/1-42 ratios in the two

SK-N controls (11.69 for SK-N.V and 11.40 for SK-N-BE(2)). Finally, in SK-N.WT (324.98 ± 9.89 pg/ml), SK-N.SWE (422.88 ± 18.26 pg/ml), and SK-N.IBE (527.72 ± 38.74 pg/ml) cells Aβ1-38 was reduced compared to the 7PA2 line (751.58 ± 59.74 pg/ml). Based on the above observations, the SK-N.NL-F line seemed most promising, as it had the smallest Aβ1-40/1-42 ratio of all lines surveyed in this experiment and the highest production of Aβ1-42.

APP and BACE1-overexpressing GI-ME-N cells showed a much subtler or no increase in Aβ and all levels remained well below those measured in 7PA2 cells (Figure 21). The pattern of relative Aβ species abundance in overexpressing GI-ME-N cells was reversed compared to overexpressing SK-N-BE(2) cells, which implies that despite the presence of mutations to modulate the relative abundance of the peptides, the overall signature of processing is determined by additional cell-specific factors. Aβ1-40 levels in these lines were lowest compared to Aβ1-38 and 1-42, except for the SK-N.SWE line where they reached the modest concentration of 30.76 ± 0.84 pg/ml. The highest amounts of Aβ1-42 were found in GI.NL-F cells (209.25 ± 10.37 pg/ml), followed by GI.WT cells (104.63 ± 5.01 pg/ml). No Aβ was detected by the assay in GI.V and GI-ME-N cells, so no conclusions could be reached about how the mutations change APP processing compared to controls. Intriguingly, even though overall amounts of Aβ were low, GI.WT, GI.IBE, and GI.NL-F also had the lowest Aβ1-40/1-42 ratios of all thirteen cell lines (0.24, 0.24, and 0.22 respectively), while GI.SWE and 7PA2 had identical ratios of 3.95. This could mean that, in fact, overexpressing GI-ME-N cells would be better at propagating exogenous seeds because of their high relative content of Aβ1-42. However, the three species detected here are by no means the only peptides produced by the amyloidogenic pathway and absolute Aβ amounts were still very low, so none of the overexpressing GI-ME-N lines were taken forward at this point. It would, however, be an interesting set of experiments to seed these lines with synthetic and AD brain-derived oligomeric material and assess their response.

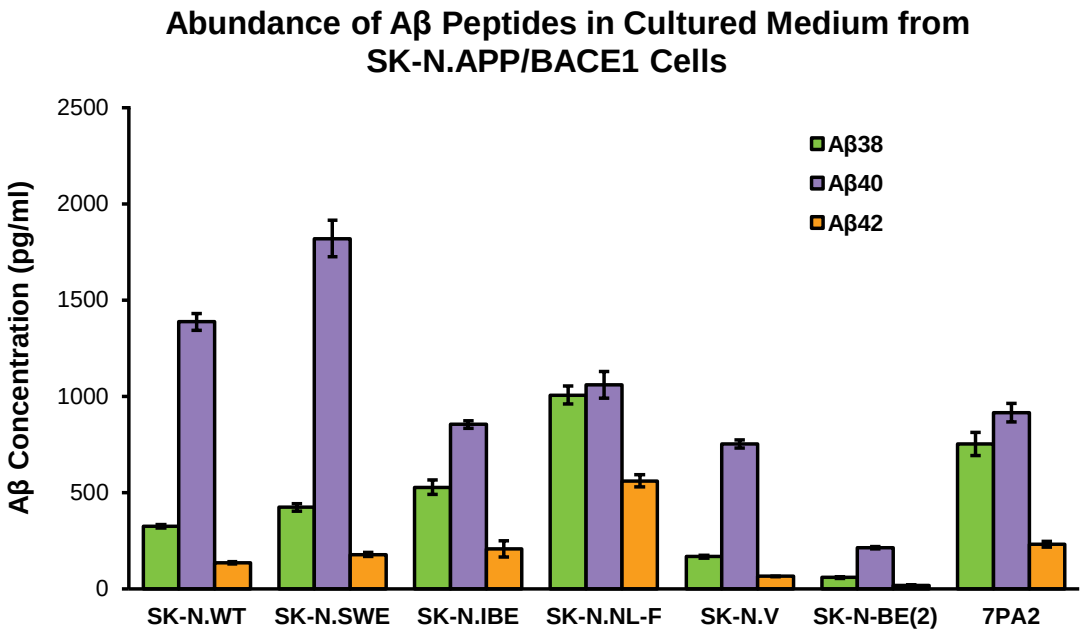

Figure 20. Quantification of Aβ1-38, 1-40, and 1-42 in SK-N-BE(2) cells overexpressing BACE1 and an APP695 variant.

Serum-free medium cultured over 17-24 h was assessed for its monomeric Aβ content via ELISA. One WT and three mutant variants were compared to a vector-only, untreated, and positive control. N = 3. Error bars represent SEM.

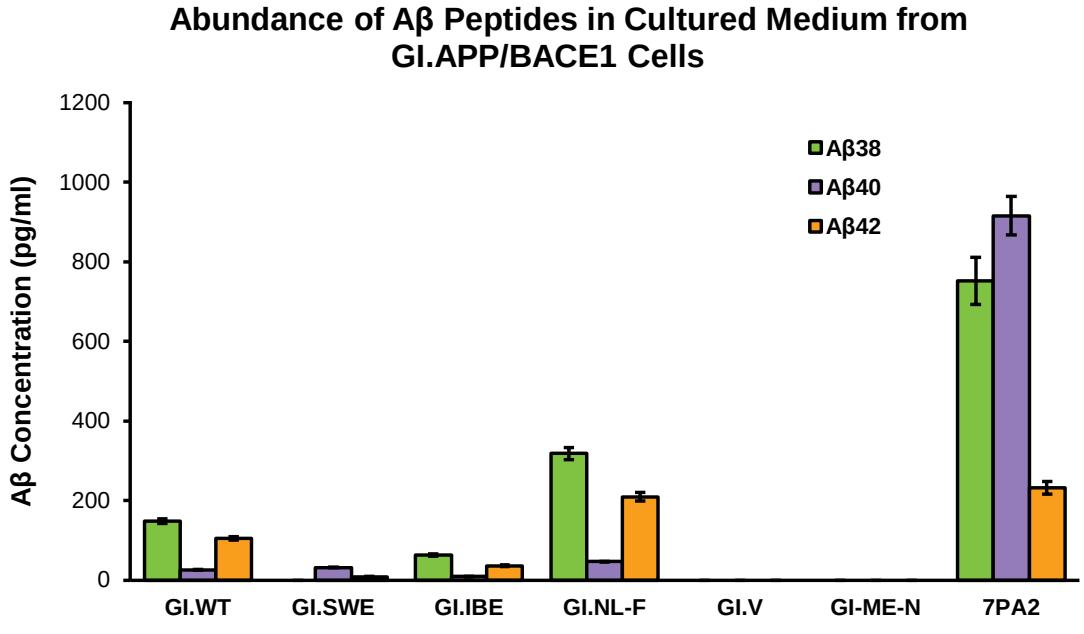

Figure 21. Quantification of Aβ1-38, 1-40, and 1-42 in GI-ME-N cells overexpressing BACE1 and an APP695 variant.

Medium from cells overexpressing a WT or one of three mutant APP variants was cultured and compared for Aβ content to that from a vector-only, untreated, and positive control as in Figure 20. N = 3. Error bars represent SEM.

4.3.3. Profiles of Secreted Aβ Species

The final step towards characterizing the differential APP processing in the overexpressing cells was to analyze their CM by mass spectrometry, in order to obtain a signature of secreted Aβ from each line beyond the scope of WB or the triplex ELISA. The peak intensity measured for each Aβ peptide was normalized to the total amount of Aβ species detected in the medium and the data were plotted as traces where each point represents the percent normalized peak intensity for an Aβ peptide (Figure 22 and Figure 23). The mass spectrometry experiments were carried out and the data were normalized by Dr. Erik Portelius and Ms. Rita Persson, under the supervision of Prof. Henrik Zetterberg. All infected SK-N-BE(2) cells showed two distinct peaks of peptides Aβ1-14 and Aβ1-19, a modest peak at Aβ11-40, and three peaks at Aβ1-34, Aβ1-38, and Aβ1-40, but most of those reached different intensities, depending on the APP variant. Short peptides were highly abundant in infected GI-ME-N cells with peaks at Aβ1-14, Aβ1-19, and Aβ1-17 for GI.SWE cells, but they did not show presence of 11-x peptides. Similarly to infected SK-N-BE(2) cells, 7PA2 and infected GI-ME-N cells also showed peaks for Aβ1-38 and Aβ1-40. GI-ME-N cells further showed modest Aβ1-28 and Aβ1-34 peaks, except for GI.SWE cells, where the peaks were more prominent. Nothing was detected in GI.V cells. Most Aβ11-x peptides were not present in 7PA2 cells either; however, the abundance of short peptides in this line was low overall, in contrast to the human lines. The most intense peak in 7PA2 cells was Aβ1-33. It is important to note that mass spectrometry traces will not necessarily follow the triplex ELISA data, as the former gives an estimate of relative abundances among 21 Aβ peptides, while the latter is a method for absolute quantification. For this reason and considering that APP is heavily processed by multiple secretases in a pattern which is cell-line dependent, it is also difficult to reach a conclusion on the effect of the introduced mutations based on the resultant traces. As this was a pilot experiment aimed at gaining an initial idea of APP processing in the generated lines, more replicates and possibly quantitative mass spectrometry would be necessary to obtain more relevant readings where statistical significance can be established and confounding technical errors can be accounted for.

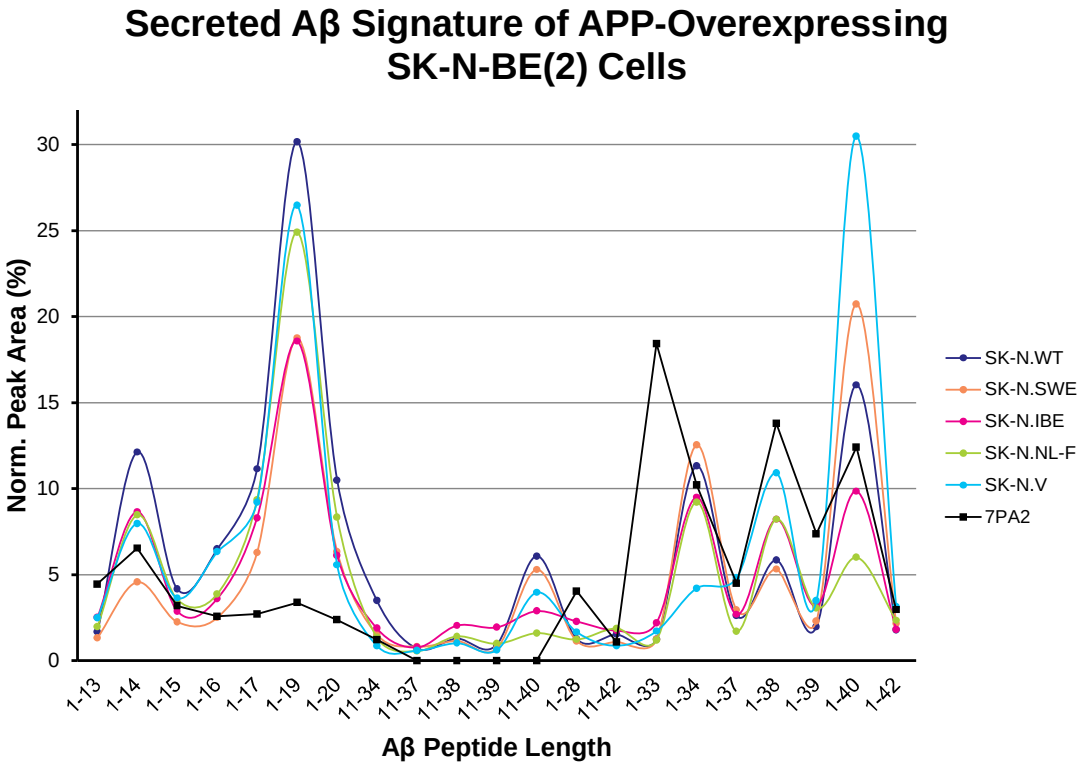

Figure 22. Mass spectrometry traces of secreted Aβ from APP and BACE1-overexpressing SK-N-BE(2) cells.

The same medium used for ELISA quantification in Figure 20 and Figure 21 was used in this experiment. Infected SK-N-BE(2) were compared to 7PA2 cells. Raw peak area intensities for each Aβ species were normalized to the total Aβ in the medium and were plotted as percentages. Each reading is the average of three biological replicates with two readings per replicate. Zero value readings were not included in the averaging where there were one or more positive reads per peptide. Error bars are hence not shown.

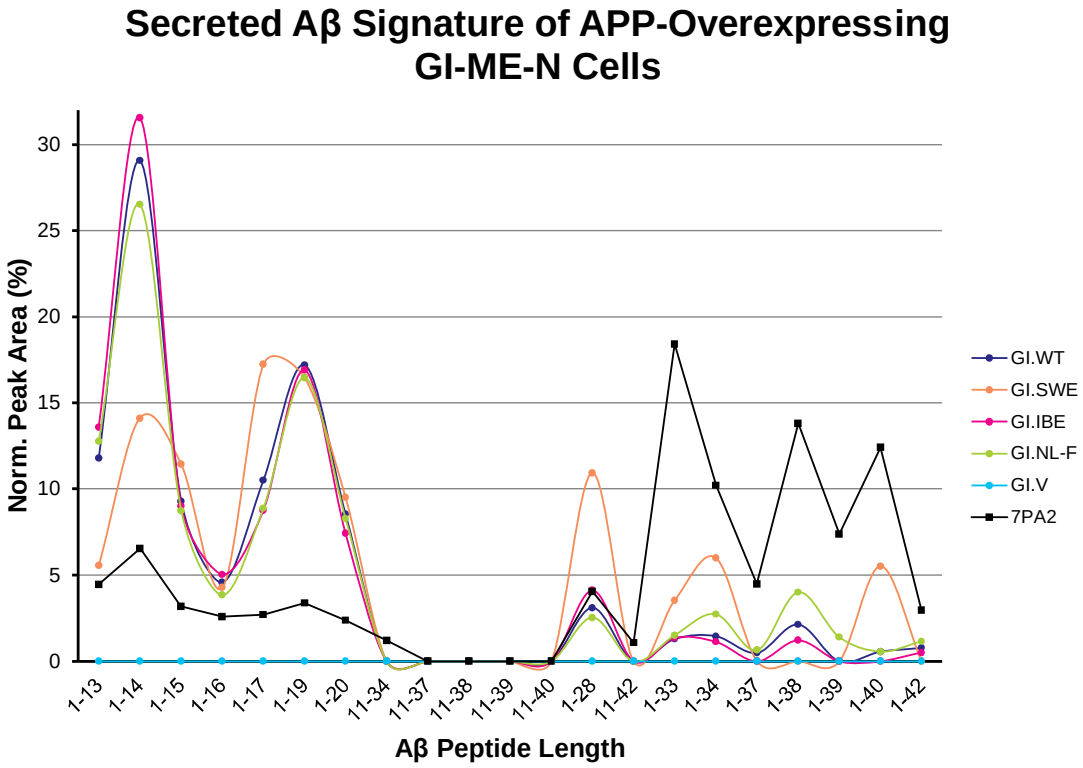

Figure 23. Mass spectrometry traces of secreted Aβ from APP and BACE1-overexpressing GI-ME-N cells.

Cultured medium from infected GI-ME-N cells was assessed and plotted as in Figure 22.

5. Capability of Aβ-Producing Cell Lines to Propagate Brain-Derived Aβ Oligomers

5.1. Characterization of Human AD and Control Brain for Intracerebral Inoculation of NL-F Mice

A set of experiments conducted by Dr. Mark Farrow, Dr. Silvia Purro, and Mr. Michael Farmer were carried out in our department to investigate the ability of patient-derived AD brain to propagate amyloidosis in the brains of young NL-F knock-in mice. The patient and control brain samples were prepared, characterized, and provided for intracerebral inoculation by Dr. Jonathan Wadsworth. The Aβ content of the brains was verified by denaturing WB (Figure 24), where a strong band corresponding to monomeric Aβ is visible at the 4 kDa marker, while the band is absent in control brain. Four months post inoculation the mice were culled and their brains were fixed, sectioned, stained, and imaged by Ms. Tamsin Wilkins. Figure 25 presents two brain slices inoculated with AD (right) and control brain (left), respectively. There is visible deposition in the hippocampus of mice treated with patient brain, while no plaques were detected in mice treated with inoculum from healthy controls. With these experiments, the seeding activity of the AD sample was proven alongside an inert control and these became available to us to test the propagative ability of APP/BACE1-overexpressing neuroblastoma.

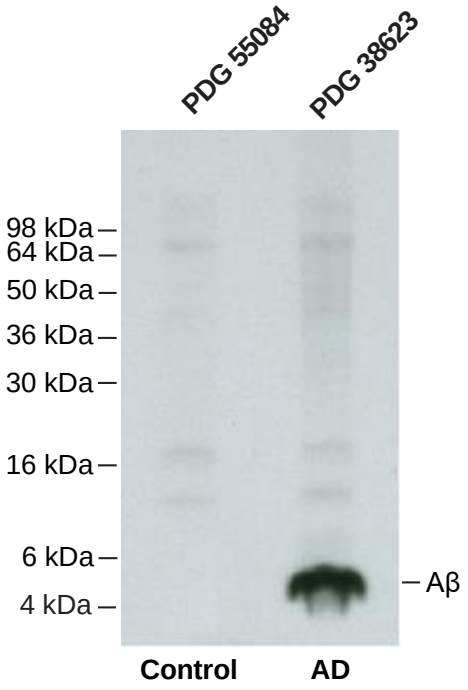

Figure 24. WB of Aβ amounts found in AD and control brain (provided by Jonathan Wadsworth).

Monomeric Aβ was detected in 10% homogenate from human brain samples PDG 38623 (AD) and PDG 55084 (control) Aβ in the AD brain sample (right) is visible as a thick band close to the 4 kDa marker.

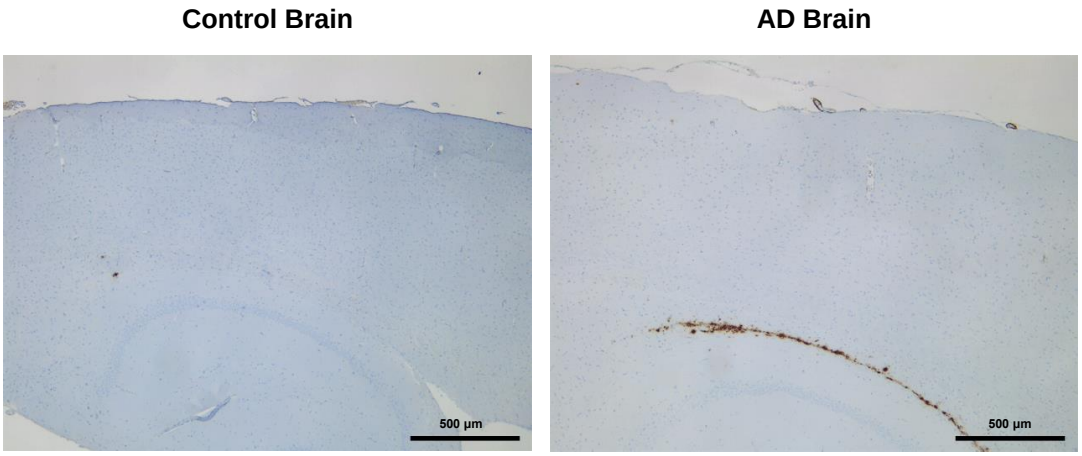

Figure 25. Slices of NL-F mouse brain four months post-inoculation with human AD and control brain (provided by Silvia Purro).

Young 6-8-week-old NL-F mice were injected with 1% w/v human AD and control brain homogenate and after four months their brains were collected and stained with 82E1 antibody. Example slices from control brain-inoculated (left) and AD brain-inoculated (right) mice are shown here. The right panel displays distinct Aβ plaque pathology in the hippocampal CA1 area (brown).

5.2. Seeding of SK-N.NL-F, 7PA2, and GI-ME-N Cells with Human AD and Control Brain

In Chapter 2, I postulated that from the panel of cell lines generated, SK-N.NL-F will be the one most likely to propagate AβO because of the amounts and proportions of Aβ1-42 it produces. As patient-derived brain material with proven ability to induce pathology in mice was available, this was used as the inoculum in the final experimental stage of the current project. 7PA2 cells were again used as a putative positive control because CM from these cells has been previously shown to also induce pathology in transgenic mice (Freir et al. 2011, Walsh et al. 2002, Welzel et al. 2014) and to contain a plethora of peptides with the Aβ sequence (Portelius et al. 2013). Finally, GI-ME-N cells were chosen as the Aβ-negative control, as CM Aβ could not be measured via ELISA or WB in this line. We expected that if the seeded cells were to truly propagate AβO, then those would be consistently observed at every passage post-seeding, long after the original inoculum has been removed. If, however, the cells were not able to sustain seeded aggregation, then a

spike would be observed immediately post-seeding, reflecting the oligomeric content of the brain homogenate, but this would drop off later on as Aβ aggregates are cleared by the cells. For these reasons, the pilot seeding experiment was set up so that both extracellular and intracellular Aβ could be monitored over three splits after inoculation with brain homogenate. CM was cultured in serum-free medium and was collected before every split and with every passage cells were also plated for immunocytochemistry. Finally, when the cells were initially seeded, this medium was also collected to account for any signal contributed by the inoculum.

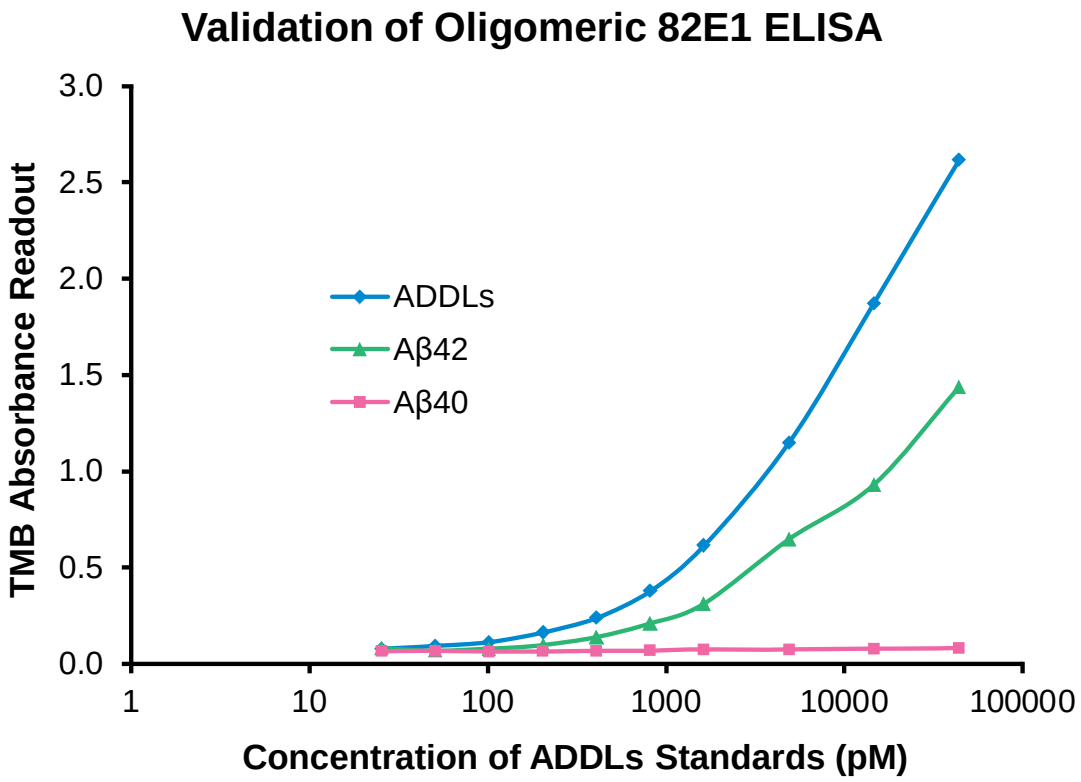

Figure 26. Validation of ELISA specificity to AβO.

Serial dilutions with equal concentrations of ADDLs and Aβ1-42 and Aβ1-40 monomer were prepared. Specificity for oligomers was confirmed by the flat line showed by the Aβ1-40 solution (pink), while both pre-formed ADDLs (blue) and freshly-prepared Aβ1-42 monomers (green) showed an increase in absorbance signal.

5.2.1. Evaluation of CM from Seeded Cells for AβO Content

In order to detect oligomers in cell CM, an already established oligomer-specific ELISA was set up (Hölttä et al. 2013). As described in detail in Materials and Methods, this assay re-

lies on the same Aβ-specific antibody for capture and detection, thereby ignoring monomeric Aβ in the readout. The specificity of this ELISA was verified with a preparation of ADDLs, monomeric Aβ1-42, and monomeric Aβ40 (Figure 26). Only the Aβ1-40 preparation actually produced a flat line as expected from a truly monomeric solution, while despite the fact that the Aβ1-42 was freshly reconstituted with HFIP to break down any preformed oligomers, it still gave off signal, which indicates that the material aggregated during handling and incubation. The standard curve for the assay was subsequently generated with a synthetic dimer missing the hydrophobic Aβ region responsible for aggregation.

SK-N.NL-F, 7PA2, and GI-ME-N cells were seeded with four dilutions of 10% AD brain homogenate (1:3000, 1:5000, 1:10000, and 1:50000), two dilutions of 10% control brain (1:3000 and 1:5000), and were also seeded with 100 nM ADDLs as a positive control treatment. The original seeded medium was run on the same plate together with all CMs collected immediately before the first and second splits post-seeding. No oligomers were detected for any of the samples tested from both SK-N.NL-F (Figure 27) and 7PA2 cells (Figure 28), except for those treated with 100 nM ADDLs. Here, the signal had completely disappeared by the second split and for this reason no CMs collected at later splits were analyzed. A 1:1000 control dilution of 10% AD brain in DPBS was the only other case to return a positive result of 42.05 pg/ml in the SK-N.NL-F plate and 26.25 pg/ml in the 7PA2 plate. However, in the latter case, the value fell below the LLOQ of 28.74 pg/ml for that assay. CM from GI-ME-N cells was not tested due to the discouraging outcome of the SK-N.NL-F and 7PA2 assays. These results could partly be explained by insufficient sensitivity, as the original ELISA was able to detect AβO found in human CSF down to 1 pg/ml (Hölttä et al. 2013), whereas the lowest LLOQ reached by this ELISA was 14.37 pg/ml. The current assay used lower volumes of antibody at the same concentration as the published ELISA because of its high price and this is most likely the reason for the lower sensitivity. However, as the decrease in signal from the cells treated with ADDLs was rapid and clear, it is unlikely that these cells propagate AβO extracellularly.

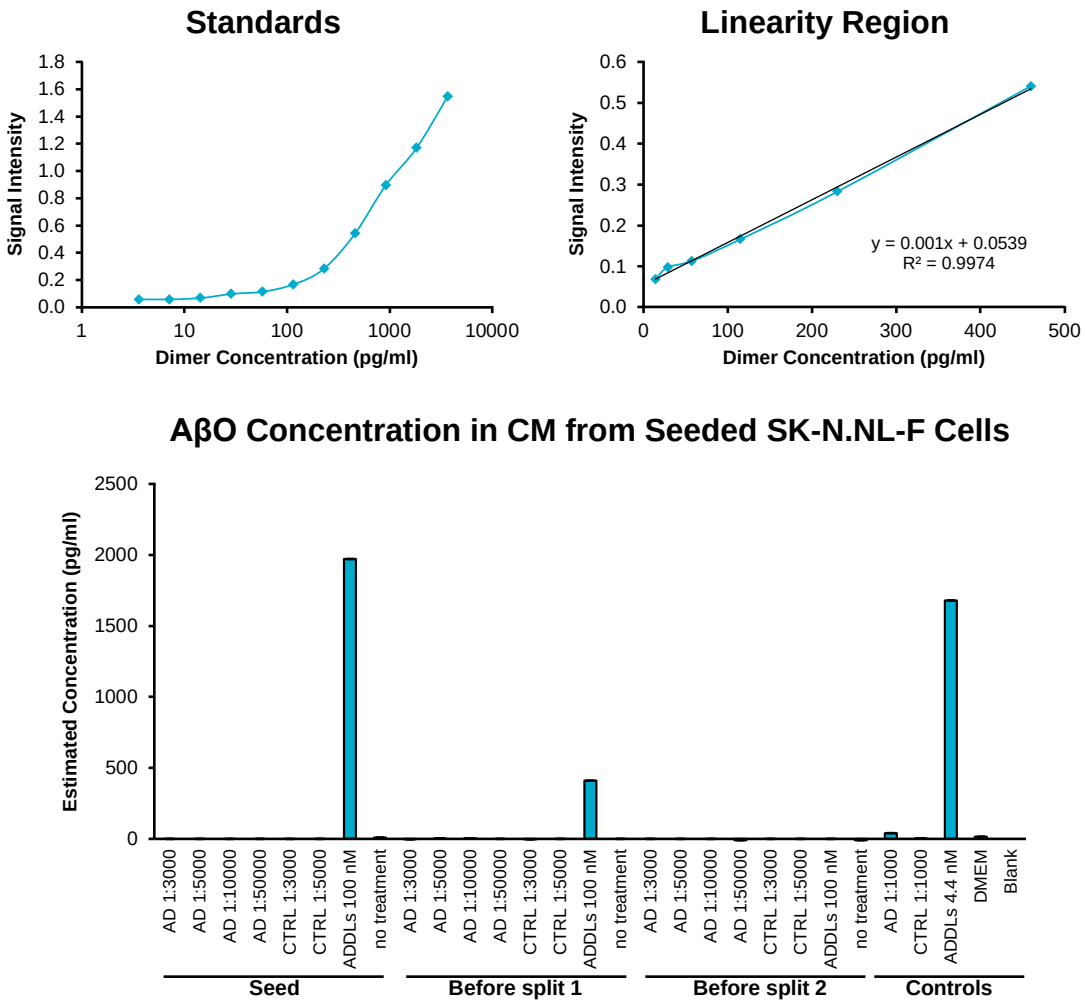

Figure 27. Detection of AβO in CM from SK-N.NL-F Cells Seeded with Human AD and Control Brain. A serial 2-fold dilution ranging from 3678.11 to 3.59 pg/ml was prepared from the synthetic Aβ1-11 dimer standard to calibrate the assay (top left). The LLOQ for this assay was 14.37 pg/ml. Oligomer content was quantified from the linearity equation (top right) and plotted for each split (bottom). Four dilutions of AD brain, two dilutions of control brain (CTRL), and a dilution of 100 nM ADDLs were used for seeding. Standards were pipetted in triplicate and samples and controls in duplicate.

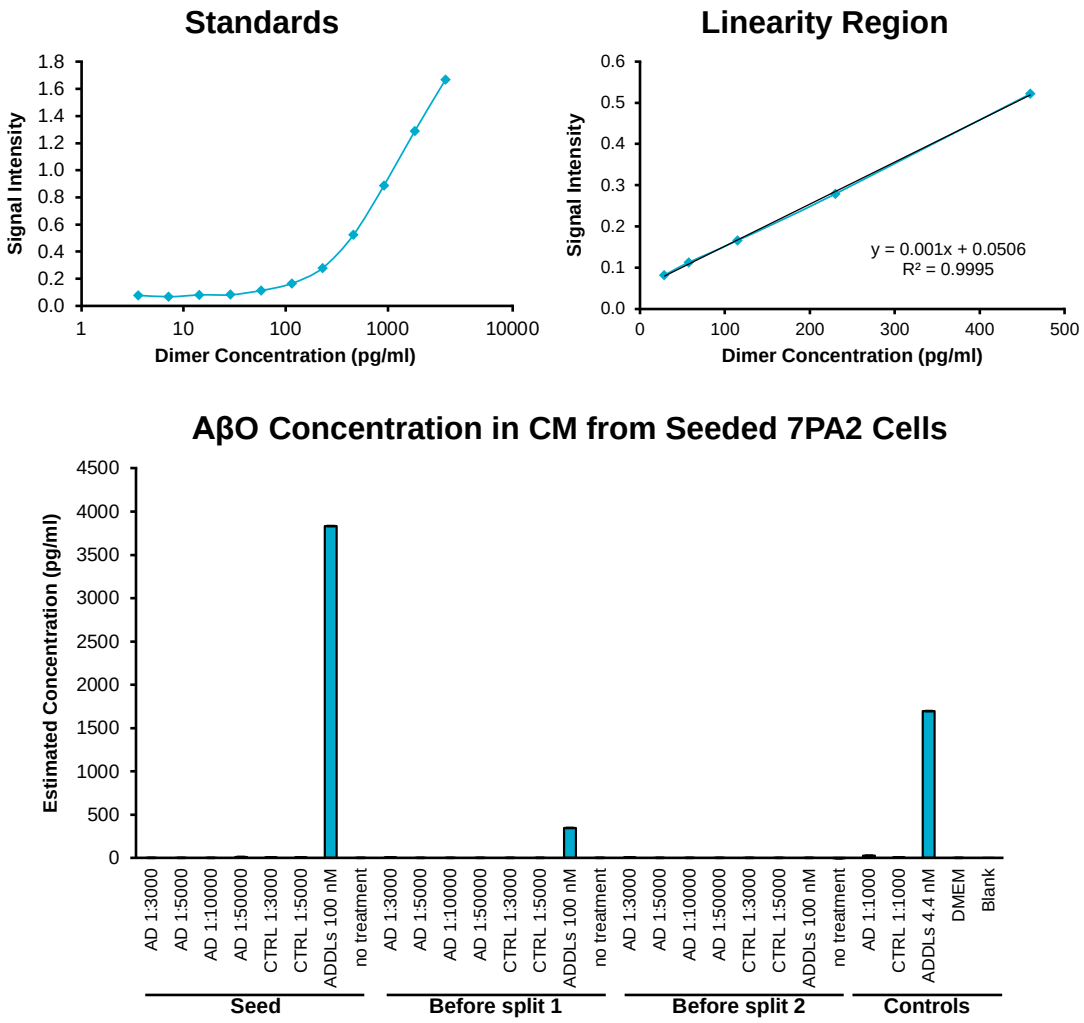

Figure 28. Detection of AβO in CM from 7PA2 Cells Seeded with Human AD and Control Brain.

The same standard dilutions (3678.11 to 3.59 pg/ml) as in Figure 27 were prepared (top left). The LLOQ for this assay was 28.74 pg/ml. Oligomer content was quantified from the linearity equation (top right) and plotted for each split as above (bottom). The same dilutions of seeding material were used here as in Figure 27. Standards were pipetted in triplicate and samples and controls in duplicate. CTRL = control brain.

5.2.2. Detection of Intracellular AβO Post-seeding

5.2.2.1. SK-N.NL-F Cells

Cells were split three times after treatment with brain homogenate and at each split a fraction was grown in chamber slides to be fixed and immunofluorescently stained for Aβ. This was done in order to visualize any intracellular and membrane-bound aggregates resulting from seeding and to assess whether those are propagated or degraded. The signal was variable across the three lines and imaging conditions were optimized for the line

with highest overall fluorescence intensity, 7PA2. Once the parameters were set and noise was reduced by adjusting the gain and laser intensity for 7PA2 cells, which showed the brightest fluorescence, it became apparent that seeded SK-N.NL-F did not show much Aβ accumulation after treatment (Figure 29). When observed by eye, many cells showed distinct immunopositive regions, but when imaged with confocal microscopy, those regions were too faint to be distinguished from noise. There appeared to be a modest increase in signal in cells seeded with AD brain after the first split, but it was difficult to determine whether there was any difference in Aβ load between the four dilutions. When quantified, normalized to cell number, and analyzed with a two-way ANOVA, the data showed that overall there was a significant spike in signal at Split 2 ($p < 0.001$), which had fallen below initial levels by Split 3 ($p < 0.0001$) (Figure 30). However, there was no significant difference between any of the treatment conditions when examined independently of split, with the exception of AD brain 1:3000 and the no treatment control where a very weak drop was measured ($p = 0.022$).

Pairwise comparisons in the two-way ANOVA were performed between treatment condition and split to assess: 1) the effect of split number on the difference in Aβ load between conditions and 2) how cells from each treatment condition handled Aβ load after each split. In the first instance, after Split 1, a significant elevation in intracellular signal compared to the no treatment control (0.24 μm^3/cell Aβ) was observed only for AD brain dilutions 1:5000 (1.36 μm^3/cell, $p = 0.008$) and 1:10000 (1.08 μm^3/cell, $p = 0.047$) and for the positive ADDLs control (1.16 μm^3/cell, $p = 0.03$). None of the other conditions were sufficiently far apart to reach significance, according to the test. At Split 2, again the positive ADDLs control (1.81 μm^3/cell, $p = 0.019$) reported a stronger signal than No Tr. (0.82 μm^3/cell), together with AD brain 1:3000 (2.42 μm^3/cell, $p < 0.0002$). With respect to the other conditions, AD brain 1:3000 contained more Aβ per cell than AD 1:5000 (1.53 μm^3/cell, $p = 0.036$), AD 1:50000 (0.71 μm^3/cell, $p < 0.0001$), and both control brain controls (1.42 μm^3/cell for 1:3000, $p = 0.019$ and 1.09 μm^3/cell for 1:5000, $p = 0.002$), but not AD 1:10000 (1.59 μm^3/cell, $p = 0.051$), which was inconsistent with the fact that AD 1:3000 was the most concentrated seeding dilution. Finally, within Split 3 there were no differences.

When looking at the performance of each condition across the three splits, all spiked at Split 2, except AD 1:50000, which declined steadily (Figure 30). The fact that the No Tr. cells followed the same pattern puts a heavy shadow of doubt over the results from this experiment, as Aβ content there was expected to remain constant. As such, even if it

would be tempting to speculate that some degree of seed proliferation is occurring between Splits 1 and 2, such a conclusion cannot be made if the negative control is not uniform. Despite this general trend, AD 1:3000 ($p = 0.001$) and CTRL 1:3000 ($p = 0.04$) were the only two conditions where the measured spike in Aβ load at Split 2 was significant. By Split 3, Aβ load was negligible, had dropped significantly from Split 1 in all AD brain conditions and the positive ADDLs control ($p < 0.022$), and ranged from 0.09 μm^3/cell for AD 1:3000 to 0.01 μm^3/cell for CTRL 1:3000; in this case the value calculated for the no treatment control was 0.02 μm^3/cell, which was higher than both AD 1:10000 and the positive ADDLs control. As such, while signal is present in all treatments up to the second split, its almost complete disappearance in the third split (Figure 30) most likely represents a suboptimal quality of staining, rather than a true biological process. When considering potential sources of error and variability i.e. staining, seed load, transfer of comparable cell numbers during splits, imaging parameters, and Aβ volume quantification protocols among others, it becomes apparent that the above observations and statistical tests are meaningless at this stage before the experiment has been replicated and more images per condition are analyzed. Unfortunately, as this experiment is exceptionally time-consuming, it was beyond the scope of the current project to faithfully replicate it.

5.2.2.2. 7PA2 Cells

Immunodetection of Aβ in 7PA2 cells was much more robust than in SK-N.NL-F cells (Figure 31), but again significance upon quantification and normalization of Aβ load as above was variable. Overall, there was a trend for Aβ load to decrease with each split, where the drop from Split 2 to Split 3 ($p < 0.0001$) was again steeper than from Split 1 to Split 2 ($p = 0.042$) (Figure 32). In addition, the only AD brain treatment which the two-way ANOVA determined to have a significantly higher Aβ volume from a control brain condition throughout the experiment, namely CTRL 1:5000, was AD 1:3000 ($p = 0.001$). The accumulation of Aβ seeds in AD 1:3000 cells was also generally elevated compared to the positive ADDLs ($p = 0.006$) and the no treatment control ($p < 0.0001$). The remaining AD brain seeding conditions contained more Aβ per cell throughout the experiment only when compared to No Tr. ($p < 0.02$), but not in relation to any of the other controls. Importantly, overall Aβ load for each condition in 7PA2 cells was roughly 10-fold higher than what was measured in SK-N.NL-F cells.

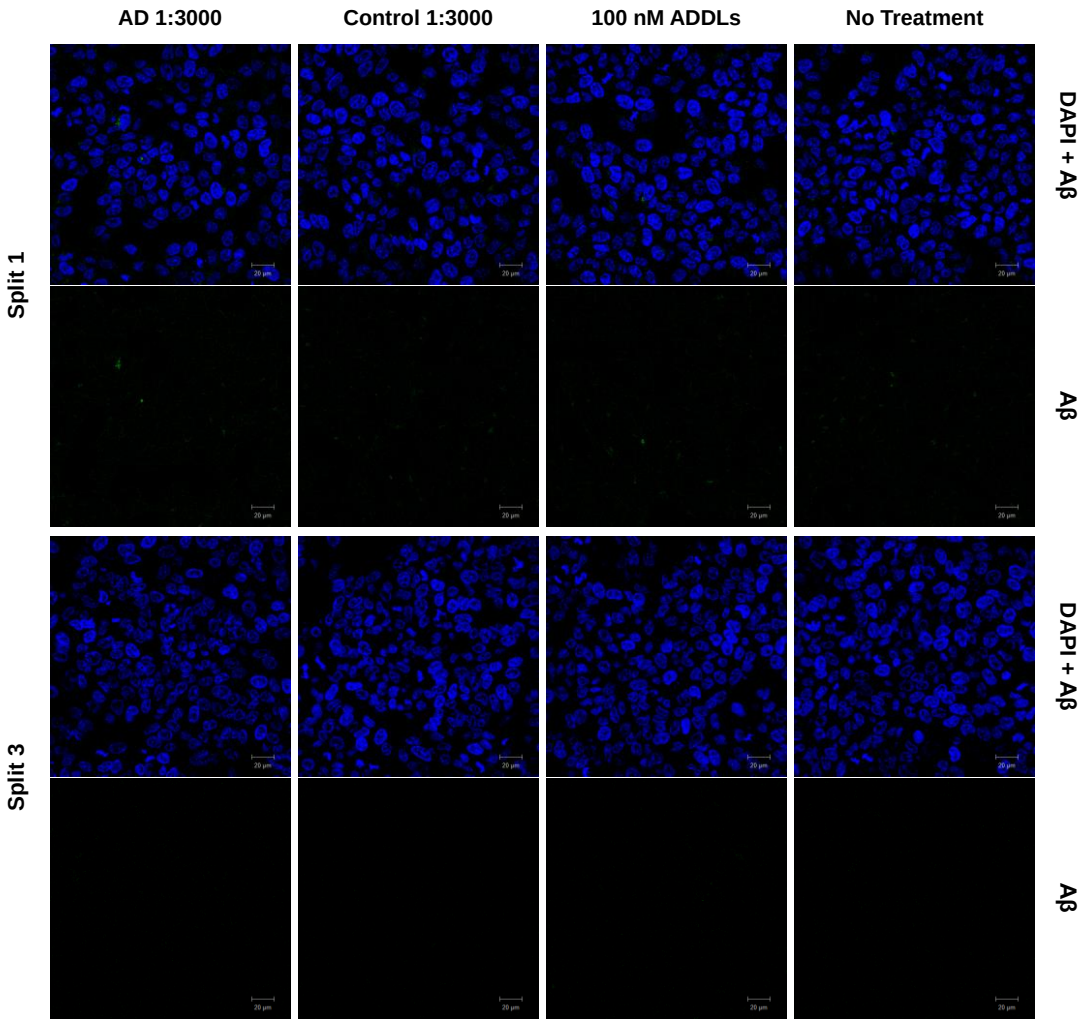

Figure 29. Intracellular Aβ after seeding SK-N.NL-F cells with human-derived brain homogenate.
Representative images of four conditions from two splits of seeded SK-N.NL-F cells are shown here. Cell nuclei are visualized with DAPI (blue) and intracellular Aβ is shown in green. Z-stacks were taken at 40x magnification and here mid-cell sections are shown. Scale bar = 20 µm.

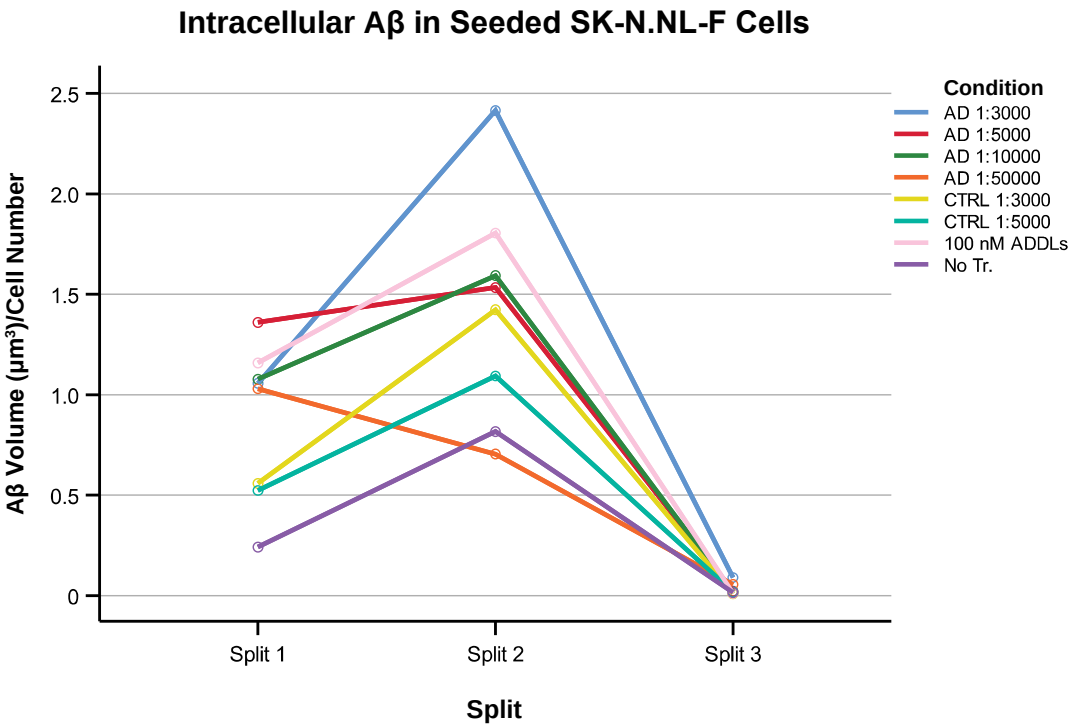

Figure 30. Quantification of intracellular Aβ from seeded SK-N.NL-F cells.

The effects of treatment dilution and split on total Aβ load (µm^3) from seeded SK-N.NL-F cells was compared with a two-way ANOVA and the Bonferroni correction for multiple pairwise comparisons was used. Plotted are the estimated marginal means obtained from averaging total Aβ load normalized to nuclear count from six z-stacks per condition. The test returned significant differences in Aβ load between the three splits ($p < 0.001$), but there were no differences when comparing treatment conditions alone. When comparing the effect of the split on each seeding condition, a few differences between conditions were observed in Splits 1 and 2 ($p < 0.05$), but none in Split 3 and details of these are discussed in the text. Although it is impossible to make specific interpretations from the current data, they do suggest that the seeding material is being degraded the longer the cells are in culture and that they are not propagating it within the experimental timeframe. CTRL = control brain. No Tr. = no treatment.

When accounting for the time the cells have spent in culture post seeding, AD 1:3000 was the only condition which always reported a higher Aβ content than other AD or control conditions, but the differences were not consistent after each split. For example, shortly after seeding at Split 1, AD 1:3000 cells contained 11.22 µm^3 Aβ/cell, which was maintained after Split 2 (11.09 µm^3/cell) but fell to 2.86 µm^3/cell after Split 3 ($p < 0.0001$). At Split 1, this result was significantly higher than AD 1:10000 only ($p = 0.029$), which reported 7.74 µm^3/cell, but not than AD 1:5000 (8.65 µm^3/cell) or AD 1:50000 (9.19 µm^3/cell), both of which are less concentrated. The fact that AD 1:50000 came up higher than both

1:5000 and 1:10000 is also puzzling, as is the fact that AD 1:50000 had equal amounts of Aβ as CTRL 1:3000 (9.71 μm^3/cell) at this stage. The remaining controls ranged from 6.48 to 5.99 μm^3/cell. In contrast, at Split 2 AD 1:3000 and AD 1:5000 (8.18 μm^3/cell) maintained their Aβ loads and were still statistically similar ($p = 0.068$); the former was significantly higher than the remaining conditions ($p < 0.009$), except ADDLs (8.07 μm^3/cell, $p = 0.058$), but the latter was only different from the No Tr. control (2.65 μm^3/cell, $p = 0.001$). The remaining two AD conditions had significantly dropped down to 5.59 and 5.04 μm^3/cell, compared to AD 1:3000 ($p < 0.001$), which also made them indistinguishable from controls at this stage. By Split 3, all AD conditions had lost a substantial amount of signal and were statistically similar. What is even more confusing is that at Split 3 AD 1:3000 had dropped so much as to be also similar to all controls (0.67 – 0.30 μm^3/cell), in contrast to the remaining AD conditions, which had less Aβ to start with, but maintained loads statistically higher that controls after three splits (5.19 – 2.86 μm^3/cell, $p \leq 0.037$).

In summary, it appears that AD 1:3000 and 1:5000 handled seeds similarly, where these were maintained for two splits (approximately a week) but lost most of them by the third split. On the other hand, AD 1:10000 and 1:50000 reached a plateau as soon as Split 2, where the drop from Split 1 to 2 was steep for 1:50000 ($p = 0.009$). This may reflect a delay in clearance mechanisms associated with excessive Aβ burden. Nevertheless, control brain treatments also demonstrated high Aβ levels initially, which fell drastically between Splits 2 and 3 ($p < 0.0001$), which is confusing because Aβ in either sample could not be detected by WB. The same pattern was followed by the positive ADDLs control, but most disturbing is that, as with SK-N.NL-F cells, the no treatment control also showed a steady decline in signal with splits, particularly between Splits 1 and 2 ($p < 0.036$). For this reason, these observations should most likely be attributed to artefacts with staining and/or measurement, as native 7PA2 cells maintained in appropriate antibiotic concentrations should not change their endogenous Aβ levels so drastically.

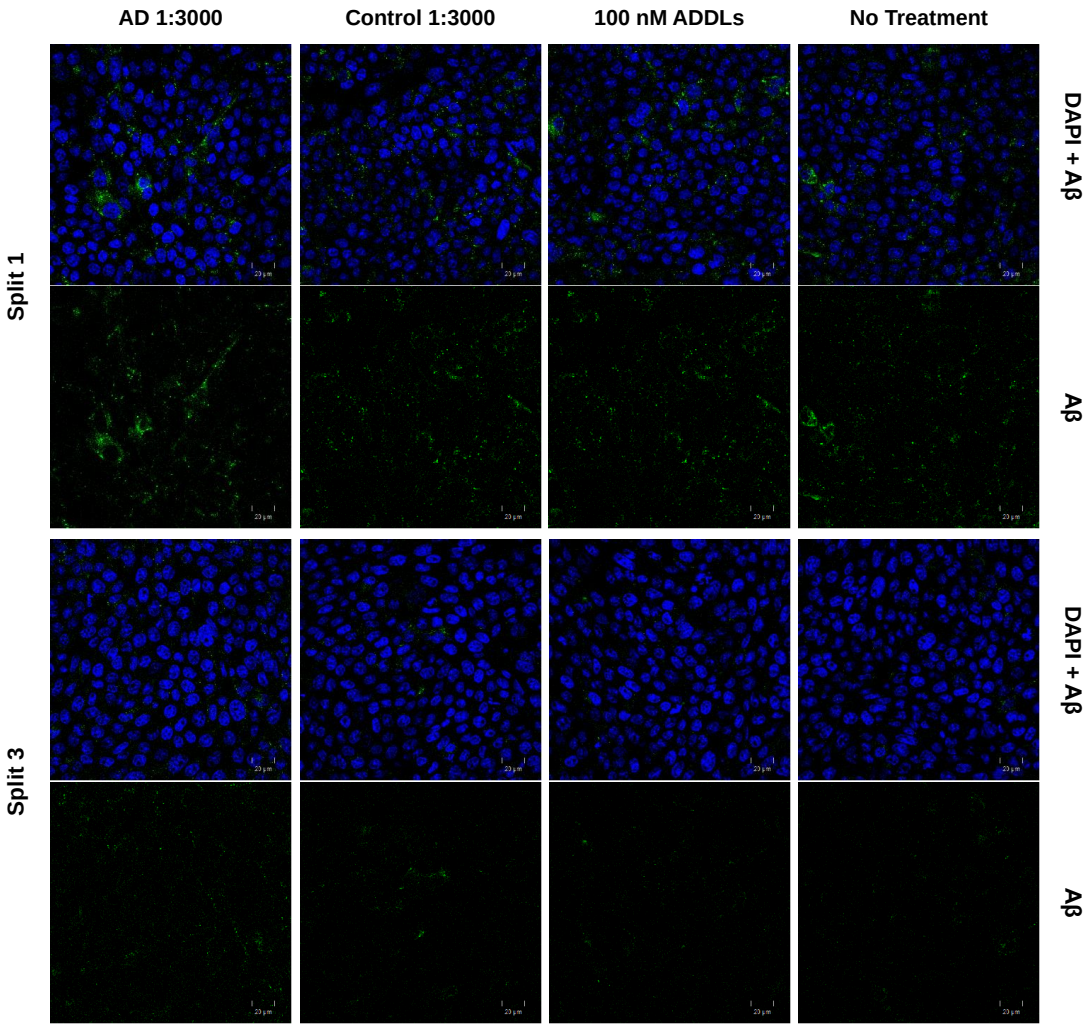

Figure 31. Intracellular Aβ seeds after treatment of 7PA2 cells with human AD brain.

Representative images of seeded 7PA2 cells are shown as in Figure 29. Aβ is shown in green and nuclei in blue. Scale bar = 20 µm.

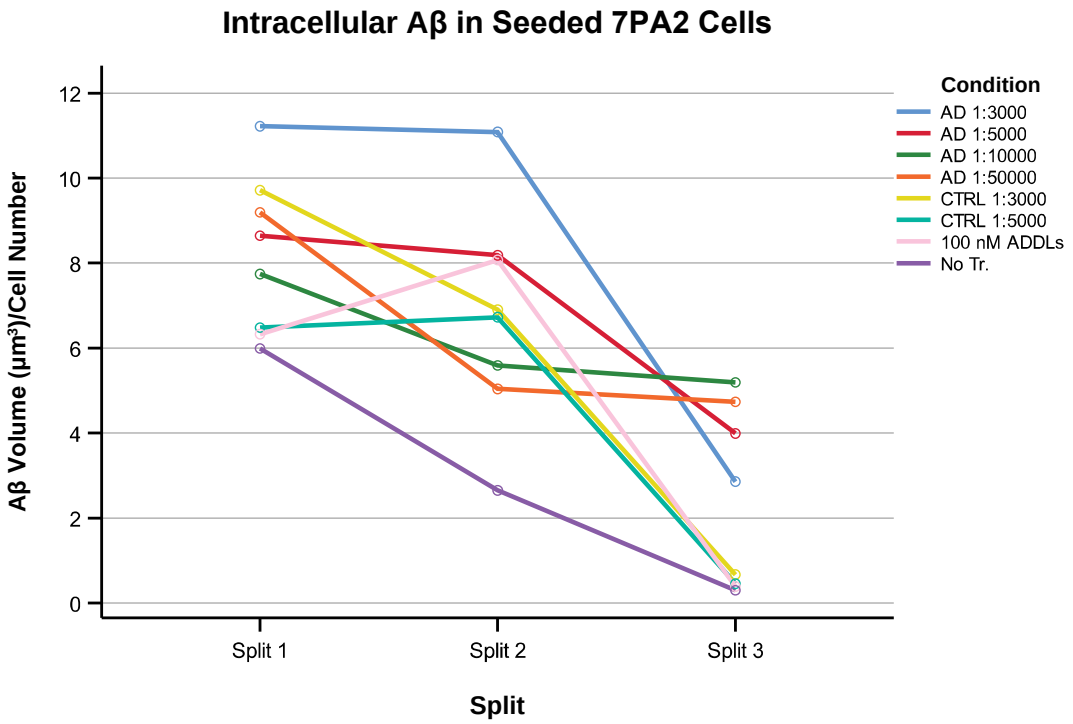

Figure 32. Quantification of intracellular Aβ from seeded 7PA2 cells.

The effects of split and dilution on total Aβ load (µm^3) normalized to nuclear count have been analyzed and plotted as in Figure 30 above. The two-way ANOVA again returned a significant decrease in Aβ signal across all three splits ($p < 0.05$), where the drop to Split 3 was drastic ($p < 0.0001$). Irrespective of split, the four AD conditions were different only from the No Tr. (no treatment) control ($p < 0.02$). Again, there were some synergistic differences between split and condition; however, as the readout for the No Tr. control was not constant, such comparisons are inconclusive. CTRL = control brain.

5.2.2.3. GI-ME-N Cells

Seeded GI-ME-N cells showed hardly any Aβ-positive staining for any of the treatments (Figure 33). The variability in signal was huge and there was no difference in seed load among splits or conditions (Figure 34). As already seen from the results from SK-N.NL-F and 7PA2 cells, variability issues with staining and detection were a running theme for the whole experiment. The survival and growth of GI-ME-N cells after splitting was poor, which may also have been due to plating density issues, so they did not survive to Split 3. In summary, at this stage there is not enough sound experimental evidence to suggest that any of the tested cells are able to propagate brain-derived Aβ seeds intracellularly and whether these are actually taken up by the cells after treatment. Should the sensitivi-

ty of the oligomeric ELISA be improved, and the immunofluorescent staining repeated, these questions could be better addressed.

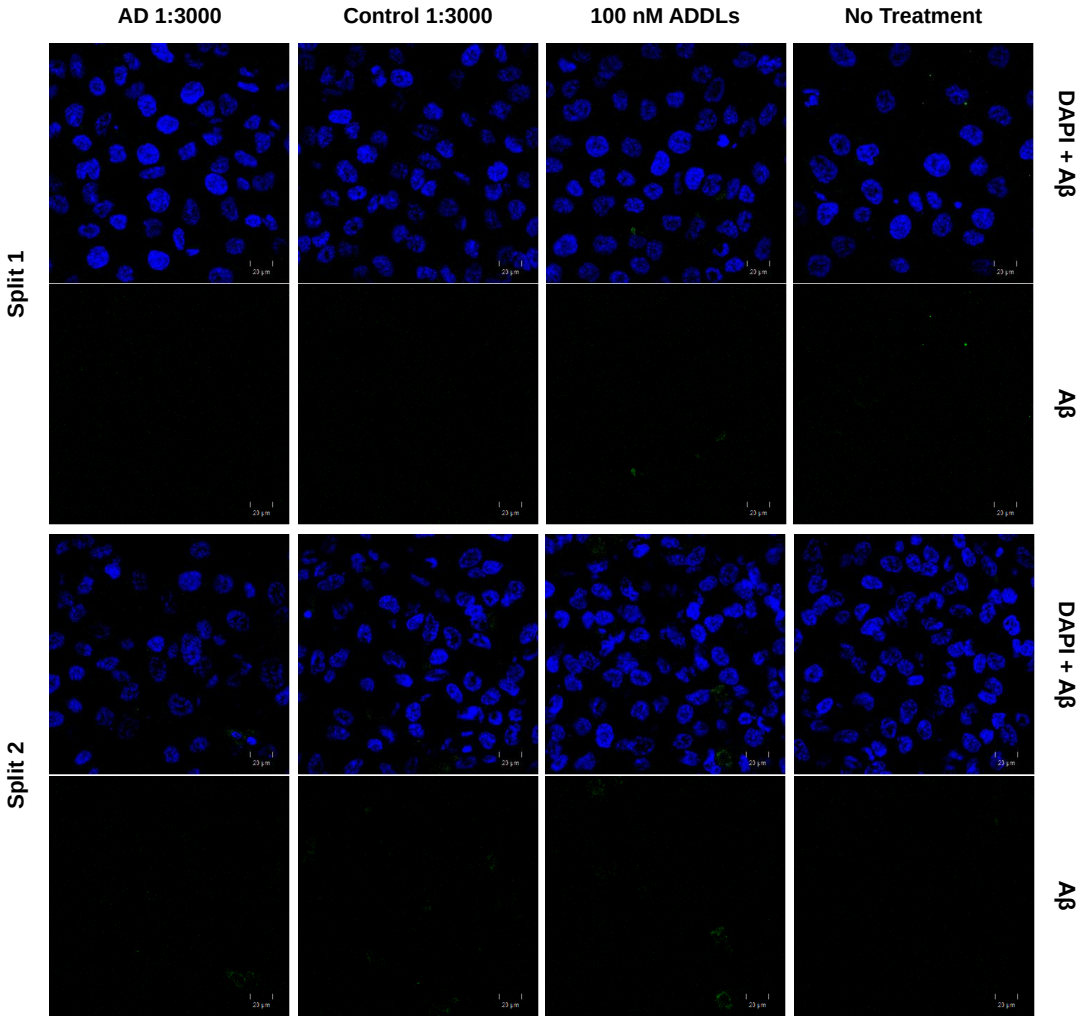

Figure 33. Intracellular Aβ in seeded GI-ME-N cells.

Representative images of seeded GI-ME-N cells are shown as in Figure 29 and Figure 31. Aβ is shown in green and nuclei in blue. Scale bar = 20 µm.

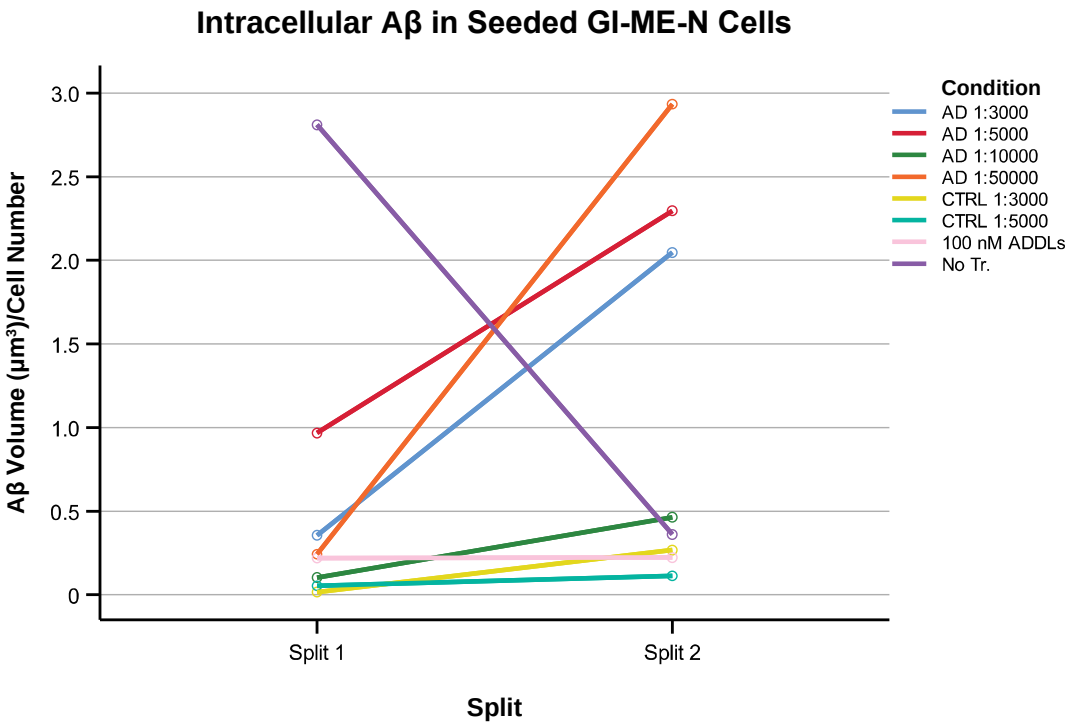

Figure 34. Quantification of intracellular Aβ from seeded GI-ME-N cells.

The data for total Aβ load (µm^3) after seeding of GI-ME-N cells were analyzed and plotted as in Figure 30 and Figure 32. The cells did not survive to Split 3, so data from only two splits are presented. As evident from the graph, all readings were too variable for any statistical differences to be established for any of the singular and combined interactions tested.

6. Discussion

6.1. Summary of Aims and Results

6.1.1. Initial Characterization of Human Neuroblastoma Cell Lines

The aim of this project was to lay the groundwork for a cell-based Aβ seeding assay, which would be able to monitor faithful propagation of patient-derived or synthetic AβO. Such a model would serve as a valuable high-throughput tool to study and modulate the mechanics of AβO strain propagation; investigate the relationship between Aβ, tau, and other AD-related proteins and how their interactions contribute to disease; and to screen for potential drug compounds and their effects. A similar model, which relies on dividing cells, already exists for prions and we investigated whether the same principle could be applied to Aβ. Therefore, a panel of human neuroblastoma cells was chosen for characterization and to test whether any one of them could be a suitable platform. Out of eleven lines, only five met the requirements of quick to moderate doubling times, growth in a monolayer, and good recovery after splitting and a further two met only two of these conditions (Table 8, p. 83). When the cells were grown in serum-free medium for 4-6 days only two cell lines, SK-N-BE(2) and its subclonal line BE(2)-M17, did not show visible changes in morphology or growth rate (Figure 7, p. 86). The growth rate of the remaining lines was reduced and most of them underwent morphological alterations to some extent, somewhat akin to differentiation.

The seven lines partly or completely meeting the crude culturing requirements were further characterized for their expression of proteins directly contributing to Aβ production. An expression spectrum was generated through WB for APP, BACE1, APH1α, NCSTN, PEN2, and PS1. There were four distinct processing patterns of APP in the seven lines, with SK-N-BE(2) and BE(2)-M17 being particularly strong expressers, while GI-ME-N cells showing hardly any presence of full-length APP (Figure 8, p. 88). In contrast, BACE1 was detected in five of the lines, where again signal in SK-N-BE(2) was very prominent, while GI-ME-N and LS yielded no detectable protein (Figure 9, p. 88). Surprisingly, APH1α was only consistently detected in two lines (Figure 10, p. 91). NCSTN expression was stronger in three lines, but because of variability in the WB signal it was difficult to establish concrete statistical differences, which was also true for the remaining two γ-secretase components, despite visible differences in the blots. An attempt to estimate the activity level of γ-secretase in the seven lines was made by taking the ratio of full-length to cleaved PS1. Interestingly, while no significant differences were established in expression, the two lines with lowest

overall PS1 amounts had higher proportions of cleaved protein compared to the remaining five.

Next, the ability of the seven lines to produce Aβ was confirmed and quantified by WB and ELISA (Figure 11 and Figure 12, p. 93 and 94). After 3-4 days in culture, CM was immunoprecipitated with two anti-Aβ antibodies targeting an N-terminal and a mid-region epitope respectively. Two out of the seven lines secreted enough Aβ to fall within the detection limit of WB and these were again SK-N-BE(2) and their subclonal BE(2)-M17 cells. The increased sensitivity of the ELISA revealed the presence of Aβ species in six out of seven lines, except for GI-ME-N cells where no Aβ could be detected. Three Aβ species were simultaneously measured; Aβ1-40 was the most abundant species in three lines, followed by Aβ1-38, and then Aβ1-42. Conversely, CHP-134 cells followed exactly the opposite pattern, while only Aβ1-40 was detected in LS and NBL-S cells. Following this initial screen, several lines could have been good candidates depending on rationale, but only two were selected for future work. SK-N-BE(2) cells expressed readily-detectable amounts of APP, BACE1, and Aβ, which made them a good candidate for a permissive cell line. On the other hand, GI-ME-N cells were taken forward as a putative negative control, as it was reasoned that the low endogenous expression of the three proteins would make them refractory to seeding. Thus, it could be investigated whether the presence and total amounts of Aβ alone are sufficient to drive seeding.

6.1.2. Generation and Overexpression of APP/BACE1 Constructs

Four gene constructs containing APP and BACE1 were cloned and overexpressed in SK-N-BE(2) and GI-ME-N cells to upregulate the amyloidogenic pathway and to also outcompete other non-amyloidogenic cleavages, since it is apparent from the APP processing signatures and the difference in secreted Aβ that the two lines cleave APP along markedly different pathways. Two commonly studied mutations were introduced into the constructs either on their own or simultaneously to expand the variety of Aβ signatures available and to see whether a particular profile would facilitate seeding. All constructs were successfully overexpressed (Figure 16 and Figure 17, p. 101 and 102). It appears that expression of APP in SK-N-BE(2) cells was already saturated, as no significant elevation of this protein was observed, while BACE1 overexpression occurred as expected. Conversely, simultaneous overexpression of APP and BACE1 into GI-ME-N cells achieved the desired effect of altering APP processing, which is evident from the band distribution in Figure 17a. In addition, while the vector-only control had no effect on BACE1 levels in GI-ME-N cells, its introduction alone appeared to elevate APP levels and partly alter its processing. Alter-

natively, it is possible that G418 selection itself exerts unforeseen stresses on GI-ME-N cells, which alters their homeostasis, or favors the survival of a sub-pool of cells with this processing signature. A comparison between G418-selected vector-only and non-infected cells would resolve this question.

Consistently with overexpression of APP and BACE1, Aβ levels in both SK-N-BE(2) and GI-ME-N cells became sufficiently elevated to be detected on WB (Figure 18 and Figure 19, p. 103). This time CM was only cultured for 17-24 h before IP, in contrast to the previous experiment where CM was cultured for several days. Untreated SK-N-BE(2) cells correspondingly did not show Aβ after the shorter incubation time. In addition, this time it was also the vector control that behaved unexpectedly, as Aβ levels were elevated, despite no detectable changes in APP or BACE1 amounts. Clearly, the treatments associated with introducing the pLNCX2 vector into either cell line exert unknown pressures on the cells and it would be interesting to see whether this effect is consistent along several other cell lines. A similar elevation of metabolic load by virtue of overexpression of the G418 resistance gene alone has been previously observed in CHO cells (Yallop & Svendsen 2001). However, strictly speaking, as the empty vector was originally intended as a negative control, the resulting positive changes in APP expression in GI-ME-N and Aβ secretion in SK-N-BE(2) cells casts doubt onto the validity of this set of results as a whole. As CM Aβ was quantified for infected cells and compared to uninfected controls, the differential effect of the vector treatment was more apparent (Figure 20 and Figure 21, p. 106). No Aβ was detected for GI.V cells, while SK-N.V cells had Aβ levels higher than control.

Overall, elevating total Aβ production in SK-N-BE(2) cells was a success for all vector conditions. SK-N.WT, SK-N.SWE, and both control lines had the same Aβ1-40/1-42 ratios. On the other hand, the ratio was reduced in SK-N.IBE and SK-N.NL-F cells. All overexpressing SK-N-BE(2) cells secreted more Aβ than the well-studied 7PA2 cells and SK-N.NL-F also had more than double the amounts of Aβ1-42. In stark contrast with the SK-N panel, CM from infected GI-ME-N cells had negligible amounts of Aβ1-40, while the other two species were more prominent. This is a likely outcome of the previous observations that APP is apparently processed in a completely different way in these cells. Again, here the NL-F mutant showed the highest Aβ1-42 and therefore the highest Aβ1-38 amounts within the GI-ME-N panel, but all concentrations were still much lower than in 7PA2 cells. At this point, the most promising line was judged to be SK-N.NL-F due to its ability to produce large amounts of Aβ1-42 at the expense of Aβ1-40.

The mass spectrometry experiments were aimed at gaining a better insight into the way the overexpressing cells handle APP (Figure 22 and Figure 23, p. 108 and 109). These data were consistent with the ELISA with respect to the effects of the mutations (discussed later). Six Aβ peptides were proportionally more abundant in the pool of total Aβ secreted by infected SK-N-BE(2) cells, namely Aβ1-40, 1-38, 1-34, 11-40, 1-19, and 1-14. This somewhat overlapped with the pattern of 7PA2 cells, which showed peaks at Aβ1-40, 1-38, and 1-14, but also at Aβ1-33 and Aβ1-28. The majority of Aβ species secreted by overexpressing GI-ME-N cells were shorter (peaks at Aβ1-14, 1-17, and 1-19), and while Aβ1-28, 1-34, 1-38, and 1-40 were also elevated, they constituted a small percentage of total Aβ. In addition, unlike infected SK-N-BE(2) cells, GI-ME-N cells revealed no Aβ peptides beginning at residue 11. Finally, Aβ in GI.V CM was not detected.

6.1.3. Inoculation with Brain Homogenate and Quantification of Seed Propagation

To investigate the ability of SK-N.NL-F cells to propagate Aβ seeds, the cells were inoculated with different dilutions of AD and control brain and were maintained over three splits to dilute out the inoculum and to observe newly formed AβO. 7PA2 and GI-ME-N cells were used as a putative positive and negative control respectively. The Aβ content of the AD sample and its ability to induce amyloidosis in Tg mice had already been demonstrated by a different group in our department (Figure 24 and Figure 25, p. 110 and 111). An ELISA using the same antibody for capture and detection was set up to detect secreted AβO in CM and its specificity was confirmed (Figure 26, p. 112). CM was collected before each split and quantified in this way. No oligomers were detected in any of the media samples, apart from the ADDLs control treatment, where the disappearance of signal by Split 2 clearly showed that only inoculum was being detected (Figure 27 and Figure 28, p. 114 and 115). Control 1:1000 dilutions of AD homogenate were also positive for AβO; this dilution was not used on cells, however, as it was found to be toxic. Staining for intracellular and membrane-bound Aβ from all seeded cell lines returned inconsistent and variable results, both within and among treatment groups (Figure 29-Figure 33, p. 118-124). In conclusion, there were many technical difficulties involving assay sensitivity and experimental design, which made pilot experiments unsuccessful in demonstrating the ability of SK-N.NL-F and 7PA2 cells to propagate exogenously-derived AβO. However, we now have a panel of well-characterized cell lines that model amyloidogenic APP processing on different genetic backgrounds and which could still yield positive results under different experimental conditions.

6.2. Selection of Cell Type and Culturing Limitations

Two of the main drivers behind the need to generate a cell-based model of Aβ seeding are the slow turnover and associated cost of similar mouse experiments. While experiment time can be shortened by using primary neurons or organotypic slice cultures (e.g. Nath et al. 2012, Novotny et al. 2016, Stancu et al. 2015), again in this case mice need to be sacrificed. Patient-derived induced pluripotent stem cells (iPSCs) are another alternative (e.g. Israel et al. 2012, Muratore et al. 2014), which comes as close as possible to the true genetic background of disease and also provides flexibility, as these cells can be differentiated to any cell type and this process can be carefully staged. These platforms are invaluable for investigating the biological effects of amyloid deposition because of their complexity, but they have high maintenance requirements and are not ideal for experiments with a high throughput. We therefore chose to use immortalized neuroblastoma cell lines, which are useful in that they can be maintained in culture over many splits and are easy to treat and modify. Of course, these cells are derived from cancers and contain chromosomal abnormalities which may bring their relevance into question, but they already have a neural progenitor background and can be easily differentiated up to a point if necessary. In addition, the huge variety of lines with substantial phenotypic differences available allows for larger-scale screens for cells suitable for the study of APP amyloidogenic processing and Aβ seeding. A valid argument can also be put forward that since the well-characterized 7PA2 hamster cells already exist, they should be the starting point for the present project. Nevertheless, we decided that human cell lines would be more suitable.

There were several problems associated with working with eleven cell lines simultaneously. It was difficult to culture all of them under the conditions recommended by the supplier, as this would have greatly increased the requirement for materials and encumbered workflow. Compromises therefore needed to be made with regards to the media and supplements, so that the cells appeared healthy, but could also be maintained easily. It would have been informative to carry out several standard viability assays to better asses the cells' response to the different culturing conditions. Quantifying the lines' health parameters in this way would have influenced the choice of cells after the subsequent protein expression characterization or at least would have indicated if adjustments of the nutrient mixtures were imperative. For example, while GI-ME-N cells were adherent, had rapid doubling times, grew in a monolayer without clumping, and were overall easy to culture, they were remarkably difficult to infect and were not tolerant to treatments like fixing and permeabilization for IF or inoculation with brain homogenate and subsequently

recovering. Although they stood out with their almost complete lack of APP expression and no amyloidogenic processing and were one of the lines with the most robust appearance, it is possible that GI-ME-N cells may have been cultured under stressful conditions, thereby impairing their performance. Nevertheless, as all lines appeared healthy and grew well over multiple splits, performing viability assays was not essential.

With Table 9 in mind, more conducive towards accurate replication would also have been to perform several rounds of timed splits where the cells from a confluent plate were counted and a known density was plated into the split plate. That way, an exact growth rate could have been calculated, which would have provided a useful criterion of comparison among cell lines and also of the overall health of a cell line after a long time in culture. In the case of lines which showed high mortality after passaging, a count of the dead cells in the culture medium after allowing a short period of re-adherence and subtracting that from the known number of cells plated would have yielded another parameter according to which culture methods could have been adjusted. Timing trypsin treatment for adherent cells would have allowed adherence to be quantified. The health of cells cultured with reduced or no serum was also estimated empirically without a more thorough quantification of homeostasis. Serum deprivation alters gene expression even during short time intervals which may induce unintended differentiation, as was most obvious in CHP-134 and NBL-S cells, arresting of the cell cycle, or apoptosis, but the high protein content of serum interferes with immunoassays through non-specific binding interactions, so a trade-off always exists between culturing healthy cells and subjecting them to stress immediately prior to an assay. Again, before-and-after viability assays would have given an indication of how well the cells were performing under this stress and whether APP processing and therefore their Aβ signatures were altered. Despite the above considerations and as informative as this systematic evaluation would have been, it was deemed non-essential and was not broached due to time constraints. Besides, we had already chosen the 7PA2 cell line as a main point of comparison and detailed protocols for its culturing medium for Aβ quantification call for serum-free conditions (Shankar et al. 2011), as Aβ's indiscriminate binding behavior means it would be very likely sequestered by proteins such as albumin, which is known to easily bind Aβ and inhibit its aggregation (Milojevic et al. 2009). This could significantly confound the readouts of assays which aim to detect both monomeric and oligomeric Aβ.

6.3. Characterization of Amyloidogenic Protein Expression – Outcomes and Considerations

Performing WB experiments for the range of proteins responsible for canonical amyloidogenic processing allowed us to gain useful insights into the behavior of the seven neuroblastoma lines which passed the initial culturing conditions screen. It was interesting to observe that while APP and γ-secretase were expressed to various degrees in all lines and BACE1 was readily detectable in five of them, these elements translated into abundant Aβ production in only BE(2)-M17 and SK-N-BE(2) – two of the seven lines. Further ELISA quantification of CM showed that Aβ is secreted by an additional four lines, in low or trace amounts (as already stated in Chapter 1, while it may appear that CHP-134 cells have higher amounts of Aβ1-42 compared to other lines, this peptide was inconsistently detected in the ELISA replicates). As BACE1 is essential for Aβ production, it was not surprising that GI-ME-N cells, where BACE1 could not be detected, secreted none of the three tested peptides. On the other hand, BACE1 could not be quantified in LS cells either, but the presence of miniscule amounts of Aβ1-40 and 1-42 in CM indicate that perhaps BACE1 is expressed at levels below the detection threshold of WB. In hindsight, blotting for CTFs and AICD would have been an additional useful method to estimate the proportion of total APP converted into Aβ.

We were also surprised that APH1α was not ubiquitously detected in our lines, particularly in the two with highest Aβ production. This could mean that, similarly to BACE1 in LS cells, the neuroblastoma lysates contain very low amounts of APH1α or that instead APH1β is expressed. Preliminary RNA sequencing (RNA-seq) data indicated that APH1α mRNA is indeed present in all lines and the highest expresser were in fact LS cells. These data are nevertheless not reported in this thesis because they were not replicated due to financial constraints and due to their tangential relevance to the core of the project. It has been shown that the endopeptidase activity of γ-secretase which cleaves the APP CTFs into p3 or Aβ and the AICD is dependent on the presenilin isoform incorporated into the complex, with PS1 being more active than PS2 and also having a preference for the Aβ1-42 → Aβ1-38 branch, while the carboxypeptidase activity of the complex is dependent on the APH1 isoform, with APH1β complexes releasing Aβ species prematurely (Acx et al. 2014). While blots for the alternative isoforms APH1β and PS2 were not performed, it would have been interesting to investigate whether complex heterogeneity exists in the neuroblastoma lines and to what extent that influences the proportions of Aβ species they produce. In addition, while in GI-ME-N and LS cells nearly all protein components

were expressed at low levels, estimated γ-secretase activation was highest based on the ratio of full-length and cleaved PS1. This activation likely has no relevance to Aβ generation, as γ-secretase has many substrates, for instance Notch which are receptors with crucial importance for development (Okochi et al. 2002). Clearly, endogenous expression of APP and the amyloidogenic secretases is not sufficient to guarantee Aβ production, so there may be other factors at play like active degradation exceeding production, for example, which limit this branch of the pathway.

It is evident from Figure 8 that APP undergoes processing in all seven cells, but this largely does not lead to Aβ production. Although neuroblastoma cells contain neuronal features, some of which may be characteristic of later stages of differentiation (Barnes et al. 1981, Cornaglia-Ferraris et al. 1990, Schlesinger et al. 1976), evidence from untreated iPSCs shows that APP is not processed at all despite its abundant expression (Bergström et al. 2016). Early neuronal differentiation causes iPSCs to cleave APP non-amyloidogenically and only in later differentiation stages do they shift towards producing Aβ (Bergström et al. 2016). There was no evidence, however, whether these changes in processing occur alongside changes in BACE1 and γ-secretase expression. Theoretically, the differences in Aβ production observed in the seven neuroblastoma lines could be a result of enzymatic activity corresponding to distinct differentiation stages, but one must be wary of interpreting the results along this line of thought because the genetic abnormalities of these cells will not cause them to behave like normal neural crest cells, which would follow a strict differentiation pattern on their path to becoming neurons. It is more likely that co-localization of APP and BACE1 is low and Aβ is therefore produced in low amounts or that other secretases are more abundant and/or active. An attempt to detect ADAM10 in the lysates was made, but no signal was detected due to the poor specificity of the antibody. Although it is necessary to reiterate that the aforementioned RNA-seq data has not been replicated or validated, it did give an indication that GI-ME-N cells express higher mRNA levels of other secretases compared to the other cells. Of note, cathepsin B mRNA was particularly abundant as is often the case with metastatic cancer cells and as the protease is known for its participation in Aβ clearance (Mueller-Steiner et al. 2006), it could be particularly active in GI-ME-N cells. In any case, it is evident that in many of the cell lines APP is processed along non-amyloidogenic pathways, despite the expression of all amyloidogenic proteins.

It would have been invaluable to complete and validate the RNA-seq data, in order to better understand the factors that contribute to Aβ seeding permissibility in neuroblastoma

cell lines and to make a more informed choice about which lines would be a good model platform. In this way a full overview of secretase activity within the chosen cell lines would have been available, which would have enabled us not only to exclude cells which favor non-amyloidogenic pathways, but to explain differences in APP processing and Aβ production in the cells. Knowing which γ-secretase complexes are active in the neuroblastomas would have allowed us to understand the drivers behind the panels of secreted Aβ species and how these are changed after overexpression of the APP/BACE1 constructs. Similarly to what was done for overexpressing SK-N-BE(2) and GI-ME-N cells later on, a mass spectrometry analysis of Aβ composition in CM, combined with validated RNA-seq would have been a great systematic evaluation of the relevance of this array of cell systems for studying APP processing and Aβ seeding. In addition, we considered performing a γ-secretase activity assay, but this was non-essential as most lines produced Aβ and this is clear evidence of the activity of the complex. Still, having reference values as a point of comparison between the lines would have been another useful method to better understand the different cell metabolisms.

6.4. Upregulating the Amyloidogenic Pathway in SK-N-BE(2) and GI-ME-N Cells

6.4.1. APP/BACE1 Construct Design

Generating the four versions of the APP/BACE1 construct for retroviral overexpression was relatively straightforward, although low transformation efficiencies greatly delayed the generation of gene-modified cells. Originally, we considered assembling two retroviral constructs to overexpress APP, BACE1, and the four γ-secretase components simultaneously, but we reasoned that APP and BACE1 overexpression only would be sufficient to substantially elevate the levels of Aβ produced by the cells and that it would be more valuable to investigate whether introducing mutations in the APP sequence would facilitate seed propagation depending on the Aβ peptides produced. Another approach would have been to overexpress C99 only, which would have simulated elevated β-secretase cleavage, but this would not have affected endogenous amyloidogenic APP processing, which as already discussed was weak in most lines. BACE1 was therefore also introduced to outcompete α-secretase activities. The Swedish and Iberian mutations were chosen for their distinct properties of elevating amyloidogenic processing and increasing Aβ1-42/1-43 production. These mutations are often used in mouse models (e.g. APP23, APPPS1; Lamb et al. 1997; Radde et al. 2006) and their effects can be synergistically combined (e.g. APP NL-F mice; Saito et al. 2014) to yield a phenotype with accelerated amyloid plaque deposition. I hoped to be able to recapitulate accelerated amyloid production in the neuroblastomas

to some extent or at least be able to compare how harboring one or both mutations affects the cells.

6.4.2. Improving Infection Efficiency

Retroviral infection was chosen as the mode of introducing the constructs because it guarantees insertion of the coding DNA directly into the host's genome and is therefore a good way to ensure stable overexpression. The virus was pseudotyped with VSV-G for maximum infectivity, as the low-density lipoprotein receptor (LDLR) which it targets is constitutively expressed in all mammalian cells, even though the packaging cell line is already designed to coat the viral particles with the dualtropic 10A1 protein. This targets the gibbon ape leukemia virus (GALV) and the amphotropic retrovirus receptor 1 (Ram-1), which are also expressed in humans. As a result, SK-N-BE(2) cells were straightforward to infect and subsequent blots revealed very high levels of both APP and BACE1, but GI-ME-N cells proved difficult, even after the protocol was adapted to consist of two rounds of infection 8 h apart, which doubled the viral titer that the cells were exposed to. Ultimately, this protocol was maintained, but the supernatant needed to be concentrated to increase the virus titer even further and ensure enough GI-ME-N cells were infected to survive selection. After antibiotic selection the surviving cells from each condition were pooled together, as isolating individual clones would have greatly expanded the workload at this point and proof-of-principle evidence was needed first.

6.4.3. Mutation Effects and Aß Production Profiles

6.4.3.1. SK-N-BE(2) Cells

Overexpression of the constructs in SK-N-BE(2) cells was successful and the relative amounts of the three Aβ species quantified by ELISA were consistent with the introduced mutations. Due to the high endogenous APP production of SK-N-BE(2) cells, further elevation of APP levels did not result in a measurable change as detected by WB and the processing pattern between infected and uninfected cells remained unaltered, but this clearly translated into significantly elevated amounts of secreted Aβ compared to uninfected cells. This was first observed by immunoprecipitating total Aβ from the CM of infected cells, where it was abundant even after an overnight-only incubation, while previously medium needed to be cultured for several days to detect Aβ from native cells. In addition, as expected, the strongest Aβ band was seen in SK-N.SWE cells, where the Swedish mutation significantly elevates total Aβ production, followed by SK-N.WT and SK-N.NL-F cells. SK-N.IBE cells showed a modest total increase of Aβ, which reflects only the overexpres-

sion of the protein, as the Iberian mutation only decreases the Aβ1-40/1-42 ratio. Why then the amounts of Aβ detected from SK-N.WT and SK-N.IBE cells appear so different is unclear, but this is consistent with previous observations made in BE(2)-M17 cells (Golde et al. 1993, Suzuki et al. 1994). It is possible that the longer Aβ species produced as a result of the Iberian mutation aggregate inside the cells and most of them are therefore not secreted. Still, this is not the case in 7PA2 cells which also overexpress APP with the similarly-acting Indiana mutation. These discrepancies could be down to APP copy number and therefore to transfection/infection efficiency or due to unknown differences between the lines' APP processing mechanisms. In any case, it is unlikely that 7PA2 cells accurately recapitulate the behavior of this mutation in neurons, due to their origin (hamster ovary).

A closer inspection of the proportion and type of secreted Aβ species revealed more details about the way APP is processed with respect to the four constructs and what shifts in Aβ species can be observed. As expected, the Aβ1-40/1-42 ratio was maintained across SK-N.WT, SK-N.SWE, SK-N.V, and SK-N-BE(2) cells despite the differences in total Aβ between the four lines. In the two constructs harboring the Iberian mutation, the Aβ1-40/1-42 ratio dropped considerably (up to ten times), where SK-N.IBE and 7PA2 cells were equal and SK-N.NL-F cells produced the most Aβ1-42 per Aβ1-40. In addition, total Aβ in SK-N.NL-F cells was higher than in SK-N.IBE, which is due to the presence of the Swedish mutation in that line. Most importantly, SK-N.NL-F cells had more than twice the amounts of Aβ1-42 compared to the well-studied 7PA2 cells, which made them a very good candidate for the seeding assay as we hypothesized that a cell line secreting large amounts of aggregate-prone Aβ would be better suited to propagate oligomeric seeds. It is unclear why the pLNCX2 vector alone elevated Aβ production enough that it was detected not only by ELISA but by WB as well. As discussed above, a comparison between SK-N.V and G418-treated uninfected SK-N-BE(2) cells would indicate whether the effect is due to antibiotic treatment or to the presence of the vector.

Mass spectrometry analysis of the secreted Aβ species was generally consistent with the quantification of Aβ1-38, 1-40, and 1-42. Nevertheless, it was somewhat unexpected to observe that while distinct elevations in the concentration of Aβ1-42 were measured by ELISA, the portion that the peptide contributed to the overall pool of secreted Aβ peptides remained uniform across all lines, including 7PA2. Whether this represents an intracellular aggregation event of this particular peptide or whether it simply reflects a corresponding increase in other species as a result of APP and BACE1 overexpression is not clear. In addition to canonical γ-secretase cleavage, which generates Aβ peptides 38-43

amino acids long, several alternative cleavage products were detected and some of these amounted to a large proportion of the total Aβ species present in CM. Apart from its primary cleavage site immediately N-terminally of the Aβ sequence, BACE1 has been shown to cleave at two alternative sites found within Aβ, between residues 10 and 11 and residues 34 and 35 (Shi et al. 2003, Vassar et al. 1999). As described in Chapter 1, BACE1 is highly expressed in untreated SK-N-BE(2) cells and that its levels were significantly elevated after overexpression of the APP/BACE1 constructs. It is therefore not surprising to detect several Aβ11-X species in infected SK-N-BE(2) cells, while these were not found in 7PA2 cells which do not overexpress BACE1. Similarly, Aβ1-34 comprised approximately 10-12% of all Aβ peptides secreted by APP/BACE1-overexpressing cells, while it only amounted to less than 5% in SK-N.V control cells, where Aβ1-40 and 1-38 also contribute to a larger proportion of the total peptides. Finally, evidence has shown that Aβ1-34 is preferentially produced from Aβ1-40 and the proportional amounts of the latter peptide are indeed reduced in all APP/BACE1-overexpressing cells (Shi et al. 2003). For these reasons, it is likely that BACE1 in particular is responsible for cleaving Aβ at residue 34 in overexpressing SK-N-BE(2) cells, but this cannot be ascertained without systematic inhibition or downregulation of BACE1, BACE2, and γ-secretase, as all three can cleave at that position (Andreasson et al. 2007, Portelius et al. 2014).

BACE2 has an alternative cleavage site, after residues 19 and 20 of Aβ (Yan et al. 2001), but γ-secretase has also been proposed to be able to hydrolyze Aβ as far N-terminally as residue 16, even though this region lies far outside of cell membrane where the complex is active (Portelius et al. 2011). Inhibition and knockdown experiments would therefore also shed light on which enzyme is responsible for the generation of Aβ1-19, which was very abundant in the tested media, and also of Aβ1-20. Even shorter C-terminally truncated Aβ species were also reported by the mass spectrometry analysis and again these could originate from several processes. It is possible that species of 14 – 16 amino acids in length are generated by ADAM10 cleavage of C99, which is known to occur in cells (Kuhn et al. 2010). Insulin-degrading enzyme (IDE) is also cleaves between residues 14 and 15 (Andreasson et al. 2007, Qiu et al. 1998) and again probing for and inhibiting it should indicate whether the modest peak at Aβ1-14 is attributable to this protease or another unknown enzyme, particularly as it seems that IDE is a major player in the clearance of Aβ (Saido & Leissring 2012). Similarly to BACE2, IDE also cleaves after residues 19 and 20 of the Aβ sequence, so it could be another candidate to explain the abundance of Aβ1-19 and Aβ1-20. It is difficult to make assumptions about the relative contributions of differ-

ent secretases without having a corresponding readout for sAPPα, sAPPβ, and p3 relative amounts.

Finally, the overall Aβ secretion signature for treated SK-N-BE(2) cells and the 7PA2 line was markedly different. The difference in peak position and intensity in 7PA2 cells (lack of a major spike at Aβ1-19, spikes at Aβ1-28 and 1-33, and a much less prominent Aβ1-40 contribution) points towards a markedly different way in which APP and therefore Aβ are processed in this line compared to its human-derived counterparts. Further investigation is needed to see which enzymes are responsible for the two alternative peaks (for example, neprilysin cleaves Aβ after residue 33, while Aβ1-28 can be produced by neprilysin, IDE, and plasmin (Andreasson et al. 2007)) and why there is such a stark reduction in α-secretase activity in 7PA2 cells. A comparison between human CSF and SH-SY5Y cell media (Figure 35) showed that the pattern of Aβ in CSF was similar to that in CM from SH-SY5Y cells (Portelius et al. 2011), and this in turn is rather similar to the pattern demonstrated by overexpressing SK-N-BE(2) cells in terms of the detected species, although there is some variety in their relative abundance. It is reasonable to hypothesize that systems which generate similar Aβ processing profiles could share similar mechanisms and are therefore more closely related, so even if the secreted Aβ does not result in seeding, these cells are likely to represent a better model of APP processing.

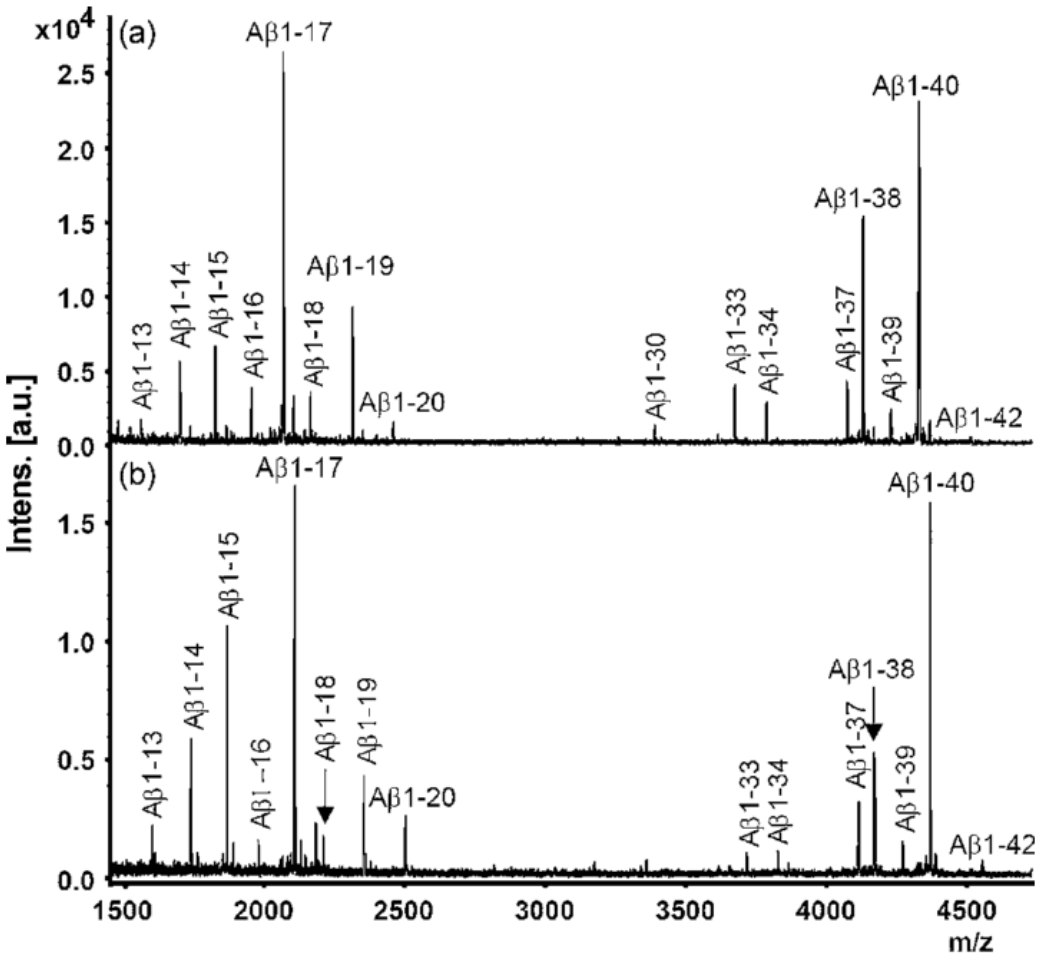

Figure 35. Representative mass spectrum patterns of Aß secretion in AD CSF (a) and untreated SH-SY5Y media (b) (from Portelius et al. 2011).

Mass-to-charge (m/z) ratio is plotted along the x-axis and intensity with arbitrary (a.u.) units is plotted on the y-axis.

6.4.3.2. GI-ME-N Cells

In contrast to infected SK-N-BE(2) cells, their GI-ME-N counterparts only showed subtle increases in Aβ production, although both APP and BACE1 were overexpressed. Unfortunately, signal variability in GI.SWE and GI.IBE cells did not allow for a statistically significant increase in APP compared to uninfected cells to be quantified, despite the visible elevation in signal. Moreover, unlike in SK-N-BE(2) cells, BACE1 overexpression in infected GI-ME-N was not uniform, which is likely due to the aforementioned difficulties with low infection efficiency. Again, here the pLNCX2 vector boosted APP expression and altered the WB band pattern to match that of the cells containing the insert, without affecting BACE1 levels. This, however, did not translate into elevated Aβ levels in GI.V cells like it did for SK-N.V cells. The increase in Aβ secreted by the remaining lines was also modest.

This time, the most Aβ was immunoprecipitated from GI.NL-F cells, while hardly anything was detected in GI.SWE cells. The IP data may appear misleading, as the 7PA2 band is much weaker than that shown for GI.NL-F cells, corresponding to more Aβ in the medium, but this was actually not the case, as shown by the ELISA quantification. The 7PA2 control sample was immunoprecipitated together with the set of SK-N-BE(2) samples and was preserved until the GI-ME-N samples were ready to blot, so it is likely that some degradation occurred before the second set of IPs could be carried out and therefore the 7PA2 signal was reduced. The blot was nevertheless not repeated because the subsequent ELISA quantification was the essential experiment.

The amounts of Aβ1-38, 1-40, and 1-42 in CM from overexpressing GI-ME-N cells were much lower than the readout from 7PA2 cells. The processing was also reversed compared to 7PA2 and SK-N-BE(2) cells – Aβ1-40 was practically nonexistent compared to Aβ1-38 and Aβ1-42. It could be that perhaps heavy preferential processing of Aβ1-40 by additional secretases in GI-ME-N and GI.WT cells, which express WT APP and also followed this pattern, is responsible. GI.WT cells secreted more Aβ than both GI.SWE and GI.IBE cells, but not more than GI.NL-F and this result confirmed the IP data. Consistently with what was observed for SK-N.IBE and SK-N.WT cells, GI.IBE also secreted less Aβ than WT. GI.NL-F cells secreted twice as much Aβ1-38 and 1-42 compared to WT cells, while their Aβ1-40 secretion levels were the same. Expression of the Swedish mutation alone reversed this tendency, but by doing so reduced all quantified Aβ species to nearly zero, which was unexpected, and which lends support to the supposition that Aβ1-40 is cut into shorter fragments by enzymatic activity or that overall Aβ degradation exceeds production. Therefore, it is also impossible to tell at this stage whether the unequal levels of BACE1 overexpression among mutant lines have led to corresponding differences in total Aβ production.

The mass spectrometry data revealed Aβ secretion signatures dominated by short C-terminally truncated species, indicative of ample α-secretase activity, but not elevated amyloidogenic processing as the ELISA data suggests. This corroborates the earlier observation from Chapter 1 that APP bands are hardly detected on WB, but that no Aβ can be recovered from CM. While the patterns of GI.WT, GI.IBE, and GI.NL-F cells closely resembled each other, the pattern of GI.SWE cells was reversed, consistently with the ELISA quantification – Aβ1-40 contributed to approximately 5% of total Aβ, while its proportions were close to nil in all other GI-ME-N lines. Correspondingly, the Aβ1-38 peak had dropped in the Swedish mutant. In addition, Aβ1-28, Aβ1-33, and Aβ1-34 were prominent,

while the contribution of Aβ1-14 was halved and Aβ1-17 was equally abundant as Aβ1-19. Again, as observed with SK-N-BE(2) cells, while Aβ1-42 was the second most abundant species out of the three quantified and its amounts varied across mutants, its contribution to the pool of total Aβ remained equally low for all lines. Despite the clear differences with SK-N-BE(2) cells, the overall secretion pattern was much more similar to the one shown by 7PA2 cells, although the latter exhibit higher β- and γ-secretase activity because of the larger amounts of longer Aβ species. A final remark needs to be made regarding the length of the Aβ species detected – there were only twenty-one species reported in the current mass spectrometry experiments, which were based on the immunoprecipitation – mass spectrometry method, while a more detailed characterization of 7PA2 cell medium was previously made when liquid chromatography was combined with high resolution tandem mass spectrometry (LS-MS/MS) to reveal more than ninety APP products (Portelius et al. 2013). Analyzing cell medium with this method would yield even more detailed results about the fate of APP and Aβ in the infected neuroblastoma cells. Nevertheless, the current data does not favor GI-ME-N cells as they clearly do not sustain Aβ production and bear few similarities with the pattern seen in human CSF, while SK-N-BE(2) cells seem to be more relevant.

6.5. Seeding of SK-N.NL-F, 7PA2, and GI-ME-N Cells with Human Brain Extracts

Although the cells were seeded with an AD brain homogenate which was unequivocally shown to accelerate amyloid plaque deposition in young APP NL-F mice in contrast to control human brain homogenate which had no detectable effect, these properties could not be reproduced in the cells I generated. There were multiple technical difficulties associated with the cell seeding experiments and these will be discussed below, but the preliminary AβO ELISA and IF data do not suggest that the cells tested under these conditions were able to propagate Aβ seeds extracellularly and were inconclusive with respect to intracellular propagation. Failure to induce seeding at this stage does not necessarily reflect a fault with the system, but it could be due to the way in which the brain sample was prepared, which would mean that it is handled differently by cells in culture and by a complete biological environment such as a mouse brain. It quickly became apparent that a 1:1000 dilution of 10% brain homogenate was toxic to the cells, but the AβO content in a 1:3000 dilution may have been insufficient to induce seeded aggregation of endogenous Aβ over short experimental timelines. It may be necessary to prepare cleaner extracts through centrifugation and therefore apply more concentrated Aβ to the culture, as the time the cells can spend in culture before being passaged will depend on their doubling.

Alternatively, an approach where cells with slower growth rates like the NBL-S line may be more appropriate.

It is necessary to point out that the brain samples were not age-matched. Nevertheless, as the experiments presented here were pilots, the samples behaved as expected in mice, and considering the difficulty in obtaining human brain for research, I made use of these homogenates left over from Dr. Silvia Purro's work. A potential limitation of this positive and negative control match that needs to be taken into account is that the two are too far removed in terms Aβ load and types of aggregates. An additional age-matched negative control will have been more informative, as it may have been enough to elicit a mild seeding response in the tested mice. However, as the object of Dr. Purro's experiments was to show a clear difference in mouse cerebral response to an Aβ-laden and an Aβ-poor brain as a proof-of-principle, which was successful, this difference in human sample age was in fact advantageous for the pilot cell seeding experiments. An age-matched control that elicits a response in mice would not have been a true negative control.

6.5.1. Troubleshooting the Aβ Oligomer-specific ELISA

Setting up the oligomeric ELISA was seemingly straightforward, but there were several difficulties associated with it, which mainly concerned the cost of the materials. Firstly, the authors of the publication describing the protocol (Hölttä et al. 2013) used an expensive custom-made synthetic Aβ dimer as the assay standard. It spans the first eleven residues of Aβ and therefore omits the C-terminal region which is responsible for the formation of amyloid structures. The dimer is therefore an ideal standard for the assay, as there is no mechanism for it to aggregate during storage and handling, unlike full-length Aβ, which is incredibly "sticky" and can form oligomers over time even when stored at -80^{o}C. In addition, using this dimer ensures that one binding event is equal to one signaling event, which allows for sensitive readouts of oligomer content. Since the same group who provided us with the mouse seeding data is also adept at preparing well-characterized ADDLs with known molarity, we initially thought that these oligomers could be a good substitute for the dimer standard. At this time, the ADDLs had been successfully employed as standards for another quantitative immunoassay in the department, but I discovered that they were unsuitable for this particular ELISA primarily because it was impossible to maintain them at the concentration at which they were originally provided.

In-house ADDLs are prepared from a monomeric solution of 100 nM Aβ1-42, which is left to aggregate unagitated at room temperature and its oligomer concentration is analyzed

at particular time points until the majority of Aβ has aggregated (Nicoll et al. 2013). At this point the molarity of oligomers is recorded and even though the solution is prepared using is Hams's F12 medium, which is routinely used as the solvent of choice for AβO (Stine et al. 2011), and is then immediately aliquoted and frozen, the concentration of oligomers continues to change over time due to Aβ1-42's remarkable ability to aggregate. This poses serious difficulties when a more sensitive assay needs to be established, as larger AβO will be quickly diluted out in lower serial dilutions of the standard curve, while at the same time they will over-saturate the high dilutions, leaving a very narrow region of linearity and corresponding upper and lower quantification limits to work with. Therefore, even though I attempted to adjust the standard curve and use the smallest possible dilution factor in an effort to maintain a homogenous ADDL solution throughout, it was impossible to quantify oligomers of a concentration lower than ~300-400 pM. This would not have posed such a problem if the AβO I aimed to detect were of high molecular weight, but as cells were expected to secrete low-n (and likely few) oligomers, using the ADDLs as a standard was incompatible with the sensitivity of the ELISA.

The second major hurdle was that the capture and detection 82E1 antibody was very expensive, which significantly drove up the cost of one experiment. I therefore began by assessing whether it would be possible to reproduce the ELISA using the 6E10 antibody, which has a similarly localized epitope at the N-terminus of Aβ and therefore detects all Aβ peptides. Nevertheless, although I tried different combinations of capture-detection antibody concentrations, I was not able to match the sensitivity offered by 82E1 with 6E10 (preliminary experiments, results not shown). As antibody pricing was still an issue, I performed the assay by halving the volume of antibody used for plate coating and sample detection, in order not to compromise the concentrations stated in the published protocol (Hölttä et al. 2013). This significantly improved detection and quantification limits and correspondingly expanded the region of linearity. When the dimer standard was used together with the published concentration of antibody at half the volume, the best LLOQ I managed to obtain was 14.37 pg/ml. This was nevertheless still at least ten-fold higher than the reported sensitivity of the ELISA, but due to time constraints I was not able to work on further improvements. Nevertheless, an experiment to quantify AβO concentration in mouse brain extracts was later performed with my help by a fellow PhD student, Justin Tosh, and this time the correct antibody concentrations and volumes were used. The assay successfully quantified oligomers in multiple mouse samples and its LLOQ was increased by twofold to 7.18 pg/ml (not shown, quoted with permission), but it was still a long way from the assay's reported lower limit of 200 fg/ml (Hölttä et al. 2013).

Given that the published protocol was followed exactly and the same parameters were not reproduced, it is possible that there were additional steps which were not reported by the authors. Pipetting by hand rather than using robots will also increase all margins of error and this could be another potential difference. With respect to the results from quantifying AβO in cell medium, either ELISA sensitivity is the primary barrier or there are simply no oligomers in the CM. Evidently, a 1:1000 dilution of 10% AD brain homogenate can be quantified, although it yields a low readout of AβO, but a 1:3000 dilution is too low for oligomers to be detected in the inoculum. Oligomers of any size should be detected by the ELISA, but as the assay is set up with the lowest possible Aβ assembly (a dimer) as a standard, the larger the oligomer is, the more inaccurate the results would be. This explains why the same molarity of ADDLs used as positive controls in both the SK-N.NL-F and 7PA2 assays (Figure 27 and Figure 28) returned such different concentrations. It is obvious in this case that the assay needs additional work to further finetune its parameters. An alternative assay format is developed by MesoScale Discovery, from where the Aβ Triplex ELISA discussed earlier was purchased. The manufactured assays are rigorously standardized and to my knowledge are the most sensitive ELISA systems available, particularly because of the use of the chemiluminescent SULFO-TAG reporter antibody conjugate, which provides better signal to the TMB colorimetric substrate which I used and which the publication quotes. Kits for in-house MSD ELISA setup can be purchased and ideally, I would have preferred to use that method for the AβO assay, but unfortunately the price per experiment would be beyond the project's budget. Still, if CM from seeded cells were quantified via this method, it could yield a positive result.

6.5.2. Approaches for the Quantification of Intracellular Aβ Seed Propagation

Interpreting the results from the quantification of intracellular Aβ seeding was difficult because the data were too variable and funding constraints made time insufficient to properly troubleshoot the protocols, as these experiments had to be performed in the few weeks leading up to the end of the project. Had there been sufficient time for optimization, the first priority would have been to see whether the apparent increase in Aβ load at Split 2 in SK-N.NL-F cells and the sustained signal between Splits 1 and 2 in 7PA2 cells are real, whether it could be maintained, and whether the inconsistent results from the no treatment controls from both cell lines reflect genetic changes in the cells akin to subcloning due to splitting. As already reported, the brain homogenates were toxic to the cells at dilutions equivalent to or lower than 1:1000, even over short incubations of a few hours, so experiments had to be restarted several times before stable cultures post-

inoculation could be maintained. Considering the dynamic nature of the setup where cells are collected at each split and the low cell count by function of the 96-well format, a compromise had to be made between maintaining sufficient cell density and plating multiple chamber slides. Again, the setup of passaging the cells several times after treatment with brain was crucial to distinguish true oligomer propagation from oligomers introduced via the inoculum. This, of course, meant that should antibody staining be unsuccessful, a second chamber slide from the same condition would not be available. It is necessary to note that at this point I was also using cells from each split for an alternative method to detect membrane-bound and intracellular Aβ seeded aggregation via an enzyme-linked immunospot (ELISPOT) assay. ELISPOT assays for membrane-bound PrP^{Sc} aggregates are performed routinely in our group as the quantitative part of the Scrapie Cell Assay, so we surmised that the method may also work for Aβ. However, when it became apparent that this would take much more time to optimize than anticipated, the method was abandoned, and I continued only with immunofluorescent detection.

Originally, I was interested in finding out whether I could employ the same principle as the oligomeric ELISA to distinguish between Aβ aggregates and pools of monomeric Aβ species on and within the cells. I therefore performed two complete rounds of primary and secondary antibody staining with non-biotinylated and biotinylated 82E1, detected with an anti-mouse AF 488 antibody and a Streptavidin 568 conjugate respectively. It was necessary to first complete staining with the non-biotinylated primary-secondary pair to minimize cross-reactivity with the biotinylated primary. Unfortunately, there was too much background cellular staining with the Streptavidin conjugate to be able to quickly determine the validity of the principle and I did not continue with attempts to improve blocking or adjust the antibody concentrations, although optimization in the future may be possible. A general disadvantage of Aβ and APP antibodies is that they are almost exclusively reared in mice and all are of the IgG1 type, which makes double labeling impossible. I therefore also considered another strategy by pairing antibodies 6E10 and 4G8 or 82E1 and 4G8; both 6E10 and 82E1 are IgG1 type, while 4G8 is an IgG2b type. Theoretically, it could have been possible to stain with isotype-specific secondary antibodies, but as the primaries do not share the same epitope and are also able to detect APP this idea was not pursued. Alternatively, oligomer-specific antibodies could have been used, but it was already too late to purchase and begin testing those out. Consequently, I had to resort to single labeling with 82E1, which recognizes the cleaved N-terminus of Aβ and has little cross-reactivity with APP, in order to be able to quantify the total Aβ load of the cells.

Coincidentally, the confocal microscope was out of order for the better part of this timeframe and an alternative machine was not available and not appropriate because the experiments were already underway, and the imaging conditions could no longer be changed. This limited the number of z-stack images that could be taken per well and consequently impaired the quantitative power of the data. It would have been possible to increase the amount of data collected by taking single-pane mid-cell level images but attempting to quantify AβO in this way would have been unrepresentative because it would have discounted aggregates bound to the membrane or closer to the cell periphery. Z-stacks allow for the full volume of the cell to be quantified and this method was preferable, despite the low number of image sequences that could be obtained. Although the earlier Aβ Triplex ELISA experiments showed that SK-N.NL-F cells have more Aβ than 7PA2 cells, fluorescence was always much lower and closer to background in SK-N.NL-F. Therefore, imaging conditions were optimized for the 7PA2 line and were then applied to SK-N.NL-F and GI-ME-N cells, but in hindsight this was likely a mistake because that way the latter two lines are imaged under stringent parameters, which would lead to loss of real signal and would increase variability depending on the quality of staining. To mitigate this, separate quantification protocols with different sensitivity were set up. A better way would have been to set separate imaging protocols for each of the three lines to begin with and then quantify in this way.

Differences in cell number presented a further problem to measuring and quantifying total Aβ volume, despite normalization to nuclear count. SK-N.NL-F and 7PA2 cells grew quickly, but the former continued to grow on top of each other, while the latter did not grow past forming a monolayer. Despite this, I did not want to split the cells earlier; it was important to maintain them in culture for several days prior to splitting so AβO have a chance to form. The opposite issue occurred with GI-ME-N cells; they are naturally large and flat, so density was always low. They were also very intolerant to all treatments; fixation, washing, and staining would cause them to float off the substratum unless the liquids were pipetted with extreme care. Even then, cells were always lost. In addition, inoculation with brain homogenate was toxic even at higher dilutions and the cells were not recovering well; they also appeared stressed by the small surface area available and the relatively low densities at which they had to be plated. Consequently, GI-ME-N cells did not survive to Split 3 and were also too sparse when they were imaged. The z-stacks for all lines were set up to image the full volume of the cells, from the basal membrane to the surface. Therefore, to maintain the distance between image slices equal, the total number of slices needed to be increased. However, this meant that while one z-stack from 7PA2

cells would take approximately five minutes, a SK-N.NL-F z-stack would take between fifteen and twenty minutes. As already stressed several times, time was a limiting factor and so instead of adhering to a strict distance between slices, the number of slices was adjusted to reflect the thickness of the imaged cell layer, but no more than eighteen images were taken per z-stack. Still, in this way a slice thickness of approximately 1 µm could be maintained.

Finally, setting up the quantification protocols was not straightforward. The difficulties associated with detecting Aβ signal among different cell types were already discussed and although the software is able to detect non-black pixels that cannot be seen by eye, some signal was likely lost because of discrepancies in imaging conditions and staining efficiency. For example, staining was suboptimal for all conditions in Split 3 of SK-N.NL-F cells and therefore quantified Aβ load is much lower than the previous two splits. This would also explain why there is a sudden drop in signal in the four control treatments in Split 3 of 7PA2 cells, as these chamber slides were processed at the same time. In addition, the nuclei of all three cell lines appeared granular and so the software had issues detecting each nucleus as an "object" – some were split into two or more pieces, while some nuclei too close together were identified as a single object, so the protocol with the least noise had to be determined empirically. Visibly, it appeared as if Aβ signal was higher in AD and ADDL treatments compared to negative controls, but from the current quantification it is impossible to tell whether there is a real decrease and also whether seeds are propagated with cell splits. When comparing images by eye it seemed as if overall Aβ load was decreasing with each split and the AβO ELISA data might also suggest that seeds are washed away or degraded, but nothing can be concluded for certain at this point. To be able to make more sound conclusions, the experiments need to be carefully repeated over a longer timeframe, conditions need to be optimized, and more data points need to be collected before SK-N.NL-F and 7PA2 cells can be truly discounted as non-seeders. However, currently it appears as though even though both lines secrete ample amounts of Aβ, neither is able to propagate AD brain-derive seeds.

6.6. Possible Reasons for the Inability of SK-N.NL-F and 7PA2 Cells to Seed Aβ Aggregation

In summary, neither SK-N.NL-F nor 7PA2 cells seeded the aggregation of Aβ oligomers; alternatively, seeding was undetectable under the pilot experimental conditions. GI-ME-N cells were used as a negative control and we were not expecting them to exhibit any seeding activity because of their complete lack of Aβ production. On the other hand, 7PA2

cells were used as a positive control because they have been reported to secrete oligomers, which we hypothesized would facilitate seeding (Walsh et al. 2002). Nevertheless, these oligomers were detected with SDS-PAGE and as argued by Benilova et al. (2012), this method is very prone to facilitate the aggregation of Aβ and therefore produce structural artefacts, which underlines the need for these cell-secreted oligomers to be proven by other methods. If cell-secreted oligomers are not an artefact, these should be more abundant in SK-N.NL-F cells because of the higher absolute and relative amounts of Aβ1-42 they secrete. If the cells indeed do not seed, there may be several reasons for this. Firstly, neuroblastoma cells might be an unsuitable platform to simulate seeding because of how far they are removed from normal neuronal cells. Nevertheless, evidence from SH-SY5Y cells showed a net accumulation of AβO following uptake of fluorescently labeled Aβ1-42 in acidic cellular compartments and these oligomers retained their seeding ability within subsequent cell lysates (Hu et al. 2009). Secondly, the mechanism of Aβ seeded aggregation is probably not governed by the same simple template-based replication principle as PrP^{C} misfolding into PrP^{Sc}, but may require additional factors, which cannot be simulated in a system with only one cell type. If, however, the process is linear and directly proportional to the concentration of seed as is the case with in vivo seeding (Morales et al. 2015), then perhaps longer incubation times will be necessary before the cells are split. This may actually call for slower-dividing cell lines, contrary to our initial assumption that it is better to use the lines with the fastest doubling times for the sake of throughput.

It is also possible that neuroblastoma cells are not able to process the brain-derived oligomers they uptake in a way that would allow them to trigger aggregation of endogenously produced monomeric Aβ or that a 1:3000 dilution is too low to induce a response over the observed timeframe. There may be a need for purification of Aβ assemblies from the 10% w/v homogenate through centrifugation to reduce the amount of unnecessary protein, thereby reducing its toxicity, and to liberate smaller soluble AβO. If time had been sufficient, I would have liked to seed the cells with 3000 *g* and 100000 *g* PBS pellets and supernatants from APP23 and APPPS1 mice to distinguish between the ability of membrane-bound, vesicle-contained, or soluble Aβ to induce seeding. It is likely that the 100000 *g* supernatant, which would be the cleanest preparation with the smallest oligomers and has been shown to be highly active in inducing seeding (Langer et al. 2011), would be well-tolerated by the cells. Since the concept of strains also exists with respect to AβO conformations, it could be that the cells studied here are not able to match the conformation of seed contained in this particular AD brain. It was recently demonstrated that despite a continuous increase in cerebral Aβ load with age, Tg mice seeded with self-

same extracts demonstrated much stronger deposition with respect to Aβ content induced by young extracts with lower Aβ1-40/1-42 ratios and therefore higher Aβ1-42 content when compared to aged extracts (Ye et al. 2017). Younger mice will have more low-n soluble AβO, which have not yet aggregated in rigid β-sheet-rich plaques, so it could be that the relative seeding activity of these homogenate preparations reflects the structural difference between these Aβ formations. It would therefore be valuable to carry out a structural analysis of the AD brain homogenate used for seeding in this PhD thesis to obtain a better understanding of its variety of AβO conformations.

6.7. Implications and Perspectives

Had I managed to detect a net increase in AβO in medium and intracellularly over several splits, the first milestone in generating a high-throughput cell-based model of Aβ seeding would have been reached and as already discussed in Sections 1.4 and 1.5 of the Introduction, this versatile tool would have been hugely important towards understanding the principles of amyloid pathology not only in AD, but also in related dementias. One avenue for further experimentation using the model would have been aimed at drawing as many parallels as possible between Aβ and PrP to prove whether Aβ is a "true" prion or simply has prion-like properties common to amyloid structures. This would have involved demonstrating that Aβ seeds are competent after multiple rounds of transmission in and between both cell and animal systems. To that end, firstly, it would have been crucial to prove whether seeds propagated by the cells after inoculation with brain homogenate are primarily intracellular or secreted and also whether they maintain their seeding potency. This could have been done by treating naïve APP/BACE1-overexpressing cells with lysate or CM from seeded cells and quantifying the resultant seeding activity over several rounds of infection, then comparing it to that observed for naïve cells seeded with the original brain sample. The next important validation step would have been to examine whether these cell-derived preparations would have been able to accelerate amyloidosis in mice and whether this would still be dose-dependent. Finally, firm support that Aβ is a prion would have come from cross-seeding experiments where brain homogenates from mice seeded with lysates or CM from seeded cells are able to propagate aggregation in naïve cells or in multiple mouse models.

Establishing the predominant cellular compartment of seed production would also have enhanced understanding of the process of seed formation, particularly with respect to the transmission of seeds between cells. If predominantly extracellular, the seeds would have to be taken up by the recipient cells either passively or through transport mechanisms

(see Figure 6), whereas if predominantly intracellular the seeds would have to be passed through direct cell-to-cell contact without much secretion, unless reuptake processes were extremely quick. In turn, this could then give clues to the potential mode of seed transmission between neurons and glia in the brain and the molecular pathways involved, which could provide insights into why Aβ pathology does not correlate with disease severity. Experiments on modulating pathways involved in Aβ and tau toxicity and measuring how seeding is subsequently affected could fill crucial gaps in the knowledge of disease mechanisms, namely: where does amyloid aggregation begin and what triggers it, what cellular factors determine its spread, does seeding impart direct cell toxicity and how, which is the crucial point of Aβ and tau interaction, and is interrupting seeding a useful therapeutic approach. Answering such questions within the limits of a neuroblastoma cell system would expand the understanding of the involvement of cell background in AD and could explain why particular cell types are vulnerable to neurodegeneration. In a manner similar to the genetic comparison of cells permissive and revertant to PrP^{Sc} propagation previously published by our lab (Marbiah et al. 2014), it would have been advantageous if detailed sequencing was performed on cells able to propagate Aβ seeds to highlight any genetic differences that might explain differential cell susceptibility to seeding in principle, but also to individual amyloid strains.

As the aim of the project was to generate the platform for an assay that would be able to propagate oligomers or strains from multiple sources, the next experimental step would have been, as touched upon above, to seed the permissive cells with a variety of human and mouse brain preparations and in this way obtain a better understanding of how seeding is affected by the size and conformation of oligomers. Similarly to the process of developing the SCA, single-cell cloning may have been necessary to facilitate permissibility and it would also have been important to test whether permissive clones could be raised against homogenates that do not seed initially. Although CSF contains soluble low-n AβO which unsurprisingly induce aggregation *in vitro*, mouse seeding experiments have so far been unsuccessful (Fritschi et al. 2014b), which is puzzling considering that low-n oligomers are thought to be acutely toxic. CSF is also a wealthy resource of potential biomarkers (Blennow et al. 2010, 2015) which may include certain AβO conformations, so it would have been particularly interesting to see whether CSF-derived AβO are able to induce seeding in the neuroblastoma cell system, since CSF can be obtained relatively easily and its "infectivity" could be a readout for disease progression. Similar attempts could be made with blood samples, although extracting Aβ in this way would be considerably more difficult. Regardless, such experiments would have made distinguishing between bioactive

and inert Aβ strains possible and the highlighted differences would likely have had direct implications towards understanding the relationship between Aβ pathology and toxicity and would have opened up the possibility of using the assay as a diagnostic tool to gauge disease advancement, expected symptoms, and tailored treatment. Importantly, investigating the effect that compounds such as antibodies against distinct Aβ strains or β- or γ-secretase modulators have on seeding could have turned the cell model into a key step in the evaluation of the suitability of potential drugs for clinical trials.

Four cell lines were generated and characterized for this thesis with the aim of assessing the contribution of APP mutations not just to seeding, but to oligomer formation as well. In particular, linking the distinct profiles of Aβ produced by each mutation to the corresponding line's seeding ability would have helped understand which species of Aβ, either alone or in tandem, are key players in misfolding and toxicity. Quantifying changes in Aβ production profiles as well as seeding in response to any cell treatment could have provided a more complete picture of APP processing and its physiological role. Structurally analyzing endogenously produced or exogenously induced oligomers would have improved the understanding of strain heterogeneity and the biophysical properties of Aβ species. In addition, this could have allowed for a detailed comparison of synthetic with cell- and patient-derived amyloid conformations and thus reveal factors that make such structures bioactive. Beyond these broader applications, had the first proof-of-principle experiments succeeded, automating and standardizing the assay, namely determining optimal cell density, dilution of inoculum, incubation times, etc., would have been a priority. It would have been advantageous if oligomers were indeed secreted in the CM, which can be easily collected and tested. Had seeding been primarily intracellular, it would have been imperative to devise a different quantification method that does not rely on laborious confocal microscopy. In addition, the neuroblastoma lines used here for their ability to rapidly proliferate in culture may not be the most suitable cell type because of their cancer background and as such another cell type, such as patient-derived iPSCs, may be more appropriate. At the current stage, however, further investment of resources is needed for the protocols described above to be optimized and the experiments revisited. Nevertheless, the potential uses of an amyloid seeding assay are virtually limitless and the current project undertook ambitious steps towards testing the hypothesis of whether APP and BACE1 overexpression is sufficient to facilitate Aβ seeding in cell lines with neural background. The resultant neuroblastoma lines are well-characterized and at present can be used to investigate APP processing and the endogenous functions of precursor and

products. It would likely only be a matter of time before strains able to propagate in these cells are discovered.

6.8. Conclusion

In conclusion, in this thesis I assessed a hypothesis-driven approach to generate cell-based models for Aβ seeding as an alternative to existing Tg mouse models, which are expensive and laborious to work with. Such a tool would fill an important gap in the field allowing for the relatively quick assessment of the bioactivity of a sample of oligomeric Aβ. This project adds to the study of APP processing and Aβ seeding by looking in more detail into a so far poorly explored system. It resulted in the generation of well-characterized APP and BACE1-overexpressing human neuroblastoma cells, which secrete a variety of Aβ peptides and represent excellent models of APP processing. The cells can be used to further explore the cellular dynamics of these two proteins. In addition, more was learned about the biology of the commonly used 7PA2 cell model, which reportedly also secretes AβO. Under the experimental conditions described in this thesis and having in mind that the key experiments were performed only once, it does not appear that either the human or the CHO model are able to propagate Aβ seeding and that mere elevation of the production of Aβ is not sufficient to facilitate this process in this platform. It was also surprising that the detection of secreted AβO in the 7PA2 line failed, which may call for a re-evaluation of its described properties. Nevertheless, it is too early to discount the usefulness of the human cell lines generated in this work because there is scope for ample further improvements of the experimental protocols and thus a more conclusive answer can be obtained. The approach used here exposes important technical and conceptual challenges and contributes towards the development of an AβO seeding model.

Reference List

Acx H, Chávez-Gutiérrez L, Serneels L, Lismont S, Benurwar M, et al. 2014. Signature amyloid β profiles are produced by different γ-secretase complexes. *J. Biol. Chem.* 289(7):4346–55

Almeida CG, Takahashi RH, Gouras GK. 2006. β-Amyloid accumulation impairs multivesicular body sorting by inhibiting the ubiquitin-proteasome system. *J. Neurosci.* 26(16):4277–88

Alzheimer's Association. 2016. 2016 Alzheimer's disease facts and figures. *Alzheimer's Dement.* 12(4):459–509

Andersson ER, Lendahl U. 2014. Therapeutic modulation of Notch signalling - are we there yet? *Nat. Rev. Drug. Discov.* 13(5):357–78

Andreasson U, Portelius E, Andersson ME, Blennow K, Zetterberg H. 2007. Aspects of β-amyloid as a biomarker for Alzheimer's disease. *Biomark. Med.* 1(1):59–78

Arbel-Ornath M, Hudry E, Boivin JR, Hashimoto T, Takeda S, et al. 2017. Soluble oligomeric amyloid-β induces calcium dyshomeostasis that precedes synapse loss in the living mouse brain. *Mol. Neurodegener.* 12(1):27

Bai X-C, Yan C, Yang G, Lu P, Ma D, et al. 2015. An atomic structure of human γ-secretase. *Nature*. 525(7568):212–17

Baranger K, Marchalant Y, Bonnet AE, Crouzin N, Carrete A, et al. 2015. MT5-MMP is a new pro-amyloidogenic proteinase that promotes amyloid pathology and cognitive decline in a transgenic mouse model of Alzheimer's disease. *Cell. Mol. Life. Sci.* 73(1):217–36

Barnes EN, Biedler JL, Spengler BA, Lyser KM. 1981. The fine structure of continuous human neuroblastoma lines SK-N-SH, SK-N-BE(2), and SK-N-MC. *In Vitro*. 17(7):619–31

Bate C, Williams A. 2011. Amyloid-β-induced synapse damage is mediated via cross-linkage of cellular prion proteins. *J. Biol. Chem.* 286(44):37955–63

Bateman RJ, Xiong C, Benzinger TLS, Fagan AM, Goate A, et al. 2012. Clinical and biomarker changes in dominantly inherited Alzheimer's disease. *N. Engl. J. Med.* 367(9):795–804

Bekris LM, Yu C-E, Bird TD, Tsuang DW. 2010. Genetics of Alzheimer disease. *J. Geriatr. Psychiatry Neurol.* 23(4):213–27

Benilova I, Karran E, De Strooper B. 2012. The toxic Aβ oligomer and Alzheimer's disease: an emperor in need of clothes. *Nat. Neurosci.* 15(3):349–57

Bennett BD, Babu-Khan S, Loeloff R, Louis J-C, Curran E, et al. 2000. Expression analysis of BACE2 in brain and peripheral tissues. *J. Biol. Chem.* 275(27):20647–51

Bergström P, Agholme L, Nazir FH, Satir TM, Toombs J, et al. 2016. Amyloid precursor protein expression and processing are differentially regulated during cortical neuron differentiation. *Sci. Rep.* 6(1):29200

Beyreuther K, Masters CL. 1991. Amyloid precursor protein (APP) and β A4 amyloid in the etiology of Alzheimer's disease: precursor-product relationships in the derangement of neuronal function. *Brain Pathol.* 1(4):241–51

Beyreuther K, Pollwein P, Multhaup G, Mönning U, König G, et al. 1993. Regulation and expression of the Alzheimer's β/A4 amyloid protein precursor in health, disease, and Down's syndrome. *Ann. N. Y. Acad. Sci.* 695(1):91–102

Bialopiotrowicz E, Szybinska A, Kuzniewska B, Buizza L, Uberti D, et al. 2012. Highly pathogenic Alzheimer's disease presenilin 1 P117R mutation causes a specific increase in p53 and p21 protein levels and cell cycle dysregulation in human lymphocytes. *J. Alzheimer's Dis.* 32(2):397–415

Bilousova T, Miller CA, Poon WW, Vinters H V, Corrada M, et al. 2016. Synaptic Amyloid-β Oligomers Precede p-Tau and Differentiate High Pathology Control Cases. *Am. J. Pathol.* 186(1):185–98

Blennow HK, Zetterberg), Blennow K, Blennow K, Hampel H, et al. 2010. Cerebrospinal fluid and plasma biomarkers in Alzheimer disease. *Nat. Rev. Neurol.* 6(16104):131–44

Blennow K, Mattsson N, Schöll M, Hansson O, Zetterberg H. 2015. Amyloid biomarkers in Alzheimer's disease. *Trends Pharmacol. Sci.* 36(5):297–309

Blennow K, Vanmechelen E. 2003. CSF markers for pathogenic processes in Alzheimer's disease: diagnostic implications and use in clinical neurochemistry. *Brain Res. Bull.* 61(3):235–42

Bloom GS. 2014. Amyloid-β and tau: the trigger and bullet in Alzheimer disease pathogenesis. *JAMA Neurol.* 71(4):505–8

Boluda S, Toledo JB, Irwin DJ, Raible KM, Byrne MD, et al. 2014. A comparison of Aβ amyloid pathology staging systems and correlation with clinical diagnosis. *Acta Neuropathol.* 128(4):543–50

Borgegård T, Gustavsson S, Nilsson C, Parpal S, Klintenberg R, et al. 2012. Alzheimer's disease:

presenilin 2-sparing γ-secretase inhibition is a tolerable Aβ peptide-lowering strategy. *J. Neurosci.* 32(48):17297–305

Braak H, Braak E. 1991. Neuropathological stageing of Alzheimer-related changes. *Acta Neuropathol.* 82(4):239–59

Braak H, Braak E. 1995. Staging of Alzheimer's disease-related neurofibrillary changes. *Neurobiol. Aging*. 16(3):271–84

Braak H, Thal DR, Ghebremedhin E, Del Tredici K. 2011. Stages of the pathologic process in Alzheimer disease: age categories from 1 to 100 years. *J. Neuropathol. Exp. Neurol.* 70(11):960–69

Braak H, Zetterberg H, Del Tredici K, Blennow K. 2013. Intraneuronal tau aggregation precedes diffuse plaque deposition, but amyloid-β changes occur before increases of tau in cerebrospinal fluid. *Acta Neuropathol.* 126(5):631–41

Brkic M, Balusu XS, Wonterghem E Van, Gorle N, Benilova I, et al. 2015. Amyloid β oligomers disrupt blood-CSF barrier integrity by activating matrix metalloproteinases. *J. Neurosci.* 35(37):12766–78

Brown P, Brandel J-P, Sato T, Nakamura Y, MacKenzie J, et al. 2012. Iatrogenic Creutzfeldt-Jakob disease, final assessment. *Emerg. Inf. Dis.* 18(6):901–7

Brown P, Liberski PR, Wolff A, Gajdusek DC. 1990. Resistance of scrapie infectivity to steam autoclaving after formaldehyde fixation and limited survival after ashing at 360 degrees C: practical and theoretical implications. *J. Infect. Dis.* 161(3):467–72

Budka H, Aguzzi A, Brown P, Brucher J-M, Bugiani O, et al. 1995. Neuropathological diagnostic criteria for Creutzfeldt-Jakob disease (CJD) and other human spongiform encephalopathies (prion diseases). *Brain Pathol.* 5(4):459–66

Canevelli M, Piscopo P, Talarico G, Vanacore N, Blasimme A, et al. 2014. Familial Alzheimer's disease sustained by presenilin 2 mutations: Systematic review of literature and genotype–phenotype correlation. *Neurosci. Biobehav. Rev.* 42:170–79

Cao X, Südhof TC. 2001. A transcriptionally [correction of transcriptively] active complex of APP with Fe65 and histone acetyltransferase Tip60. *Science (80-.).* 293(5527):115–20

Castellano JM, Kim J, Stewart FR, Jiang H, Demattos RB, et al. 2011. Human apoE isoforms differentially regulate brain amyloid-β peptide clearance. *Sci. Transl. Med.* 3(89):89ra57

Castro-Seoane R, Hummerich H, Sweeting T, Tattum MH, Linehan JM, et al. 2012. Plasmacytoid dendritic cells sequester high prion titres at early stages of prion infection. *PLoS Pathog.* 8(2):e1002538

Chávez-Gutiérrez L, Bammens L, Benilova I, Vandersteen A, Benurwar M, et al. 2012. The mechanism of γ-Secretase dysfunction in familial Alzheimer disease. *EMBO J.* 31(10):2261–74

Christensen DZ, Schneider-Axmann T, Lucassen PJ, Bayer TA, Wirths O. 2010. Accumulation of intraneuronal Aβ correlates with ApoE4 genotype. *Acta Neuropathol.* 119(5):555–66

Clavaguera F, Akatsu H, Fraser G, Crowther RA, Frank S, et al. 2013. Brain homogenates from human tauopathies induce tau inclusions in mouse brain. *Proc. Natl Acad. Sci. USA*. 110(23):9535–40

Clavaguera F, Bolmont T, Crowther RA, Abramowski D, Frank S, et al. 2009. Transmission and spreading of tauopathy in transgenic mouse brain. *Nat. Cell Biol.* 11(7):909–13

Cohen M, Appleby B, Safar JG. 2016. Distinct prion-like strains of amyloid β implicated in phenotypic diversity of Alzheimer's disease. *Prion*. 10(1):9–17

Cole SL, Vassar R. 2007. The basic biology of BACE1: a key therapeutic target for Alzheimer's disease. *Curr. Genomics*. 8(8):509–30

Collinge J. 2016. Mammalian prions and their wider relevance in neurodegenerative diseases. *Nature*. 539(7682):217–26

Corder EH, Saunders AM, Strittmatter WJ, Schmechel DE, Gaskell PC, et al. 1993. Gene dose of apolipoprotein E type 4 allele and the risk of Alzheimer's disease in late onset families. *Science (80-.).* 261(5123):921–23

Cornaglia-Ferraris P, Ponzoni M, Montaldo P, Mariottini GL, Donti E, et al. 1990. A new human highly tumorigenic neuroblastoma cell line with undetectable expression of N-myc. *Pediatr. Res.* 27(1):1–6

Costanzo M, Zurzolo C. 2013. The cell biology of prion-like spread of protein aggregates: mechanisms and implication in neurodegeneration. *Biochem. J*. 452(1):1–17

Das P, Murray B, Belfort G. 2015. Alzheimer's protective A2T mutation changes the conformational landscape of the Aβ1–42 monomer differently than does the A2V mutation. *Biophys. J.* 108(3):738–47

Davis RC, Marsden IT, Maloney MT, Minamide LS, Podlisny MB, et al. 2011. Amyloid β dimers/trimers potently induce cofilin-actin rods that are inhibited by maintaining cofilin-phosphorylation. *Mol. Neurodegener.* 6(1):10

Davis SA, Gan KA, Dowell JA, Cairns NJ, Gitcho MA. 2017. TDP-43 expression influences amyloid β plaque deposition and tau aggregation. *Neurobiol. Dis.* 103:154–62

De Kimpe L, Van Haastert ES, Kaminari A, Zwart R, Rutjes H, et al. 2013. Intracellular accumulation of aggregated pyroglutamate amyloid beta: Convergence of aging and Aβ pathology at the lysosome. *Age (Omaha).* 35(3):673–87

De Strooper B. 2003. Aph-1, Pen-2, and Nicastrin with Presenilin generate an active γ-Secretase complex. *Neuron*. 38(1):9–12

De Strooper B. 2014. Lessons from a failed γ-secretase Alzheimer trial. *Cell*. 159(4):721–26

De Strooper B, Iwatsubo T, Wolfe MS. 2012. Presenilins and γ-secretase: structure, function, and role in Alzheimer Disease. *Cold Spring Harb. Perspect. Med.* 2(1):a006304

De Strooper B, Saftig P, Craessaerts K, Vanderstichele H, Guhde G, et al. 1998. Deficiency of presenilin-1 inhibits the normal cleavage of amyloid precursor protein. *Nature*. 391(6665):387–90

De Strooper B, Vassar R, Golde T. 2010. The secretases: enzymes with therapeutic potential in Alzheimer disease. *Nat. Rev. Neurol.* 6(2):99–107

DeMattos RB, Cirrito JR, Parsadanian M, May PC, O'Dell MA, et al. 2004. ApoE and clusterin cooperatively suppress Aβ levels and deposition: evidence that ApoE regulates extracellular Aβ metabolism in vivo. *Neuron*. 41(2):193–202

DeMattos RB, O'Dell MA, Parsadanian M, Taylor JW, Harmony JAK, et al. 2002. Clusterin promotes amyloid plaque formation and is critical for neuritic toxicity in a mouse model of Alzheimer's disease. *Proc. Natl. Acad. Sci. U. S. A.* 99(16):10843–48

Dickson DW, Kouri N, Murray ME, Josephs KA. 2011. Neuropathology of frontotemporal lobar degeneration-tau (FTLD-tau). *J. Mol. Neurosci.* 45(3):384–89

Dineley KT, Westerman M, Bui D, Bell K, Ashe KH, Sweatt JD. 2001. β-Amyloid activates the mitogen-activated protein kinase cascade via hippocampal α7 nicotinic acetylcholine receptors: In vitro and in vivo mechanisms related to Alzheimer's disease. *J. Neurosci.* 21(12):4125–33

Domert J, Rao SB, Agholme L, Brorsson AC, Marcusson J, et al. 2014. Spreading of amyloid-β peptides via neuritic cell-to-cell transfer is dependent on insufficient cellular clearance. *Neurobiol. Dis.* 65:82–92

Doody RS, Raman R, Farlow M, Iwatsubo T, Vellas B, et al. 2013. A phase 3 trial of semagacestat for treatment of Alzheimer's disease. *N. Engl. J. Med.* 369(4):341–50

Duran-Aniotz C, Morales R, Moreno-Gonzalez I, Hu PP, Fedynyshyn J, Soto C. 2014. Aggregate-depleted brain fails to induce Aβ deposition in a mouse model of Alzheimer's disease. *PLoS One*. 9(2):e89014

Dyrks T, Weidemann A, Multhaup G, Salbaum JM, Lemaire H-G, et al. 1988. Identification, transmembrane orientation and biogenesis of the amyloid A4 precursor of Alzheimer's disease. *EMBO J.* 7(4):949–57

Eisele YS, Bolmont T, Heikenwalder M, Langer F, Jacobson LH, et al. 2009. Induction of cerebral β-amyloidosis: intracerebral versus systemic Aβ inoculation. *Proc. Natl. Acad. Sci. U. S. A.* 106(31):12926–31

Eisele YS, Fritschi SK, Hamaguchi T, Obermüller U, Füger P, et al. 2014. Multiple factors contribute to the peripheral induction of cerebral β-amyloidosis. *J. Neurosci.* 34(31):10264–73

Eisele YS, Obermüller U, Heilbronner G, Baumann F, Kaeser SA, et al. 2010. Peripherally applied Aβ-containing inoculates induce cerebral β-amyloidosis. *Science (80-.).* 330(6006):980–82

Eisenberg D, Jucker M. 2012. The amyloid state of proteins in human diseases. *Cell*. 148(6):1188–1203

Elad N, De Strooper B, Lismont S, Hagen W, Veugelen S, et al. 2015. The dynamic conformational landscape of γ-secretase. *J. Cell Sci.* 128(3):589–98

Evangelisti E, Cascella R, Becatti M, Marrazza G, Dobson CM, et al. 2016. Binding affinity of amyloid oligomers to cellular membranes is a generic indicator of cellular dysfunction in protein misfolding diseases. *Sci. Rep.* 6(32721):1–14

Ferreira ST, Lourenco M V, Oliveira MM, De Felice FG. 2015. Soluble amyloid-β oligomers as synaptotoxins leading to cognitive impairment in Alzheimer's disease. *Front. Cell Neurosci.* 9:191

Fillenbaum GG, Van Belle G, Morris JC, Mohs RC, Mirra SS, et al. 2008. CERAD (Consortium to Establish a Registry for Alzheimer's Disease) The first 20 years. *Alzheimers Dement.*

4(2):96–109

Freir DB, Fedriani R, Scully D, Smith IM, Selkoe DJ, et al. 2011. Aβ oligomers inhibit synapse remodelling necessary for memory consolidation. *Neurobiol. Aging*. 32(12):2211–18

Fritschi SK, Cintron A, Ye L, Mahler J, Bühler A, et al. 2014a. Aβ seeds resist inactivation by formaldehyde. *Acta Neuropathol.* 128(4):477–84

Fritschi SK, Langer F, Kaeser SA, Maia LF, Portelius E, et al. 2014b. Highly potent soluble amyloid-β seeds in human Alzheimer brain but not cerebrospinal fluid. *Brain*. 137(11):2909–15

Frost B, Hemberg M, Lewis J, Feany MB. 2014. Tau promotes neurodegeneration through global chromatin relaxation. *Nat. Neurosci.* 17(3):357–66

Gajdusek DC. 1977. Unconventional viruses and the origin and disappearance of kuru. *Science (80-.).* 197(4307):943–60

Galasko D, Chang L, Motter R, Clark CM, Kaye J, et al. 1998. High cerebrospinal fluid tau and low amyloid β42 levels in the clinical diagnosis of Alzheimer disease and relation to apolipoprotein E genotype. *Arch. Neurol.* 55(7):937–45

George S, Rönnbäck A, Gouras GK, Petit GH, Grueninger F, et al. 2014. Lesion of the subiculum reduces the spread of amyloid β pathology to interconnected brain regions in a mouse model of Alzheimer's disease. *Acta Neuropathol. Commun.* 2(1):17

Geser F, Martinez-Lage M, Kwong LK, Lee VM-Y, Trojanowski JQ. 2009. Amyotrophic lateral sclerosis, frontotemporal dementia and beyond: the TDP-43 diseases. *J. Neurol.* 256(8):1205–14

Gessel MM, Bernstein S, Kemper M, Teplow DB, Bowers MT. 2012. Familial Alzheimer's disease mutations differentially alter amyloid β-protein oligomerization. *ACS Chem. Neurosci.* 3(11):909–18

Getsios D, Blume S, Ishak KJ, Maclaine G, Hernández L. 2012. An economic evaluation of early assessment for Alzheimer's disease in the United Kingdom. *Alzheimer's Dement.* 8(1):22–30

Golde TE, Cai X-D, Shoji M, Younkin SG. 1993. Production of Amyloid β Protein from Normal Amyloid β-Protein Precursor (βAPP) and the Mutated βAPPS Linked to Familial Alzheimer's Diseasea. *Ann. N. Y. Acad. Sci.* 695(1):103–8

Goold R, Rabbanian S, Sutton L, Andre R, Arora P, et al. 2011. Rapid cell-surface prion protein conversion revealed using a novel cell system. *Nat. Commun.* 2(281):1–11

Guardia-Laguarta C, Pera M, Clarimón J, Molinuevo JL, Sánchez-Valle R, et al. 2010. Clinical, neuropathologic, and biochemical profile of the amyloid precursor protein I716F mutation. *J. Neuropathol. Exp. Neurol.* 69(1):53–59

Guerreiro R, Wojtas A, Bras J, Carrasquillo M, Rogaeva E, et al. 2013. TREM2 variants in Alzheimer's disease. *N. Engl. J. Med.* 10(3682):117–27

Guerreiro RJ, Baquero M, Blesa R, Boada M, Brás JM, et al. 2010. Genetic screening of Alzheimer's disease genes in Iberian and African samples yields novel mutations in presenilins and APP. *Neurobiol. Aging*. 31(5):725–31

Gunn AP, Wong BX, Johanssen T, Griffith JC, Masters CL, et al. 2016. Amyloid-β peptide Aβ3pE-42 induces lipid peroxidation, membrane permeabilization, and calcium influx in neurons. *J. Biol. Chem.* 291(12):6134–45

Guo JL, Lee VMY. 2014. Cell-to-cell transmission of pathogenic proteins in neurodegenerative diseases. *Nat. Med.* 20(2):130–38

Ha S, Furukawa R, Fechheimer M. 2011. Association of AICD and Fe65 with Hirano bodies reduces transcriptional activation and initiation of apoptosis. *Neurobiol. Aging*. 32(12):2287–98

Haapasalo A, Kovacs DM. 2011. The many substrates of presenilin/γ-secretase. *J. Alzheimer's Dis.* 25(1):3–28

Hamaguchi T, Eisele YS, Varvel NH, Lamb BT, Walker LC, Jucker M. 2012. The presence of Aβ seeds, and not age per se, is critical to the initiation of Aβ deposition in the brain. *Acta Neuropathol.* 123(1):31–37

Hampel H, Blennow K, Shaw LM, Hoessler YC, Zetterberg H, Trojanowski JQ. 2009. Total and phosphorylated tau protein as biological markers of Alzheimer's disease. *Exp. Gerontol.* 45(1):30–40

Hardy J, Allsop D. 1991. Amyloid deposition as the central event in the aetiology of Alzheimer's disease. *Trends Pharmacol. Sci.* 12(10):383–88

Hardy J, Higgins GA. 1992. Alzheimer's disease: the amyloid cascade hypothesis. *Science (80-.).* 256(5054):184–85

Hatch RJ, Wei Y, Xia D, Götz J. 2017. Hyperphosphorylated tau causes reduced hippocampal CA1 excitability by relocating the axon initial segment. *Acta Neuropathol.* 133(5):717–30

Heilbronner G, Eisele YS, Langer F, Kaeser SA, Novotny R, et al. 2013. Seeded strain-like transmission of β-amyloid morphotypes in APP transgenic mice. *EMBO Rep.* 14(11):1017–22

Henley DB, Sundell KL, Sethuraman G, Dowsett SA, May PC. 2014. Safety profile of semagacestat, a gamma-secretase inhibitor: IDENTITY trial findings. *Curr. Med. Res. Opin.* 30(30):2021–32

Herrup K. 2015. The case for rejecting the amyloid cascade hypothesis. *Nat Neurosci*. 18(6):794–99

Holmes BB, Furman JL, Mahan TE, Yamasaki TR, Mirbaha H, et al. 2014a. Proteopathic Tau seeding predicts tauopathy in vivo. *Proc. Natl. Acad. Sci. U. S. A.* 111(41):E4376–85

Holmes O, Paturi S, Selkoe DJ, Wolfe MS. 2014b. Pen-2 is essential for γ-secretase complex stability and trafficking but partially dispensable for endoproteolysis. *Biochemistry*. 53(27):4393–4406

Hölttä M, Hansson O, Andreasson U, Hertze J, Minthon L, et al. 2013. Evaluating Amyloid-β Oligomers in Cerebrospinal Fluid as a Biomarker for Alzheimer's Disease. *PLoS One*. 8(6):e66381

Hu W, Zhang X, Tung YC, Xie S, Liu F, Iqbal K. 2016. Hyperphosphorylation determines both the spread and the morphology of tau pathology. *Alzheimer's Dement.* 12(10):1066–77

Hu X, Crick SL, Bu G, Frieden C, Pappu R V, Lee J-M. 2009. Amyloid seeds formed by cellular uptake, concentration, and aggregation of the amyloid-β peptide. *Proc Natl. Acad. Sci. U. S. A.* 106(48):20324–29

Huang C-C, Chung C-M, Leu H-B, Lin L-Y, Chiu C-C, et al. 2014. Diabetes mellitus and the risk of Alzheimer's disease: a nationwide population-based study. *PLoS One*. 9(1):e87095

Israel MA, Yuan SH, Bardy C, Reyna SM, Mu Y, et al. 2012. Probing sporadic and familial Alzheimer's disease using induced pluripotent stem cells. *Nature*. 482(7384):216–22

Ittner LM, Fath T, Ke YD, Bi M, Van Eersel J, et al. 2008. Parkinsonism and impaired axonal transport in a mouse model of frontotemporal dementia. *Proc. Natl Acad. Sci.* 105(41):15997–2

Ittner LM, Ke YD, Delerue F, Bi M, Gladbach A, et al. 2010. Dendritic function of tau mediates amyloid-β toxicity in Alzheimer's disease mouse models. *Cell*. 142(3):387–97

Jaunmuktane Z, Mead S, Ellis M, Wadsworth JDF, Nicoll AJ, et al. 2015. Evidence for human transmission of amyloid-β pathology and cerebral amyloid angiopathy. *Nature*. 525(7568):247–50

Jin M, Shepardson N, Yang T, Chen G, Walsh DM, Selkoe DJ. 2011. Soluble amyloid β-protein dimers isolated from Alzheimer cortex directly induce Tau hyperphosphorylation and neuritic degeneration. *Proc. Natl. Acad. Sci. U. S. A.* 108(14):5819–24

Johnston JA, Cowburn RF, Norgren S, Wiehager B, Venizelos N, et al. 1994. Increased β-amyloid release and levels of amyloid precursor protein (APP) in fibroblast cell lines from family members with the Swedish Alzheimer's disease APP670/671 mutation. *FEBS Lett.* 354(3):274–78

Jones SE, Jomary C. 2002. Clusterin. *Int. J. Biochem. Cell Biol.* 34(5):427–31

Jonsson T, Atwal JK, Steinberg S, Snaedal J, Jonsson P V., et al. 2012. A mutation in APP protects against Alzheimer's disease and age-related cognitive decline. *Nature*. 488(7409):96–99

Jonsson T, Stefansson H, Steinberg S, Jonsdottir I, Jonsson P V., et al. 2013. Variant of TREM2 associated with the risk of Alzheimer's disease. *N. Engl. J. Med.* 368(2):107–16

Josephs KA, Whitwell JL, Weigand SD, Murray ME, Tosakulwong N, et al. 2014. TDP-43 is a key player in the clinical features associated with Alzheimer's disease. *Acta Neuropathol.* 127(6):811–24

Kane MD, Lipinski WJ, Callahan MJ, Bian F, Durham RA, et al. 2000. Evidence for seeding of β-amyloid by intracerebral infusion of Alzheimer brain extracts in β-amyloid precursor protein-transgenic mice. *J. Neurosci.* 20(10):3606–11

Kang J, Lemaire H-G, Unterbeck A, Salbaum JM, Masters CL, et al. 1987. The precursor of Alzheimer's disease amyloid A4 protein resembles a cell-surface receptor. *Nature*. 325(6106):733–36

Karch CM, Goate AM. 2015. Alzheimer's disease risk genes and mechanisms of disease pathogenesis. *Biol. Psychiatry*. 77(1):43–51

Kaufman S, Sanders D, Thomas T, Ruchinskas A, Vaquer-Alicea J, et al. 2016. Tau prion strains dictate patterns of cell pathology, progression rate, and regional vulnerability in vivo.

Neuron. 92(4):796–812

Kim J, Onstead L, Randle S, Price R, Smithson L, et al. 2007. Aβ40 inhibits amyloid deposition In vivo. *J. Neurosci.* 27(3):627–33

Kimberly WT, Lavoie MJ, Ostaszewski BL, Ye W, Wolfe MS, Selkoe DJ. 2003. γ-Secretase is a membrane protein complex comprised of presenilin, nicastrin, aph-1, and pen-2. *Proc. Natl. Acad. Sci. U. S. A.* 100(11):6382–6287

Klöhn P-C, Stoltze L, Flechsig E, Enari M, Weissmann C. 2003. A quantitative, highly sensitive cell-based infectivity assay for mouse scrapie prions. *Proc. Natl. Acad. Sci. U. S. A.* 100(20):11666–71

Kögel D, Concannon CG, Müller T, König H, Bonner C, et al. 2012. The APP intracellular domain (AICD) potentiates ER stress-induced apoptosis. *Neurobiol. Aging*. 33(9):2200–2209

Koo EH, Squazzo SL. 1994. Evidence that production and release of amyloid β-protein involves the endocytic pathway. *J. Biol. Chem.* 269(26):17386–89

Köpke E, Tung Y-C, Shaikh S, Alonso A del C, Iqbal K, Grundke-Iqbal I. 1993. Microtubule-associated protein tau. Abnormal phosphorylation of a non-paired helical filament pool in Alzheimer disease. *J. Biol. Chem.* 268(32):24374–84

Krako N, Magnifico MC, Arese M, Meli G, Forte E, et al. 2013. Characterization of mitochondrial dysfunction in the 7PA2 cell model of Alzheimer's disease. *J. Alzheimer's Dis.* 37(4):747–58

Kuhn P-H, Wang H, Dislich B, Colombo A, Zeitschel U, et al. 2010. ADAM10 is the physiologically relevant, constitutive α-secretase of the amyloid precursor protein in primary neurons. *EMBO J.* 29(17):3020–32

Kuperstein I, Broersen K, Benilova I, Rozenski J, Jonckheere W, et al. 2010. Neurotoxicity of Alzheimer's disease Aβ peptides is induced by small changes in the Aβ42 to Aβ40 ratio. *EMBO J.* 29(19):3408–20

LaFerla FM, Green KN, Oddo S. 2007. Intracellular amyloid-β in Alzheimer's disease. *Nat. Rev. Neurosci.* 8(7):499–509

Lamb BT, Call LM, Slunt HH, Bardel KA, Lawler AM, et al. 1997. Altered metabolism of familial Alzheimer's disease-linked amyloid precursor protein variants in yeast artificial chromosome transgenic mice. *Hum. Mol. Genet.* 6(9):1535–41

Langer F, Eisele YS, Fritschi SK, Staufenbiel M, Walker LC, Jucker M. 2011. Soluble Aβ seeds are potent inducers of cerebral β-amyloid deposition. *J. Neurosci.* 31(41):14488–95

Lasagna-Reeves CA, Castillo-Carranza DL, Sengupta U, Guerrero-Munoz MJ, Kiritoshi T, et al. 2012. Alzheimer brain-derived tau oligomers propagate pathology from endogenous tau. *Sci. Rep.* 2(700):1–7

Laurén J, Gimbel DA, Nygaard HB, Gilbert JW, Strittmatter SM. 2009. Cellular prion protein mediates impairment of synaptic plasticity by amyloid-β oligomers. *Nature*. 457(7233):1128–32

LaVoie MJ, Fraering PC, Ostaszewski BL, Ye W, Kimberly WT, et al. 2003. Assembly of the γ-secretase complex involves early formation of an intermediate subcomplex of Aph-1 and nicastrin. *J. Biol. Chem.* 278(39):37213–22

Lee CYD, Tse W, Smith JD, Landreth GE. 2011. Apolipoprotein E promotes β-amyloid trafficking and degradation by modulating microglial cholesterol levels. *J. Biol. Chem.* 287(3):2032–44

Lei M, Xu H, Li Z, Wang Z, O 'malley TT, et al. 2016. Soluble Aβ oligomers impair hippocampal LTP by disrupting glutamatergic/GABAergic balance. *Neurobiol. Dis.* 85:111–21

Li B, Chohan MO, Grundke-Iqbal I, Iqbal K. 2007. Disruption of microtubule network by Alzheimer abnormally hyperphosphorylated tau. *Acta Neuropathol.* 113(5):501–11

Li C, Götz J. 2017. Somatodendritic accumulation of Tau in Alzheimer's disease is promoted by Fyn-mediated local protein translation. *EMBO J.* 36(21):3120–38

Li J, Browning S, Mahal SP, Oelschlaegel AM, Weissmann C. 2010. Darwinian evolution of prions in cell culture. *Science (80-.).* 327(5967):869–72

Li N, Liu K, Qiu Y, Ren Z, Dai R, et al. 2016. Effect of presenilin mutations on APP cleavage; Insights into the pathogenesis of FAD. *Front. Aging Neurosci.* 8(eCollection 2016):51

Lichtenthaler SF, Wang R, Grimm H, Uljon SN, Masters CL, Beyreuther K. 1999. Mechanism of the cleavage specificity of Alzheimer's disease γ-secretase identified by phenylalanine-scanning mutagenesis of the transmembrane domain of the amyloid precursor protein. *Proc. Natl. Acad. Sci. U. S. A.* 96(6):3053–58

Liu G, Yao L, Liu J, Jiang Y, Ma G, et al. 2014. Cardiovascular disease contributes to Alzheimer's disease: evidence from large-scale genome-wide association studies. *Neurobiol. Aging*. 35(4):786–92

Llewelyn CA, Hewitt PE, Knight RSG, Amar K, Cousens S, et al. 2004. Possible transmission of variant Creutzfeldt-Jakob disease by blood transfusion. *Lancet*. 363(9407):417–21

Lu J-X, Qiang W, Yau W-M, Schwieters CD, Meredith SC, Tycko R. 2013. Molecular structure of β-amyloid fibrils in Alzheimer's disease brain tissue. *Cell*. 154(6):1257–68

Marbiah MM, Harvey A, West BT, Louzolo A, Banerjee P, et al. 2014. Identification of a gene regulatory network associated with prion replication. *EMBO J.* 33(14):1–21

Marcinkiewicz M, Seidah NG. 2002. Coordinated expression of β-amyloid precursor protein and the putative β-secretase BACE and α-secretase ADAM10 in mouse and human brain. *J. Neurochem.* 75(5):2133–43

Marzesco A-M, Flötenmeyer M, Bühler A, Obermüller U, Staufenbiel M, et al. 2016. Highly potent intracellular membrane-associated Aβ seeds. *Sci. Rep.* 6:28125

Mayeux R, Stern Y. 2012. Epidemiology of Alzheimer disease. *Cold Spring Harb. Perspect. Med.* 2(8):a006239

McCarron M, McCallion P, Reilly E, Mulryan N. 2014. A prospective 14-year longitudinal follow-up of dementia in persons with Down syndrome. *J. Intellect. Disabil. Res.* 58(1):61–70

McKhann GM, Drachman D, Folstein M, Katzman R, Price D, Stadlan EM. 1984. Clinical diagnosis of Alzheimer's disease: report of the NINCDS-ADRDA Work Group under the auspices of Department of Health and Human Services Task Force on Alzheimer's Disease. *Neurology*. 34(7):939–44

McKhann GM, Knopman DS, Chertkow H, Hyman BT, Jack CR, et al. 2011. The diagnosis of dementia due to Alzheimer's disease: recommendations from the National Institute on Aging-Alzheimer's Association workgroups on diagnostic guidelines for Alzheimer's disease. *Alzheimer's Dement.* 7(3):263–69

Merino-Serrais P, Benavides-Piccione R, Blazquez-Llorca L, Kastanauskaite A, Rá A, et al. 2013. The influence of phospho-tau on dendritic spines of cortical pyramidal neurons in patients with Alzheimer's disease. *Brain*. 136(6):1913–28

Meyer-Luehmann M, Coomaraswamy J, Bolmont T, Kaeser S, Schaefer C, et al. 2006. Exogenous induction of cerebral β-amyloidogenesis is governed by agent and host. *Science (80-.).* 313(September):1781–84

Milojevic J, Raditsis A, Melacini G. 2009. Human serum albumin inhibits Aβ fibrillization through a "monomer-competitor" mechanism. *Biophys. J.* 97(9):2585–94

Mirbaha H, Chen D, Morozova OA, Ruff KM, Sharma A, et al. 2018. Inert and seed-competent tau monomers suggest structural origins of aggregation. *bioRxiv*. 163394

Morales R, Bravo-Alegria J, Duran-Aniotz C, Soto C. 2015. Titration of biologically active amyloid-β seeds in a transgenic mouse model of Alzheimer's disease. *Sci. Rep.* 5:9349

Morales R, Duran-Aniotz C, Castilla J, Estrada L, Soto C. 2011. De novo induction of amyloid-β deposition in vivo. *Mol. Psychiatry*. 17(12):1347–53

Morris GP, Clark IA, Vissel B. 2014. Inconsistencies and controversies surrounding the amyloid hypothesis of Alzheimer's disease. *Acta Neuropathol. Commun.* 2(1):135

Morris JC, Roe CM, Xiong C, Fagan AM, Goate AM, et al. 2010. APOE predicts amyloid-β but not tau Alzheimer pathology in cognitively normal aging. *Ann. Neurol.* 67(1):122–31

Motter R, Vigo-Pelfrey C, Kholodenko D, Barbour R, Johnson-Wood K, et al. 1995. Reduction of β-amyloid peptide42 in the cerebrospinal fluid of patients with Alzheimer's disease. *Ann. Neurol.* 38(4):643–48

Mueller-Steiner S, Zhou Y, Arai H, Roberson ED, Sun B, et al. 2006. Antiamyloidogenic and neuroprotective functions of cathepsin B: implications for Alzheimer's disease. *Neuron*. 51(6):703–14

Mullan M, Crawford F, Axelman K, Houlden H, Lilius L, et al. 1992. A pathogenic mutation for probable Alzheimer's disease in the APP gene at the N-terminus of β-amyloid. *Nat. Genet.* 1(5):345–47

Müller UC, Deller T, Korte M. 2017. Not just amyloid: physiological functions of the amyloid precursor protein family. *Nat. Rev. Neurosci.* 18(5):281–98

Muratore CR, Rice HC, Srikanth P, Callahan DG, Shin T, et al. 2014. The familial Alzheimer's disease APPV717I mutation alters APP processing and Tau expression in iPSC-derived neurons. *Hum. Mol. Genet.* 23(13):3523–36

Murrell J, Farlow M, Ghetti B, Benson MD. 1991. A mutation in the amyloid precursor protein associated with hereditary Alzheimer's disease. *Science (80-.).* 254(5028):97–99

Nath S, Agholme L, Roshan Kurudenkandy F, Granseth B, Marcusson J, Hallbeck M. 2012. Spreading of neurodegenerative pathology via neuron-to-neuron transmission of β-amyloid. *Neurobiol. Dis.* 32(26):8767–77

Nicoll AJ, Panico S, Freir DB, Wright D, Terry C, et al. 2013. Amyloid-β nanotubes are associated

with prion protein-dependent synaptotoxicity. *Nat. Commun.* 4:2416

Nilsson P, Saito T, Saido TC. 2014. New mouse model of Alzheimer's. *ACS Chem. Neurosci.* 5(7):499–502

Nomura S, Umeda T, Tomiyama T, Mori H. 2013. The E693Δ (Osaka) mutation in amyloid precursor protein potentiates cholesterol-mediated intracellular amyloid β toxicity via its impaired cholesterol efflux. *J. Neurosci. Res.* 91(12):1541–50

Novotny R, Langer F, Mahler J, Skodras A, Vlachos A, et al. 2016. Conversion of synthetic Aβ to In Vivo active seeds and amyloid plaque formation in a hippocampal slice culture model. *J. Neurosci.* 36(18):5084–93

Oddo S, Caccamo A, Shepherd JD, Murphy MP, Golde TE, et al. 2003. Triple-transgenic model of Alzheimer's disease with plaques and tangles: intracellular Aβ and synaptic dysfunction. *Neuron*. 39(3):409–21

Oelschlegel AM, Weissmann C. 2013. Acquisition of drug resistance and dependence by prions. *PLoS Pathog.* 9(210):e1003158

Oesch B, Westaway D, Waichli M, McKinley MP, Kent SBH, et al. 1985. A cellular gene encodes scrapie PrP 27-30 protein. *Cell*. 40(4):735–46

Ohnishi H, Murata Y, Okazawa H, Matozaki T. 2011. Src family kinases: modulators of neurotransmitter receptor function and behavior. *Trends Neurosci.* 34(12):629–37

Okochi M, Steiner H, Fukumori A, Tanii H, Tomita T, et al. 2002. Presenilins mediate a dual intramembranous γ-secretase cleavage of Notch-1. *EMBO J.* 21(20):5408–16

Omtri RS, Davidson MW, Arumugam B, Poduslo JF, Kandimalla KK. 2012. Differences in the cellular uptake and intracellular itineraries of amyloid β proteins 40 and 42: ramifications for the Alzheimer's drug discovery. *Mol. Pharm.* 9(7):1887–97

Pan K-M, Baldwin M, Nguyen J, Gasset M, Serban A, et al. 1993. Conversion of α-helices into β-sheets features in the formation of the scrapie prion proteins. *Proc. Natl. Acad. Sci. U. S. A.* 90(23):10962–66

Park HJ, Shabashvili D, Nekorchuk MD, Shyqyriu E, Jung JI, et al. 2012. Retention in endoplasmic reticulum 1 (RER1) modulates amyloid-β (Aβ) production by altering trafficking of γ-secretase and amyloid precursor protein (APP). *J. Biol. Chem.* 287(48):40629–40

Peila R, Rodriguez BL, Launer LJ. 2002. Type 2 diabetes, APOE gene, and the risk for dementia and related pathologies: the Honolulu-Asia aging study. *Diabetes*. 51(4):1256–62

Pensalfini A, Albay Iii R, Rasool S, Wu JW, Hatami A, et al. 2014. Intracellular amyloid and the neuronal origin of Alzheimer neuritic plaques. *Neurobiol. Dis.* 71:53–61

Petkova AT, Leapman RD, Guo Z, Yau W-M, Mattson MP, Tycko R. 2005. Self-propagating, molecular-level polymorphism in Alzheimer's β-amyloid fibrils. *Science (80-.).* 307(5707):262–65

Podlisny MB, Ostaszewski BL, Squazzo SL, Koo EH, Rydell RE, et al. 1995. Aggregation of secreted amyloid β-protein into sodium dodecyl sulfate-stable oligomers in cell culture. *J. Biol. Chem.* 270(16):9564–70

Polanco JC, Li C, Bodea L-G, Martinez-Marmol R, Meunier FA, Götz J. 2018. Amyloid-β and tau complexity — towards improved biomarkers and targeted therapies. *Nat. Rev. Neurol.* 14(1):22–39

Polydoro M, Dzhala VI, Pooler AM, Nicholls SB, McKinney AP, et al. 2014. Soluble pathological tau in the entorhinal cortex leads to presynaptic deficits in an early Alzheimer's disease model. *Acta Neuropathol.* 127(2):257–70

Ponte P, Gonzalez-DeWhit P, Schilling P, Miller J, Hsu D, et al. 1988. A new A4 amyloid mRNA contains a domain homologous to serine proteinase inhibitors. *Nature*. 331(6156):525–27

Portelius E, Bogdanovic N, Gustavsson MK, Volkmann I, Brinkmalm G, et al. 2010. Mass spectrometric characterization of brain amyloid β isoform signatures in familial and sporadic Alzheimer's disease. *Acta Neuropathol.* 120(2):185–93

Portelius E, Dean RA, Andreasson U, Mattsson N, Westerlund A, et al. 2014. β-site amyloid precursor protein-cleaving enzyme 1(BACE1) inhibitor treatment induces Aβ5-X peptides through alternative amyloid precursor protein cleavage. *Alzheimers. Res. Ther.* 6:75

Portelius E, Olsson M, Brinkmalm G, Rüetschi U, Mattsson N, et al. 2013. Mass spectrometric characterization of amyloid-β species in the 7PA2 cell model of Alzheimer's disease. *J. Alzheimer's Dis.* 33(1):85–93

Portelius E, Price E, Brinkmalm G, Stiteler M, Olsson M, et al. 2011. A novel pathway for amyloid precursor protein processing. *Neurobiol. Aging*. 32(6):1090–98

Portelius E, Tran AJ, Andreasson U, Persson R, Brinkmalm G, et al. 2007. Characterization of amyloid β peptides in cerebrospinal fluid by an automated immunoprecipitation

procedure followed by mass spectrometry. *J. Proteome Res.* 6(11):4433–39

Prince M, Bryce R, Albanese E, Wimo A, Ribeiro W, Ferri CP. 2013. The global prevalence of dementia: A systematic review and metaanalysis. *Alzheimer's Dement.* 9(1):63–75.e2

Prusiner SB. 1982. Novel proteinaceous infectious particles cause scrapie. *Science (80-.).* 216(9):136–44

Prusiner SB. 1998. Prions. *Proc. Natl. Acad. Sci. U. S. A.* 95(23):13363–83

Qiang W, Yau W-M, Lu J-X, Collinge J, Tycko R. 2017. Structural variation in amyloid-β fibrils from Alzheimer's disease clinical subtypes. *Nature*. 541(7636):217–21

Qiu WQ, Walsh DM, Ye Z, Vekrellis K, Zhang J, et al. 1998. Insulin-degrading enzyme regulates extracellular levels of amyloid β-protein by degradation. *J. Biol. Chem.* 273(49):32730–38

Radde R, Bolmont T, Kaeser SA, Coomaraswamy J, Lindau D, et al. 2006. Aβ42-driven cerebral amyloidosis in transgenic mice reveals early and robust pathology. *EMBO Rep.* 7(9):940–46

Ripoli C, Cocco S, Li Puma DD, Piacentini R, Mastrodonato A, et al. 2014. Intracellular accumulation of amyloid-β (Aβ) protein plays a major role in Aβ-induced alterations of glutamatergic synaptic transmission and plasticity. *J. Neurosci.* 34(38):12893–903

Ritchie DL, Barria MA, Peden AH, Yull HM, Kirkpatrick J, et al. 2017. UK Iatrogenic Creutzfeldt–Jakob disease: investigating human prion transmission across genotypic barriers using human tissue-based and molecular approaches. *Acta Neuropathol.* 133(4):579–95

Rogaeva E, Meng Y, Lee JH, Gu Y, Kawarai T, et al. 2007. The neuronal sortilin-related receptor SORL1 is genetically associated with Alzheimer disease. *Nat. Genet.* 39(2):168–77

Rönnbäck A, Sagelius H, Bergstedt KD, Näslund J, Westermark GT, et al. 2012. Amyloid neuropathology in the single Arctic APP transgenic model affects interconnected brain regions. *Neurobiol. Aging*. 33(4):831.e11-831.e19

Rosen RF, Fritz JJ, Dooyema J, Cintron AF, Hamaguchi T, et al. 2012. Exogenous seeding of cerebral β-amyloid deposition in βAPP-transgenic rats. *J. Neurochem.* 120(5):660–66

Rovelet-Lecrux A, Hannequin D, Raux G, Le Meur N, Laquerrière A, et al. 2006. APP locus duplication causes autosomal dominant early-onset Alzheimer disease with cerebral amyloid angiopathy. *Nat. Genet.* 38(1):24–26

Rudge P, Jaunmuktane Z, Adlard P, Bjurstrom N, Caine D, et al. 2015. Iatrogenic CJD due to

pituitary-derived growth hormone with genetically determined incubation times of up to 40 years. *Brain*. 138(11):3386–99

Saido T, Leissring MA. 2012. Proteolytic degradation of amyloid β-protein. *Cold Spring Harb. Perspect. Med.* 2(6):a006379

Saito T, Matsuba Y, Mihira N, Takano J, Nilsson P, et al. 2014. Single App knock-in mouse models of Alzheimer's disease. *Nat. Neurosci.* 17(5):661–63

Saito T, Suemoto T, Brouwers N, Sleegers K, Funamoto S, et al. 2011. Potent amyloidogenicity and pathogenicity of Aβ43. *Nat. Neurosci.* 14(8):1023–32

Sanchez-Mejias E, Navarro V, Jimenez S, Sanchez-Mico M, Sanchez-Varo R, et al. 2016. Soluble phospho-tau from Alzheimer's disease hippocampus drives microglial degeneration. *Acta Neuropathol.* 132(6):897–916

Sandberg MK, Al-Doujaily H, Sharps B, Clarke AR, Collinge J. 2011. Prion propagation and toxicity in vivo occur in two distinct mechanistic phases. *Nature*. 470(7335):540–42

Sandberg MK, Al-Doujaily H, Sharps B, Wiggins De Oliveira M, Schmidt C, et al. 2014. Prion neuropathology follows the accumulation of alternate prion protein isoforms after infective titre has peaked. *Nat. Commun.* 5(4347):1–7

Sanders DW, Kaufman SK, Devos SL, Sharma AM, Mirbaha H, et al. 2014. Distinct tau prion strains propagate in cells and mice and define different tauopathies. *Neuron*. 82(6):1271–88

Saunders AM, Strittmatter WJ, Schmechel D, George-Hyslop PH, Pericak-Vance MA, et al. 1993. Association of apolipoprotein E allele epsilon 4 with late-onset familial and sporadic Alzheimer's disease. *Neurology*. 43(8):1467–72

Scheltens P, Blennow K, Breteler MMB, De Strooper B, Frisoni GB, et al. 2016. Alzheimer's disease. *Lancet*. 388(10061):505–17

Schlesinger HR, Gerson JM, Moorhead PS, Maguire H, Hummeler K. 1976. Establishment and characterization of human neuroblastoma cell lines. *Cancer Res.* 36:3094–3100

Schneider JA, Arvanitakis Z, Bang W, Bennett DA. 2007. Mixed brain pathologies account for most dementia cases in community-dwelling older persons. *Neurology*. 69(24):2197–2204

Selkoe DJ. 2011. Resolving controversies on the path to Alzheimer's therapeutics. *Nat. Med.*

17(9):1060–65

Selkoe DJ, Hardy J. 2016. The amyloid hypothesis of Alzheimer's disease at 25 years. *EMBO Mol. Med.* 8(6):595–608

Serneels L, Dejaegere T, Craessaerts K, Horré K, Jorissen E, et al. 2005. Differential contribution of the three Aph1 genes to γ-secretase activity in vivo. *Proc. Natl. Acad. Sci. U. S. A.* 102(5):1719–24

Serrano-Pozo A, Frosch MP, Masliah E, Hyman BT. 2011. Neuropathological alterations in Alzheimer disease. *Cold Spring Harb. Perspect. Med.* 1(1):a006189

Shah S, Lee S-F, Tabuchi K, Hao Y-H, Yu C, et al. 2005. Nicastrin functions as a γ-secretase-substrate receptor. *Cell*. 122(3):435–47

Shankar GM, Li S, Mehta TH, Garcia-Munoz A, Shepardson NE, et al. 2008. Amyloid-β protein dimers isolated directly from Alzheimer's brains impair synaptic plasticity and memory. *Nat. Med.* 14(8):837–42

Shankar GM, Welzel AT, McDonald JM, Selkoe DJ, Walsh DM. 2011. Isolation of low-n amyloid β-protein oligomers from cultured cells, CSF, and brain. *Methods Mol. Biol.* 670:33–44

Shariati SAM, De Strooper B. 2013. Redundancy and divergence in the amyloid precursor protein family. *FEBS Lett.* 587(13):2036–45

Sharples RA, Vella LJ, Nisbet RM, Naylor R, Perez K, et al. 2008. Inhibition of gamma-secretase causes increased secretion of amyloid precursor protein C-terminal fragments in association with exosomes. *FASEB J.* 22:1469–78

Shen J, Bronson RT, Chen DF. 1997. Skeletal and CNS defects in Presenilin-1-deficient mice. *Cell*. 89(4):629–39

Shi X-P, Tugusheva K, Bruce JE, Lucka A, Wu G-X, et al. 2003. β-Secretase cleavage at amino acid residue 34 in the amyloid β peptide is dependent upon γ-secretase activity. *J. Biol. Chem.* 278(23):21286–94

Shipton OA, Leitz JR, Dworzak J, Acton CEJ, Tunbridge EM, et al. 2011. Tau protein is required for amyloid β-induced impairment of hippocampal long-term potentiation. *J. Neurosci.* 31(5):1688–92

Smith LM, Strittmatter SM. 2017. Binding sites for amyloid-β oligomers and synaptic toxicity. *Cold Spring Harb. Perspect. Med.* 7(5):a024075

Song H-L, Shim S, Kim D-H, Won S-H, Joo S, et al. 2014. β-Amyloid is transmitted via neuronal connections along axonal membranes. *Ann. Neurol.* 75(1):88–97

Stancu I, Vasconcelos B, Ris L, Wang P, Villers A, et al. 2015. Templated misfolding of Tau by prion-like seeding along neuronal connections impairs neuronal network function and associated behavioral outcomes in Tau transgenic mice. *Acta Neuropathol.* 129(6):875–94

Stine WB, Jungbauer L, Yu C, Ladu MJ. 2011. Preparing synthetic Aβ in different aggregation states. *Methods Mol. Biol.* 670:13–32

Stöhr J, Condello C, Watts JC, Bloch L, Oehler A, et al. 2014. Distinct synthetic Aβ prion strains producing different amyloid deposits in bigenic mice. *Proc. Natl. Acad. Sci. U. S. A.* 111(28):10329–34

Stöhr J, Watts JC, Mensinger ZL, Oehler A, Grillo SK, et al. 2012. Purified and synthetic Alzheimer's amyloid beta (Aβ) prions. *Proc. Natl. Acad. Sci. U. S. A.* 109(27):11025–30

Strobel G. *What Is Early Onset Familial Alzheimer Disease (eFAD)?* Alzforum. https://www.alzforum.org/early-onset-familial-ad/overview/what-early-onset-familial-alzheimer-disease-efad

Struhl G, Adachi A. 2000. Requirements for presenilin-dependent cleavage of notch and other transmembrane proteins. *Mol. Cell*. 6(3):625–36

Sturchler-Pierrat C, Abramowski D, Duke M, Wiederhold K-H, Mistl C, et al. 1997. Two amyloid precursor protein transgenic mouse models with Alzheimer disease-like pathology. *Proc. Natl. Acad. Sci. U. S. A.* 94(24):13287–92

Suzuki N, Cheung TT, Cai X-D, Odaka A, Otvos L, et al. 1994. An increased percentage of long amyloid β protein secreted by familial amyloid β protein precursor (β APP717) mutants. *Science (80-.).* 264(5163):1336–40

Swerdlow AJ, Higgins CD, Adlard P, Jones ME, Preece MA. 2003. Creutzfeldt-Jakob disease in United Kingdom patients treated with human pituitary growth hormone. *Neurology*. 61(6):783–91

Szaruga M, Munteanu B, Lismont S, Hopf C, De Strooper B, et al. 2017. Alzheimer's-Causing Mutations Shift Aβ Length by Destabilizing γ-Secretase-Aβn Interactions. *Cell*. 170(3):443–56

Szaruga M, Veugelen S, Benurwar M, Lismont S, Sepulveda-Falla D, et al. 2015. Qualitative changes in human γ-secretase underlie familial Alzheimer's disease. *J. Exp. Med.*

121(12):2003–13

Tamaoka A, Odaka A, Ishibashi Y, Usami M, Sahara N, et al. 1994. APP717 missense mutation affects the ratio of amyloid β protein species (Aβ1-42/43 and Aβ1-40) in familial Alzheimer's disease brain. *J. Biol. Chem.* 269(52):32721–24

Taneo J, Adachi T, Yoshida A, Takayasu K, Takahara K, Inaba K. 2015. Amyloid β oligomers induce interleukin-1β production in primary microglia in a cathepsin B- and reactive oxygen species-dependent manner. *Biochem. Biophys. Res. Commun.* 458(3):1–7

Telling GC, Parchi P, DeArmond SJ, Cortelli P, Montagna P, et al. 1996. Evidence for the conformation of the pathologic isoform of the prion protein enciphering and propagating prion diversity. *Science (80-.).* 274(5295):2079–82

Terry C, Wenborn A, Gros N, Sells J, Joiner S, et al. 2016. Ex vivo mammalian prions are formed of paired double helical prion protein fibrils. *Open Biol.* 6(5):160035

Thal DR, Rüb U, Orantes M, Braak H. 2002. Phases of Aβ-deposition in the human brain and its relevance for the development of AD. *Neurology*. 58(12):1791–1800

Thinakaran G, Borchelt DR, Lee MK, Slunt HH, Spitzer L, et al. 1996. Endoproteolysis of presenilin 1 and accumulation of processed derivatives In Vivo. *Neuron*. 17(1):181–90

Tofoleanu F, Buchete N-V. 2012. Alzheimer Aβ peptide interactions with lipid membranes. *Prion*. 6(4):339–45

Tokutake T, Kasuga K, Yajima R, Sekine Y, Tezuka T, et al. 2012. Hyperphosphorylation of Tau induced by naturally secreted amyloid-β at nanomolar concentrations is modulated by insulin-dependent Akt-GSK3β signaling pathway. *J. Biol. Chem.* 287(42):35222–25233

Tomiyama T, Nagata T, Shimada H, Teraoka R, Fukushima A, et al. 2008. A new amyloid β variant favoring oligomerization in Alzheimer's-type dementia. *Ann. Neurol.* 63(3):377–87

Trevitt CR, Hosszu LLP, Batchelor M, Panico S, Terry C, et al. 2014. N-terminal domain of prion protein directs its oligomeric association. *J. Biol. Chem.* 289(37):25497–508

Umeda T, Kimura T, Yoshida K, Takao K, Fujita Y, et al. 2017. Mutation-induced loss of APP function causes GABAergic depletion in recessive familial Alzheimer's disease: analysis of Osaka mutation-knockin mice. *Acta Neuropathol. Commun.* 5(1):59

Vasconcelos B, Stancu IC, Buist A, Bird M, Wang P, et al. 2016. Heterotypic seeding of Tau fibrillization by pre-aggregated Abeta provides potent seeds for prion-like seeding and

propagation of Tau-pathology in vivo. *Acta Neuropathol.* 131(4):1–21

Vassar R, Bennett BD, Babu-Khan S, Kahn S, Mendiaz E a, et al. 1999. Beta-secretase cleavage of Alzheimer's amyloid precursor protein by the transmembrane aspartic protease BACE. *Science (80-.).* 286(5440):735–41

Vassar R, Kuhn PH, Haass C, Kennedy ME, Rajendran L, et al. 2014. Function, therapeutic potential and cell biology of BACE proteases: current status and future prospects. *J. Neurochem.* 130(1):4–28

Veugelen S, Saito T, Saido TC, Chávez-Gutiérrez L, De Strooper B. 2016. Familial Alzheimer's disease mutations in presenilin generate amyloidogenic Aβ peptide seeds. *Neuron*. 90(2):410–16

Villemagne VL, Burnham S, Bourgeat P, Brown B, Ellis KA, et al. 2013. Amyloid β deposition, neurodegeneration, and cognitive decline in sporadic Alzheimer's disease: a prospective cohort study. *Lancet Neurol.* 12(4):357–67

Voytyuk I, De Strooper B, Chávez-Gutiérrez L. 2018. Modulation of γ- and β-secretases as early prevention against Alzheimer's disease. *Biol. Psychiatry*. 83(4):320–27

Wadsworth JDF, Joiner S, Linehan JM, Asante EA, Brandner S, Collinge J. 2008a. The origin of the prion agent of kuru: molecular and biological strain typing. *Philos. Trans. R. Soc. Lond. B. Biol. Sci.* 363(1510):3747–53

Wadsworth JDF, Powell C, Beck JA, Joiner S, Linehan JM, et al. 2008b. Molecular diagnosis of human prion disease. *Methods Mol. Biol.* 459:197–227

Wakabayashi T, De Strooper B. 2008. Presenilins: members of the gamma-secretase quartets, but part-time soloists too. *Physiology*. 23(67):194–204

Walker ES, Martinez M, Brunkan AL, Goate A. 2005. Presenilin 2 familial Alzheimer's disease mutations result in partial loss of function and dramatic changes in Aβ 42/40 ratios. *J. Neurochem.* 92(2):294–301

Walker LC, Jucker M. 2015. Neurodegenerative diseases: expanding the prion concept. *Annu. Rev. Neurosci.* 38:87–103

Walker LC, Schelle J, Jucker M. 2016. The prion-like properties of amyloid-β assemblies: implications for Alzheimer's disease. *Cold Spring Harb. Perspect. Med.* 6(7):a024398

Walsh DM, Klyubin I, Fadeeva J V, Cullen WK, Anwyl R, et al. 2002. Naturally secreted

oligomers of amyloid β protein potently inhibit hippocampal long-term potentiation in vivo. *Nature*. 416(6880):535–39

Wang H-Y, Li W, Benedetti NJ, Lee DHS. 2003. α7 nicotinic acetylcholine receptors mediate β-amyloid peptide-induced tau protein phosphorylation. *J. Biol. Chem.* 278(34):31547–53

Wang HY, Lee DH, D'Andrea MR, Peterson PA, Shank RP, Reitz AB. 2000. β-Amyloid(1-42) binds to α7 nicotinic acetylcholine receptor with high affinity. Implications for Alzheimer's disease pathology. *J. Biol. Chem.* 275(8):5626–32

Wang Y, Mandelkow E. 2015. Tau in physiology and pathology. *Nat. Rev. Neurosci.* 17(1):22–35

Watts JC, Condello C, Stöhr J, Oehler A, Lee J, et al. 2014. Serial propagation of distinct strains of Aβ prions from Alzheimer's disease patients. *Proc. Natl. Acad. Sci. U. S. A.* 111(28):10323–28

Welzel AT, Maggio JE, Shankar GM, Walker DE, Ostaszewski BL, et al. 2014. Secreted amyloid β-proteins in a cell culture model include N-terminally extended peptides that impair synaptic plasticity. *Biochemistry*. 53(24):3908–21

West E, Osborne C, Bate C. 2017. The cholesterol ester cycle regulates signalling complexes and synapse damage caused by amyloid-β. *J. Cell Sci.* 130(18):3050–59

Will R., Ironside J., Zeidler M, Estibeiro K, Cousens S., et al. 1996. A new variant of Creutzfeldt-Jakob disease in the UK. *Lancet*. 347(9006):921–25

Willem M, Tahirovic S, Busche MA, Ovsepian S V., Chafai M, et al. 2015. η-Secretase processing of APP inhibits neuronal activity in the hippocampus. *Nature*. 526(7573):443–47

Wilson RS, Segawa E, Boyle PA, Anagnos SE, Hizel LP, Bennett DA. 2012. The natural history of cognitive decline in Alzheimer's disease. *Psychol. Aging*. 27(4):1008–17

Wirths O, Bayer TA. 2012. Intraneuronal Aβ accumulation and neurodegeneration: Lessons from transgenic models. *Life Sci.* 91(23–24):1148–52

Wolfe MS, Selkoe DJ, Xia W, Ostaszewski BL, Diehl TS, Kimberly WT. 1999. Two transmembrane aspartates in presenilin-1 required for presenilin endoproteolysis and gamma-secretase activity. *Nature*. 398(6727):513–17

Wood WG, Eckert GP, Igbavboa U, Müller WE. 2003. Amyloid β-protein interactions with membranes and cholesterol: causes or casualties of Alzheimer's disease. *Biochim. Biophys. Acta*. 1610(2):281–90

Xia W, Ostaszewski BL, Kimberly WT, Rahmati T, Moore CL, et al. 2000. FAD mutations in presenilin-1 or amyloid precursor protein decrease the efficacy of a γ-secretase inhibitor: evidence for direct involvement of PS1 in the γ-secretase cleavage complex. *Neurobiol. Dis.* 7(6):673–81

Xiao Q, Gil S-C, Yan P, Wang Y, Han S, et al. 2012. Role of phosphatidylinositol clathrin assembly lymphoid-myeloid leukemia (PICALM) in intracellular amyloid precursor protein (APP) processing and amyloid plaque pathogenesis. *J. Biol. Chem.* 287(25):21279–89

Yallop CA, Svendsen I. 2001. The effects of G418 on the growth and metabolism of recombinant mammalian cell lines. *Cytotechnology*. 35(2):101–14

Yan R, Munzner JB, Shuck ME, Bienkowski MJ. 2001. BACE2 functions as an alternative α-secretase in cells. *J. Biol. Chem.* 276(36):34019–27

Yang T, Li S, Xu H, Walsh DM, Selkoe DJ. 2017. Large soluble oligomers of amyloid β-protein from Alzheimer brain are far less neuroactive than the smaller oligomers to which they dissociate. *J. Neurosci.* 37(1):152–63

Ye L, Fritschi SK, Schelle J, Obermüller U, Degenhardt K, et al. 2015a. Persistence of Aβ seeds in APP null mouse brain. *Nat. Neurosci.* 18(11):1559–61

Ye L, Hamaguchi T, Fritschi SK, Eisele YS, Obermüller U, et al. 2015b. Progression of seed-induced Aβ deposition within the limbic connectome. *Brain Pathol.* 25(6):743–52

Ye L, Rasmussen J, Kaeser SA, Marzesco A-M, Obermüller U, et al. 2017. Aβ seeding potency peaks in the early stages of cerebral β-amyloidosis. *EMBO Rep.* 18(9):1536–44

Yeh FL, Wang Y, Tom I, Gonzalez LC, Sheng M. 2016. TREM2 binds to apolipoproteins, including APOE and CLU/APOJ, and thereby facilitates uptake of amyloid-β by microglia. *Neuron*. 91(2):328–40

Yoshiyama Y, Higuchi M, Zhang B, Huang S-M, Iwata N, et al. 2007. Synapse loss and microglial activation precede tangles in a P301S tauopathy mouse model. *Neuron*. 53(3):337–51

Youssef I, Florent-Béchard S, Malaplate-Armand C, Koziel V, Bihain B, et al. 2008. N-truncated amyloid-β oligomers induce learning impairment and neuronal apoptosis. *Neurobiol. Aging*. 29(9):1319–33

Zetterberg H, Mattsson N. 2014. Understanding the cause of sporadic Alzheimer's disease. *Expert Rev. Neurother.* 14(6):621–30

Zhang Z, Song M, Liu X, Su Kang S, Duong DM, et al. 2015. Delta-secretase cleaves amyloid precursor protein and regulates the pathogenesis in Alzheimer's disease. *Nat. Commun.* 6:8762

Zhou F, Gong K, Song B, Ma T, van Laar T, et al. 2012. The APP intracellular domain (AICD) inhibits Wnt signalling and promotes neurite outgrowth. *Biochim. Biophys. Acta*. 1823(8):1233–41

Zou K, Kim D, Kakio A, Byun K, Gong J-S, et al. 2003. Amyloid β-protein (Aβ)1-40 protects neurons from damage induced by Aβ1-42 in culture and in rat brain. *J. Neurochem*. 87(3):609–19